A technical description of ACCESS-OM2, The Consortium of Ocean-Sea Ice Modelling in Australia's global ocean and sea ice model

Andrew Kiss, Andy Hogg, Kial Stewart, Adele Morrison, Aidan Heerdegen (ANU);
Nicholas Hannah (Double Precision); Marshall Ward (NCI);
Paul Spence, Matthew England, Ryan Holmes, Alfonso Acosta Goncalves (UNSW);
Russell Fiedler, Simon Marsland (CSIRO);
Fabio Dias, Abhishek Savita (UTas);
Petra Heil (AAD & ACE CRC, UTas);
Fanghua Wu (Beijing Climate Center);
Stephen Griffies (GFDL); James Munroe (Memorial U. Newfoundland)

TODO: consolidate author list and add anyone who's missing (order is arbitrary at this stage)

The latest version of this document is available from
GitHub: https://github.com/COSIMA/ACCESS-OM2-1-025-010deg-report

This version: typeset 2023-06-30 14:55:59 +10:00
Last commit: git hash: b26d655 2023-06-30 14:54:04 +1000,
committed to branch "master" by Andrew Kiss
77 commit(s) since release 1.0
NB: git hash does not reflect any uncommitted changes to this document.

CONTRIBUTORS PLEASE NOTE:

- please sign up with GitHub and click "watch" on https://github.com/COSIMA/ACCESS-OM2-1-025-010deg-report to be kept informed of discussions
- to discuss aspects of the paper, please post an issue at https://github.com/COSIMA/ACCESS-OM2-1-025-010deg-report/issues instead of using email. You can tag relevant parts of the .tex file with \ISSUE{num} (where "num" is the issue number) to link to the issue page (change tag to \CISSUE{num} if the issue is closed, so it is easily changed back if the issue is reopened).
- note contributors for sections in the .tex file with \CONTRIBUTORS{...}
- add "to do" items to the .tex file with \TODO{...}
- note errors and problems with \FIXME{...} in the .tex file
- to make git diffs easier, please try to write each sentence in the .tex file on a separate line
- use a bare number (no leading v) if you do git tags (for compatibility with the gitinfo2 package used here)
- see https://github.com/COSIMA/ACCESS-OM2-1-025-010deg-report for how to add or edit figures

Contents

List of Figures

List of Tables

1 Purpose of this document

This document serves two purposes:

1. This is a technical report to document the configuration and performance of the ACCESS-OM2 suite of models at 1°, 0.25° and 0.1° horizontal resolution (http://cosima.org.au/index.php/models/), intended to be a resource for the user community (e.g. COSIMA) and readily updated. This approach was partly inspired by Griffies (2015).

2. It forms the basis of one or more journal papers to announce and assess the performance of these models, e.g. Kiss et al. (2020).

TODO: Auto-update figures by programatically running COSIMA notebooks, so you could have a jenkins job or somesuch checking the COSIMA tech paper notebooks are all up to date and working correctly http://tritemio.github.io/smbits/2016/01/02/execute-notebooks/ and http://nbconvert.readthedocs.io/en/latest/execute_api.html

TODO: copy things from Nic's talk http://cosima.org.au/wp-content/uploads/2018/06/COSIMA2018-Hannah.pdf, Marshall's COSIMA 2018 workshop talk

2 Introduction

This technical report documents the ACCESS-OM2 ocean-sea ice model configurations at nominal horizontal resolutions of 1°, 0.25° and 0.1° developed by the Consortium for Ocean-Sea Ice Modelling in Australia (COSIMA, http://cosima.org.au). COSIMA is both a collaborative consortium within Australia's ocean and sea ice modelling community that integrates capability from different groups, and an ARC Linkage Project (involving the Australian National University, the University of New South Wales, the University of Tasmania, the Bureau of Meteorology, CSIRO and the Australian Antarctic Division) to develop the ACCESS-OM2 model suite described here, intended for nationwide use by Australia's ocean and sea ice modelling community, and to be incorporated into future versions of the Bluelink ocean reanalysis and forecasting system and the ACCESS coupled climate model.

The model configuration suite is designed to be accessible, well-documented and straightforward for new users to set up, run and analyse. Model development is public (https://github.com/COSIMA/access-om2) and all model code, configuration files and inputs are available to download and ready to run on NCI's Gadi supercomputer. Model run configurations are also tracked with git, with input files and executables tagged with git hashes for reproducibility. Output from all significant runs will be published on the NCI data repository, and the COSIMA Cookbook (https://github.com/COSIMA/cosima-cookbook) provides Python analysis tools to handle the large data volumes produced by the high-resolution runs.

3 Model Configuration

CONTRIBUTORS: Andrew Kiss to coordinate

TODO: incorporate things from https://github.com/COSIMA/access-om2/wiki/System-description

3.1 Overview

The ACCESS-OM2 model suite is described by Kiss et al. (2020); additional technical details are provided here. Model configurations at three horizontal resolutions have been developed, named

ACCESS-OM2 (nominally 1° horizontal resolution), ACCESS-OM2-025 (nominally 0.25°) and ACCESS-OM2-01 (nominally 0.1°). The suite of three resolutions is also collectively referred to as ACCESS-OM2. Configurations (e.g. run parameters and forcing) are as consistent as possible across the three resolutions (see Table 2 and Appendix A) to facilitate studies of resolution dependence and subgridscale parameterisations. The coarser models served as testbeds for developing correct configurations at higher resolutions, and are suitable for long experiments covering climatological timescales of hundreds of years, but are not eddy-resolving. They are intended for incorporation into future versions of the ACCESS-CM global coupled climate model. In contrast, the ACCESS-OM2-01 configuration resolves the first baroclinic deformation radius away from shelves and equatorward of about 50° (Hallberg, 2013), and therefore resolves the mesoscale in most of the world ocean. It is suitable for runs of several decades and is intended to form the basis of the next generation of the Bluelink operational ocean forecasting system.

ACCESS-OM2 consists of two-way coupled ocean and sea ice models driven by a prescribed atmosphere (see Figure 1). The model source code is hosted at https://github.com/COSIMA/access-om2. The ocean model component is the Modular Ocean Model (MOM) version 5.1 from the Geophysical Fluid Dynamics Laboratory (https://mom-ocean.github.io). The sea ice component (https://github.com/COSIMA/cice5/) is a fork from the Los Alamos sea ice model (CICE) version 5.1.2 from Los Alamos National Laboratories (https://github.com/CICE-Consortium/CICE-svn-trunk/tree/cice-5.1.2) which we keep up to date with https://github.com/CICE-Consortium/CICE-svn-trunk. **TODO:** cite CICE doi and let CICE consortium know of publications: http://cice-consortium-cice.readthedocs.io/en/master/intro/citing.html These components are forced by prescribed atmospheric conditions taken from the 55-year Japanese Reanalysis for driving oceans (JRA55-do, Tsujino et al., 2018a) via YATM (https://github.com/COSIMA/libaccessom2/). The model components are coupled together via Ocean Atmosphere Sea Ice Soil (OASIS3-MCT) version 2.0 from CERFACS and CNRS, France (https://portal.enes.org/oasis). The exact source code and inputs used for the experiments discussed here are listed in Table 2. The following subsections provide further details on these model components.

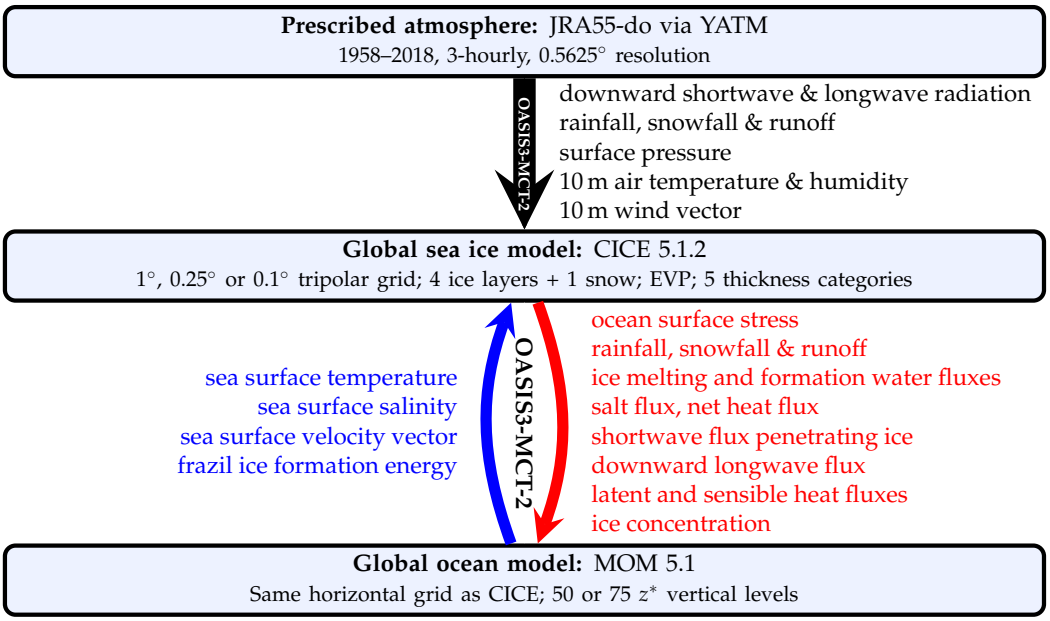

Figure 1: Coupling between model components by OASIS3-MCT-2 as specified in the namcouple file (which matches the atmosphere-CICE coupling fields specified in atmosphere/forcing.json and the CICE-MOM coupling fields specified in mom_oasis3_interface_nml in ocean/input.nml). Notice that MOM receives atmospheric forcing via CICE rather than directly from YATM (CICE has the same global domain as MOM). Surface pressure is used in the surface fluxes routines in CICE to calculate the saturated vapour pressure. It is also passed from CICE to MOM, but we don't show it here because MOM ignores it in the current configuration since use_full_patm_for_sea_level=false and max_ice_thickness=0. Similarly, the sea surface slope vector is passed from MOM to CICE but is unused (use_ocnslope is false, so the sea surface slope is instead calculated from the sea surface velocity vector, assuming geostrophy) so is not shown here. Also see https://github.com/COSIMA/access-om2/wiki/System-description.

	ACCESS-OM2	ACCESS-OM2-025	ACCESS-OM2-01
Experiment	1deg_jra55v13_iaf_spinup1_B1	025deg_jra55v13_iaf_gmredi6	01deg_jra55v13_iaf
MOM			
source	https://github.com/mom-ocean/MOM5/tree/afe80bfd	https://github.com/mom-ocean/MOM5/tree/afe80bfd	https://github.com/mom-ocean/MOM5/tree/afe80bfd
executable	/g/data/ik11/inputs/access-om2/bin/fms_ACCESS-OM_afe80bfd.x	/g/data/ik11/inputs/access-om2/bin/fms_ACCESS-OM_afe80bfd.x	/g/data/ik11/inputs/access-om2/bin/fms_ACCESS-OM_afe80bfd.x
inputs	/g/data/ik11/inputs/access-om2/input_236a3011/mom_1deg	/g/data/ik11/inputs/access-om2/input_236a3011/mom_025deg	/g/data/ik11/inputs/access-om2/input_38570c62/mom_01deg
CICE			
source	https://github.com/COSIMA/cice5/tree/076b14f2	https://github.com/COSIMA/cice5/tree/076b14f2	https://github.com/COSIMA/cice5/tree/076b14f2
executable	/g/data/ik11/inputs/access-om2/bin/cice_auscom_360x300_24p_-076b14f2.exe	/g/data/ik11/inputs/access-om2/bin/cice_auscom_1440x1080_480p_-076b14f2.exe	/g/data/ik11/inputs/access-om2/bin/cice_auscom_3600x2700_1392p_-076b14f2.exe
inputs	/g/data/ik11/inputs/access-om2/input_236a3011/cice_1deg	/g/data/ik11/inputs/access-om2/input_236a3011/cice_025deg	/g/data/ik11/inputs/access-om2/input_38570c62/cice_01deg
YATM			
source	https://github.com/COSIMA/libaccessom2/tree/e8ad3723	https://github.com/COSIMA/libaccessom2/tree/e8ad3723	https://github.com/COSIMA/libaccessom2/tree/e8ad3723
executable	/g/data/ik11/inputs/access-om2/bin/yatm_e8ad3723.exe	/g/data/ik11/inputs/access-om2/bin/yatm_e8ad3723.exe	/g/data/ik11/inputs/access-om2/bin/yatm_e8ad3723.exe
inputs	/g/data/ik11/inputs/access-om2/input_236a3011/yatm_1deg	/g/data/ik11/inputs/access-om2/input_236a3011/yatm_025deg	/g/data/ik11/inputs/access-om2/input_38570c62/yatm_01deg
common inputs	/g/data/ik11/inputs/access-om2/input_236a3011/common_1deg_jra55	/g/data/ik11/inputs/access-om2/input_-236a3011/common_025deg_jra55	/g/data/ik11/inputs/access-om2/input_38570c62/common_01deg_jra55
outputs	/g/data/hh5/tmp/cosima/access-om2/1deg_jra55v13_iaf_spinup1_B1	/g/data/hh5/tmp/cosima/access-om2-025/025deg_jra55v13_iaf_gmredi6	/g/data/hh5/tmp/cosima/access-om2-01/01deg_jra55v13_iaf
run summary	/g/data/hh5/tmp/cosima/access-om2-run-summaries/run_summary_1deg_-jra55v13_iaf_spinup1_B1.csv	/g/data/hh5/tmp/cosima/access-om2-run-summaries/run_summary_025deg_-jra55v13_iaf_gmredi6.csv	/g/data/hh5/tmp/cosima/access-om2-run-summaries/run_summary_01deg_-jra55v13_iaf.csv

Table 2: Sources and NCI paths to executables, inputs and outputs for the experiments in this document. These are based on the final run of each experiment; consult run summary spreadsheets for information on any changes within these experiments and details on computational resource use. Namelist changes within runs are tabulated in Appendix B. Note that the last cycle of 1deg_jra55v13_iaf_spinup1_B1 was repeated with extra diagnostics in 1deg_jra55v13_iaf_spinup1_B1_lastcycle. The final source code and run configurations used here are at https://doi.org/10.5281/zenodo.2653246 (or equivalently at https://github.com/COSIMA/access-om2/releases/tag/GMD2019). The individual final run configurations are at https://github.com/COSIMA/1deg_jra55_iaf/releases/tag/1.0, https://github.com/COSIMA/025deg_jra55_iaf/releases/tag/1.0 and https://github.com/COSIMA/01deg_jra55_iaf/releases/tag/1.0

Model	n	Δz_{min} (m)	Δz_{median} (m)	Δz_{max} (m)	H_{max} (m)
ACCESS-OM2	50	2.3	93.0	219.6	5363.5
ACCESS-OM2-025	50	2.3	93.0	219.6	5363.5
ACCESS-OM2-01	75	1.1	42.6	198.4	5808.7

Table 4: Vertical grid parameters: n levels, with spacing of Δz_{min} and Δz_{max} at the surface and maximum depth H_{max}, respectively, and median spacing Δz_{median}. Figure 2 shows the distribution with depth. **TODO:** check that I'm correctly using the notation in Stewart et al. (2017)

3.2 MOM configurations

MOM parameters for the three model resolutions are tabulated in Appendix A.2. We discuss the choices of key parameters here.

The primary MOM5 reference is Griffies (2012). Griffies et al. (2008) provides many useful technical details (despite being for MOM4).

The ocean formulation is hydrostatic and Boussinesq (volume-conserving), with a free surface and z^* vertical coordinate.

The Boussinesq reference density is rho0 = 1035.0 kgm^{-3}, the default value.

3.2.1 Vertical grid

The configurations use a z^* vertical coordinate (vertical_coordinate='zstar'; Griffies, 2012, section 5.1.4), with partial cells (see section 3.2.3). The vertical grid is staggered, with vertical velocity points offset from tracer points. Vertical grid parameters are summarised in Tables 4 and 9 and Figure 2. The vertical grids are specified in the input file ocean_vgrid.nc for each configuration. Vertical grid data is also available in the ocean.nc output files (see variables st_ocean, st_edges_ocean, sw_ocean, sw_edges_ocean).

The vertical grids are optimised for resolving baroclinic modes (Stewart et al., 2017). The vertical grids in ACCESS-OM2 and ACCESS-OM2-025 are slightly modified versions of KDS50 (Stewart et al., 2017, table 1), with 50 levels and 2.3 m spacing at the surface, increasing smoothly to 219.6 m by the bottom at 5363.5 m. The vertical grid in ACCESS-OM2-01 is a slightly modified version of KDS75 (Stewart et al., 2017, table 1), with 75 levels and 1.1 m spacing at the surface, increasing smoothly to 198.4 m by the bottom at 5808.7 m. The 75 level vertical grid is finer than OFAM3 at all depths other than 100 – 260 m and finer at all depths than GFDL50 and NEMO46 (as defined by Stewart et al., 2017).

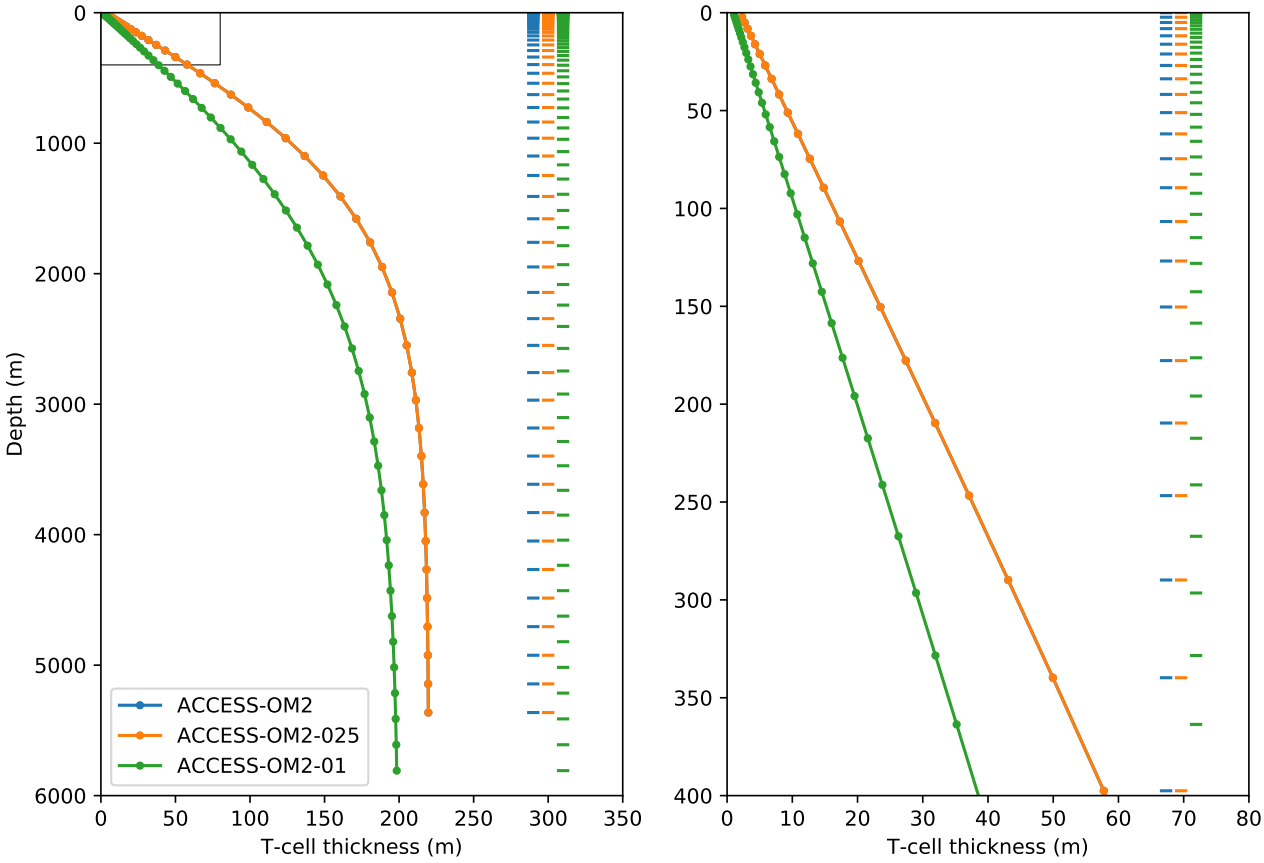

Figure 2: Vertical grid spacing for the ACCESS-OM2 simulations. ACCESS-OM2 and ACCESS-OM2-025 use the same vertical grid. Left: the full depth range. Right: the upper ocean. The horizontal lines show the top and bottom of T cells. Table 2 provides further details.

	Global			North of 60°N			South of 60°S		
	min	median	max	min	median	max	min	median	max
ACCESS-OM2 dx	23.8	91.7	111.2	24.7	32.7	54.8	23.8	43.0	54.6
ACCESS-OM2 dy	15.4	51.4	111.2	15.4	47.4	56.6	27.5	57.5	76.1
ACCESS-OM2 dx/dy	0.49	0.92	3.04	0.49	0.74	3.04	0.72	0.75	0.91
ACCESS-OM2-025 dx	6.0	18.1	27.8	6.2	8.1	13.9	6.0	11.3	13.9
ACCESS-OM2-025 dy	6.0	18.1	27.8	6.0	11.1	13.9	11.7	11.7	13.9
ACCESS-OM2-025 dx/dy	0.51	1.0	1.82	0.53	0.8	1.82	0.51	0.96	1.0
ACCESS-OM2-01 dx	2.19	7.16	11.12	2.47	3.29	5.55	2.19	4.52	5.55
ACCESS-OM2-01 dy	0.88	7.16	11.12	0.88	4.39	5.55	4.7	4.7	5.55
ACCESS-OM2-01 dx/dy	0.47	1.0	5.1	0.52	0.81	5.1	0.47	0.96	1.0

Table 6: Statistics of ocean T-cell horizontal dimensions (in km) and aspect ratios; global distributions are shown in Figure 5.

3.2.2 Horizontal grid

Grid parameters are summarised in Tables 6 and 9. The horizontal grids are specified in the file ocean_hgrid.nc for each configuration.

In the horizontal, MOM and CICE use the same orthogonal curvilinear Arakawa B-grid with velocity components co-located at the northeast corner of tracer cells. Model configurations have been developed with zonal resolutions of 1°, 0.25° and 0.1° south of 65°N. Figures 3, 4 and 5 and Table 6 show the grid spacing at the three resolutions. Globally, the median cell size is 92 km, 18.1 km and 7.2 km, respectively, at 1°, 0.25° and 0.1° resolution. Although the CICE model is global, the sea ice is mostly confined to latitudes higher than 60°, where most cell dimensions are finer than 47.4 km, 11.3 km and 4.5 km, respectively, at the three resolutions.

The horizontal meshes are 360 × 300, 1440 × 1080 and 3600 × 2700 at 1°, 0.25° and 0.1°, respectively. In all cases the grid covers the global ocean, extending from the North Pole to the Antarctic shelf edge but omitting the Antarctic landmass. The T-grid extends to 77.8766233766234°S at 1°, 81.0770008338366°S at 0.25°, and 81.1297513555451°S at 0.1°. The ocean extends to the southernmost cell at 1°, but the other resolutions have a land mask covering the southernmost cells, giving southernmost ocean T-cell latitudes of 78.22584°S at 0.25°, and 79.58801°S at 0.1°.

The longitude range is −280°E to +80°E, placing the join in the middle of the Indian Ocean. In all configurations the grid is tripolar (Murray, 1996) north of 65°N (so the grid directions are not zonal and meridional in this region), with the tripoles placed on land at 65°N, −100°E and 65°N, 80°E. In the 0.25° and 0.1° configurations the grid is Mercator (i.e. the meridional spacing scales as the cosine of latitude) between 65°N and 65°S; south of 65°S, the meridional grid spacing is held at the same value (in km) as at 65°S. The meridional variation of meridional grid spacing is more complicated in the 1° model (Figure 5), and incorporates a refinement to 1/3° (of latitude) within 10° of the Equator (Bi et al., 2013b; Bi and Marsland, 2010).

The 0.1° configuration had a misaligned CICE grid in both the IAF run and the preceding RYF spinup — see https://github.com/COSIMA/access-om2/issues/190. ⚠

TODO: maps of grid spacing divided by local 1st baroclinic Rossby radius from CheltonDeSzoekeSchlaxEl-NaggarSiwertz1998a http://www-po.coas.oregonstate.edu/research/po/research/rossby_radius/index.html?

3.2.3 Bathymetry

CONTRIBUTORS: Russ Fiedler

Topography tools:

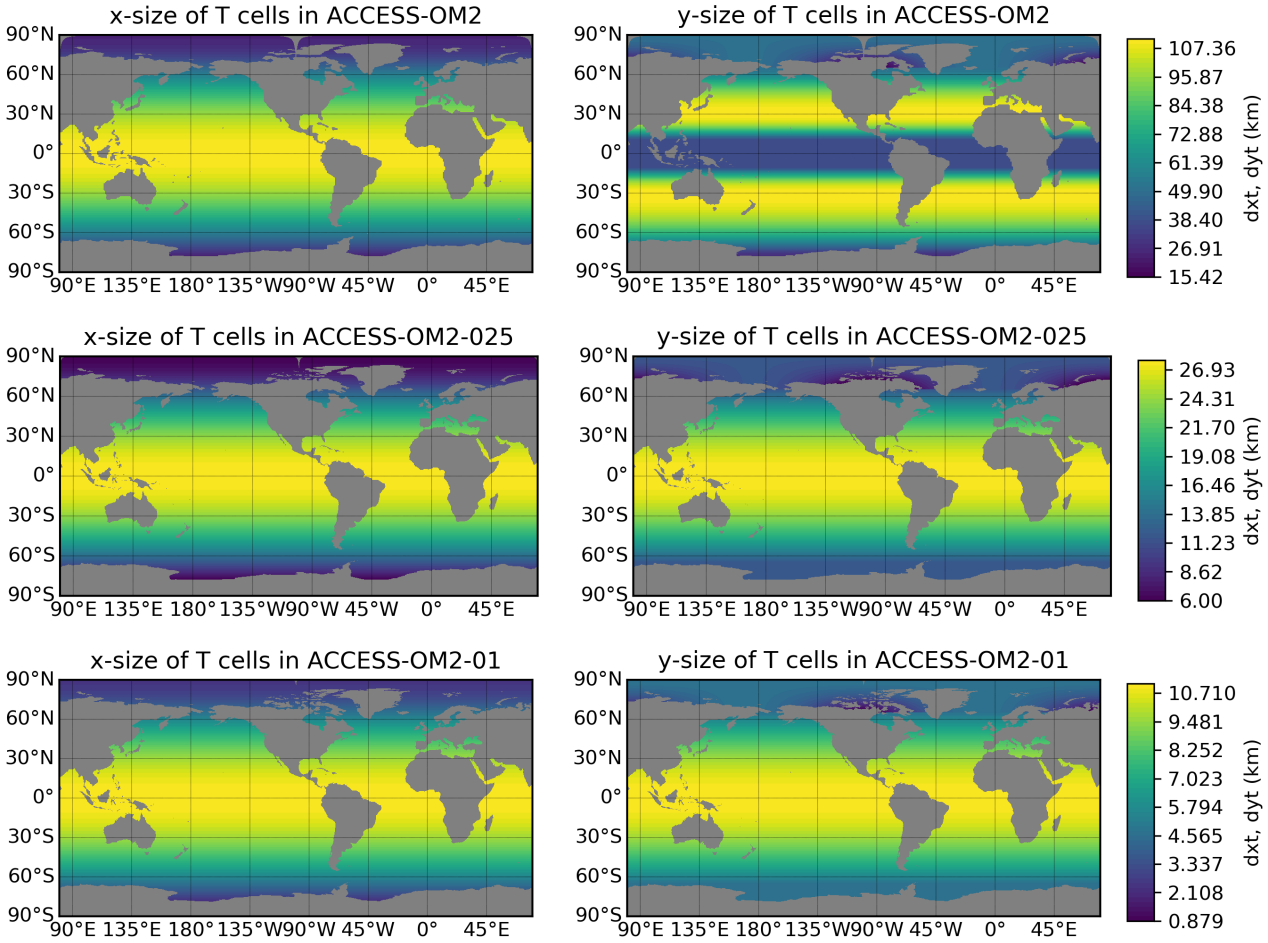

Figure 3: Horizontal grid spacing for the ACCESS-OM2 simulations. The colorbar limits show the minimum and maximum values. Note the meridional refinement near the equator in the 1° grid. **TODO:** also plot aspect ratio? see Bi and Marsland (2010)

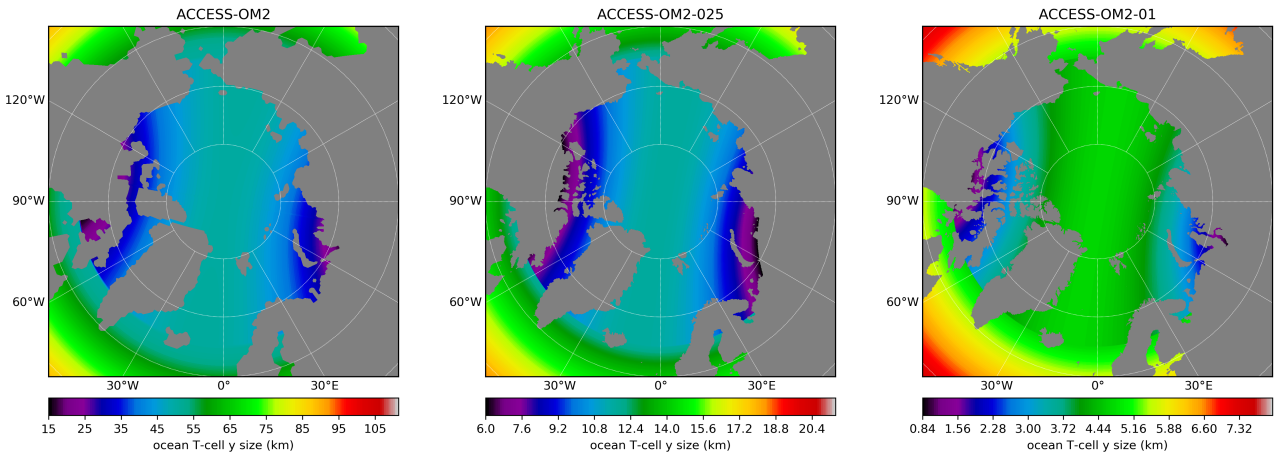

Figure 4: Land masks and T cell y-size in the Arctic tripolar region in the three resolutions.

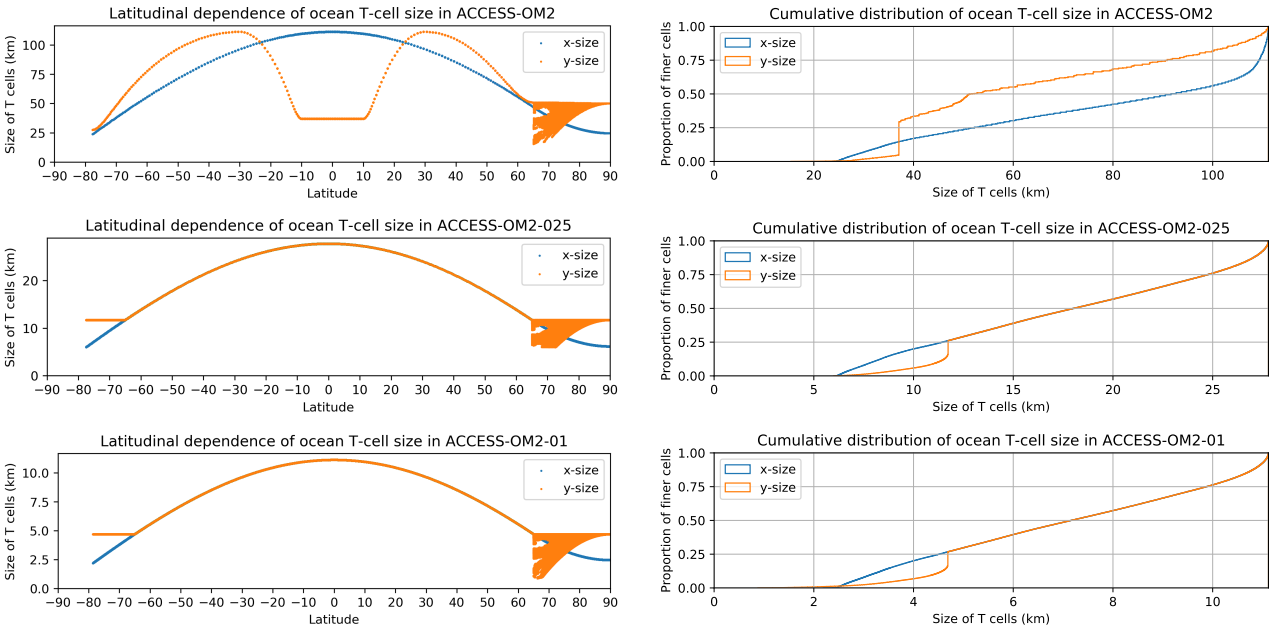

Figure 5: Latitudinal variation of ocean cell dimensions (left), and cumulative histograms of horizontal grid spacing for ocean cells (right) in the ACCESS-OM2 simulations. Table 6 provides further statistics.

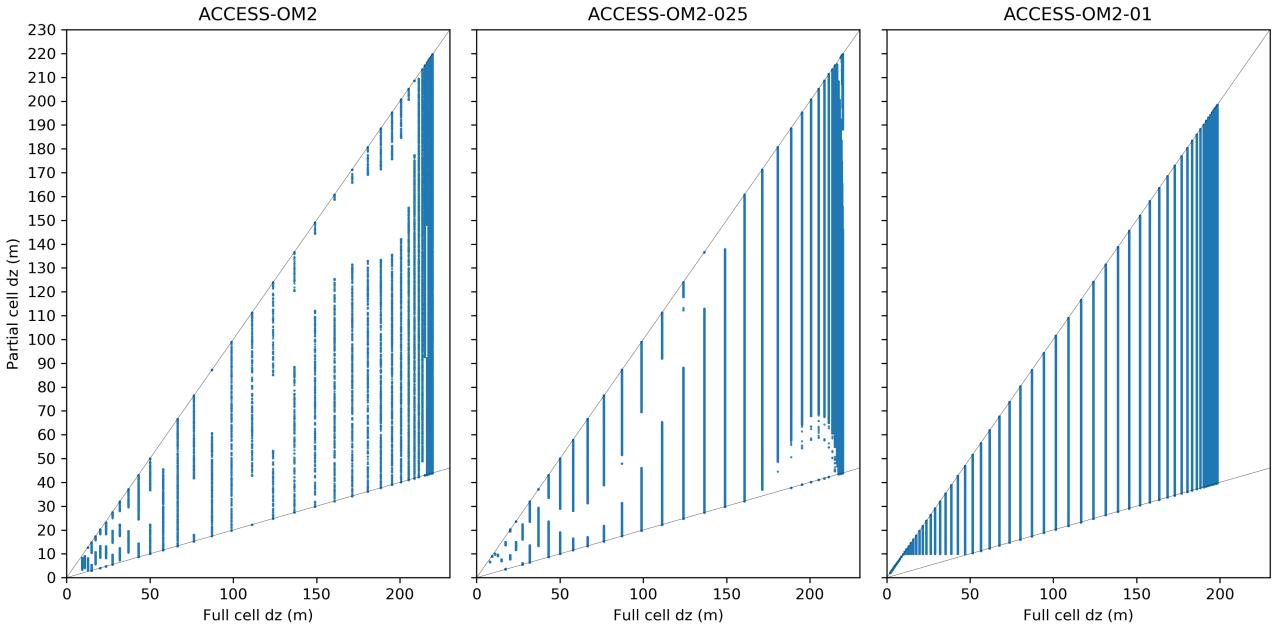

Figure 6: Scatter plots of partial cell thickness versus full cell thickness in the three configurations. The upper and lower lines have slopes of 1 and 0.2, respectively. For ACCESS-OM2-01 the cells are full-depth when thinner than 10 m (i.e. the points fall on the upper line).

Various iterations of the 0.1° bathymetry are in /g/data/hh5/tmp/cosima/bathymetry; see /g/data/hh5/tmp/cosima/bathymetry and /short/v45/aek156/access-om2/input/mom_01deg/README-topog.txt and /home/156/aek156/payu/01deg_jra55v13_ryf8485_-spinup6/README-topog.txt.

kmt_min: minimum number of vertical cells

The topog.nc seafloor topography (bathymetry) files were set up at each resolution with the help of https://github.com/COSIMA/topogtools and https://github.com/mom-ocean/MOM5/blob/master/src/tools/make_topog/topog.c and are read in by https://github.com/mom-ocean/MOM5/blob/master/src/mom5/ocean_core/ocean_topog.F90 at runtime. This reads work/ocean/INPUT/topog.nc which points to /short/v45/aek156/access-om2/input/mom_01deg/topog.nc - OR DOES IT? This in turn is the same as /g/data/hh5/tmp/cosima/bathymetry/topog_13_06_2018.baffin.nc. At 0.1° /short/v45/aek156/access-om2/control/01deg_-jra55_iaf/config.yaml specifies /short/public/access-om2/input_38570c62/mom_01deg/topog.nc, which is the same as /g/data/hh5/tmp/cosima/bathymetry/topog_13_06_2018.baffin.nc. At 0.25° the topography is specified in /home/157/amh157/payu/0-jra55_iaf_gmredi/config.yaml as /g/data/ua8/MOM/grids/025/topog/KDS50/ **TODO:** what's the 1 deg topog? **FIXME:** update all this

The land mask in the two coarser resolutions was enlarged near the tripoles to remove small wet points, but this was not done at 0.1° (figure 4). Consequently the 0.1° bathymetry retains the Gulf of Ob in Siberia and many channels in the Canadian Archipelago which are absent at coarser resolution.

There are no ice shelf cavities as these are not supported in MOM5.1.

Mention the integrity checks and scripts used to generate the data (e.g. in /g/data/hh5/tmp/cosima/bathymetry/tools/cor — should these be made publicly available? Also https://github.com/aekiss/notebooks/blob/master/non-advective.ipynb.

The minimum depth is 45.11 m (10 levels) in ACCESS-OM2, 40.36 m (9 levels) in ACCESS-OM2-025, and 10.43 m (7 levels) in ACCESS-OM2-01 — see

⚠

1° and 0.25° The 1° and 0.25° topography files originate from the OCCAM model, from which they inherit a number of flaws such as anomalous 'pits' on the shelves (for example excessive depth in the Gulf of Carpentaria and also the East Siberian and Chukchi seas south of Wrangel Island); see https://github.com/mom-ocean/MOM5/issues/172. They also have land masks that differ from each other and ⚠ also from the 0.1° topography; see https://github.com/COSIMA/access-om2/issues/158. The 1° and 0.25° topography files were based on previously-generated files with the GFDL50 vertical grid and a (presumably 20%) minimum partial cell thickness. When adapted to KDS50 the GFDL50 minimum cell thickness ⚠ produces gaps in the thickness distribution (figure 6), i.e. the small terraces produced by the GFDL minimum partial cell thickness are inherited by the topography on the KDS50 vertical grid. See https://github.com/COSIMA/access-om2/issues/141.

0.1° The 0.1° bathymetry was generated from scratch by Russ Fiedler, and is therefore unaffected by the flaws that afflict the topography at 1° and 0.25°. It is based on GEBCO 2014 30 arcsecond gridded data **FIXME:** which version? http://www.gebco.net/data_and_products/gridded_bathymetry_data/gebco_30_second_grid/ GEBCO is has 1 m vertical resolution but this is averaged within each model grid cell, so the model topography is smoother (at least, before later processing). The topography data used in the runs is /short/v45/aek156/access-om2/input/mom_01deg/topog.nc also /g/data/hh5/tmp/cosima/bathymetry/topog_latest.nc **FIXME:** update

Topography ends at a vertical wall at the ice shelf edge (the calving line, not the grounding line). A narrow strip along the southern boundary of the model is all land because the latitude range of the model was chosen for consistency with the previous MOM-SIS bathymetry which stopped at the grounding line.

TODO: plot or stats on how much model bathy differs from gebco plot bathymetry for the 3 resolutions – incl difference from gebco and from 0.1deg as maps, scatter plots, histograms, and differences between the 3 resolutions, eg in Canadian archipelago

TODO: mention main places where bathy tweaks were made – see /g/data/hh5/tmp/cosima/bathymetry/README

/g/data/hh5/tmp/cosima/bathymetry/README: "Enforced minimum of 7 levels (approx 10m). Excavated not filled in so land mask kept. Partial cells: Enforced thickness of max(10,0.2*dz). If partial cell were thinner than half this then the cell was removed."

We use partial cells (Adcroft et al., 1997; Pacanowski and Gnanadesikan, 1998) to obtain a more accurate representation of bottom topography. For ACCESS-OM2-01 the minimum height of partial cells is 20% of the full cell height, or $\min(10\,\mathrm{m}, \Delta z)$, whichever is greater (depth:min_thick=10 in topog.nc; this modification is done by https://github.com/mom-ocean/MOM5/blob/master/src/tools/make_topog/topog.c#L858). This means the minimum thickness is greater than 20% of the full cell thickness if this is less than 50 m (i.e. for depths shallower than 543 m) and the cells are full-depth if they thinner than 10 m (i.e. for depths shallower than 103 m) — see figure 6 and https://github.com/COSIMA/access-om2/issues/99). This produces terraces in shallow water. This problem is fixed in more recent versions.

3.2.4 Tracers

CONTRIBUTORS: Ryan Holmes

At all three resolutions tracers (salt, temperature and age) are advected horizontally and vertically by the multidimensional piecewise parabolic method (Colella and Woodward, 1984), with a monotonicity-preserving flux limiter following Suresh and Huynh (1997) (horizontal-advection-scheme=vertical-advection-scheme='mdppm' and ppm_hlimiter=ppm_vlimiter=3 for temp, salt and age in ocean/field_table; also see https://github.com/mom-ocean/MOM5/blob/master/src/mom5/ocean_tracers/ocean_tracer_advect.F90). **TODO:** check: is this monotonicity-preserving under all conditions? https://github.com/mom-ocean/MOM5/blob/99168b44ab45f4f5b4fa2544a0c3f644f0afb666/src/mom5/ocean_tracers/ocean_tracer_advect.F90 As the 0.1° configuration does not include a mesoscale eddy parameterization or explicit isopycnal or lateral diffusion (see section 3.2.5), the suppression of large lateral tracer gradients near the grid-scale in this configuration is achieved solely though spurious numerical mixing in this tracer advection scheme. **TODO:** Reference to Holmes et al numerical mixing article/s

3.2.5 Sub-grid scale lateral / neutral physics

CONTRIBUTORS: Ryan Holmes

A sub-grid scale parameterization for mesoscale eddies is included in the 1° and 0.25° models (ocean_nphysics_nml use_this_module=true), but not at 0.1° as this resolution is considered "eddy-resolving". In the two coarser configurations the Gent and McWilliams (1990) (GM) parameterization is used to represent the down-gradient isopycnal thickness flux associated with mesoscale eddies, and the along-isopycnal eddy tracer transport is parameterised by a Redi diffusivity (Redi, 1982). The namelist group ocean_nphysics_util_nml controls these parameterisations; see Griffies (2012, section 23.8) for further explanation. Note that the namelists are a bit confusing, as many ignored parameters are specified — see https://github.com/COSIMA/access-om2/issues/197. Their parameters are recalculated from scratch for each run, rather than being picked up from restarts (nphysics_util_zero_init=true).

The GM parameterization is implemented as a skew diffusive flux (Griffies, 1998). In common with many GFDL configurations, we use the ocean_nphysicsC formulation (use_nphysicsc=true) which differs from the default (use_nphysicsa) in that the skew diffusive flux calculation is based on a vector streamfunction built from a sum of baroclinic modes. The associated diffusivity is depth-independent but flow-dependent (agm_closure=true, agm_closure_baroclinic=true), and is the product of agm_closure_scaling, an inverse timescale, a squared length scale, and a grid scaling factor (see https://github.com/mom-ocean/MOM5/blob/4d60fad0e56/src/mom5/ocean_param/neutral/ocean_nphysics_util.F90#L2860). The length scale (agm_closure_length) is 50 km at 1° and 20 km at 0.25° (agm_closure_length is used because agm_closure_baroclinic=true — see https://github.com/mom-ocean/MOM5/blob/4d60fad0e5619fe15a630732ace4f0e3b3c6f23e/src/mom5/ocean_param/neutral/ocean_nphysics_util.F90#L2756). The inverse timescale is an Eady growth rate determined from the horizontal density gradient averaged between agm_closure_upper_depth=100 m and agm_closure_lower_depth=2000 m using a constant buoyancy frequency of agm_closure_buoy_freq=0.004 s^{-1} (these three values are the defaults). The Eady growth rate

is subject to a limiter (agm_closure_eady_cap) and is smoothed both vertically and horizontally (agm_closure_eady_smooth_horz=true, agm_closure_eady_smooth_vert=true) and vertically averaged in the mixed layer (agm_closure_eady_ave_mixed=true). The grid scaling (agm_closure_grid_scaling=true) reduces the GM diffusivity in proportion to how well the numerical grid resolves the first baroclinic Rossby radius (or the equatorial Rossby radius within $\pm 5^\circ$ latitude), as suggested by (Hallberg, 2013). The GM diffusivity is limited to the ranges 50–600 $m^2 s^{-1}$ at 1° and 1–200 $m^2 s^{-1}$ at 0.25° set by agm_closure_min and agm_closure_max. It is not smoothed in space (agm_smooth_space=false) or time (agm_smooth_time=false).

The along-isopycnal Redi tracer diffusion (Redi, 1982) in the two coarser configurations has a diffusivity that differs from GM (aredi_equal_agm=false). A constant coefficient of aredi=600 $m^2 s^{-1}$ is used at 1°. At 0.25° the Redi coefficient is scaled by the resolution of the grid relative to either the first baroclinic Rossby radius, or the equatorial Rossby radius for latitudes between $\pm 5^\circ$N (aredi_diffusivity_grid_scaling=true), with a diffusivity no greater than aredi= 200 $m^2 s^{-1}$.

drhodz_mom4p1 is true at 1° but false at 0.25°.

Further testing of spatially- and temporally-dependent Redi and GM schemes has not yet been undertaken. However, given the sensitivity of the overturning circulation in the Southern Ocean and the formation of bottom water to the presence of these schemes exposed in a preliminary study in the 0.25° configuration, such a sensitivity study should be high on the agenda.

All three configurations include a parameterization for re-stratification in the surface mixed layer due to submesoscale eddies (Fox-Kemper et al., 2008); see namelist group ocean_submesoscale_nml. This parameterization applies an overturning circulation dependent on the horizontal buoyancy gradients within the mixed layer. The optional horizontal diffusive portion of this parameterization is not used (submeso_diffusion=false, so submeso_diffusion_biharmonic and submeso_diffusion_scale are ignored).

Horizontal friction is implemented with a biharmonic operator and an isotropic Smagorinsky scaling (k_smag_iso=2.0, k_smag_aniso=0.0) for the viscosity coefficient (Griffies and Hallberg, 2000); also see Griffies (2012, chapter 25). Our choice of k_smag_iso=2.0 is below the lower limit of $\pi/\sqrt{2} \approx 2.2$ suggested by Griffies and Hallberg (2000) and much less than the values of k_smag_iso=3.0, k_smag_aniso=3.0 used in OFAM3 (Appendix F.1), but matches what is used in ACCESS-CM2 (Appendix F.4) and does not seem to cause numerical stability problems. The 1° configuration also has a grid spacing-dependent isotropic (vel_micom_aniso=0.0) biharmonic background viscosity set by the velocity scale vel_micom_iso=0.04 $m s^{-1}$; there is no background viscosity at the other resolutions. The NCAR viscosity scheme is also applied at 1° (ncar_boundary_scaling=true), to enhance the background horizontal viscosity at western boundaries in order to ensure the western boundary currents are resolved (ncar_boundary_scaling=true at 0.25° and 0.1° but this has no effect because vel_micom_iso and vel_micom_aniso are both zero). This increases the background viscosity at 1° by a factor that is 4 on the i-maximum side of land cells at each depth, and decreases to 1 as a function of distance in the i direction (NB: this is not eastward distance in the tripole), with a profile that is a Gaussian with length scale 500 km (the inverse of ncar_vconst_4 in cm), raised to the power ncar_rescale_power=2. The background viscosity is inconsistent along the tripole seam with ncar_boundary_scaling=true — see https://github.com/mom-ocean/MOM5/issues/282. At 1° there is also background Laplacian viscosity at the bottom set by the velocity scale vel_micom_bottom=0.01 $m s^{-1}$ and calculated by a 5-point Laplacian operator (bottom_5point=true). The overall biharmonic viscosity is limited to visc_crit_scale=25% of the numerical instability threshold in ACCESS-OM2, or 100% in the other two configurations (see Griffies, 2004, equation (18.26)). The Smagorinsky biharmonic viscosity A_4 varies spatially by orders of magnitude (Figure 7). A viscous western boundary current has a width of about 3.6 times the length scale $(A_4/\beta)^{1/5}$ (see Haidvogel et al., 1992, Appendix B). This thickness is about 350 km in ACCESS-OM2, 100 km in ACCESS-OM2-025, and 60 km in ACCESS-OM2-01 (Figure 8), which is well-resolved by the grid in all cases. The lateral boundary condition for velocity is no-slip, as a consequence of using a B-grid (Griffies, 2012).

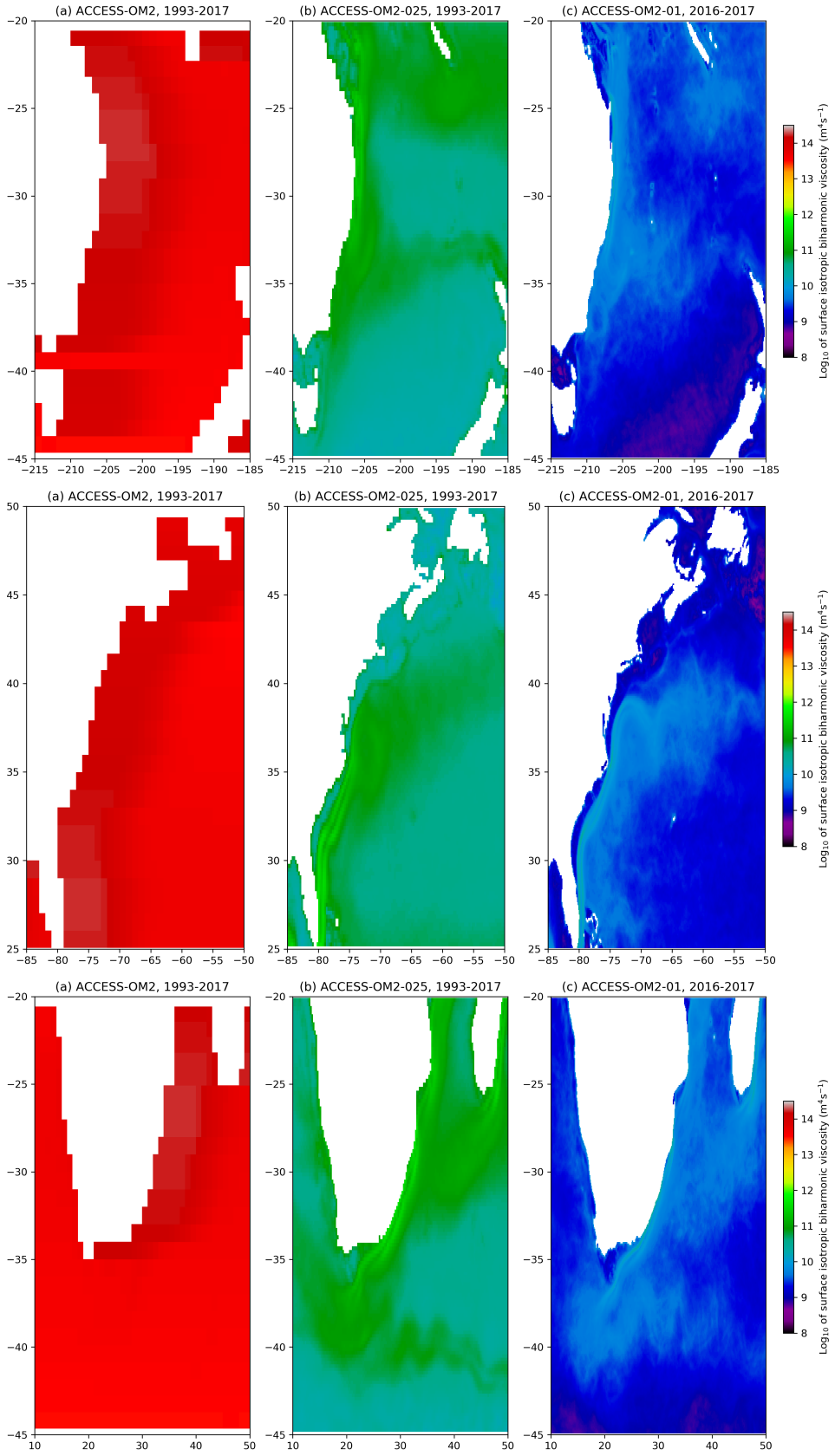

Figure 7: Time-mean surface isotropic biharmonic viscosity A_4 in several western boundary regions.

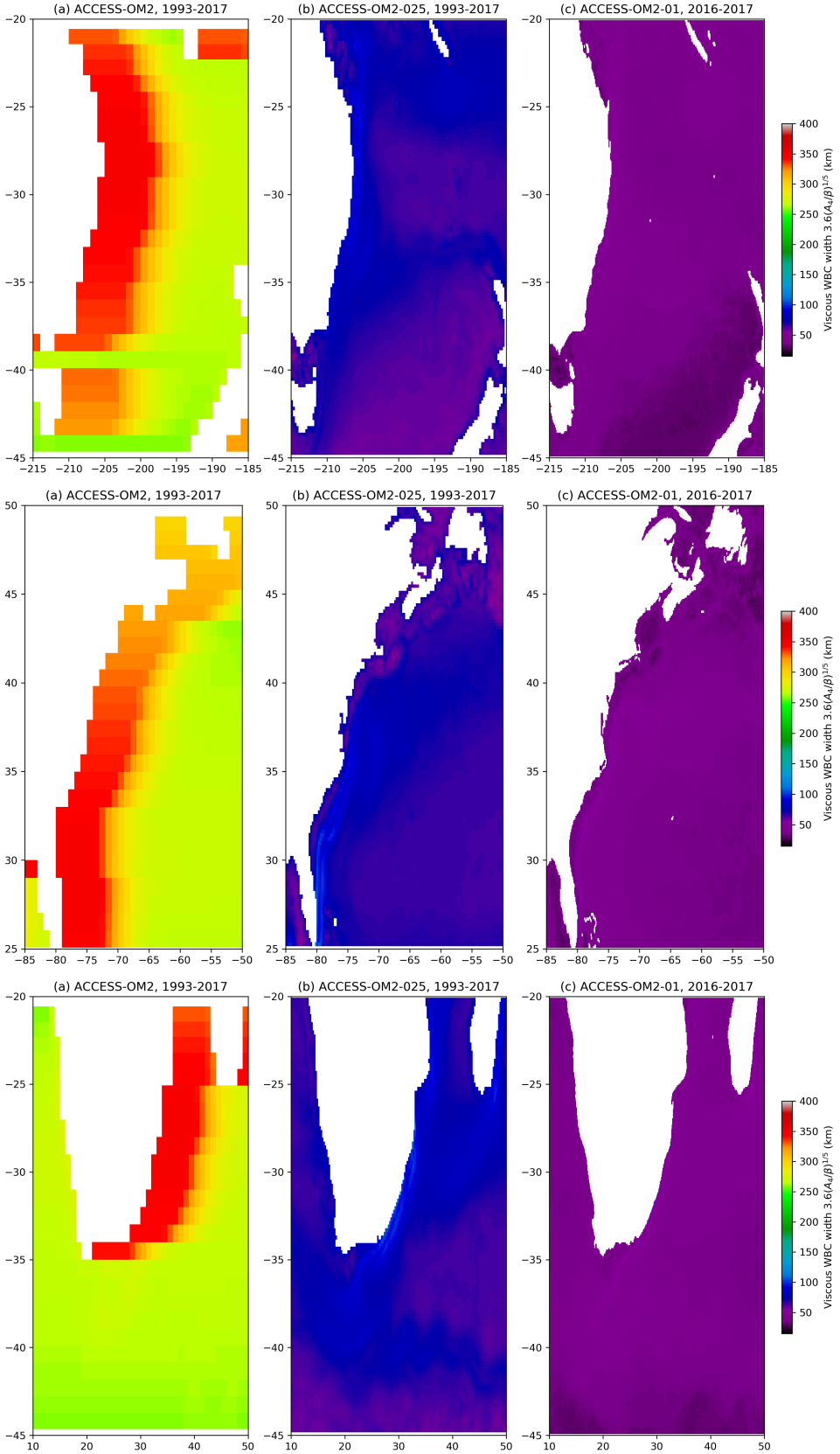

Figure 8: Biharmonic western boundary current width $3.6(A_4/\beta)^{1/5}$ in several western boundary regions, based on the time-mean surface isotropic biharmonic viscosity A_4 (figure 7).

3.2.6 Sub-grid scale vertical physics

CONTRIBUTORS: Ryan Holmes

Vertical diffusion of both tracers and momentum is parameterized using the K-profile parameterization (KPP, Large et al., 1994, vert_mix_scheme='kpp_mom4p1'), which governs mixing within the surface boundary layer, as well as interior convection (when the stratification is unstable), Richardson number-based shear instability (active mainly in the equatorial undercurrents), internal wave breaking, and double-diffusion. **TODO:** Comment on applicability of KPP at our high vertical resolution - see Van Roekel et al. (2018) KPP maintains static stability by applying large vertical diffusivity in regions with small or negative Richardson number; therefore explicit convective adjustment is not used at any resolution (see ocean_convect_nml). At 1° the Jochum (2009) latitudinally-dependent, depth-independent background vertical tracer diffusivity scheme is used (j09_diffusivity=true), with diffusivity j09_bgmax=$5 \times 10^{-6}\,\mathrm{m^2 s^{-1}}$ poleward of j09_lat=±20°N, reducing to j09_bgmin=$1 \times 10^{-6}\,\mathrm{m^2 s^{-1}}$ at the equator via a cosine profile, similar to observations (Gregg et al., 2003). The background vertical tracer diffusivity is zero in ACCESS-OM2-025 and ACCESS-OM2-01 (j09_diffusivity is unspecified, and the default is false). There is no additional non-tidal, non-KPP background vertical diffusivity at any resolution (background_diffusivity=0.0).

There are no explicit tides, but we include vertical tracer diffusivity and vertical viscosity from parameterised internal and barotropic tidal processes. Turbulent mixing and viscosity due to breaking internal tides is parameterised by the Simmons et al. (2004) scheme (use_wave_dissipation=true) with a vertical decay scale decay_scale=500 m, zero background vertical diffusivity (background_diffusivity=0.0), a constant background vertical viscosity of background_viscosity=$1 \times 10^{-4}\,\mathrm{m^2 s^{-1}}$, tidal current speed read from the file tideamp.nc (read_tide_speed) and bottom roughness amplitude read from the file roughness_amp.nc (read_roughness=true and reading_roughness_amp=true). The Lee et al. (2006) scheme is used to parameterise vertical mixing and viscosity due to the drag of barotropic tides on the bottom (use_drag_dissipation). Further parameters are in the ocean_vert_tidal_nml namelist group. **TODO:** investigate whether newer dissipation estimates/methods should be used, e.g. are de Lavergne et al. (2019) and https://doi.org/10.17882/58105 relevant?

Bottom drag is calculated from the law of the wall using prescribed spatially-varying bottom roughness and tidal current speed (cdbot_roughness_uamp=true), with residual current uresidual=$0.05\,\mathrm{m s^{-1}}$. Tidal current speed is read from the file tideamp.nc and bottom roughness is read from the file roughness_cdbot.nc. The bottom drag coefficient is restricted to the range cdbot_lo to cdbot_hi, where cdbot_lo takes its default value 0.001 and cdbot_hi=0.007 (larger than the default value 0.003). cdbot is unused, since cdbot_law_of_wall=false (the default).

The tidal speed data in tideamp.nc probably originates from Jayne and St. Laurent (2001) if it came from GFDL.**TODO:** try to confirm this? The bottom roughness files seem basically the same, except that roughness_amp.nc is on T points and roughness_cdbot.nc is on U points. They probably originate from Jayne and St. Laurent (2001) or Jayne (2009), which in turn are derived from Smith and Sandwell (1997).**TODO:** try to confirm this?

TODO: What is drag_coeff in ocean_grid.nc??

3.2.7 Rayleigh drag

Rayleigh drag is a velocity tendency term proportional to the velocity, with a negative coefficient whose inverse magnitude is the *e*-folding time for velocity decay. It is a momentum sink that is employed as an engineering fix to improve model stability and/or realism in a few selected locations in the 1° and 0.1° configurations, specified in ocean/field_table, as shown in figure 9. At 1° it is used to improve the Indonesian Throughflow transport; a damping timescale of 1.5 hr is applied at all but the bottom 2 (3) U-cells in Lombok (Ombai) Strait and for 3/4 of the width of the Torres Strait at all depths (these omissions were not intended, and could be corrected in ocean/field_table in new configurations: https://github.com/COSIMA/access-om2/issues/156). At 0.1° a damping timescale of 1.5 hr is used at all depths across

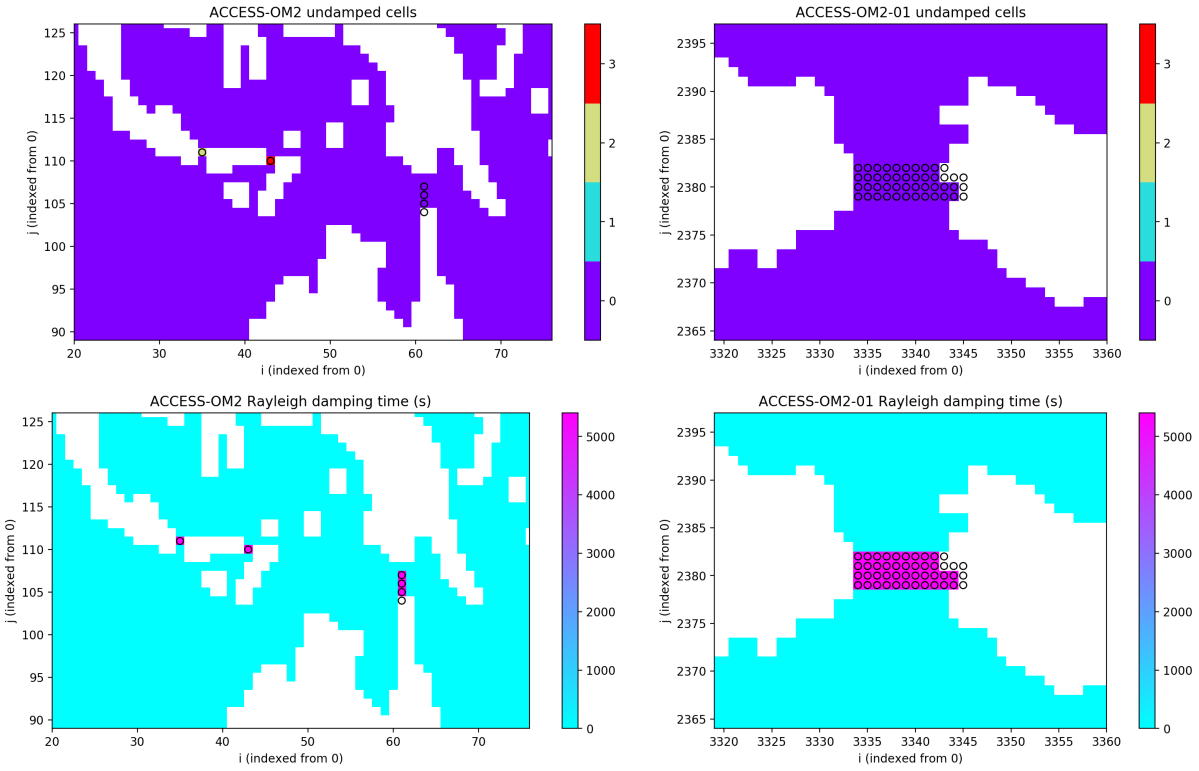

Figure 9: Rayleigh damping locations and magnitudes. Circles indicate where Rayleigh damping is defined in ocean/field_table and white cells are the U-grid land mask. Top row: Rayleigh damping locations at 1° (left; in the Lombok, Ombai and Torres Straits) and 0.1° (right; in the Kara Strait); colours in the circled cells indicate how many U-cells are not damped in each column. Bottom row: Rayleigh damping timescale (or zero if not defined) at 1° (left) and 0.1° (right). Where defined, damping timescales are all 5400 s. There is no Rayleigh damping at 0.25°.

the full width of Kara Strait to constrain the velocity, which otherwise leads to numerical instability unless an unfeasibly small timestep is used. There is no Rayleigh drag in the 0.25° configuration.

3.2.8 Other model physical parameters

We use the Jackett et al. (2006) pre-TEOS-10 seawater equation of state and freezing temperature (eos_preteos10=true and freezing_temp_preteos10=true). The prognostic temperature variable is conservative temperature in the 1° and 0.25° configurations (temperature_variable='conservative_temp'), and potential temperature[1] in the 0.1° configuration (temperature_variable='potential_temp'). However the 1° and 0.25° configurations mistakenly had pottemp_equal_contemp=true, which meant that incorrect temperatures were passed to the coupler https://github.com/COSIMA/access-om2/issues/148. The 0.1° simulation also had pottemp_equal_contemp=true, but the coupler fluxes are correct (since it used temperature_variable='potential_temp') but the conservative temperature output diagnostic is actually potential temperature. Since we use pre-TEOS-10, practical salinity is the prognostic variable for salt for all the ACCESS-OM2 configurations (https://github.com/mom-ocean/MOM5/blob/99168b44ab45f4f5b4fa2544a0c3f644f0afb666/src/mom5/ocean_core/ocean_density.F90#L209). If we switched to TEOS-10 (Roquet et al., 2015) we'd need to use two salinity variables (Preformed Salinity and Absolute Salinity anomaly) instead of practical salinity: see https://github.com/mom-ocean/MOM5/blob/99168b44ab45f4f5b4fa2544a0c3f644f0afb666/src/mom5/ocean_tracers/ocean_tempsalt.F90#L60 and https://github.com/mom-ocean/MOM5/blob/99168b44ab45f4f5b4fa2544a0c3f644f0afb666/src/mom5/ocean_core/ocean_density.F90#L203 and https://github.com/COSIMA/access-om2/issues/140. Frazil production is not confined to the top model layer (frazil_only_in_surface=false) **TODO:** check - ignored since we use auscom? and uses the pre-TEOS-10 freezing temperature (freezing_temp_preteos10)=true.

[1] This was an oversight: https://github.com/COSIMA/access-om2/issues/97, and has been corrected in the new 0.1° RYF configuration, which uses conservative temperature: https://github.com/COSIMA/access-om2/projects/1.

The Red Sea fix was not used (redsea_gulfbay_sfix=false or unspecified).

Overflow schemes are not used (see ocean_overflow_nml and ocean_overexchange_nml). Downslope transport and mixing schemes are only used at 1°, where we have sigma transport (Beckmann and Döscher, 1997; Campin and Goosse, 1999; Döscher and Beckmann, 2000) with default parameters (ocean_sigma_transport_nml) and downslope mixing (ocean_mixdownslope_nml) with mixdownslope_npts=4 (the default is 1).

Ice is massless / levitating (max_ice_thickness=0) to avoid coupled ice-ocean instabilities (Hallberg, 2014), but this alters the pressure applied to the ocean by the sea ice and precludes exact mass conservation in the coupled ocean and sea ice system (although mass is conserved within MOM5 itself, i.e. mass change rate equals net mass flux **TODO:** strictly speaking, should "mass" be "volume"?). See https://github.com/mom-ocean/MOM5/blob/7c8bb96/src/mom5/ocean_core/ocean_sbc.F90#L321. We also have use_full_patm_for_sea_level=false. In combination with max_ice_thickness=0 this eliminates the inverse barometer and ice mass signals from eta_t: https://github.com/mom-ocean/MOM5/blob/ac2aeaab3753f1170f8dc9d1db4c7a5f3bbf7359/src/mom5/ocean_core/ocean_sbc.F90#L3936

3.2.9 Timestepping

The MOM baroclinic timestep is ice_ocean_timestep in accessom2.nml. ice_ocean_timestep is also the CICE thermodynamic timestep, overriding dt in cice_in.nml. ice_ocean_timestep is chosen to be a factor of the JRA55-do forcing period of 3 hr = 10800 s, for example one of 100, 108, 120, 135, 144, 150, 180, 200, 216, 225, 240, 270, 300, 360, 400, 432, 450, 540, 600, 675, 720, 900, 1080, 1200, 1350, 1800, 2160, 2700, 3600 or 5400 s. Typical values are given in Table 8. We use split timestepping, with the baroclinic timestep barotropic_split = 80 times longer than the barotropic timestep. Note that in going from baroclinic timestep n to $n+1$ the barotropic solver integrates over a time interval covering baroclinic steps n to $n+2$ in order to give a centred time-average at baroclinic step $n+1$; thus there are 160 times more barotropic timesteps than baroclinic timesteps (Griffies, 2012, section 11.6).

The barotropic dynamics use a predictor-corrector method (Griffies, 2012, sections 11.2.5 and 11.5), with the recommended method (barotropic_time_stepping_a=true; see Griffies, 2012, section 11.8.1) and default dissipation parameter pred_corr_gamma=0.2 and smoothing smooth_eta_t_laplacian=true, vel_micom_lap=0.05 ms^{-1}. (smooth_eta_diag_laplacian and smooth_pbot_t_laplacian are ignored since we use a depth-based (z^*) vertical coordinate, and eta_max and frac_crit_cell_height are ignored because truncate_eta is false.)

Two-level volume- and tracer-conserving timestepping schemes are used for the baroclinic dynamics (time_tendency='twolevel'), with a staggered second-order forward method (tracer advection and lateral mixing of tracer and velocity calculated at timestep n and pressure gradients calculated at timestep $n+\frac{1}{2}$ **TODO:** check - see Griffies (2012, chapter 11)), implicit vertical mixing (aidif=1.0) and bottom drag (bmf_implicit=true), and semi-implicit Coriolis (acor=0.5) calculations. The tracer timestep is the same as the baroclinic dynamics timestep (baroclinic_split = 1). Velocity advection uses a second-order centred operator in space (velocity_advect_centered=true by default) and third-order Adams-Bashforth timestepping (adams_bashforth_third=true). See Griffies (2012, sections 11.3–11.6 and 11.8.1).

3.3 CICE sea ice model configurations

The sea-ice component in the ACCESS-OM2 suite is based on CICE version 5.1.2 (https://github.com/CICE-Consortium/CICE-svn-trunk/tree/cice-5.1.2). We have maintained our own fork at https://github.com/COSIMA/cice5 which includes additional code such as the auscom drivers used in these runs. We periodically update this fork to match the latest from the CICE consortium https://github.com/CICE-Consortium/CICE-svn-trunk. The model runs reported here used commit 076b14f2 (table 2; https://github.com/COSIMA/cice5/commit/076b14f2) which was the 117th commit in our fork after an import of CICE 5.1.2 on 24 June 2015 (https://github.com/COSIMA/cice5/commit/1110bae87). Commit 076b14f2 did not include several bug fixes which we have since imported from the CICE consortium (see commits cbf4c62 through to 320a796 at https://github.com/COSIMA/cice5/commits/master). **TODO:** check whether these bugs were relevant to our configs

The primary CICE5 reference is Hunke et al. (2015). CICE parameters for the three model resolu-

tions are tabulated in Appendix A.3; see https://ncar.github.io/CICE/users_guide/ice_nml_var.html for additional details. We discuss the choices of key parameters here. The parameters are based on those of ACCESS-OM **TODO:** check (Bi et al., 2013b), which used CICE4.1 and was the ocean-sea ice component of the ACCESS-CM coupled climate model (Bi et al., 2013a; Dix et al., 2013). ACCESS-CM has now been superseded by ACCESS-CM2; CICE namelist differences between our ACCESS-OM2 1° configuration and ACCESS-CM2 are are tabulated in Appendix F.4.2.

CICE5 uses the same horizontal grid as MOM (see section 3.2.2). Its thermodynamic timestep is ice_ocean_timestep, the same as the MOM baroclinic timestep, but its dynamic and elastic timesteps are reduced by the factors ndtd and ndte×ndtd (respectively) as explained below.

Bailey et al. (2018)?

CICE parameter sensitivities: Hunke (2010).

Parameter sensitivities: Uotila et al. (2012) found that sea ice volume and area are sensitive to albedo, snow patchiness, turning angle, ocean-ice heat transfer coefficient, and a ridging parameter. Miller et al. (2006) documented a sensitivity of ice thickness, speed and extent to ice strength and the air-ice drag coefficient, whilst Kim et al. (2006) found sensitivity of ice thickness to ice density, conductivity, maximum salinity, ice-ocean drag coefficient and ridging parameters. Urrego-Blanco et al. (2016) found a sensitivity to snow parameters and melt pond drainage. Also see Massonnet et al. (2014) (NEMO-LIM3).

cf. Andrew Roberts RASM cice namelist (Petra email 6 June) **TODO:** get permisssion which was used in Roberts et al. (2015); Cassano et al. (2017); Hamman et al. (2017); Jin et al. (2018); Roberts et al. (2018) see Appendix F.3

See Andrew Roberts' comments on Roberts et al. (2015) in email from Petra email 6 June — inertial coupling can be essential for stability

The CICE biogeochemistry code (group zbgc_nml) is not used.

3.3.1 Thickness redistribution

We use 5 thickness categories (specified at compile time in build.sh by NICECAT). We use kcatbound=0, so the lower bound of ice categories is 0, 0.6445072, 1.391433, 2.470179 and 4.567288 m (from NCAT in CICE output files), as in Hunke et al. (2015, table 2).

We use the Lipscomb et al. (2007) ridging scheme (krdg_partic=1), with an e-folding scale parameter mu_rdg=3 $\mathrm{m}^{1/2}$, which is the default value and matches ACCESS-CM2 (Appendix F.4.2) but is smaller than the value 2 $\mathrm{m}^{1/2}$ used in ACCESS-OM (Bi et al., 2013b, table 2). maxraft (the maximum thickness of rafted ice) takes the default value of 1.0 m in ACCESS-OM2, ACCESS-OM and ACCESS-CM.

3.3.2 Dynamics

TODO: check I (AK) haven't misunderstood anything here – this is based on only a quick skim of most of these papers

We are currently using "classic EVP" [2] (kdyn=1, revised_evp = false) (Hunke and Dukowicz, 1997, 2002; Hunke, 2001). This represents the internal ice stresses by a visco-plastic (VP) rheology (Hibler, 1979), to which a fictitious elastic term is added to facilitate efficient numerical convergence to the visco-plastic solution via damped elastic waves which are supposed to decay to negligible amplitude during ndte=120 sub-timesteps within each dynamic timestep (Hunke et al., 2015,

[2] Another CICE option is the "revised EVP" method (Bouillon et al., 2013; Hunke et al., 2015, section 3.5.3) which corrects an error in the "classic EVP" stress formulation and may also improve the convergence rate of the elastic sub-timesteps and reduce the incidence of spurious grid-aligned linear kinematic features ("leads"). **TODO:** try this out? Bouillon et al. (2013) argue that this is superior to using "classic EVP", but see warnings by Kimmritz et al. (2017, 2015) that numerical instability may dominate over convergence as the greatest source of error.**FIXME:** wrong references? they don't say this as far as I can see.

sections 3.5.2 and 4.4; note that Δt should be replaced by Δt_{dyn} throughout section 3.5: see https://github.com/CICE-Consortium/CICE/pull/83).

There is an ongoing debate regarding the suitability of visco-plastic ice rheology, particularly to represent sea ice on fine scales (Nye, 1973; Weiss et al., 2007; Lindsay et al., 2003; Kwok et al., 2008; Girard et al., 2009; Dansereau et al., 2016; Hutter et al., 2018; Weiss and Dansereau, 2017; Hutter et al., 2018). An alternative supported by CICE is the elastic-anisotropic-plastic (EAP) model (Weiss and Schulson, 2009; Wilchinsky and Feltham, 2006; Tsamados et al., 2013), but this seems relatively untested and uncalibrated at this stage.

If we accept the VP formulation, there is also the question of how well the EVP sub-timesteping converges to the VP solution with no residual elastic wave effects. Like many comparable models we use ndte=120 sub-timestep iterations, but Losch and Danilov (2012); Lemieux et al. (2012); Kimmritz et al. (2017, 2015) show that full convergence may take thousands of iterations even with the revised EVP method (particularly at high resolution), which would be prohibitively expensive unless an accelerated method (e.g. Koldunov et al., 2019b) was used. We must therefore expect our sea ice stress distribution to contain artefacts due to residual elastic waves. These artefacts may include spurious grid-scale noise and long linear features in the shear and divergence fields (Lemieux et al., 2012). We note that the default ndte has been increased to 240 in CICE6.

see Lemieux and Tremblay (2009)

Horizontal advection of conserved properties is handled by the incremental remapping scheme of Dukowicz and Baumgardner (2000) and Lipscomb and Hunke (2004), documented in Hunke et al. (2015, section 3.2). We find that the CFL condition associated with this method usually sets the maximum CICE dynamic timestep, which is shorter than the CICE thermodynamic timestep (and MOM baroclinic timestep) by the factor ndtd. This CFL condition becomes very restrictive at 0.1° due to the very fine grid spacing in ocean cells near the tripole (table 6 and figures 3 and 5) so we set ndtd=3 to allow MOM to run with a longer timestep. We have not found this to be necessary in the coarser configurations, so these have ndtd=1. Using ndtd=3 slows down CICE relative to MOM, altering the load balance. We mitigate this by increasing the proportion of cores allocated to CICE in the 0.1° configuration (table 8 and figure 12) so that MOM does not spend so much time waiting for CICE, but this configuration still appears to be CICE-bound. Newer configurations have greatly improved efficiency, partly by altering the bathymetry to eliminate the very smallest ocean cells.

In all three configurations the vertical grid resolution is fine enough to resolve the surface Ekman layer (Table 4), so we use a turning angle of zero (cosw=1.0, sinw=0.0), consistent with ACCESS-OM (Bi et al., 2013b, table 2) and ACCESS-CM2 (appendix F.4.2; values unspecified but cosw=1.0, sinw=0.0 are the defaults). (Is zero turning angle reasonable? see Uotila et al. (2012); Park and Stewart (2016); McPhee (2008); Leppäranta (2011) — we are using 10m ageostrophic winds and can resolve the ocean Ekman layer.)

We use an ice-ocean drag coefficient of dragio=0.00536, consistent with ACCESS-OM (Bi et al., 2013b, table 2) and very close to the value of 0.0054 measured at 0.5 m below first-year landfast ice by Shirasawa and Ingram (1997). A wide range of values have been used in the literature (Lu et al., 2011; Martinson and Wamser, 1990; Leppäranta, 2011, table 5.3), but the coefficient also depends on the water velocity and depth at which it is measured, the ice roughness, and the upper ocean stratification (Leppäranta, 2011; Waters and Bruno, 1995). Sensitivity to this parameter has been investigated by Uotila et al. (2012); Urrego-Blanco et al. (2016); Kim et al. (2006).

Sea ice drag coefficients and turning angles: Heorton et al. (2019)

3.3.3 Thermodynamics

The albedo configuration is described in section 3.5.

We use 4 ice layers and one snow layer (specified at compile time in build.sh by NICELYR and

NSNWLYR, respectively).

We use the mushy ice formulation of Turner et al. (2013) (ktherm=2, tfrz_option='mushy') at 0.1°. At other resolutions we use the Bitz and Lipscomb (1999) formulation (ktherm=1, tfrz_option='linear_salt'). In both cases the freezing point depends on salinity. We also use a constant freezing temperature tocnfrz=-1.8C — should we switch to having a function of SSS that is consistent with tfrz_option? — see Uotila et al. (2012). These freezing points also differ from the frazil freezing point in MOM, for which we use freezing_temp_preteos10 = true. See Andrew Roberts' comments on mushy thermo in email from Petra email 6 June 2018 "First, we are using mushy-layer thermodynamics, and this needs to be carefully coupled so that the temperature in the ocean model's upper layer matches the liquidus temperature in CICE, but the ocean model still conserves salt." **TODO:** make freezing points consistent?

We use the NCAR CCSM3 shortwave distribution method (shortwave='default'), which has implicit melt ponds. Explicit melt ponds require the delta-Eddington radiation (shortwave='dEdd'), so the parameters in ponds_nml are ignored in our configuration **TODO:** check. See Andrew Roberts' comments on melt ponds in email from Petra email 6 June 2018.

Do we include lateral melting? see Roach et al. (2018).

Consistent with ACCESS-OM (Bi et al., 2013b, table 2) we use the Pringle et al. (2007) thermal conductivity parameterisation (conduct='bubbly'), which improves the otherwise slow Antarctic ice growth rate (Hunke, 2010), and an ice-ocean heat transfer coefficient of chio=0.006 (this is the value actually used, since the namelist value chio=0.004 was ignored — see https://github.com/COSIMA/cice5/issues/55) with minimum friction velocity ustar_min=5×10^{-3} ms^{-1}. ⚠

3.4 Coupling

See https://github.com/COSIMA/access-om2/wiki/System-description

Figure 1 shows the fields that are transferred between the coupled model components. The prescribed atmosphere drives the global ice model, which is two-way coupled to the ocean model. Coupling is implemented using the Ocean Atmosphere Sea Ice Soil (OASIS3-MCT, Valcke et al., 2013) coupler version 2.0, developed at CERFACS and CNRS, France (https://portal.enes.org/oasis), which uses the Model Coupling Toolkit (MCT, https://www.mcs.anl.gov/research/projects/mct/) for routing between individual processors in each model component. The OASIS3-MCT-2 user guide is here: http://www.cerfacs.fr/oa4web/papers_oasis/oasis3mct_UserGuide_2.0.pdf. The coupling strategy is based on the ACCESS-OM model (Bi and Marsland, 2010), but we use a newer version of OASIS which is capable of parallel coupling.

The default remapping method used within OASIS3-MCT-2 (SCRIP https://github.com/SCRIP-Project/SCRIP) does not scale to 0.1°. Instead the grid remapping interpolation weights are calculated using the RegridWeightGen application which is part of the ESMF framework https://www.earthsystemcog.org/projects/esmf/. Conservative interpolation is used to remap flux fields (2nd order at 1° and 0.25°, first order for 0.1°: https://github.com/COSIMA/access-om2/issues/71). For scalar fields we use a technique called patch recovery (Kritsikis et al., 2017a; Khoei and Gharehbaghi, 2007) to produce very smooth destination fields. This is particularly important for the the 0.25° and 0.1° configurations because they have finer resolution than the forcing dataset. However the 2nd order conservative remapping method produces spurious extrema (including nonsensical incorrect signs such as negative runoff or negative downwelling shortwave fluxes): https://github.com/COSIMA/access-om2/issues/74#issuecomment-454660871. The creation of interpolation weights is documented at https://github.com/COSIMA/access-om2/wiki/Technical-documentation#creating-remapping-weights. ⚠

The atmosphere-to-ice coupling timestep is determined by the frequency of the atmospheric forcing dataset (i.e. 3 hourly for JRA55-do). Ice-to-ocean coupling takes place on every timestep (ice_ocean_timestep, the ocean baroclinic timestep and ice thermodynamic timestep), since baroclinic_split=1.

3.5 Forcing

There is no direct coupling from YATM to MOM5. Surface forcing is handled globally by CICE5, which obtains atmospheric data from YATM, interpolates it in time **TODO:** check!, and calculates various forcing fluxes to pass on to MOM5 via the OASIS3-MCT coupler (figure 1).

The entire 0.1° deg run was affected by a forcing bug: https://github.com/marshallward/payu/issues/138 and https://github.com/COSIMA/access-om2/issues/123. The coarser model runs discussed here were not affected. ⚠

We have mass exchange of surface freshwater fluxes as in Bi et al. (2013b) **TODO:** confirm

JRA55-do v1.3 atmospheric forcing (1984-5, 1990-1 or 2003-4 repeat-year, 0.5625° (∼55km), 3-hourly) in addition to CORE NYF (2° (∼200 km), 6-hourly)

JRA-55-do v1.3 forcing is supported at all three resolutions, and CORE2 forcing is supported at 1 degree resolution. JRA-55-do repeat-year forcing forcing (RYF) and interannual forcing (IAF) are currently supported.

Ocean surface roughness following Beljaars (1995) (CICE parameter rough_scheme='beljaars'; note that this is also specified in MOM in ocean_rough_nml, but this is for SIS and is therefore ignored).

The sea ice roughness iceruf=5×10^{-3} m matches that used in ACCESS-OM (Bi et al., 2013b, table 2).

Ocean albedo is constant (cst_ocn_albedo=true), with the value ocn_albedo=0.1, which is larger than the value 0.06 used in ACCESS-OM (Bi et al., 2013b). (This has been changed to the Large and Yeager (2009) latitude-dependent ocean albedo (cst_ocn_albedo=false) in more recent versions.) The MOM parameter ocean_albedo_option is ignored. In CICE5 we use the same NCAR CCSM3 shortwave distribution method (shortwave='default'), ice and snow albedos in the visible (≤ 700 nm) and infrared (≥ 700 nm) bands (albicev, albicei, albsnowv, albsnowi) and melt albedo parameters (dalb_mlt and ahmax) **TODO:** explain these as in ACCESS-OM (Bi et al., 2013b, their table 2), but we use the default snow patchiness parameter snowpatch = 0.02 m instead of the value 0.01 m used in ACCESS-OM. (We also set the same dt_mlt=1.0°C as ACCESS-OM but this Delta-Eddington parameter is ignored since shortwave='default'.) The albedo parameters differ from those in Hunke et al. (2015) and in JRA-55 (Kobayashi et al., 2015). We use the default CCSM3 albedo type (albedo_type='default'). **TODO:** explain what this does

Shortwave penetration into the ocean is handled by the GFDL scheme (ocean_shortwave_gfdl_nml), with Manizza et al. (2005) optics (optics_manizza=true). The Manizza et al. (2005) scheme splits the shortwave radiation flux equally into red and blue/green bands, and determines separate exponential decay scales for each band, with a term depending on chlorophyll-a concentration and a constant term for the absorption by pure seawater. We use a prescribed monthly surface chlorophyll-a climatology (read_chl=true) from the file chl.nc. This climatology is based on SeaWiFS data from 1998–2006 **TODO:** check: Griffies (2015, sec 3.14.2) says 1998–2007 and is presumably **TODO:** check the same as used in GFDL's CM2.5 and CM2.6 (Delworth et al., 2012; Griffies et al., 2015) based on the method of Sweeney et al. (2005). The 0.25° and 0.1° chl.nc files have patches of missing data in the far north and south: https://github.com/COSIMA/access-om2/issues/273. ⚠ In the GFDL implementation this surface chlorophyll-a concentration is crudely approximated as independent of depth. We also set a maximum penetration of zmax_pen=300 m. This limit is unlikely to have a noticeable effect, since even the slowest-decaying component (the blue/green band in clear water) has a decay scale $k = 0.0232\,\mathrm{m}^{-1}$, so the neglected fraction is at most $\frac{1}{2}\exp(-k\,\mathrm{zmax\_pen}) = 4.7 \times 10^{-4}$, and probably very much less. **TODO:** set zmax_pen to 1e6? see comments in code

There is no representation of geothermal heating (use_geothermal_heating=false).

3.5.1 JRA55-do interannual and repeat-year forcing

The ACCESS-OM2 configurations are forced with the JRA55-do v1.3 atmospheric reanalysis (Tsujino et al., 2018a, and http://www.cesm.ucar.edu/events/wg-meetings/2018/presentations/omwg/kim.pdf and https://climate.mri-jma.go.jp/

~htsujino/jra55do.html) which has significantly improved bias, spatial and temporal resolution (55 km, 3-hourly), temporal extent (1958–2018), and dynamical self-consistency compared to the CORE dataset (200 km, 6-hourly, 1948–2009) used in many previous studies. We use recent calving and basal melt estimates from Depoorter et al. (2013), which are spatially variable and somewhat larger than the uniform values in CORE (Tsujino et al., 2018a). JRA55-do will also be regularly updated, allowing real-time experiments. The improved spatial resolution of wind is important for better representation of coastal polynyas (Stössel et al., 2011; Zhang et al., 2015). JRA55-do has higher spatial and temporal resolution and longer temporal extent than ERA-Interim (80 km, 6-hourly, 1979–present) but is coarser and somewhat shorter than the upcoming ERA5 reanalysis (31 km, 3-hourly, 1950–present): https://confluence.ecmwf.int//pages/viewpage.action?pageId=74764925.

JRA55-do data are available from https://esgf-node.llnl.gov/search/input4mips/?institution_id=MRI. It has been downloaded to NCI in a few places: /g/data/qv56/replicas/input4MIPs/CMIP6/OMIP/MRI/ (note that MRI-JRA55-do-1-3 is actually v1.3.1) and also /g/data/ua8/JRA55-do/v1-3 (note that 1-3 is actually 1.3.0; this is what was used for the ACCESS-OM2 v1.0 runs). Also see http://climate-cms.unsw.wikispaces.net/JRA55-do and https://github.com/COSIMA/access-om2/issues/120.

The JRA55-do forcing file paths are constructed from the paths in atmosphere/forcing.json, with INPUT replaced by the paths in the atmosphere input section of config.yaml and {{year}} replaced by the model years over the range set in accessom2.nml.

See JRA55_RYF_justification.ipynb for biases in each RYF year.

JRA55-do (Tsujino et al., 2018a) is a surface-atmospheric reanalysis product derived from the 55-year Japanese reanalysis (JRA55, http://jra.kishou.go.jp/JRA-55/index_en.html) and intended for driving oceans models. We use JRA55-do version 1.3 to drive our ice and ocean models. The temporal coverage is from 1st January 1958 to 1st February 2018, but it is regularly updated to near present day.

JRA55-do v1.3 user manual: Tsujino et al. (2018b)

For the latest information on the dataset status and citation: http://goo.gl/r8up31.

see http://amaterasu.ees.hokudai.ac.jp/~tsujino/JRA55-do-v1.3/00README_v1_3.1st JRA-55: Kobayashi et al. (2015) JRA55-do: Tsujino (2015b,a, 2016); Tsujino et al. (2018a), Tsujino et al. (2016), Kim et al. (2018)

http://www.clivar.org/omdp/japan2016

JRA55-do version 1.3 provides 3-hourly liquid and solid precipitation, downwelling surface longwave and shortwave radiation, sea level pressure, 10m wind velocity components, 10m specific humidity and 10m air temperature (NB: humidity and temperature are shifted from 2m in JRA55 to 10m in JRA55-do — see Tsujino et al., 2018a, , appendix A2) on a TL319 grid (0.5625° resolution), and daily river flux at 0.25° resolution.

TODO: check: what do we use for glacier runoff? groundwater? evaporation? upwelling longwave radiation?

"Runoff from Greenland and Antarctica are replaced by climatological runoff. Greenland runoff is based on Bamber et al. (2012) and Antarctica runoff is based on Depoorter et al. (2013)." (http://amaterasu.ees.hokudai.ac.jp/~tsujino/JRA55-do-v1.3/00README_v1_3.1st)

The Antarctic runoff is spatially variable in JRA55-do (Tsujino et al., 2018a), in contrast to CORE .

we made a start on this: https://github.com/COSIMA/matm/issues/5

currently fresh water is input at the ice shelf edges.

cf. runoff (iceberg discharge scheme) used in ACCESS-CM2 - see AMOS2018 notes on Dave Bi's talk and https://accessdev.nci.org.au/trac/wiki/CMIP6workshop — this is discharged only at the surface. See Siobhan's email 2018-06-04

Runoff - incl distributed iceberg melt? Ask Adele? basal melt needs to be at depth - notebook p561, Mathiot et al. (2017). We have the data but waiting on it being published. Veronique has regridded this - see email 2017-11-16 Merino et al. (2016) and Depoorter et al. (2013) Paul: "The Antarctic

ice berg data is published and the data is publicly available here: http://neichin.github.io/personalweb/publications/ However, the Antarctic basal melt fluxes are not published yet and the data has not been made public." Also see Merino et al. (2018); Donat-Magnin et al. (2017); Mathiot et al. (2017); Hammond and Jones (2016); Stössel et al. (2015)

JRA55-do river runoff is from Suzuki et al. (2018); this is daily, interannually varying runoff from the JRA55 land surface model at 0.25° resolution, adjusted to match the observational estimates of Dai et al. (2009). River runoff is combined with climatological monthly solid runoff for Greenland (Bamber et al., 2012) and spatially-variable annual mean climatological basal melt and calving from Antarctica (Depoorter et al., 2013). Calving and liquid runoff are combined (discharge_combine_runoff_calve defaults to true). River discharge is inserted at the coast in the top river_insertion_thickness=40 m, but other runoff is inserted only at the surface (runoff_insertion_thickness and calving_insertion_thickness default to zero) at the ice shelf edge. Total runoff is remapped (and spread horizontally if needed to keep the flux below a threshold) in real time by YATM — see section 3.5.5.

runoff tools: https://github.com/COSIMA/runoff_tools

RYF: cite (Stewart et al., 2020); cf. Röske (2006).

discuss choice of year for RYF — will use 1984-5 for high-res runs – refer to Kial's paper

RYF generated by https://github.com/aidanheerdegen/make_ryf.

These 12-month periods were identified as particularly "neutral": 1 May 1984 - 30 April 1985, 1 May 1990 - 30 April 1991, 1 May 2003 - 29 April 2004 (we keep 29 Feb 2004 and ditch 30 April 2004 so as to keep 365 days per year). We have run ocean-sea ice spinups forced by all three JRA55-do v1.3 repeat years at 1° but we are concentrating on 1984-5 for the 0.1° spinup as it has less of the warming signal and also gives us more of the JRA55 dataset for subsequent interannual runs.

Kial's email 2018-03-05:

> -1st of January is in the peak of the northern winter and southern summer, meaning the variability in forcing fields (ie. weather) is quite high. This is a problem for surface buoyancy fluxes in the north Atlantic and Labrador & Nordic Sea regions, where NADW formation is notoriously sensitive to changes in surface forcing. The day of the year with lowest variability (least weather) is going to be closer to the equinoxes, and in JRA55 DO it turns out to be 1 May.
>
> -The three candidate years have been selected as the 12-month periods with climate indices closest to neutral. The climate indices of interest are the SOI, SAM and NAO. Removing the criteria that a 12-month period follows the calendar year allows us to find "years" that are closer to climatologically neutral.
>
> -Having the jump at 1 May allows us to run the model harder. The model tends to fall over at 1 Jan if the jump is there, meaning we have to back off the timestep and nurse it through. Having the jump at 1 May does not require any such nursing. Currently we are running the ACCESS-OM2 1° with 5400 sec timesteps from initialization and getting through 90 years per day.

TODO: plots of anomalies from climatology for the time-mean (or seasonal-mean) RYF forcing fields

see https://github.com/COSIMA/access-om2/issues/52 and http://www.earthsystemmodeling.org/esmf_releases/last_built/ESMF_refdoc/node3.html#SECTION03020000000000000000

All versions of JRA55-do up to and including v1.4.1 had some tropical cyclones in the Northeast Pacific and the North Atlantic from 1959 to 1987 erroneously represented as anti-cyclonic vortices: https://github.com/COSIMA/access-om2/issues/186. RYF8485 (1 May 1984 - 30 April 1985) has four faulty North Atlantic storms but RYF9091 and RYF0304 are OK. This issue is fixed in JRA55-do v1.5. ⚠

SST suddenly gets worse at end of 1990's at all resolutions, and stays that way (Kiss et al., 2020, figure 3b) — is there a persistent problem with JRA55-do? Or is it just that the 18°C offset is wrong?

The new IAF configuration will use JRA55-do 1.4.0 from /g/data/qv56/replicas/input4MIPs/CMIP6/OMIP/MRI/MRI-JRA55-do-1-4-0. At present this extends to 5 Jan 2019, which is as much as is currently available from https://esgf-node.llnl.gov/search/input4mips/ but this will be extended close to the present day from time to time — e.g. there is a beta version v1.4.0.1beta extending to 11 Jan 2020: https://climate.mri-jma.go.jp/~htsujino/jra55do.html. The JRA55-do v1.4.0 user manual is here: https://climate.mri-jma.go.jp/~htsujino/docs/JRA55-do/v1_4-manual/User_manual_jra55_do_v1_4.pdf (Tsujino et al., 2019).

3.5.2 Restoring

The only restoring we apply is to surface salinity. This is restored to interpolated **TODO:** state interpolation method – Smoothing at 0.1deg to deal with spurious discontinuities and noise in WOA13v2: https://github.com/COSIMA/access-om2/issues/103 World Ocean Atlas 2013 v2 monthly climatology (https://www.nodc.noaa.gov/OC5/woa13/); the interpolated salinity file is salt_sfc_restore.nc. The restoring timescale is set by salt_restore_tscale; we use 10 days at 0.1° and 21.28 days for the coarser resolutions. The "piston velocity" (surface vertical grid spacing divided by restoring timescale) is more physically relevant than the restoring timescale. This is 0.11 m/day at all resolutions due to the differing vertical resolution (see Table 4). This piston velocity is within the range of values used for CORE-II models, but is somewhat weaker restoring than the 50 m/300 days (i.e. 0.167 m/day) used for GFDL's MOM simulations (Danabasoglu et al., 2014, table 2).

We apply salinity restoring via a salt flux (use_waterflux = true, salt_restore_as_salt_flux = true) and restore everywhere, including under ice (salt_restore_under_ice = true). A spatially constant offset is added to the salt restoring to ensure that the net salt restoring flux is zero for each timestep (zero_net_salt_restore = true). In order to avoid excessively large fluxes the SSS mismatch is limited to max_delta_salinity_restore = 0.5 psu for the purposes of calculating the restoring flux at 0.25° and 0.1° (but not at 1°). We don't use salinity_restore_limit_lower or salinity_restore_limit_upper, so max_delta_salinity_restore applies even in regions of extremely low or high salinity (see https://github.com/mom-ocean/MOM5/issues/203).

We close the water budget by imposing a constraint of zero net water flux into the combined ocean-sea ice system from the coupler (zero_net_water_coupler = true) by removing the area-mean of $P - E + R$ (precipitation - evaporation + runoff) from $P - E$ (also adjusting liquid_precip for consistency) so that the area-integrated $P - E + R = 0$ at each timestep; this does not constrain water exchanges with the sea ice (see section 4.12.5). Note that the MOM diagnostics pme_river and total_pme_river report the water fluxes into the ocean model component (not the total ocean-sea ice system), so are non-zero due to water exchange with sea ice due to freezing and melting. See these code sections for documentation on zero_net_water_coupler, addition of ice melt to pme, adjustment to ensure zero water flux, and output of pme_river and total_pme_river diagnostics.

These salt restoring and freshwater parameter choices are typical of CORE-II models (Danabasoglu et al., 2014, table 2).

See Griffies et al. (2016, section 2.3) and Danabasoglu et al. (2014, Appendix C). Sensitivity to restoring: Behrens et al. (2013).

2nd order conservative interpolation: Kritsikis et al. (2017b)

3.5.3 Sea ice formation salt flux limiter

The model sea ice has a fixed bulk salinity; we use the default ice_salt_concentration = 0.005 kg salt / kg ice, matching the CICE5 parameter ice_ref_salinity defined in drivers/auscom/ice_constants.F90 (but differing from the ACCESS-OM value of 0.004 kg salt / kg ice, Bi et al., 2013b, table 2). This salt is obtained from the seawater when sea ice is formed, and we found this could drive ocean salinity below zero in regions fresher than ice_salt_concentration, for example during the spring melt in the shallow Siberian gulfs that are resolved in the 0.1° model bathymetry. This problem was resolved by setting the local ocean-ice salt flux to zero in regions where the seawater salinity is less than ocean_ice_salt_limit

= 0.006 kg salt / kg ice. Since we use zero_net_salt_restore = true, in these regions the sea ice salt is instead obtained from the global surface ocean at large. Over a sea ice formation and melt cycle this produces a small unphysical transport of salt from the global surface ocean to regions where such sea ice melts. Sea ice formed in regions saltier than ocean_ice_salt_limit obtains its salt locally as usual. **TODO:** get Russ to check this https://github.com/mom-ocean/MOM5/commit/2d76b70ca66173f8dfcfdb0597c9b148ef4a7510 This limiter is only applied in the 0.1° model.

3.5.4 Bulk formulas used

These are specified in the AUSCOM ocean drivers for CICE5.

see https://github.com/COSIMA/cice5/blob/master/source/ice_atmo.F90, https://github.com/COSIMA/cice5/blob/master/source/ice_forcing.F90, https://github.com/COSIMA/cice5/blob/master/drivers/auscom/surface_flux_mod.F90 https://github.com/COSIMA/cice5/blob/master/drivers/auscom/cpl_forcing_handler.F90

The stress applied to the ocean surface is a mixture of the air-ocean and ice-ocean stresses, weighted in proportion to the ice concentration (see here, lines 725–6).

We use Large and Yeager (2004) turbulent flux bulk formulas (ncar_ocean_flux=true, ncar_ocean_flux_orig=false), for the air-ocean drag coefficient, evaporative transfer coefficient and sensible heat transfer coefficient (eq. 6–10 in Large and Yeager, 2004). This is implemented in https://github.com/COSIMA/cice5/blob/master/drivers/auscom/surface_flux_mod.F90#L824. The calculation uses the air-ocean velocity difference with an additional component to account for gustiness (the gust component is derived from **FIXME:** what? and is not modified: alt_gustiness, gust_const, gust_min). Note that the implementation differs from Large and Yeager (2004) in having a $0.5\,\mathrm{m\cdot s^{-1}}$ floor for the 10 m relative windspeed, a ceiling of 10 for the absolute value of the stability parameter ζ, and a floor of 1 for the parameter $X = (1 - 16\zeta)^{\frac{1}{4}}$ (though the last of these should have no effect). We used n_itts=2 Monin-Obukhov iterations, which Large and Yeager (2004) state is appropriate for over the ocean, but less than their suggested value of 5 for over sea ice. **FIXME:** or is this only applied over the ocean?

TODO: comment on whether bulk formula is still applicable despite the fine vertical resolution – see Van Roekel et al. (2018)

Large and Yeager (2009)

- relative or absolute wind? See Abel et al. (2017). We use relative wind over ocean: https://github.com/COSIMA/cice5/blob/master/drivers/auscom/surface_flux_mod.F90#L558 - relative to ice as well as ocean? Relative winds are used over ocean, but absolute winds over ice: https://github.com/COSIMA/access-om2/issues/138.

We don't use high-frequency coupling (we don't specify highfreq in group forcing_nml so it defaults to false). highfreq implements the RASM coupling method of Roberts et al. (2015, 2011); also see http://www.oc.nps.edu/NAME/RASM_overview.pdf. It uses relative ice-atmosphere velocities for calculating stresses, so should probably be turned on for consistency, since relative velocity is used for the ocean.[3] **TODO:** check this is correct - ssuo is passed to surface_flux as u_surf There is now an option to use absolute winds to force the ocean via the boolean absolute_wind in namelist surface_flux_nml — see https://github.com/COSIMA/access-om2/issues/137. So absolute wind on both ocean and ice requires absolute_wind=true and highfreq=false, whereas relative wind on both ocean and ice requires absolute_wind=false and highfreq=true.

See Tsujino et al. (2018a, section 3.4.3): raw JRA55 winds have been adjusted in JRA55-do to agree with time-mean scatterometer and radiometer winds, which are relative to the ocean current. So subtracting the ocean surface current may be unnecessary. Tsujino (2018) recommend adding the Rio et al. (2014) climatological surface current distributed with the forcing dataset to better approximate the absolute wind. see Wu et al. (2017) and https://arccss.slack.com/archives/C6PP0GU9Y/p1511825314000106?thread_ts=1511802000.000465&cid=C6PP0GU9Y and https://jra55-do.slack.com/archives/C7LEZT4KY/p1511963905000047 and https://github.com/COSIMA/access-om2/issues/79. In addition to the adjustment in JRA55-do, the underlying JRA55 reanalysis ingests scatterometer winds (Kobayashi et al., 2015), so presumably includes the imprint of eddies. This

[3] This has been corrected in the new 0.1° RYF configuration, which uses relative velocities for both ice and ocean: https://github.com/COSIMA/access-om2/projects/1.

would not be corrected by adding climatological mean ocean currents. There may be significant impacts of western boundary currents — see Renault et al. (2019a, 2016).

We follow current recommended practice to calculate wind stress from relative wind, but this is still a matter of debate. The issue is that the JRA55-do mean winds are set to equal the scatterometer mean, and this is a relative measurement so includes the effect of mean currents. But if absolute wind is used in the stress calculation it will omit eddy stress damping. This is quite a complex issue, particularly since ocean-only models also lack important feedbacks that modulate the stresses (e.g. Renault et al., 2020).

TODO: should bulk formulas match what was used in JRA55-do? do we need something like ncar_ocean_fluxes but for JRA-55? https://github.com/COSIMA/cice5/blob/master/drivers/auscom/surface_flux_mod.F90#L820 NB: Tsujino et al. (2018a) use formulas from Gill (1982) and recommend using these rather than Large and Yeager (2004, 2009). Also see Brodeau et al. (2017).

see Roberts et al. (2015) appendix A - RASM uses nonzero ice velocity for stress calculation

cf. appendix C of Griffies et al. (2009).

3.5.5 YATM and libaccessom2

CONTRIBUTORS: Nic Hannah

ACCESS-OM2 uses a new atmospheric driver, known as YATM, which implements a file-based atmosphere and replaces MATM used in ACCESS-OM (Bi et al., 2013b). Its purpose is to track model time and, when necessary, read the appropriate forcing fields from files and deliver them to the coupler. This is implemented via an associated library (libaccessom2, https://github.com/COSIMA/libaccessom2) that is linked into YATM, CICE and MOM to provide shared functionality and an interface to inter-model communication and synchronisation tasks.

YATM is also responsible for remapping runoff (combined river, calving and basal melt) in real-time. This is done separately from the other forcing fields because it is difficult to do in a distributed memory setting — ensuring runoff is on coastal points may require interprocess communication. Remapping is done in two steps: firstly it is moved to the destination grid using conservative interpolation, and then distributed from land to coastal points using an efficient nearest neighbour algorithm based on a pre-computed k-dimensional tree (k-d tree) data structure (Bentley, 1975). The Fortran k-d tree implementation is called KDTREE2 (https://github.com/jmhodges/kdtree2).

To prevent high concentrations of runoff a method for spatially variable conservative flux limiting has been implemented. Values are set by runoff_caps in units of $\mathrm{kg\,m^{-2}\,s^{-1}}$; i-index start and end regions are set by runoff_caps_is and runoff_caps_ie, and j-index start and end regions are set by runoff_caps_js and runoff_caps_je. The 0.25° and 1° configurations use the default runoff cap of $0.03\,\mathrm{kg{\cdot}m^{-2}s^{-1}}$ globally. At 0.1° there are reduced caps of 0.001 and $0.003\,\mathrm{kg{\cdot}m^{-2}s^{-1}}$ at the mouths of some Arctic rivers to produce broader spreading and avoid excessively low salinity, and a cap of $0.03\,\mathrm{kg{\cdot}m^{-2}s^{-1}}$ everywhere else. **TODO:** Tabulate / plot runoff caps or runoff distribution in all models

YATM parameters for the three model resolutions are tabulated in Appendix A.4.

3.6 Initial conditions and spinup

The ACCESS-OM2 and ACCESS-OM2-025 runs were started at rest, with zero sea level, with temperature and salinity from World Ocean Atlas 2013 v2 (WOA13, Locarnini et al., 2013; Zweng et al., 2013, https://www.nodc.noaa.gov/OC5/woa13/) and run for five 60-year cycles (1 Jan 1958 – 31 Dec 2017) of JRA55-do. The temperature and salinity initial condition is created by the script /g/data/hh5/tmp/cosima/observations/postprocessing/woa13/WOA_initial_conditions.py. It is composed of the January 0.25° climatology /g/data/v45/akm157/data/WOA13v2/averaged_decades/woa13_decav_s01_04v2.nc over the full range of depths for which it is available (0–1500 m) and the

boreal Winter (January-March) 0.25° climatology /g/data/v45/akm157/data/WOA13v2/averaged_decades/woa13_decav_s13_04v2.nc below that, with in-situ temperature converted to potential temperature referenced to 0 dbar via the TEOS-10 formulas as implemented in https://pypi.org/project/gsw/. Note that an initial condition of potential temperature was mistakenly used, which does not match the model prognostic conservative temperature used at 1° and 0.25° — see section 3.2.8 and https://github.com/COSIMA/access-om2/issues/206. We use the "decav" WOA13 product, which is the average of the decadal averages, so uses data from 1955–2012: https://data.nodc.noaa.gov/woa/WOA13/DOC/woa13documentation.pdf. Since it's the average of the decadal averages it won't be biased towards recent data. This initial condition is the same as for OMIP (Griffies et al., 2016), except that we use potential temperature and practical salinity rather than conservative temperature and absolute salinity.

The ACCESS-OM2-01 experiment 01deg_jra55v13_iaf ran for 33 years from 1 Jan 1985 – 31 Dec 2017. It was started on 1 January from restart 431 from 01deg_jra55v13_ryf8485_spinup6, i.e. after 40 years of JRA55-do 1 May 1984 – 30 April 1985 repeat-year forcing (RYF, Stewart et al., 2020), which in turn began from the same World Ocean Atlas 2013 v2 initial condition as the coarser runs. The 01deg_jra55v13_ryf8485_spinup6 RYF spinup contained some parameter changes, detailed in /g/data/hh5/tmp/cosima/access-om2-run-summaries/run_summary_01deg_jra55v13_ryf8485_spinup6.csv. The most significant of these was changing the ice turning angle from 16.26° **TODO:** in which direction? presumably depends on hemisphere(cosw=0.96, sinw=0.28) to zero (cosw=1.0, sinw=0.0) at the start of August in the 12th year (run 113). Before this change the Arctic ice volume was building up significantly (and unrealistically) in the thickest category, but it began a slow decline when the turning angle was set to zero (figure 10) which persisted into the first ∼ 6 years of the IAF run (figure 35). This change in the turning angle also caused a small increase in Antarctic sea ice thickness which rapidly stabilised at its new level. The 1984–85 repeat-year forcing contained some biases relative to climatology; for example, biases in the North Pacific wind stress curl produced late separation of the Kuroshio Current. For details see Stewart et al. (2020).

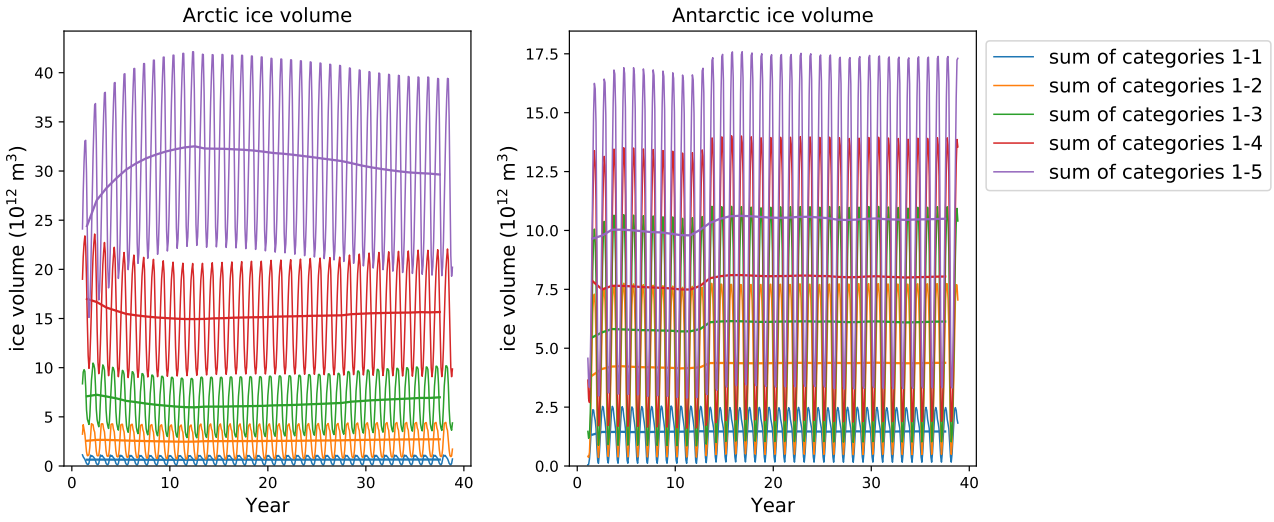

Figure 10: Sea ice volume (cumulative by category) in the RYF run used as the initial condition for the IAF run at 0.1°.

The sea ice and snow initial conditions are set in subroutine set_state_var in ice_init.F90 — see https://github.com/COSIMA/cice5/blob/5583ce54fd8822c1b8aef0549090167ca5f36d10/source/ice_init.F90#L1412. The first run has restart=false (see Appendix B.3.1), so uses ice_ic='default'. This sets a uniform ice concentration and thickness (100% and around 2.5 m, respectively) in regions north of 70°N and south of 60°S where the sea surface temperature is less than 1°C above freezing (see aice and hi in /g/data/hh5/tmp/cosima/access-om2-01/01deg_jra55v13_ryf8485_spinup6/output000/ice/OUTPUT/iceh.0001-01-01.nc). Ice area has a parabolic distribution across the five ice thickness categories. The initial snow thickness in each category is 0.2 m or 20% of the ice thickness in that category, whichever is smaller. The total sea ice and snow volumes in this initial condition are very close to the adjusted state (figure 11, top eight panels), displaying only a small

	ACCESS-OM2	ACCESS-OM2-025	ACCESS-OM2-01
Zonal resolution	1°	0.25°	0.1°
Ocean grid	360 × 300 × 50	1440 × 1080 × 50	3600 × 2700 × 75
MOM5 tile size	23 × 20	30 × 27	45 × 36
MOM5 number of tiles	240	1920	6000
MOM5 cores	216	1455	4358
CICE5 block size	15 × 300	30 × 27	36 × 30
CICE5 number of blocks	24	1920	9000
CICE5 cores (NTASK)	24 (24)	361 (480)	1600 (1392)
CICE5 processor_shape	'slenderX1'	'square-ice'	'square-ice'
CICE5 distribution_type	'cartesian'	'roundrobin'	'roundrobin'
Queue	normalbw	normal	normal
Timestep (s)	5400	1350–1800	450
CPU hr / model year	118	4,700	118,000*
Walltime hr / model year	0.38	2.6	19.9*
Memory (Gb)	83	522	2689

Table 8: Typical computational details and resource requirements for the three configurations. Full details are given in the run summary spreadsheets in Table 2, and namelist changes within runs are tabulated in Appendix B. Total core count in the spreadsheets is rounded up to a multiple of the cores per node (24 in the normalbw queue, 16 in the normal queue). The number of tiles (blocks) includes land-only tiles (blocks), but these are not allocated to a processor core. Multiple CICE5 blocks are allocated to each core at 0.25° and 0.1°. MOM5 tile size is determined by the horizontal grid dimension divided by the number of tiles in that direction as set by layout. CICE5 block size (BLCKX×BLCKY) and NTASK are defined at compile time via https://github.com/COSIMA/cice5/blob/076b14f2/bld/config.nci.auscom.360x300, https://github.com/COSIMA/cice5/blob/076b14f2/bld/config.nci.auscom.1440x1080 and https://github.com/COSIMA/cice5/blob/076b14f2/bld/config.nci.auscom.3600x2700 in ACCESS-OM2, ACCESS-OM2-025 and ACCESS-OM2-01, respectively. The timestep is the MOM5 baroclinic timestep, equal to the CICE5 thermodynamic timestep. *More recent configuration improvements have halved the ACCESS-OM2-01 walltime and SU cost.

reduction of ice mass in category 4 in both hemispheres, and an increase in category 5 in the Arctic. Consequently there is no significant drift in total ocean salt as the sea ice spins up (figure 11 bottom row).

3.7 Model computational details and performance

CONTRIBUTORS: Marshall, Nic

3.7.1 Resource requirements

Typical model computational resource requirements are shown in Table 8; further details are provided in the run summary spreadsheets (see Table 2).

Some of the factors underlying these parameter choices are discussed in section 3.3.2. Newer configurations have greatly improved efficiency than is shown here.

This demonstrates efficient scaling well beyond the 512 cores investigated by Schmidt (2007).

cf. MOM-SIS-01: 50–60kSU/day?

cf. Matt Chamberlain's 2016 talk: global MOM-SIS at 0.1° and 50 levels, 960 CPUs (50x23 layout, 200 masked), dt=720s, month ~100min: http://cosima.org.au/wp-content/uploads/2016/06/ofam_global.mac_.pdf — this is as fast as ACCESS-OM2-01 but about 6x cheaper!

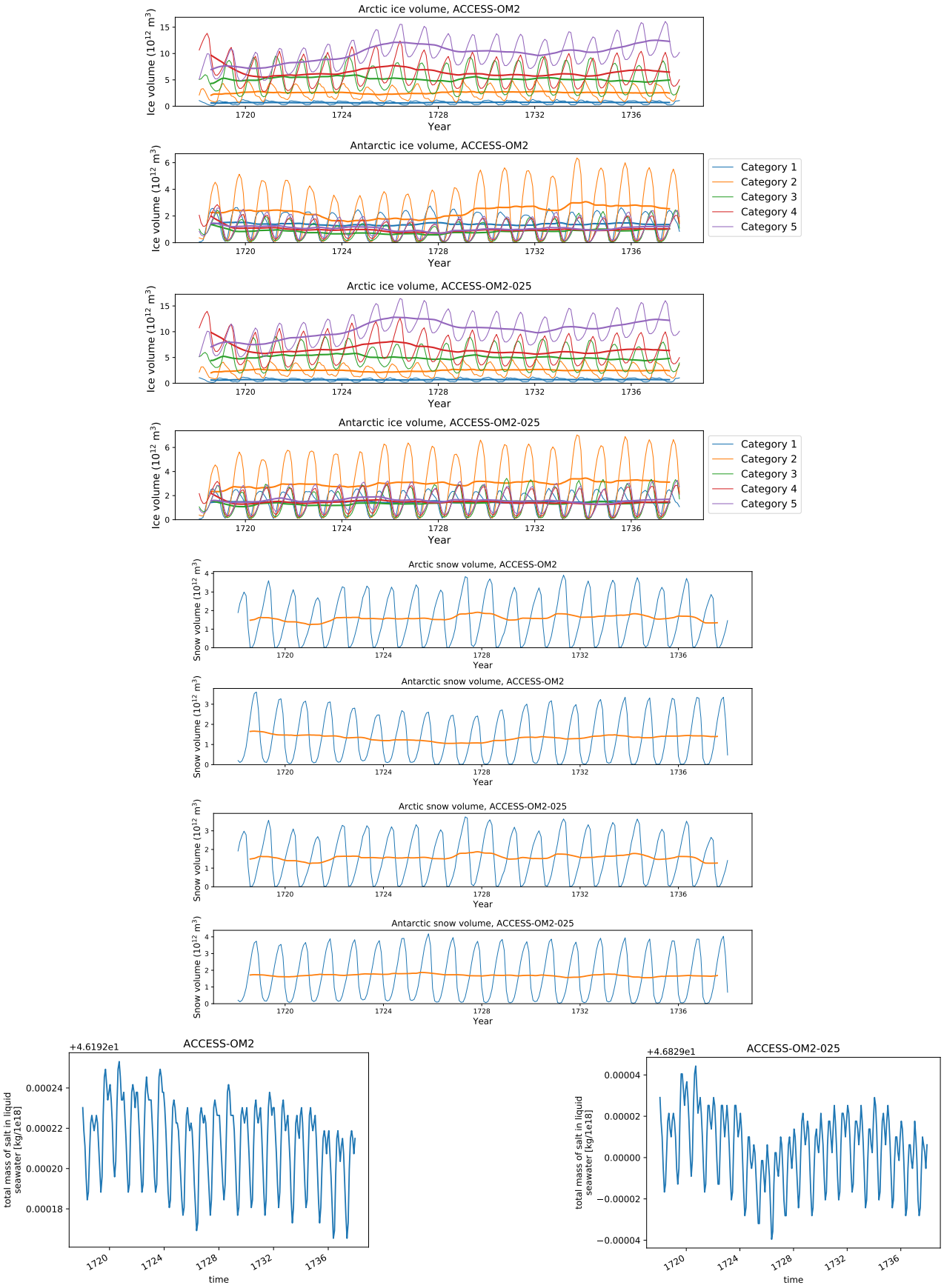

Figure 11: Top four plots: Arctic and Antarctic sea ice volume by category in initial spinup at 1° and 0.25°. Next four plots: Arctic and Antarctic snow volume in initial spinup at 1° and 0.25°. Bottom row: monthly mean total mass of ocean salt in the first several years at 1° (left) and 0.25° (right). The top eight plots show monthly means and 12-month rolling means. The ocean salt plots have large offsets indicated at the top of the y-axes. The annual cycles are due to sea ice formation and melting, which vary the total ocean salt by less than one part in 10^6.

3.7.2 Tiling in MOM and CICE

TODO: plot MOM tiling, showing dry tiles and bathymetry for each resolution?

TODO: plot CICE tiling/blocks, showing idle tiles for each resolution?

See table 8. CICE5 has the ability to subdivide the computational domain horizontally into tiles (termed "blocks"), and then parallelise by allocating one or more blocks to each CPU. This can improve load balancing if a similar number of ice-containing and ice-free blocks are allocated to each CPU. The maximum number of blocks per CPU is given by the environment variable MXBLCKS which is calculated from the CPU count[4] (NTASK) by the build.sh compilation script: https://github.com/COSIMA/cice5/blob/076b14f2/bld/build.sh#L72; the actual number of blocks is reported in the output file ice_diag.d. NTASK is included in the executable name, with a 'p' suffix. There are tools for investigating load balance with various masking and CPU choices at https://github.com/russfiedler/masking (currently only for distribution_type='roundrobin').

The final CICE5 configurations of the runs reported here used distribution_type='roundrobin' with processor_shape='square-ice' at 0.25° and 0.1° (Craig et al., 2015), which omits land-only blocks and also improves the load balance. At 1° we use distribution_type='cartesian' and processor_shape='slenderX1', which allocates pole-to-pole meridional strips to each processor in the interests of load balancing. We also use halo masking at all resolutions (maskhalo_bound, maskhalo_dyn and maskhalo_remap are all true), which eliminates MPI updates in ice-free halos.

3.7.3 Parallel scaling

TODO: cannibalise NCMAS application

Raijin hardware details: http://nci.org.au/systems-services/peak-system/raijin/, https://github.com/marshallward/optiflop/blob/master/doc/microbench.rst.

In all cases the initial condition was 1st January from spun-up runs (1 January 2003 in 5th cycle at 1°, 1 January 2000 in 5th cycle at 0.25°, and 1 January 2000 at 0.1°).

See figure 12.

cf. Koldunov et al. (2019a)

The profiling runs were nearly identical to the final configurations of the production runs (Appendix A), in particular having the same ndtd=3 and mushy ice (ktherm=2), but they did have a few differences which are tabulated in Appendix C. We note here the main differences that may affect runtime.

- The profiled runs used executables compiled with Intel compiler suite 2019 and OpenMPI 3.0.3, whereas the production runs used Intel compiler suite 2017 (17.0.1.132) and OpenMPI 1.10.2.
- The profiled runs used Sandy Bridge nodes, whereas the production runs used the faster Broadwell nodes.
- The profiled 1° MOM5 runs used redsea_gulfbay_sfix, but this wasn't used in production runs. This is expected to be insignificant as it used Russ' fixed version which has a negligible impact on runtime.

[4] For example, at 0.1°, MXBLCKS= trunc$(3600 \times 2700/(\text{BLCKX} \times \text{BLCKY} \times \text{NTASK}))$, where BLCKX and BLCKY are the tile dimensions (see table 8). Note that NTASK only sets a rough lower bound for the CPU count. The number of CICE cores actually used in a run is specified via ncpus in the ice section of config.yaml, which must equal nprocs in cice_in.nml **TODO:** check - is this ensured by payu?. nprocs can exceed NTASK, but should not be much less than NTASK, since CICE will abort if it requires more than MXBLCKS blocks per core. It is best not to have nprocs far in excess of NTASK, since this will increase the load imbalance within CICE (because the number of blocks per core decreases), and is also memory-inefficient.

- The profiled CICE5 runs used distribution_type='sectrobin' at both 0.25° and 0.1°, but the production runs used 'roundrobin' at both resolutions (apart from the first 114 runs at 0.1° which used 'cartesian'). 'sectrobin' has a smaller communication overhead than 'roundrobin' but may have poorer load balancing (Hunke et al., 2015).
- The profiled 1° CICE5 runs used an ice-ocean stress turning angle of 16.26° (cosw=0.96, sinw=0.28), instead of zero.
- ice_ocean_timestep was 1800 s and 400 s at 0.25° and 0.1° (respectively) in the profiled runs; these differ from 1350 s and 450 s in Appendix A, but are within the range of the values used in the production runs (Appendix B).

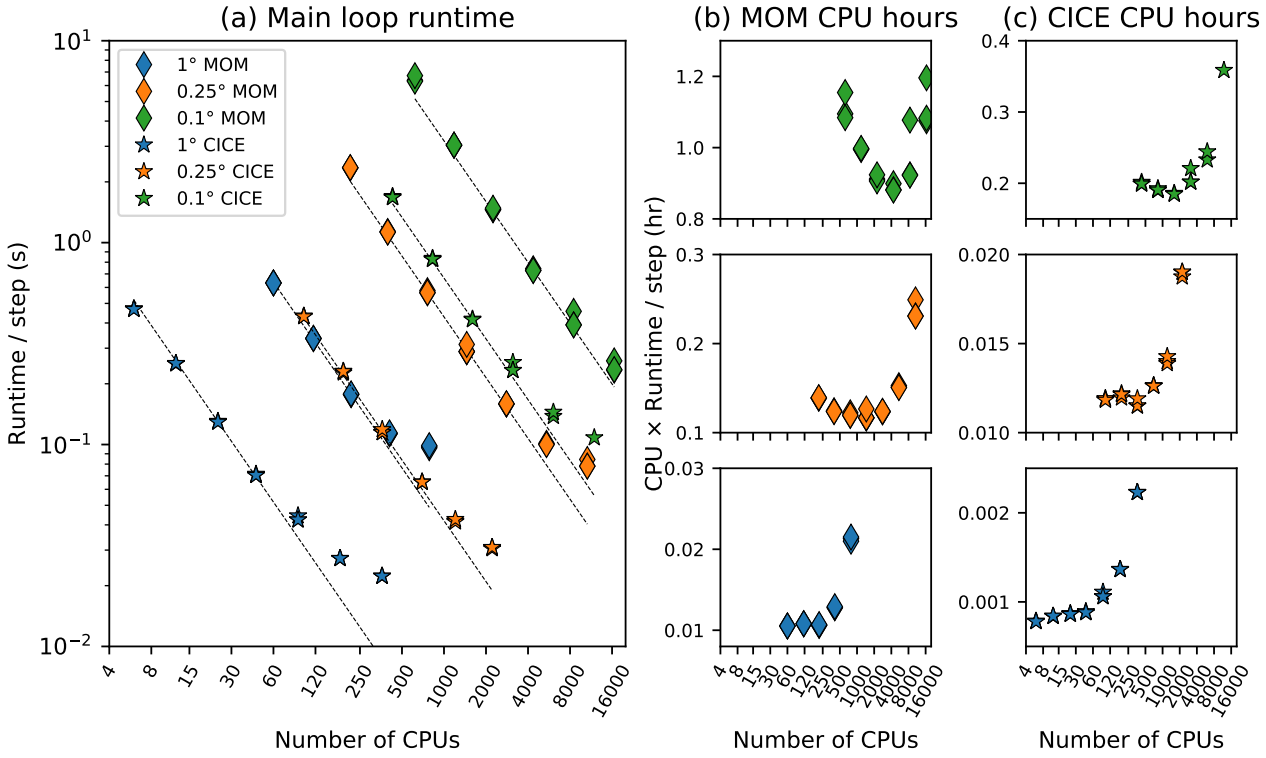

Figure 12: MOM5 and CICE5 scaling on Raijin.

3.8 Comparison with similar models

Iovino et al. (2016)

Namelists of MOM-based models are compared in Appendix F.

3.8.1 OFAM3

TODO: make the links point to the relevant appendix

ACCESS-OM2-01 MOM namelist differences from OFAM3 are shown in Appendix F.1, and Table 9 summarises differences in their grids. Also see Matt Chamberlain's email 28 May 2018.

monin_obukhov_nml neutral is false for OFAM2017 but true for the others.

The biharmonic Smagorinsky parameters differ. ACCESS-OM2-01 uses k_smag_aniso=0.0 and k_smag_iso=2.0, so is less viscous than the two OFAM configurations which use k_smag_aniso=3.0 and k_smag_iso=3.0, as well as background anisotropic and isotropic viscosities (set by vel_micom_aniso and

Table 9: ACCESS-OM2 compared to ACCESS-OM and OFAM3.

	ACCESS-OM	OFAM3	ACCESS-OM2
Ocean	MOM 4.1	MOM 4.1	MOM 5.1
Sea ice	CICE 4.1	—	CICE 5.1
Coupler	OASIS 3.25	—	OASIS3-MCT-2
Grid	global tripolar, z^*	75°S–75°N only, z^*	global tripolar, z^*
Resolution	1°, 360×300×50	0.1°, 3600×1500×51, $\Delta z = 5 - 1000$ m	1°, 360×300×50, $\Delta z = 10.0 - 334.7$ m or 0.25°, 1440×1080×50, $\Delta z = 2.3 - 219.6$ m or 0.1°, 3600×2700×75, Δz=1.1 – 198.4 m

vel_mico_iso). Although vel_micom_bottom is nonzero in the OFAM configurations, it is ignored because bottom_5point=false.

cf. oceanMAPS3.0 http://cosima.org.au/wp-content/uploads/2016/06/Brassington_Ocean_modelling_and_forecasting_v3.pptx.pdf

The vertical resolution has also been improved relative to OFAM3 (Oke et al., 2013). The resolution is finer tham OFAM3 at all depths other than 100–260 m, particularly at the surface and in the deep ocean, with 75 levels ranging from 1.1 m thick at the surface to 198 m thick at 5808 m (compared to 51 levels ranging from 5 m to 1000 m thick currently in OFAM3/Bluelink). Of particular relevance for coastal studies is the improved vertical resolution in the upper ocean, with 31 levels in the top 200 m and a minimum water depth of 10 m (rather than 24 levels and a minimum depth of 15 m for OFAM3), providing better resolution of shelf processes and a closer match to coastlines. Vertical spacing is optimised for resolving baroclinic modes, considerably reducing the error in their representation compared to the 51-level OFAM3 grid (Stewart et al., 2017, table 1).

Feng et al. (2016)

3.8.2 ACCESS, ACCESS-CM2, ACCESS-ESM

See Appendix F.4.

ACCESS-OM2 uses the same MOM, CICE and OASIS versions as ACCESS-CM2 (1°) Bi et al. (2016), http://cosima.org.au/wp-content/uploads/2016/06/BI-COSIMA-Hobart-20160526.ppt.pdf

In ACCESS-OM and ACCESS-CM2 the ocean_sigma_transport_nml parameters sigma_advection_sgs_only, sigma_umax, thickness_sigma_layer, thickness_sigma_min, tracer_mix_micom and vel_micom differ from the default values used in ACCESS-OM2 at 1°.

ACCESS-CM2 also uses Langmuir circulation parameterization in KPP (do_langmuir), which helps with getting realistic AAIW (Bi et al., 2019).

ACCESS-CM2 uses a different 50-level vertical grid from ACCESS-OM2, with 10 m spacing at the surface rather than 2.3 m.

ACCESS-CM2 code harmonised with ACCESS-OM2: https://github.com/mom-ocean/MOM5/releases/tag/CM2-0.1

https://www.dropbox.com/s/lktfwl3da0jpzp6/Fabio2018_Namelist_meeting_final.pdf?dl=0 section 2 shows that Rayleigh drag (see section 3.2.7) is also weaker in the Lombok and Torres Straits (longer timescale: 3600 s instead of 5400 s) in ACCESS-OM and (presumably) doesn't have any undamped cells at the bottom (unlike

ACCESS-OM2 — see figure 9 (a)), since it uses the GFDL50 grid.

See https://accessdev.nci.org.au/trac/wiki/CMIP6workshop There's an ACCESS-CM2 report available - ask Arnold Sullivan. And data is available on NCI to members of p66 and NCI access groups

cf. ACCESS Bi et al. (2013a,b); Dix et al. (2013). The ocean and sea ice components are essentially the same in ACCESS 1.0 and 1.3, which are based on MOM4p1 and CICE4.1 (https://confluence.csiro.au/display/ACCESS/Home). Also see https://accessdev.nci.org.au/trac/wiki/access/ACCESS_AMIP_testcases.

Bi et al. (2013b)

cf. ACCESS-ESM https://www.google.com.au/url?sa=t&rct=j&q=&esrc=s&source=web&cd=2&ved=0ahUKEwjvjsmH0rjZAhWEnpQKHb7VC-EQFgg0MAE&url=https%3A%2F%2Faccessdev.nci.org.au%2Ftrac%2Fraw-attachment%2Fwiki%2FScienceDay%2Fziehn_access_esm1.pdf&usg=AOvVaw1bYwLzey6vpy7g6v7W0aF0

3.8.3 MOM-SIS-01

cf. MOM-SIS-01 Spence et al. (2017) - forced by 2° CORE NYF - 75 levels; ACCESS-OM2-01 has newer bathy, CICE, JRA55-do, and probably different vertical grid

ACCESS-OM2-01 has newer forcing and bathymetry, and a different sea ice model than MOM-SIS-01 Spence et al. (2017).

3.8.4 GFDL CM2, CM2.5, CM2.6

cf. CM2-1deg CM2.5 CM2.6 (they were MOM v5) and discuss resolving eddies: Griffies et al. (2015) Delworth et al. (2012) Dunne et al. (2012) Griffies (2015)

cf. CORE (Griffies et al., 2009), CORE-II (Danabasoglu et al., 2014)

minimum depth = 40m ?

3.8.5 UKMO GO6, GO7, GC3.0, GC3.1

cf. UKMO GO6, GO7 Storkey et al. (2018) - based on NEMO.

GO7 has cavities under the ice shelves, whereas GO6 is similar to ACCESS-OM2-x in having no cavities and fresh water input at the ice shelf edges.

cf. UKMO GC3.0, GC3.1 Williams et al. (2018)

cf. UKMO HadGEM3-GC3.1 Ridley et al. (2018); Roberts et al. (2019)

cf. UKMO Global Sea Ice 6.0 CICE configuration used in the Met Office global coupled configuration GC2.0 (Rae et al., 2015)

3.8.6 RASM and others?

Cassano et al. (2017); Hamman et al. (2017); Jin et al. (2018); Roberts et al. (2018), http://www.oc.nps.edu/NAME/RASM_overview.pdf

Key RASM differences from ACCESS-OM2-01:

- ndte=600 (cf 120)
- highfreq=true
- differing pond parameters hs0 and rfracmax — presumably ignored, since we don't use shortwave='dEdd'

- lots of differences in shortwave_nml — NB: we use shortwave='default' rather than 'dEdd'
- differing thermo parameter dSdt_slow_mode=-1.5e-07 (cf. -5e-08)

RASM is 1/12° but on a rotated-pole grid so the Arctic resolution is ∼9 km (Roberts et al., 2015), considerably coarser than ACCESS-OM2-01 (Table 6).

Also RIOPS http://science.gc.ca/eic/site/063.nsf/eng/h_97632.html, GIOPS http://science.gc.ca/eic/site/063.nsf/eng/h_97631.html, https://www.godae.org/~godae-data/GOVST-VIII/presentations/5.9-GOVST8_Nov18_ScienceDay_GSmith.pdf

3.8.7 Whole Antarctic Ocean Model (formerly known as the Antarctic Tidal Ocean Model)

The Whole Antarctic Ocean Model (Richter et al., 2020) is a regional circum-Antarctic model based on ROMS. Key differences from ACCESS-OM2-01 include: circulation within cavities under ice shelves, tidal forcing, shelf melting and higher resolution (2km, 31 sigma layers). There is no sea ice model component.

4 Model evaluation

CONTRIBUTORS: Andy Hogg to coordinate

Kiss et al. (2020) present evaluations of the ACCESS-OM2 model suite; additional details are provided here.

Data from all experiments are stored on NCI in `/g/data/hh5/tmp/cosima` and can be accessed and analysed via the COSIMA Cookbook (https://github.com/COSIMA/cosima-cookbook). Table 2 specifies the subset of these experiments used for the comparisons in this section. Run configuration details are available on NCI in `/g/data/hh5/tmp/cosima/access-om2-run-summaries` for hh5 group members (apply for group membership if interested). Data are also publicly available at https://doi.org/10.4225/41/5a2dc8543105a and https://researchdata.ands.org.au/cosima-model-output-collection/993052. **TODO:** put data here

resolution dependence: Kirtman et al. (2012)

use obs dataset and methods from CLIVAR Repository for Evaluating Ocean Simulations? http://www.clivar.org/clivar-panels/omdp/reos

cf Ocean Modelling CORE-II Special Issue (Virtual) http://www.sciencedirect.com/science/journal/14635003/vsi/10PSR6J3BV4

OMIP - Griffies et al. (2016) - does BOM/CSIRO already have code to do this for CMIP6? ask Marsland

cf Oke et al. (2013) - reproduce some of these obs comparisons

cf http://www.cesm.ucar.edu/working_groups/Ocean/metrics.html?

cf esmvaltool https://www.esmvaltool.org/?

See Fanghua's observation comparison notebooks (should be on github) and also her presentation from 2018-01-25 and https://github.com/FanghuaWu/cosima-cookbook/tree/master/notebooks

see HighResMIP (Haarsma et al., 2016)

cf. http://www.globcurrent.org?

4.1 Barotropic streamfunction

4.2 Surface current speed and variability

FIXME: we calculate magnitude of time-mean velocity which is not the same as time-mean speed. Is this what Lumpkin et al do, or should we save speed in diag_table?

Laurindo et al. (2017) Archer et al. (2017a,b, 2018) Wijeratne et al. (2018)

See figures 17–24.

Mean Gulf Stream separation is poor (late) at 0.25deg (Figure 24), and too variable.

Mean Gulf Stream separation is OK at 0.1deg, but separation location is too variable, occasionally separating 2-3 degrees too far north.

4.3 Deep circulation

Ollitrault and Colin de Verdière (2014)

Zilberman et al. (2023)

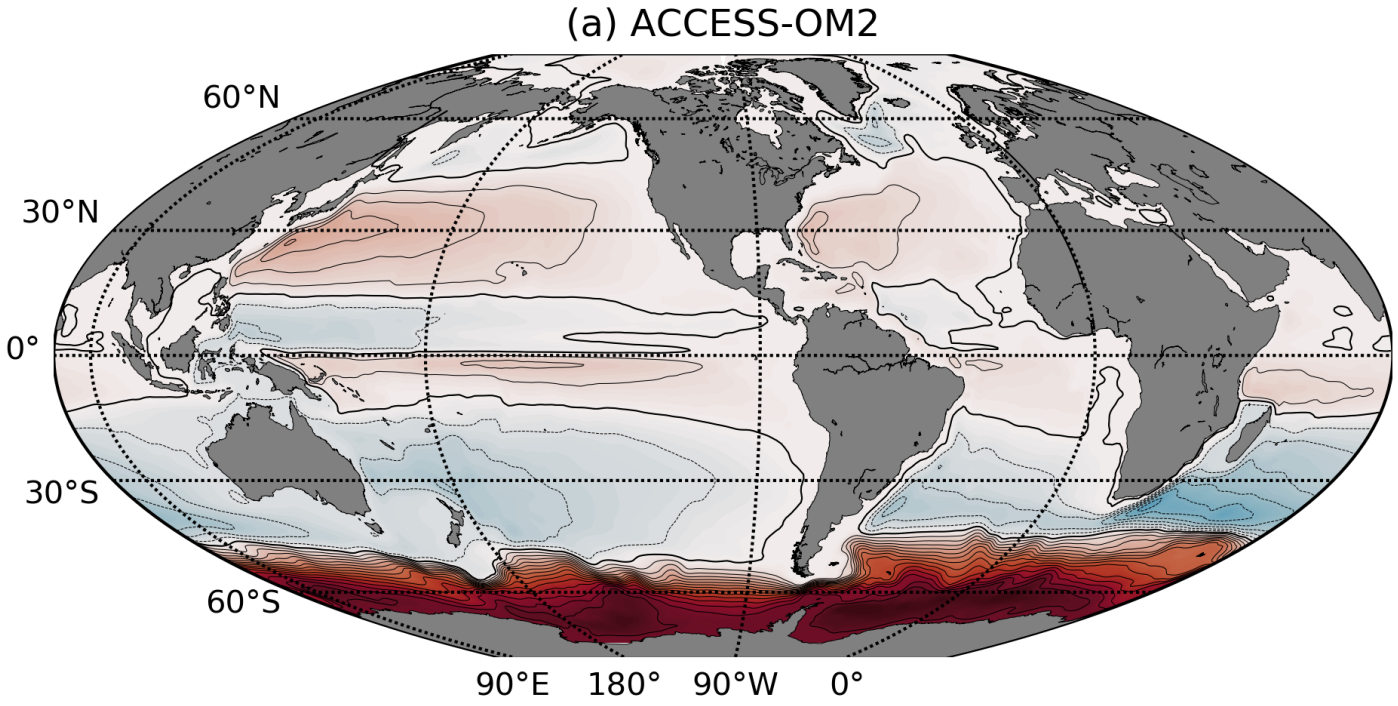

Figure 13: Global barotropic streamfunction for ACCESS-OM2 simulations.**TODO:** averaged over what years?

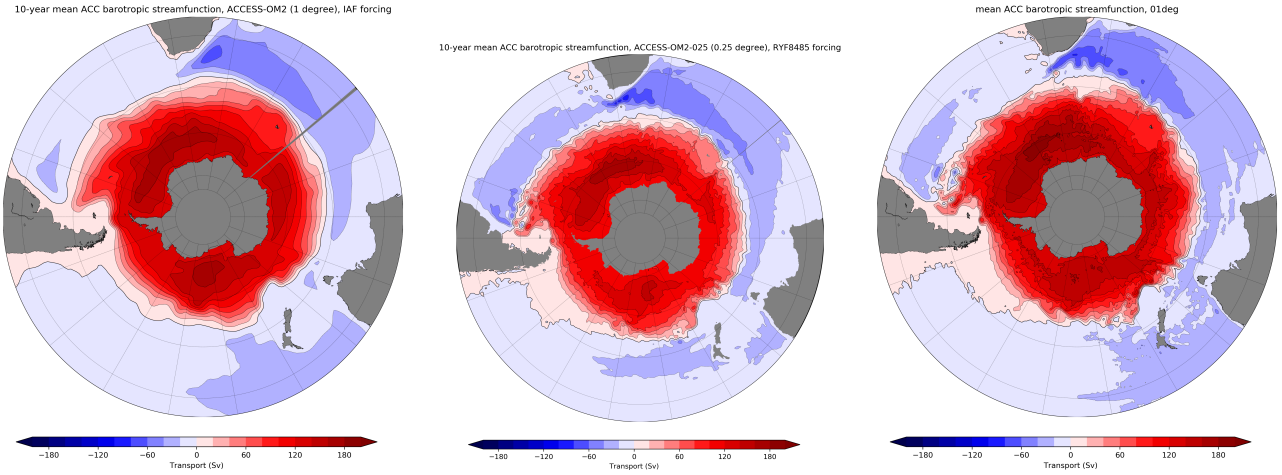

Figure 14: Antarctic Circumpolar Current barotropic streamfunction for ACCESS-OM2 simulations. **TODO:** Compare with Colin de Verdière and Ollitrault (2016) figure 9: https://journals.ametsoc.org/na101/home/literatum/publisher/ams/journals/content/phoc/2016/15200485-46.1/jpo-d-15-0046.1/20160222/images/large/jpo-d-15-0046.1-f9.jpeg

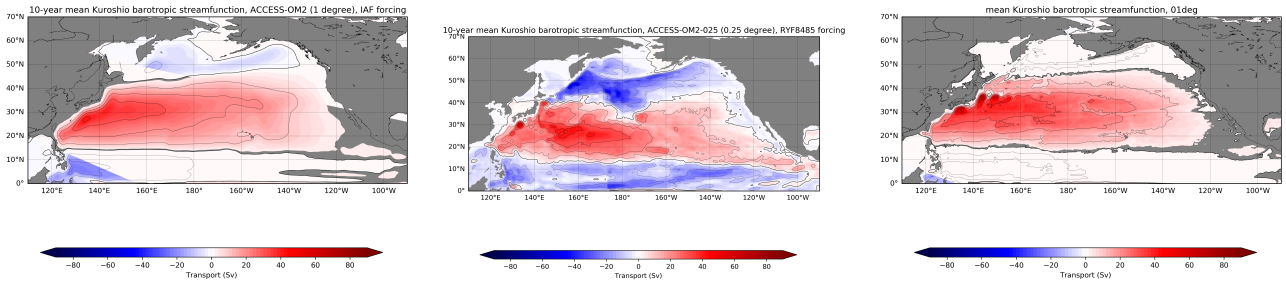

Figure 15: Kuroshio barotropic streamfunction for ACCESS-OM2 simulations. **TODO:** Compare with Colin de Verdière and Ollitrault (2016) figure 7: https://journals.ametsoc.org/na101/home/literatum/publisher/ams/journals/content/phoc/2016/15200485-46.1/jpo-d-15-0046.1/20160222/images/large/jpo-d-15-0046.1-f7.jpeg

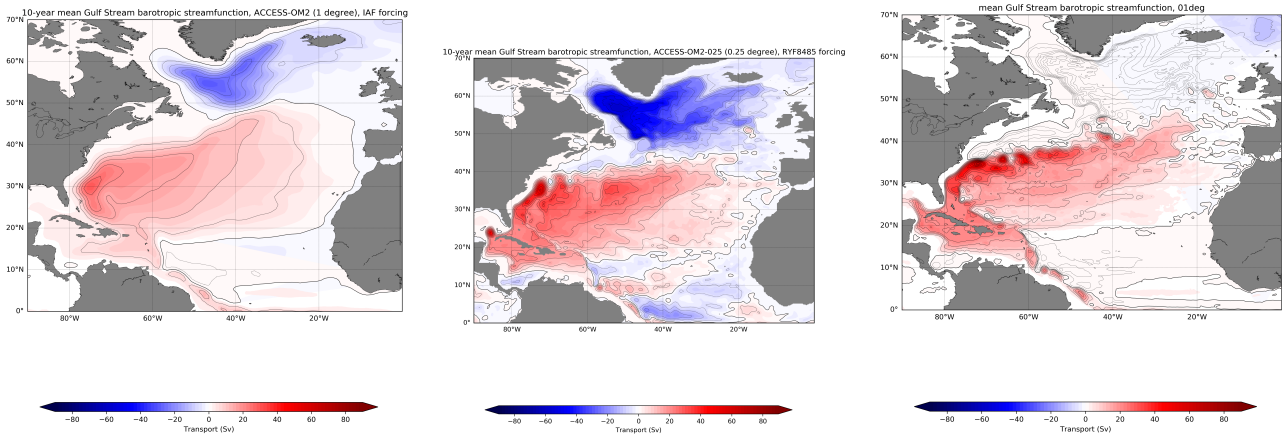

Figure 16: Gulf Stream barotropic streamfunction for ACCESS-OM2 simulations. **TODO:** Compare with Colin de Verdière and Ollitrault (2016) figure 3: https://journals.ametsoc.org/na101/home/literatum/publisher/ams/journals/content/phoc/2016/15200485-46.1/jpo-d-15-0046.1/20160222/images/large/jpo-d-15-0046.1-f3.jpeg

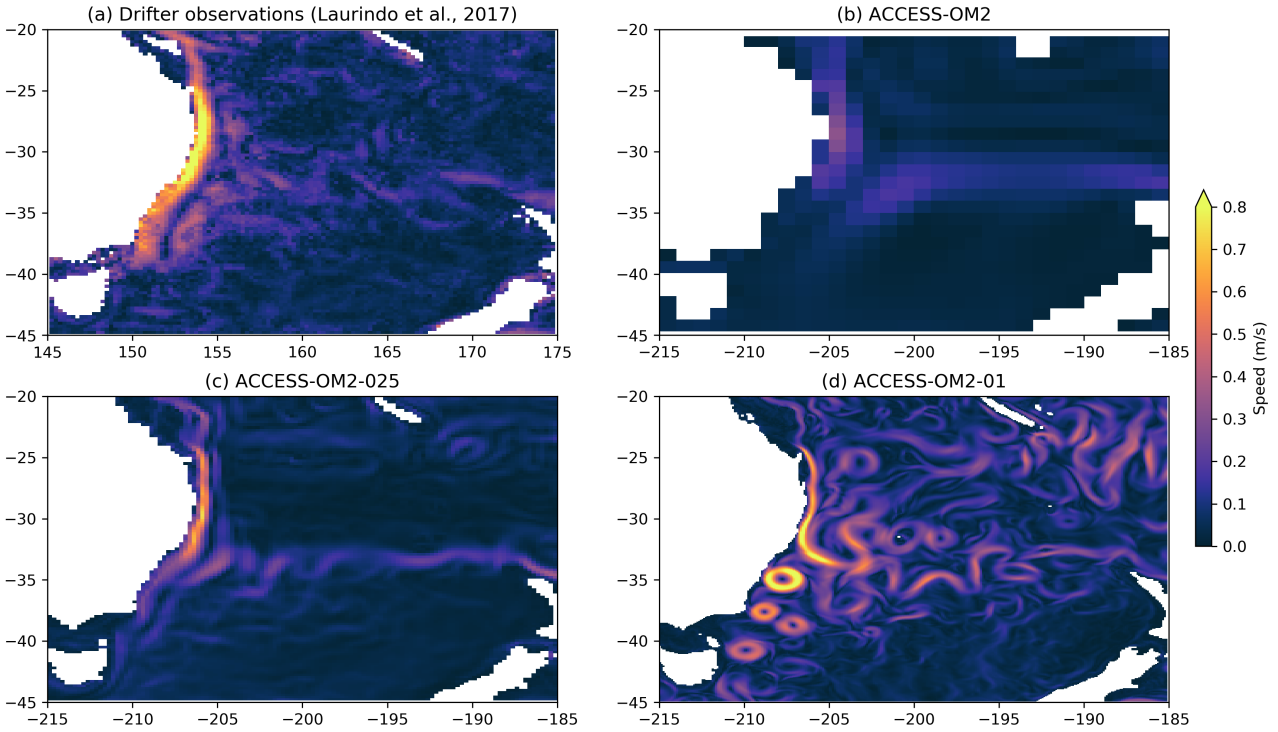

Figure 17: East Australian Current surface speed from (a) observations (1979–2015 mean from drifters at 15 m; Laurindo et al., 2017) and snapshots **FIXME:** daily mean at 0.1 deg and annual mean at 0.25 and 1 deg? what date? from ACCESS-OM2 simulations at (b) 1° resolution; (c) 0.25° resolution and (d) 0.1° resolution.

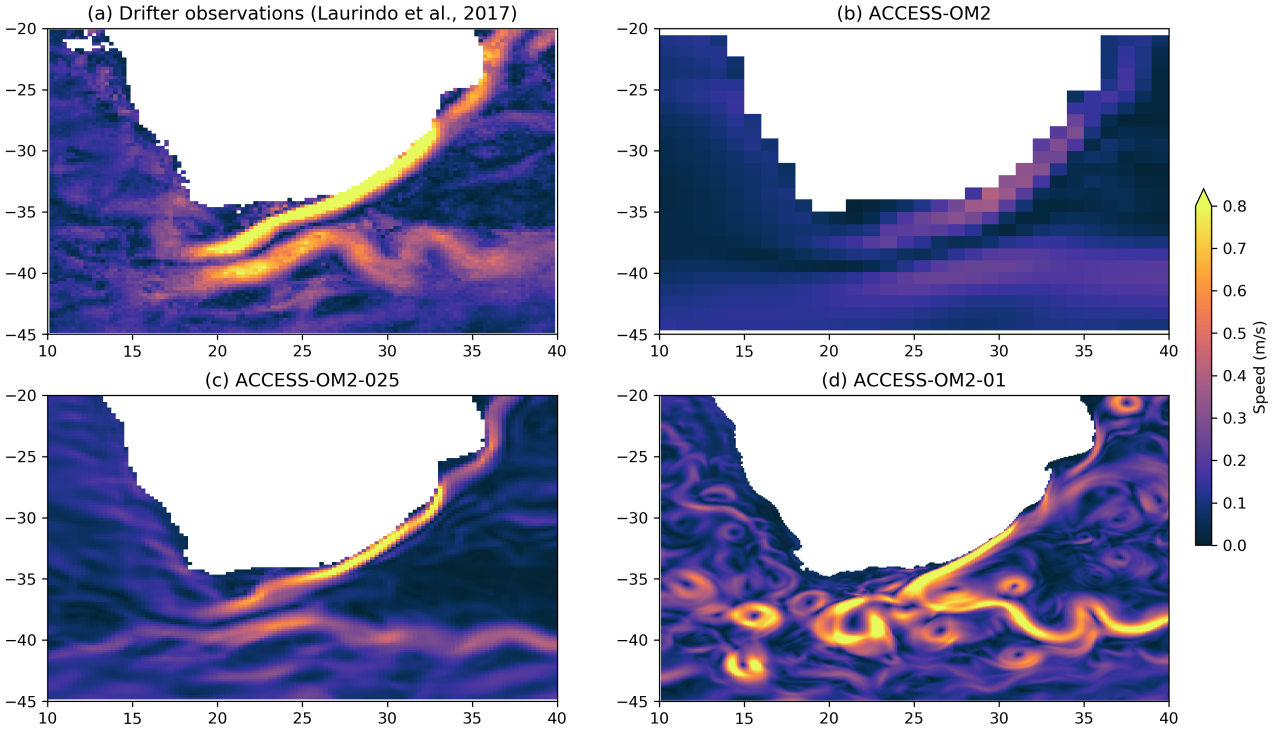

Figure 18: Agulhas Current surface speed from (a) observations (1979–2015 mean from drifters at 15 m; Laurindo et al., 2017) and snapshots **FIXME:** daily mean at 0.1 deg and annual mean at 0.25 and 1 deg? what date? from ACCESS-OM2 simulations at (b) 1° resolution; (c) 0.25° resolution and (d) 0.1° resolution.

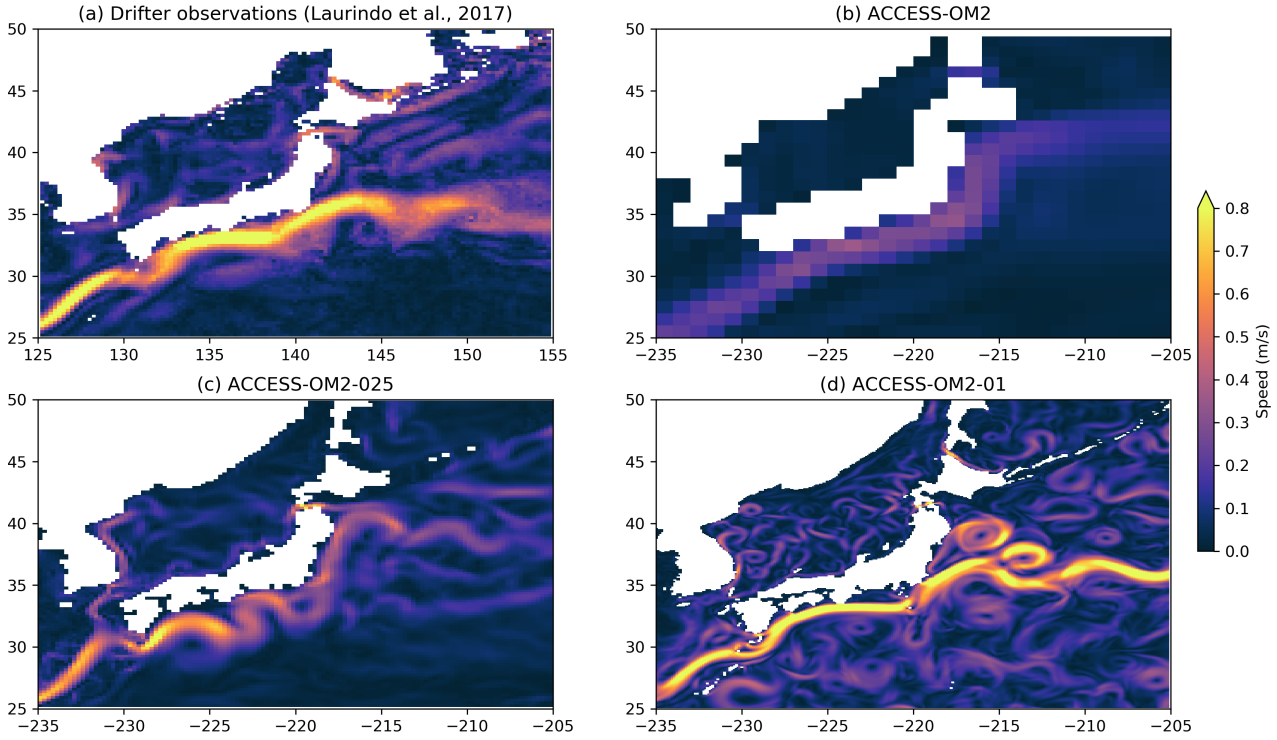

Figure 19: Kuroshio surface speed from (a) observations (1979–2015 mean from drifters at 15 m; Laurindo et al., 2017) and snapshots **FIXME:** daily mean at 0.1 deg and annual mean at 0.25 and 1 deg? what date? from ACCESS-OM2 simulations at (b) 1° resolution; (c) 0.25° resolution and (d) 0.1° resolution.

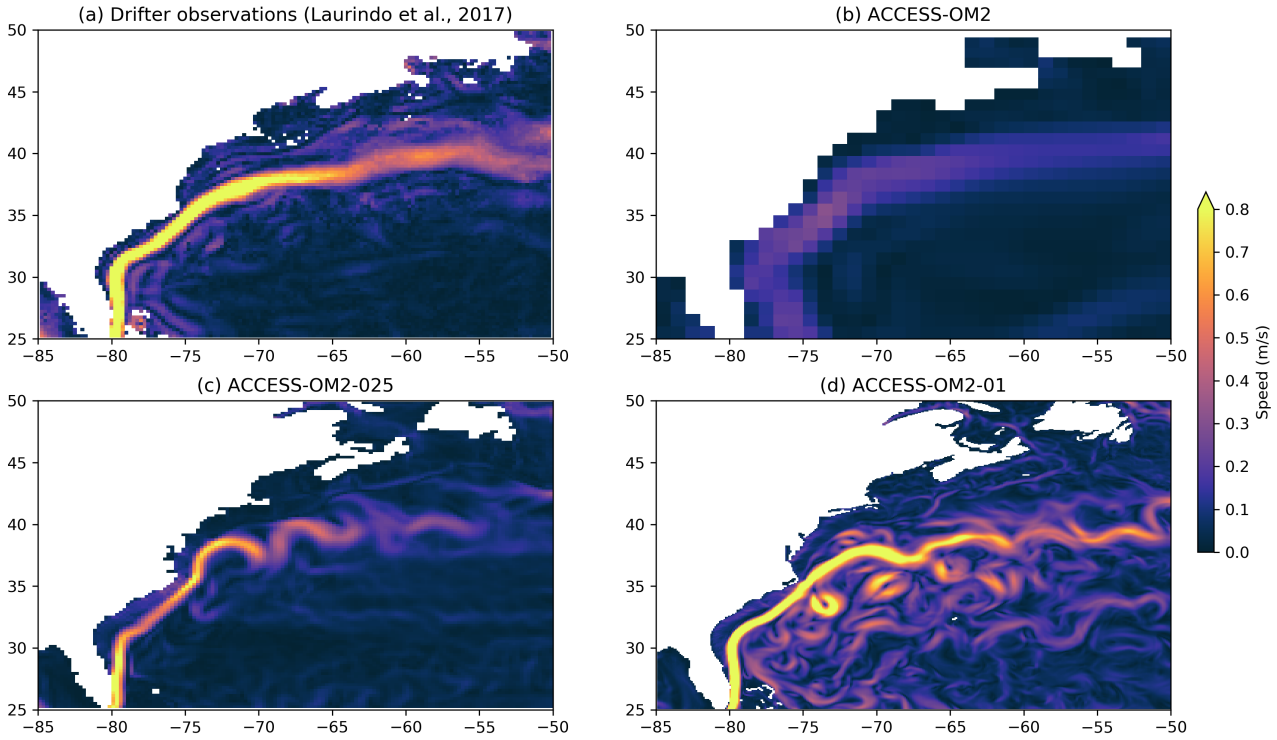

Figure 20: Gulf Stream surface speed from (a) observations (1979–2015 mean from drifters at 15 m; Laurindo et al., 2017) and snapshots **FIXME:** daily mean at 0.1 deg and annual mean at 0.25 and 1 deg? what date? from ACCESS-OM2 simulations at (b) 1° resolution; (c) 0.25° resolution and (d) 0.1° resolution.

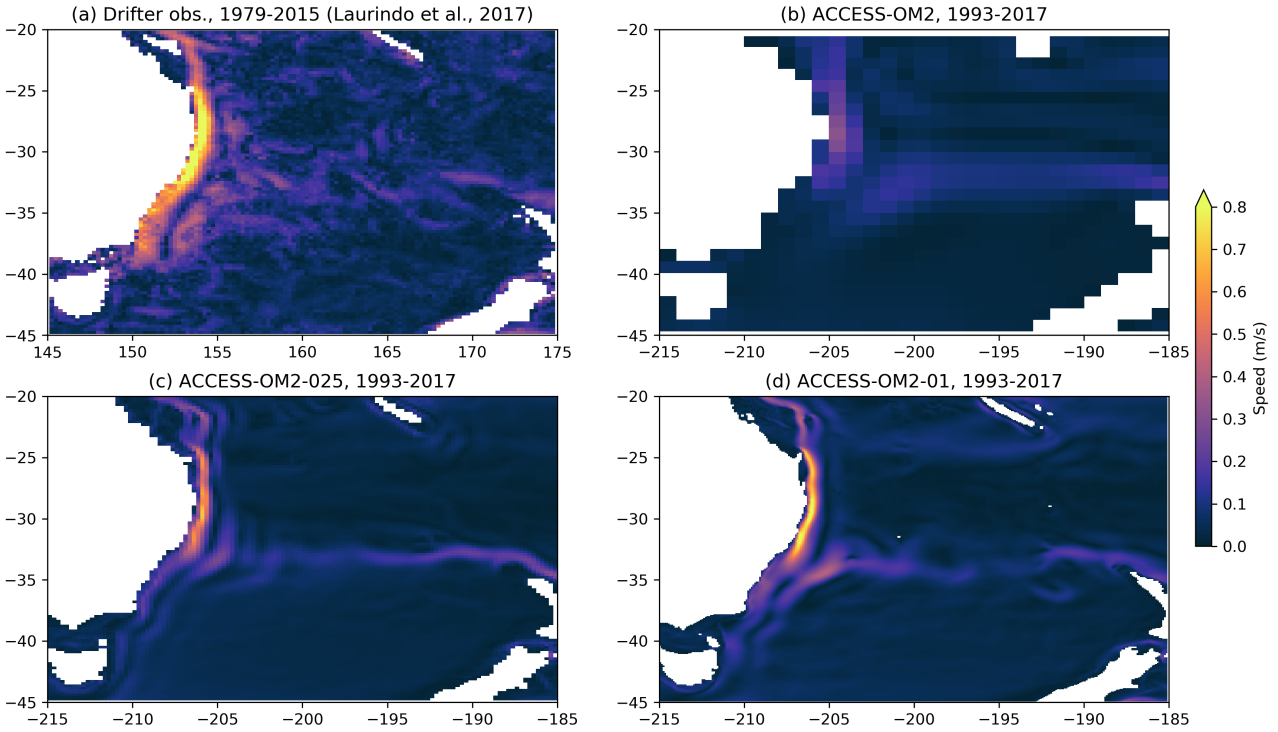

Figure 21: East Australian Current surface speed from (a) observations (1979–2015 mean from drifters at 15 m; Laurindo et al., 2017) and climatology from ACCESS-OM2 simulations at (b) 1° resolution; (c) 0.25° resolution and (d) 0.1° resolution.

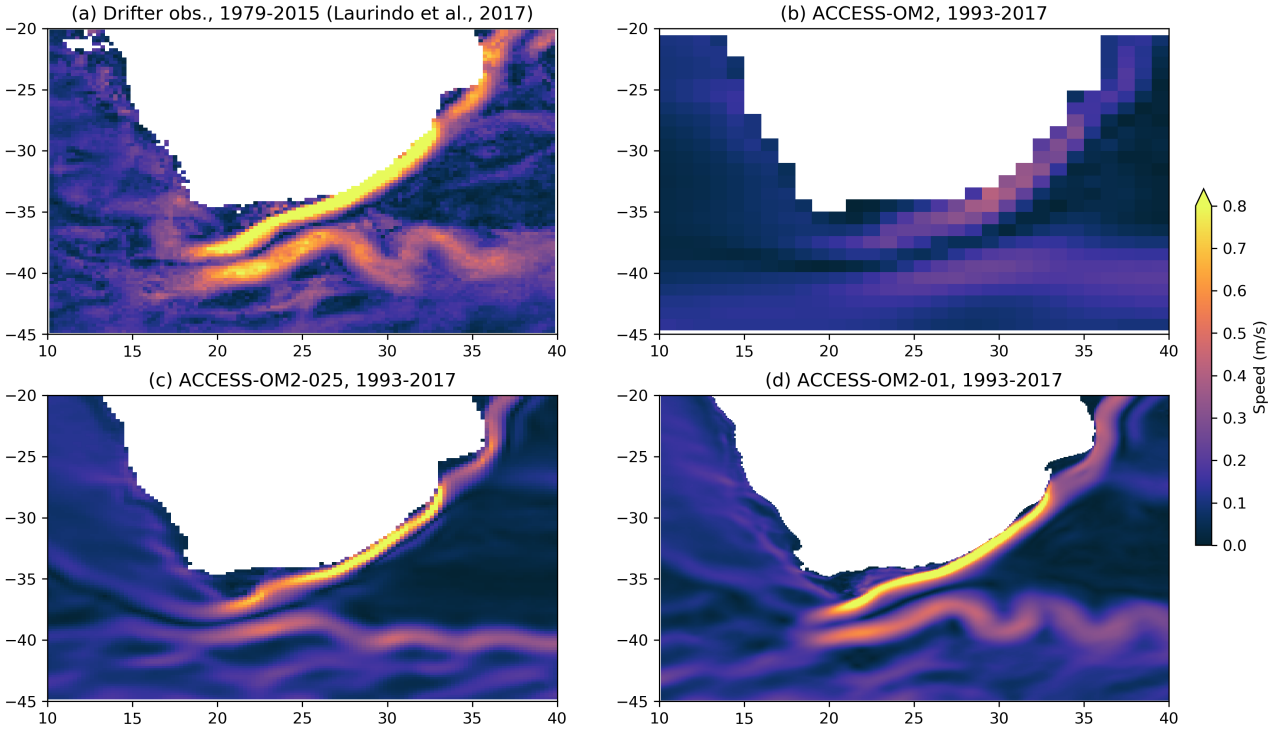

Figure 22: Agulhas Current surface speed from (a) observations (1979–2015 mean from drifters at 15 m; Laurindo et al., 2017) and climatology from ACCESS-OM2 simulations at (b) 1° resolution; (c) 0.25° resolution and (d) 0.1° resolution.

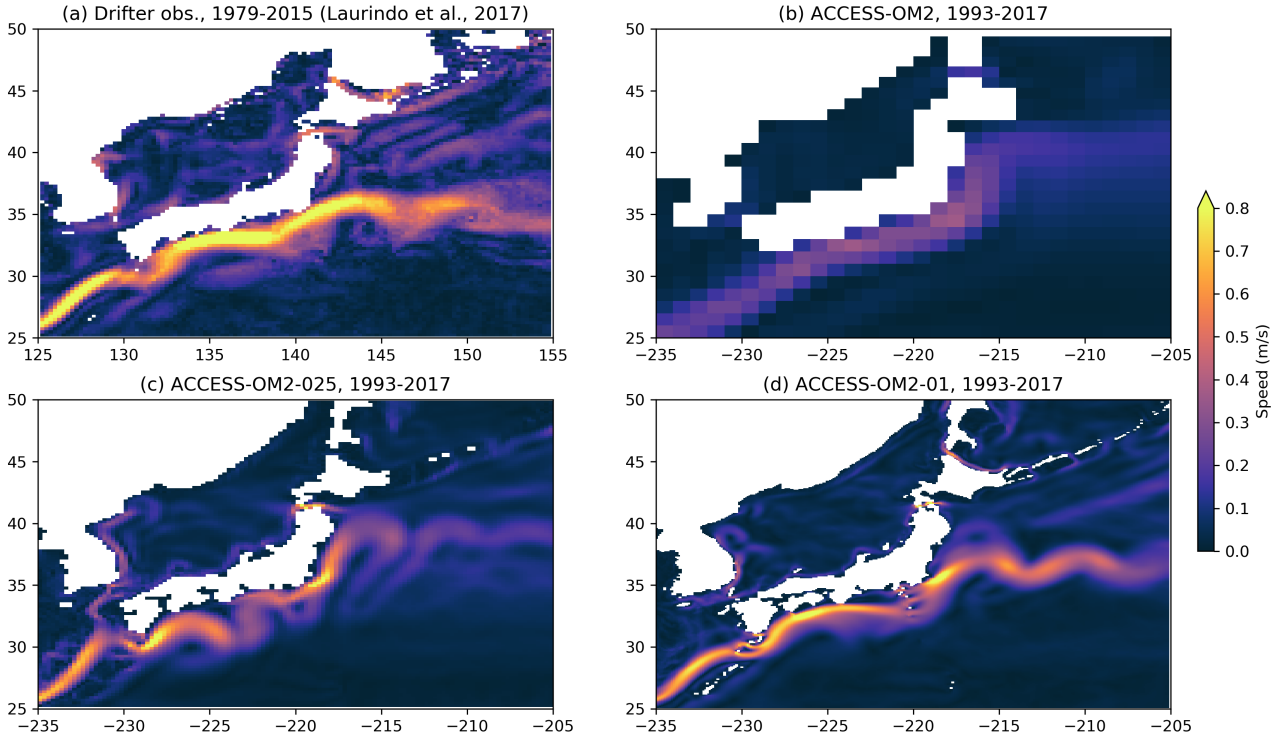

Figure 23: Kuroshio surface speed from (a) observations (1979–2015 mean from drifters at 15 m; Laurindo et al., 2017) and climatology from ACCESS-OM2 simulations at (b) 1° resolution; (c) 0.25° resolution and (d) 0.1° resolution.

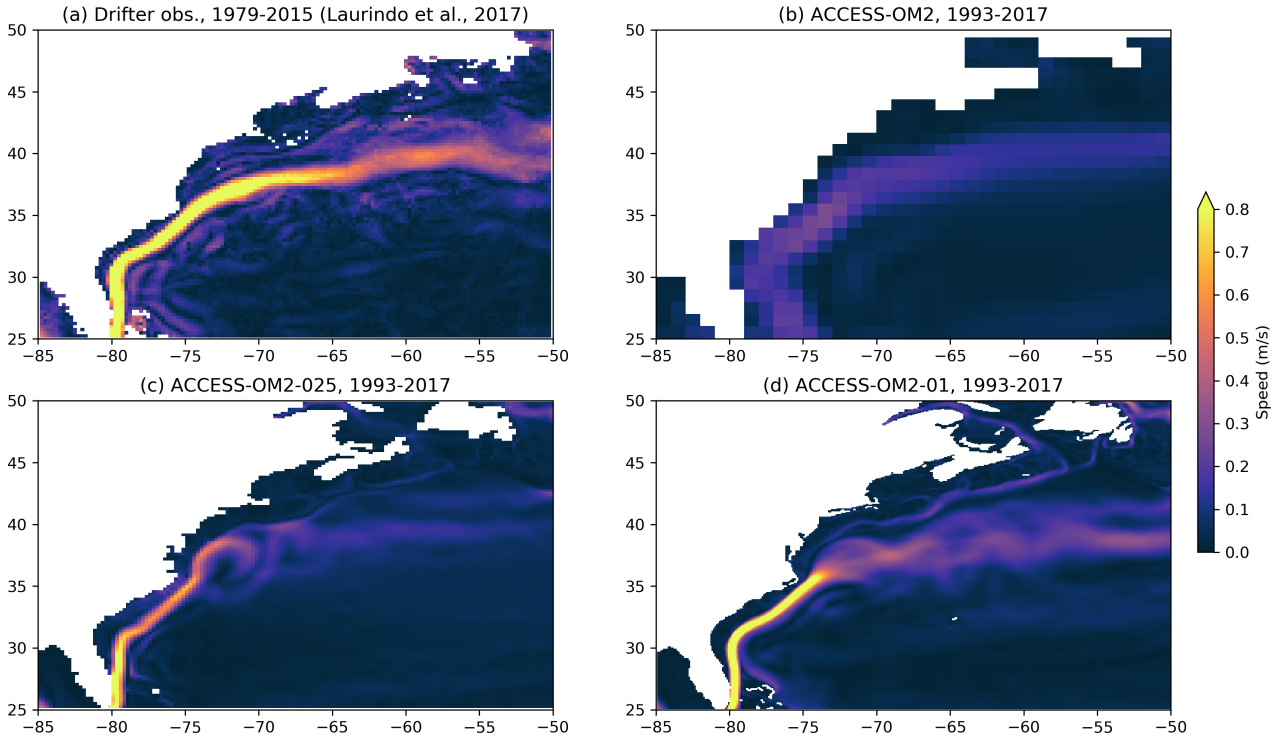

Figure 24: Gulf Stream surface speed from (a) observations (1979–2015 mean from drifters at 15 m; Laurindo et al., 2017) and climatology from ACCESS-OM2 simulations at (b) 1° resolution; (c) 0.25° resolution and (d) 0.1° resolution.

4.4 Transports through key straits and boundary currents

See Figure 25

See Griffies et al. (2016, figure J1) for standard CMIP6/OMIP sections.

use zigzag method in tripolar region? - see appendix C4 in Griffies et al. (2016)

TODO: output vertical sections at high spatiotemporal resolution in diag_table

Figure 25: Transports through key straits. **TODO:** update **TODO:** fix Lombok, fix ranges, include 1 deg, label panels (a), (b) etc **FIXME:** meridional transports are wrong - see https://github.com/COSIMA/ACCESS-OM2-1-025-010deg-report/issues/47

4.4.1 ITF

TODO: See "Océane Richet - Indonesian Seas model assessment" dir

transports through straits - cf INSTANT array obs and Sprintall et al. (2009); Hautala et al. (2001)

Marsland 12 Apr 2018: ACCESS (1°) used Rayleigh drag to shift transport from westernmost to easternmost strait to match obs. Also cf. Perth-Jakarta line (XBT?)

TODO: check that water mass transformation between inflow and outflow resembles obs — may need enhanced mix-

ing to represent the strong tidal mixing in this region (Koch-Larrouy et al., 2008a,b; Atmadipoera et al., 2009).

4.4.2 Drake Passage

CONTRIBUTORS: Andy Hogg

Drake passage transport is about 135 Sv at 0.1° resolution and about 105 Sv 0.25° (see Figure 25), **TODO:** keep these up to date significantly below the observed values of 173.3 Sv (Donohue et al., 2016) and 175 Sv (Colin de Verdière and Ollitrault, 2016).

ACC transport is increased by spurious deep convection (Cheon et al., 2014; Martin et al., 2012) — so perhaps the reduced DP transport at 0.1deg is related to reduced spurious deep convection?

4.5 Equatorial current velocity and temperature structure

CONTRIBUTORS: Ryan Holmes

See Figure 26.

cf. TOGA?

4.6 Overturning

The overturning circulation on density surfaces for all three resolutions is shown in Fig. 27. This figure ...

Farneti et al. (2015)

Lumpkin and Speer (2007)

Talley (2013)

4.7 Meridional heat transport

CONTRIBUTORS: Ryan Holmes, Adele Morrison

AMOC: do transect at 26.5N to cf RAPID array http://www.rapid.ac.uk/rapidmoc/ Smeed et al. (2018)

Could also split AMOC into western and eastern components for comparison on OSNAP (Lozier et al., 2017, 2019; Holliday et al., 2018). Data: https://www.o-snap.org

AMOC reviews: Zhang et al. (2019), Frajka-Williams et al. (2019) and Hirschi et al. (2020).

Caesar et al. (2018); Böning et al. (2016); Rahmstorf et al. (2015)

cf. Newsom et al. (2016)? But this is just another model analysis?

Could also compare to reanalysis products, as done in Griffies et al. (2015), Figure 7. Ganachaud and Wunsch (2003) is another obs estimate to compare with.

4.8 Model bias assessments

Minimal model bias important for BOM for data assimilation in oceanMAPS, but is difficult to assess with repeat-year forcing as the mean of RYF is not climatology, so after many repeats of RYF the slowly-adjusting ocean features will match neither climatology nor the state in the repeat year, even if the model itself is unbiased.

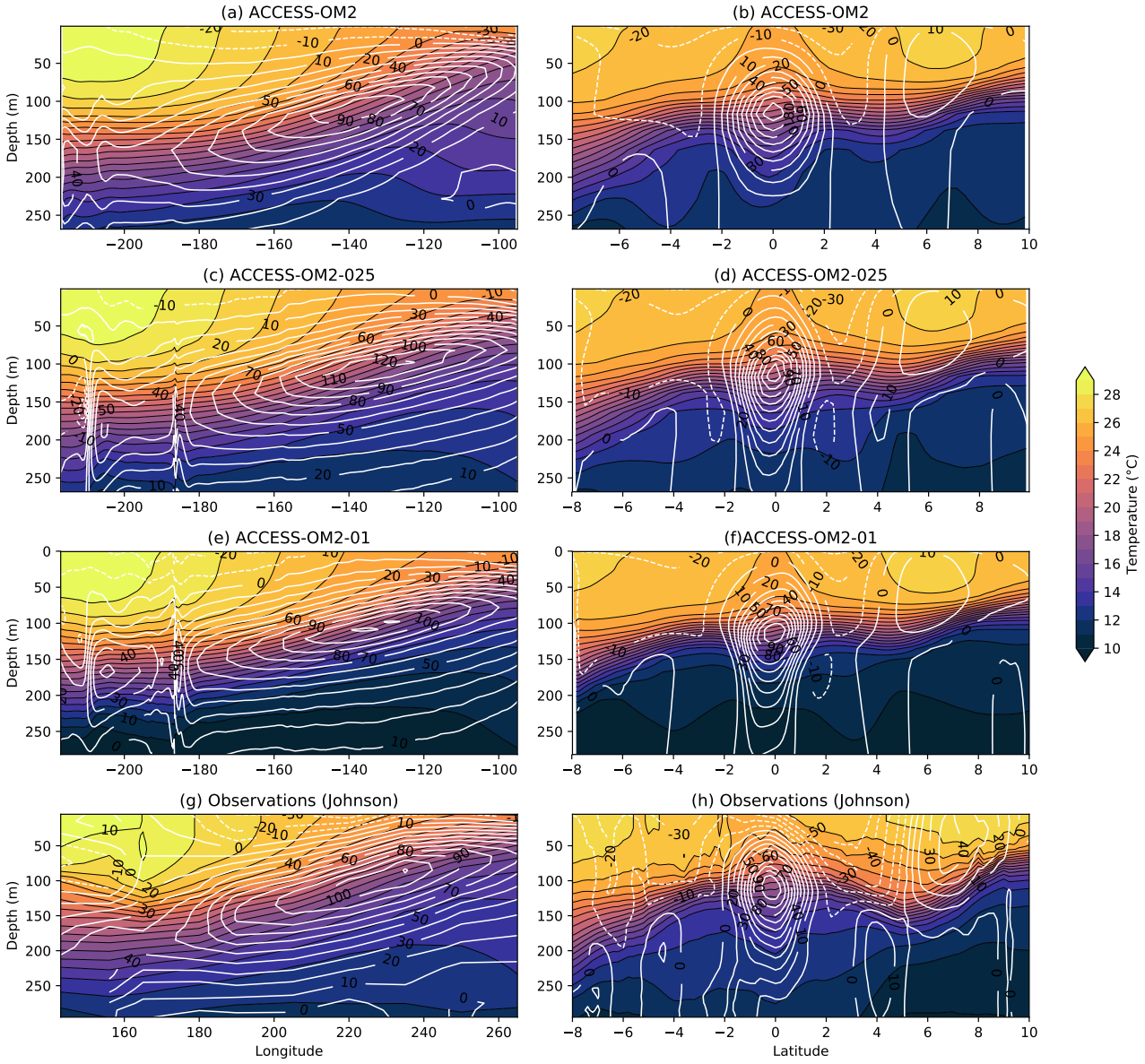

Figure 26: Transects in the upper equatorial Pacific versus longitude at the Equator (left) and versus latitude at 220°E (right) for the model configurations **TODO:** averaged over which years? and observations from Johnson et al. (2002) **TODO:** averaged over which years? **TODO:** check this is the correct reference. Colours show temperature in °C and white contours with black labels are eastward velocity isotachs (in cm s^{-1}; westward contours are dashed).

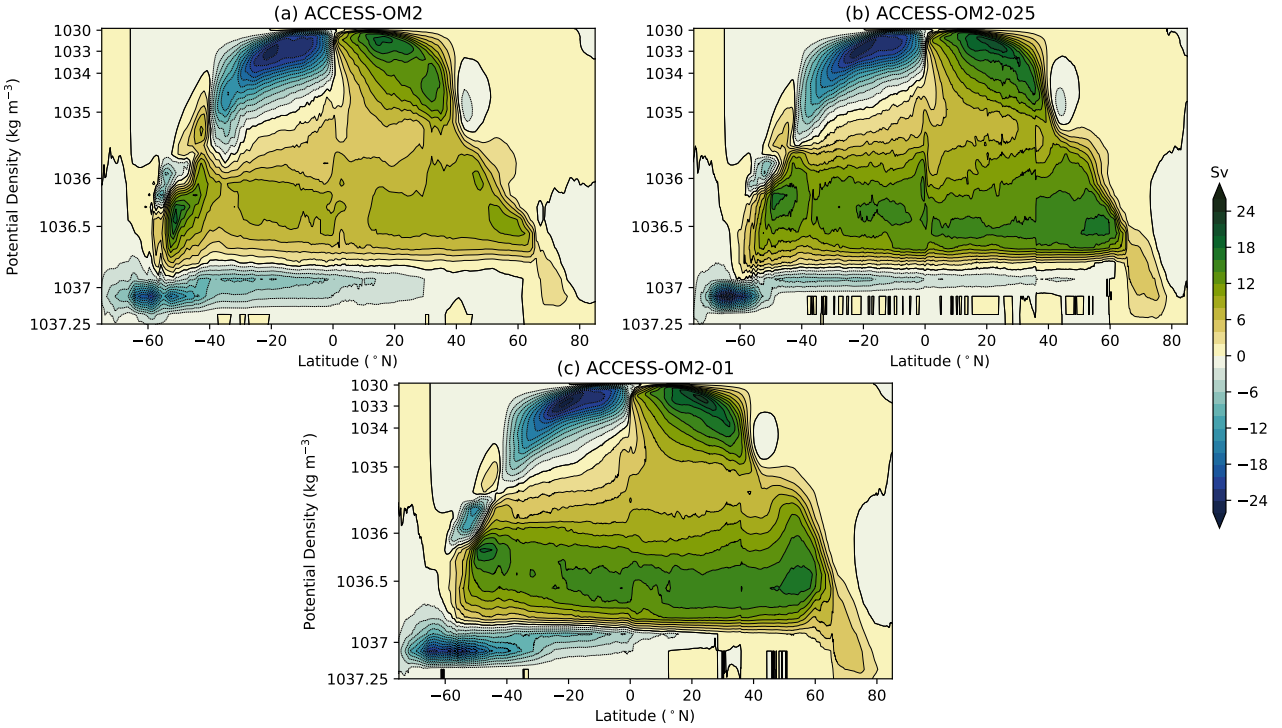

Figure 27: Global overturning circulation on density surfaces (σ_2) for ACCESS-OM2 simulations at (a) 1° resolution; (b) 0.25° resolution and (c) 0.1° resolution.

cf BRAN

cf Kerry et al. (2016)

4.9 Water mass properties and structure

CONTRIBUTORS: Adele Morrison

4.10 Mixed layer depth (MLD)

TODO: cf. MLD obs from Holte et al. (2017); Schmidtko et al. (2013); de Boyer Montégut et al. (2004)? **TODO:** plot MLD and check to see that consistent definitions are used - see notebooks that compare model with IFREMER and MILA_GPV obs The mld diagnostic is mixed layer depth determined by density criteria. It is the depth at which the buoyancy exceeds the surface buoyancy by more than the default buoyancy criterion buoyancy_crit=0.0003 ms^{-2}. Since buoyancy is $g\Delta\sigma/\rho$, this very nearly identical to the $\Delta\sigma = 0.03\,\mathrm{kgm}^{-3}$ density criterion used by Sallée et al. (2013) and advocated by Downes et al. (2009); Sallée et al. (2006) and de Boyer Montégut et al. (2004).

CMIP5 models tend to underestimate winter MLD (Sallée et al., 2013).

Full-depth convection in the Antarctic has been observed only once, in the 1974–6 Weddell Polynya (Gordon, 1978). Otherwise, Antarctic MLD is shallower than 1000 m (Schmidtko et al., 2013). All 3 resolutions display regions of anomalously deep (often full-depth) convection. This covers large areas in the eastern Weddell Sea and western Ross Sea every winter and spring in the 1° and 0.25° simulations, but is much reduced in the 0.1° simulation, and confined to a much smaller region in the northwest Weddell Sea, with significant interannual variability.

The behaviour of the two coarser models is typical of CMIP5 models, which produce bottom water by spurious deep-ocean convection rather than down-slope flows (Heuzé et al., 2013, 2015).

Connection to polynyas: see Goosse and Fichefet (2001); Heuzé et al. (2015); Kjellsson et al. (2015),

section 4.15.7.

see Uotila et al. (2019)

use Argo data

and MEOP southern ocean seal data http://www.meop.net?

4.10.1 T/S diagrams

4.10.2 Deep water formation / transformation rates, locations, properties

Farneti et al. (2015) Abernathey et al. (2016) Downes et al. (2011) Pellichero et al. (2018)

4.11 Heat conservation, bias and drift

CONTRIBUTORS: Chris Chapman, Ryan Holmes

use XBT data from Chris Chapman?

cf FAFMIP? Gregory et al. (2016)

4.11.1 SST bias

WOA13v2 0.25-degree Arctic SST has spurious steps - see https://github.com/COSIMA/access-om2/issues/103

new sst obs datasets: see Pilo email 2018-11-05

cf. SSTARS (Wijffels et al., 2018), available via https://portal.aodn.org.au/?

Daily 0.25 deg JMA MGDSST Reanalysis and Real Time MGDSST Analysis: 1982 - present https://www.data.jma.go.jp/gmd/goos/data/pub/JMA-product/mgd_sst_glb_D Canadian Meteorological Centre's (CMC) 0.2 degree SST analysis: 1991–2017: https://podaac.jpl.nasa.gov/dataset/CMC0.2deg-CMC-L4-GLOB-v2.0 Canadian Meteorological Centre's (CMC) 0.1 degree SST analysis: 2016 - present: https://podaac.jpl.nasa.gov/dataset/CMC0.1deg-CMC-L4-GLOB-v3.0?ids=&values=&search=CMC For assessment and validation of these analyses, see Fiedler et al. (2019).

4.11.2 lat/depth T sections and bias

4.11.3 Drift: depth/time T hovmollers

4.11.4 zonally averaged surface heat flux terms

4.12 Salt conservation, bias and drift

cf FAFMIP? Gregory et al. (2016)

4.12.1 SSS bias

WOA13v2 0.25-degree Arctic SSS has spurious steps - see https://github.com/COSIMA/access-om2/issues/103

4.12.2 lat/depth S sections and bias

4.12.3 Drift: depth/time S hovmollers

4.12.4 zonally averaged surface salt/freshwater flux terms

4.12.5 Variation of ocean volume

Over a 60-year forcing cycle the global mean SSH increases by about 3.5 cm and the global mean salinity falls by about 0.0002 psu (figure 28). This is due to ocean-ice mass exchange, as P-E+R is constrained to be zero (section 3.5.2). The 3.5 cm SSH change represents an increase in ocean volume of about 1.26×10^{13} m^3. This is in close agreement with a roughly 1.3×10^{13} m^3 sea ice decline over 40 years (Figure 35).

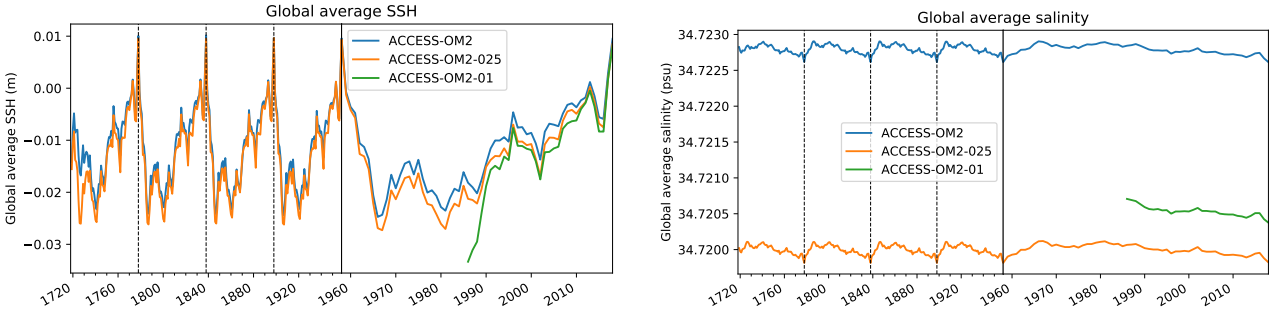

Figure 28: Global mean sea surface height (left) and salinity (right) for the 3 runs.

4.13 Variability

Danabasoglu et al. (2016)

4.13.1 Western boundary current variability

4.13.2 EKE spatial distribution and wavenumber spectrum

EKE near 1000dbar: Ollitrault and Colin de Verdière (2014)

also check EKE spectrum to see if it follows the expected slope - eg Capet et al. (2008)

cf. SSH spectrum obs: Xu and Fu (2011, 2012)

Scott Bachman recommends 2D Laplacian Leith (or his new QG Leith, currently being tested in MOM 6) over Smagorinsky, as Smagorinsky over-damps the fine scales. However Leith is not implemented in MOM5. O'Kane finds good agreement between 0.25 and 0.1 deg despite using Smag biharmonic

See Errico (1985); Durran et al. (2017)

4.14 Sea level

Griffies et al. (2014)

4.15 Sea ice

See the obs datasets used in SITool: Lin et al. (2021) https://github.com/XiaLinUCL/Sea-Ice-Evaluation-Tool

Year of Polar Prediction (YOPP) data portal: https://yopp.met.no, e.g. http://thredds.met.no/thredds/fou-hi/arctic20km.html?dataset=arctic20km_24h_be

discuss linear kinematic features (leads): Hutchings et al. (2005); Wang et al. (2016a); Wang and Wang (2009); Losch et al. (2014); Hutter et al. (2018). These are too fine to be resolved by the large footprint of the SSM/I and SSMIS passive microwave sensors (Lemieux et al., 2015). But can be detected in ice drift http://rkwok.jpl.nasa.gov/envisat/index.html (Hutter et al., 2018).

See Uotila et al. (2013)

see Smith et al. (2015)

see https://medium.com/pangeo/polar-deployment-of-pangeo-96865774287c

see Schroeter et al. (2018); Barthélemy et al. (2017); Uotila et al. (2017); Schweiger et al. (2011)

see Vaughan et al. (2013); Flato et al. (2013); Dorn et al. (2018)

problems comparing models to obs: Notz et al. (2013)

see Naughten (2018); Naughten et al. (2018); Roach et al. (2020)

see NAS (2017), Hobbs et al. (2016); Uotila et al. (2019)

special issue: https://agupubs.onlinelibrary.wiley.com/doi/toc/10.1002/(ISSN)2169-9291.NICE1

see Kial's RYF sea ice assessment at 1deg

cf. ACCESS-OM (Uotila et al., 2012, 2013)

wavy ice features in 0.25deg — poor EVP convergence? https://github.com/COSIMA/access-om2/issues/87

Too much ice south of Svalbard in 0.10deg — **TODO:** check Gulf Stream in 0.1deg – is it carrying heat far enough north?

TODO: put probe points at narrowest point of northern Nares Str between Greenland and Ellesmere - compare ice export to Kwok et al. (2010)

TODO: summary plot of sea ice extent min and max contours for the 3 models and obs in NH and SH

We have quite thick ice in small, isolated locations in some Arctic embayments (up to about 22m **TODO:** check) but at least it's not hundreds of metres as in Delworth et al. (2012).

Reanalyses for possible comparison with model (from Helen Beggs' email 21 Mar 2018):

- Reanalyses of sea ice observations: The OSI-SAF reanalysis is available in 10 km resolution from: http://osisaf.met.no/p/ice/index.html#conc-reproc It covers the period from 1978 to 2009 with consistent algorithm processing. PUM and validation reports are available at the website as well. OSI-SAF Daily sea ice concentration analyses are being ingested into the new Decadal OFAM Climate Model by Sakov and Sandery.
- http://osisaf.met.no: ice concentration, edge, drift and emissivity on both hemispheres, as well as climate consistent time series
- Bremen/Hamburg University and their AMSR2 based products
- NCEP (Bob Grumbine), http://polar.ncep.noaa.gov/seaice/ - BoM uses NCEP 1/12° Daily Global Sea Ice Analyses as operational inputs into their SST analyses, used as the boundary condition to the NWP models

http://psc.apl.uw.edu/research/projects/arctic-sea-ice-volume-anomaly/

TODO: check: are there katabatic winds in JRA55? if not, does this explain our lack of coastal polynyas? see Zhang et al. (2015); Stössel et al. (2011) **TODO:** Alex Fraser suggestion at AUV workshop: check formation rate – is it just thin frazil in the model, so we actually do have coastal polynyas? could also look at category 1 ice thickness

see Ice_Validation_ACCESS-OM2-01.ipynb https://github.com/aekiss/cosima-cookbook/blob/master/notebooks/Ice_Validation_ACCESS-OM2-01.ipynb uses data from http://nsidc.org

see SIMIP Notz et al. (2016)

see Toyota and Kimura (2018) - plastic rheology applies in MIZ

and check convergence Bouillon et al. (2013); Kimmritz et al. (2015); Losch and Danilov (2012); Lemieux and Tremblay (2009)

Wang et al. (2016b)

Downes et al. (2015)

cf Heil et al. (2011) **ISSUE 3**

4.15.1 Seasonal cycle of extent and area

ISSUE 1 **ISSUE 2**

We adopt the usual definition of sea ice extent as the area in which sea ice concentration exceeds 15%.

See Figures 33 and 34. **FIXME:** land mask area differs between the three configurations (figure 4) and differs from obs, especially in the Canadian Archipelago and River Ob - how to remove this bias in the total extent, area and volume?

Note that there are significant differences between passive microwave observational products (Ivanova et al., 2015; Roach et al., 2018; Meier et al., 2014) and https://nsidc.org/support/faq/what-difference-between-nasa-team-algorithm-ar Fritzner et al. (2018) use both methods: Bootstrap primarily for observations with low SIC, and Bristol for high SIC. Sea ice extent is generally consistent, but sea ice area or concentration distributions differ significantly and this should be taken into account when assessing model performance (Roach et al., 2018). NAS (2017): " As a general rule of thumb, said Dr. Massom, overall accuracies in ice concentration retrieval ranging from ±5% to ±15% are expected. Errors are largest in summer, over regions of predominantly thin/new ice, and year round in the marginal ice zone (MIZ) (up to ±30%) (Brucker et al., 2014; Comiso et al., 2011)."

NOAA/NSIDC Climate Data Record of Passive Microwave Sea Ice Concentration, Version 3 Meier et al. (2017); Peng et al. (2013), http://nsidc.org/data/G02202 This has a nominal resolution of 25 km, considerably coarser than both the 0.25° and 0.1° models (Table 6). Leads are too fine to be resolved by the large footprint of the SSM/I and SSMIS passive microwave sensors (Lemieux et al., 2015).

TODO: cf. Melsheimer and Spreen (2019); Melsheimer (2019): 6.25km daily SIC, July 2012 - Dec 2019

TODO: show March and Sept ice concentration vs. obs obs: 1988–1997 climatology from NOAA/NSIDC Climate Data Record of Passive Microwave Sea Ice Concentration, v3

Sea Ice Index, Version 3 (Fetterer et al., 2017, updated daily, http://nsidc.org/data/g02135).

Sea ice extent — see Ivanova et al. (2016)

We capture the 2016 decline in Antarctic sea ice extent (Meehl et al., 2019; Wang et al., 2019).

4.15.2 Sea ice thickness and volume

TODO: also plot snow thickness timeseries hs

TODO: maps of summer and winter mean snow thickness

See Figure 35: the growth of Arctic ice volume is due to increasing category 5, presumably due to ridging. We use kcatbound=0, so lower bound of ice categories is 0, 0.64, 1.39, 2.47, 4.57m (Hunke et al., 2015, table 2). So by year 9 most of the ice volume (not area) is more than 4.57m thick, including in the summer minimum.

thickness: http://psc.apl.uw.edu/sea_ice_cdr/

cf. IceSat data 2003–2008 (Kurtz and Markus, 2012)

Compare thickness with cryosat data? - from late 2010 onwards http://science-pds.cryosat.esa.int Schröder et al. (2019); Fons et al. (2022b,a)

Or GIOMAS (see Uotila et al., 2013)? - though this is output from a data-assimilated model (Zhang and Rothrock, 2003) at about 1 degree resolution, monthly data from 1/1979 to present http://psc.apl.washington.edu/zhang/Global_seaice/model.html and http://psc.apl.uw.edu/data/global-sea-ice-giomas-data-sets/ Or Worby et al. (2008)? Or Kwok and Cunningham (2008)? or Kwok and Rothrock (2009)? or Kwok (2018)?

See Petra email 2018-11-26: Ron Kwok's data

or PIOMAS? Schweiger et al. (2011), from ftp://pscftp.apl.washington.edu/zhang/PIOMAS/data/v2.1/, used by Ridley et al. (2018) and others

Axel's APL Zice Arctic climate record http://psc.apl.uw.edu/sea_ice_cdr/data_tables.html

New SIT estimates: https://www.aviso.altimetry.fr/en/data/products/altimetry-ice-products/altimetry-sea-ice-products-from-ctoh.html

SIT and snow depth monthly 12.5km: Guerreiro et al. (2017), Guerreiro and Fleury (2017) now includes Antarctic http://ctoh.legos.obs-mip.fr/data/sea-ice-products

Snow depth: Garnier et al. (2021)

TODO: include maps of monthly mean concentration bias relative to passive microwave at the 3 resolutions: Sept and March in NH, Feb and Sept in SH

4.15.3 Age

4.15.4 Formation rate

ice production rate in coastal polynyas (Tamura et al., 2008; Tamura and Ohshima, 2011; Tamura et al., 2016; Nihashi and Ohshima, 2015; Ohshima et al., 2016) - see Adele's email 9 Mar 2018 - includes a script and netcdf version. Looks like you can download the data set here: http://www.lowtem.hokudai.ac.jp/wwwod/polar-seaflux/ what diagnostics give us production in CICE? f_congel gives basal growth – not relevant? meltb, meltl,melts, meltt? frazil?

See Pellichero et al. (2018)

4.15.5 Drift

cf. Kimura ice motion dataset - 60km Petra is getting a 30km dataset

Giles et al. (2011) Sumata et al. (2014, 2015b,a); Szanyi et al. (2016) Kwok et al. (2017)

4.15.6 Ice deformation

cf. Hutchings et al. (2011)

scaling - see Hutter et al. (2018), Girard et al. (2009) and reviews by Weiss (2003, 2017); Weiss and Dansereau (2017)

4.15.7 Polynyas

How good are katabatic winds in JRA55? cf. polar WRF?

Morales Maqueda (2004) review polynya observations and dynamics.

Uotila et al. (2013) Kwok et al. (2008)

Polynyas are occasionally seen at 1° in the monthly mean sea ice thickness near Maud Rise but they don't persist from year to year. No open-ocean polynyas are seen in the Weddell or Ross Seas at 0.25° in Sept in any year in the final cycle—so occurrence is less than observed, not more. No open-ocean polynyas are seen in Weddell or Ross Seas at 0.1° in September.

Dufour et al. (2017) see quasi-continouous deep convection at 0.25° but no polynyas

Also see section 4.10.

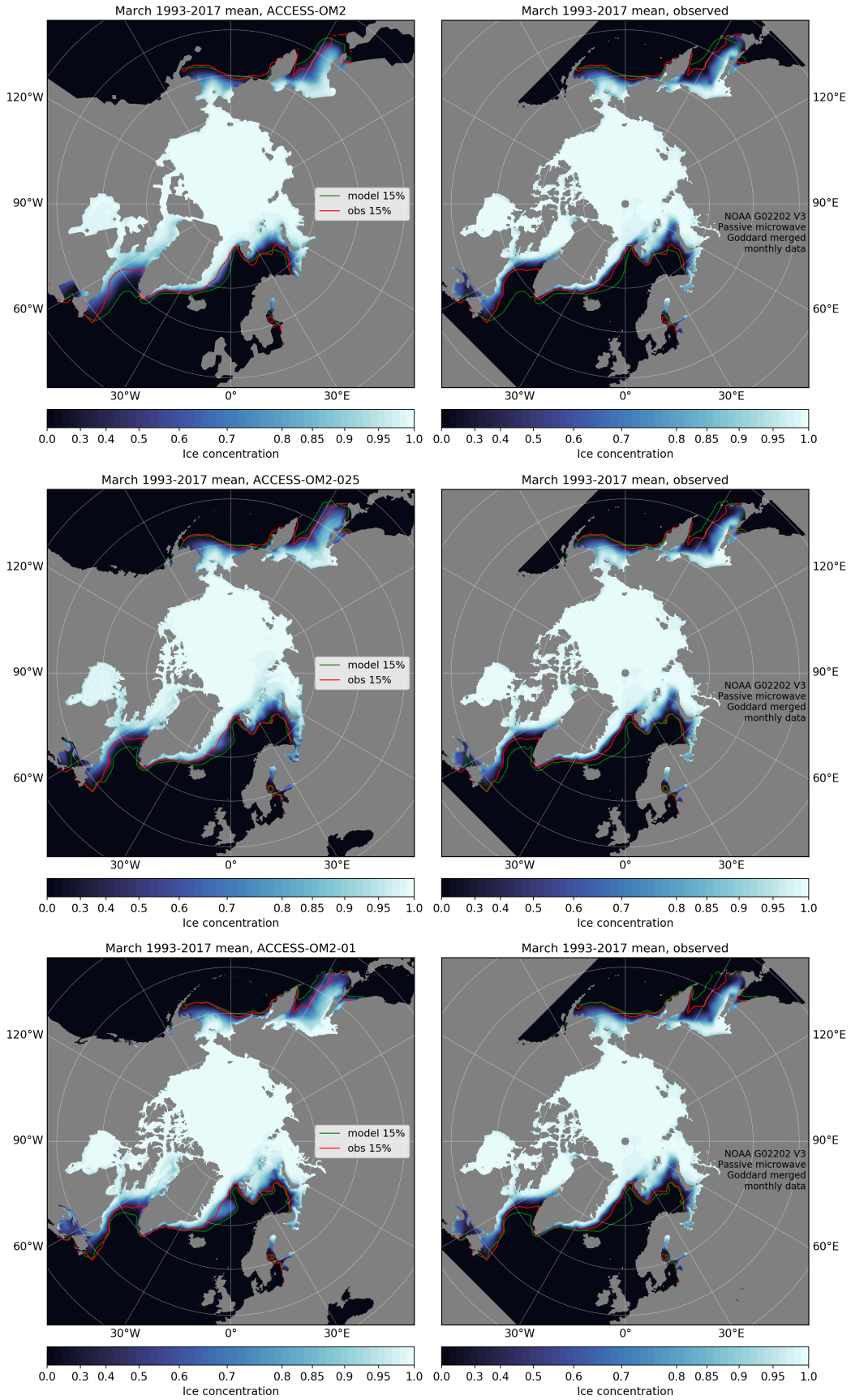

Figure 29: Arctic sea ice concentration from the ACCESS-OM2 suite (left) and passive microwave (right), March mean. Green (red) line is the 15% concentration contour in the model (observations). The scale is nonlinear to highlight differences at high concentrations. **TODO:** make this more compact - no need to repeat obs 3 times

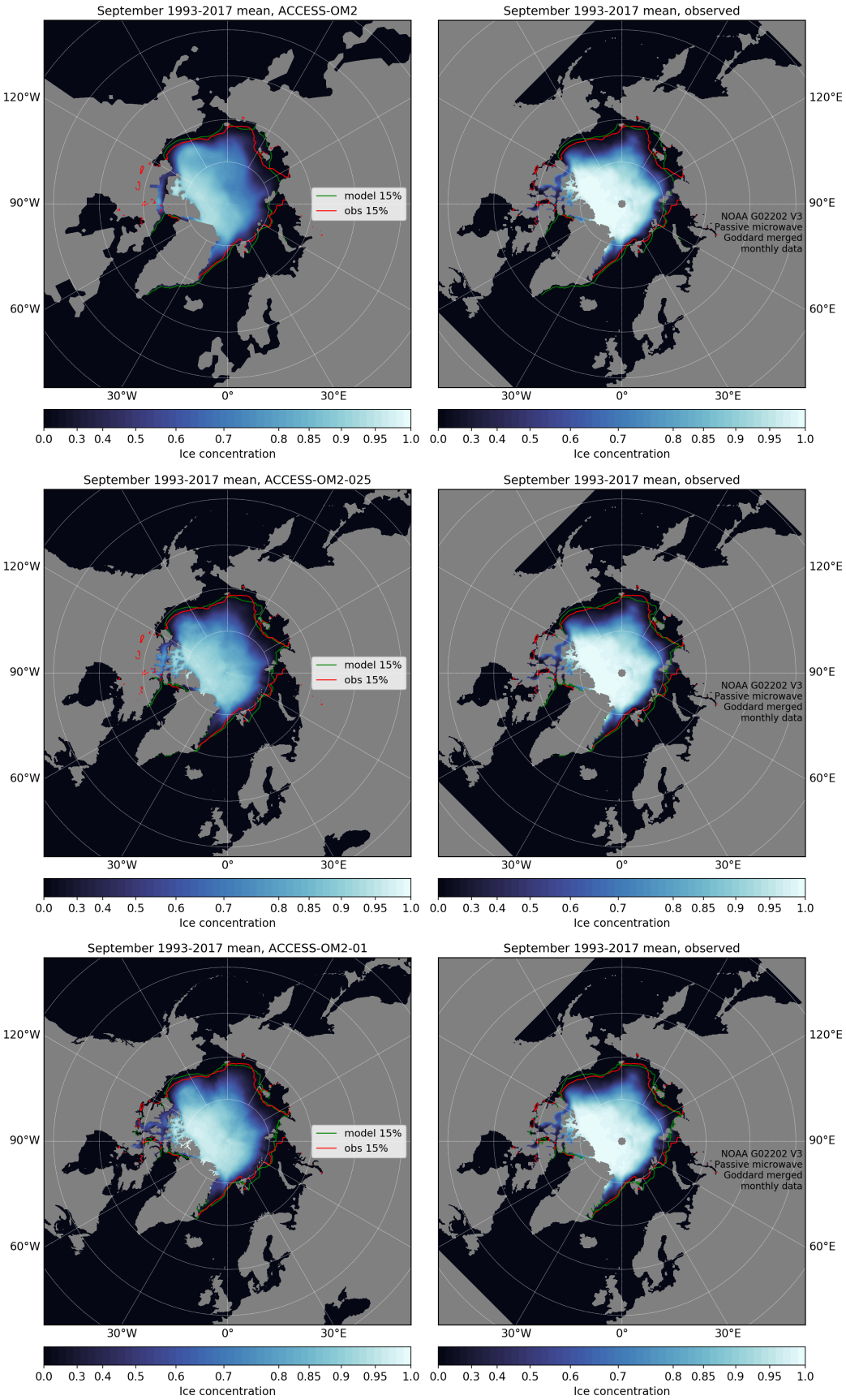

Figure 30: Arctic sea ice concentration from the ACCESS-OM2 suite (left) and passive microwave (right), September mean. Green (red) line is the 15% concentration contour in the model (observations). The scale is nonlinear to highlight differences at high concentrations. **TODO:** make this more compact - no need to repeat obs 3 times

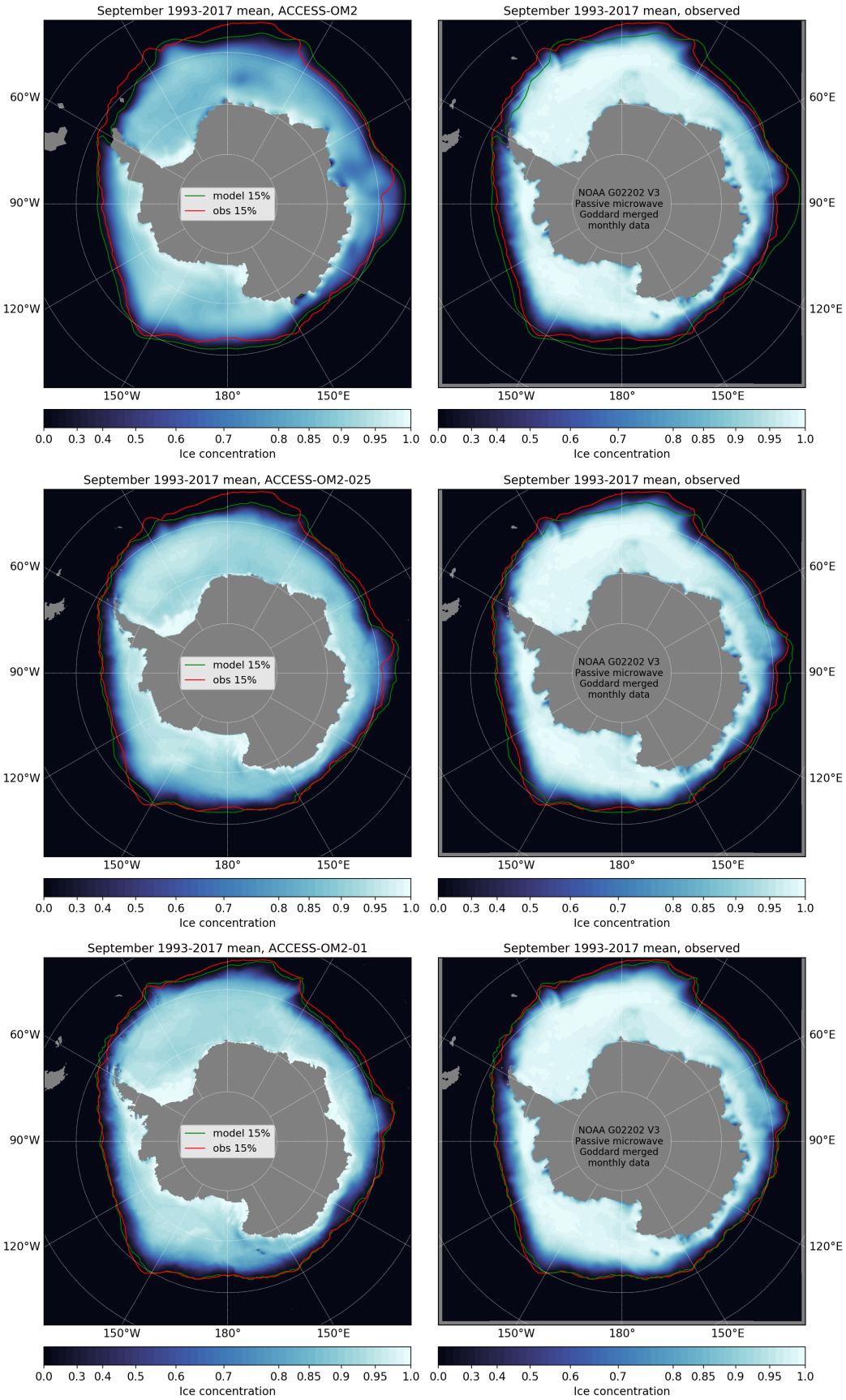

Figure 31: Antarctic sea ice concentration from the ACCESS-OM2 suite (left) and passive microwave (right), September mean. Green (red) line is the 15% concentration contour in the model (observations). The scale is nonlinear to highlight differences at high concentrations. **TODO:** make this more compact - no need to repeat obs 3 times

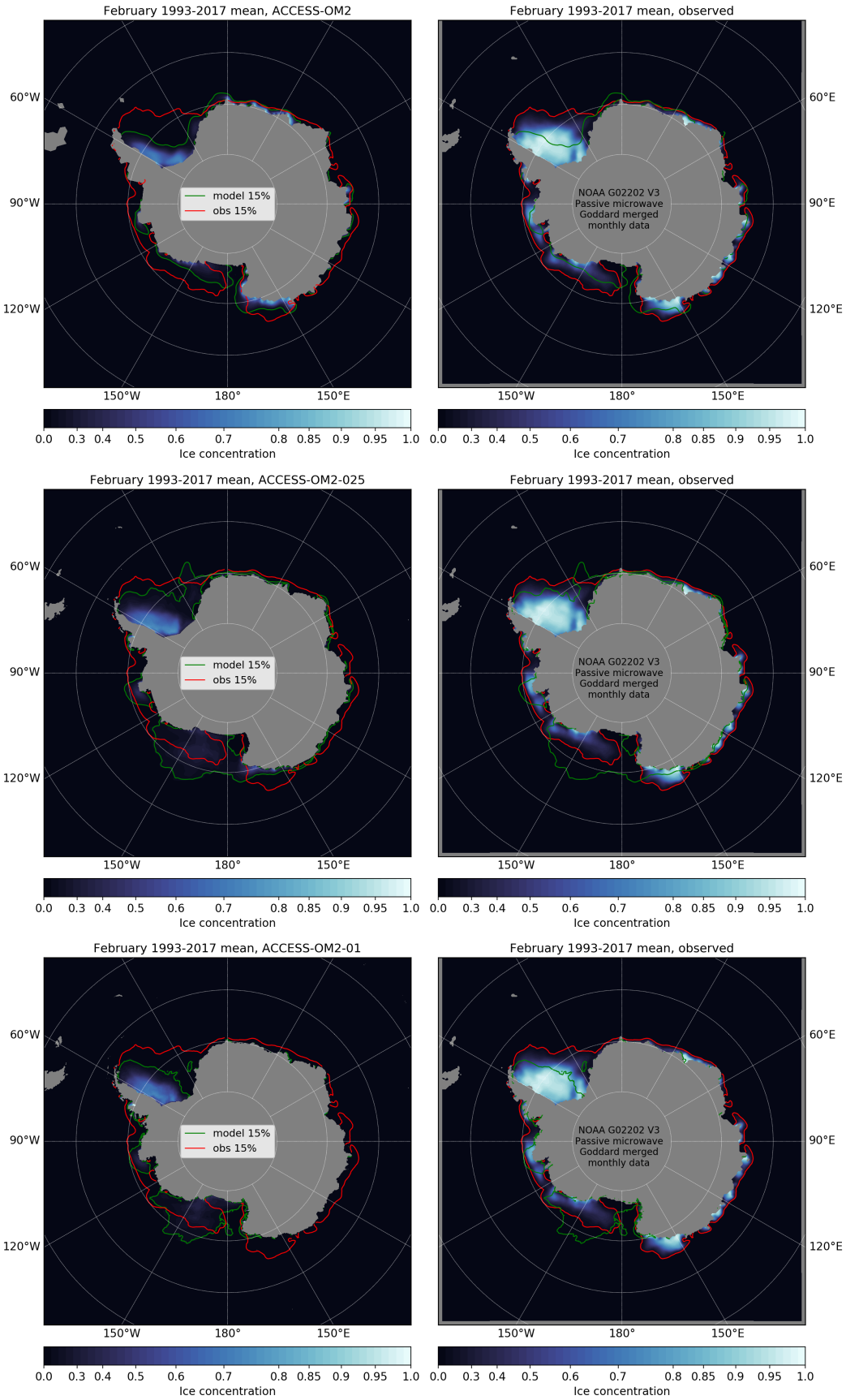

Figure 32: Antarctic sea ice concentration from the ACCESS-OM2 suite (left) and passive microwave (right), February mean. Green (red) line is the 15% concentration contour in the model (observations). The scale is nonlinear to highlight differences at high concentrations. **TODO:** make this more compact - no need to repeat obs 3 times

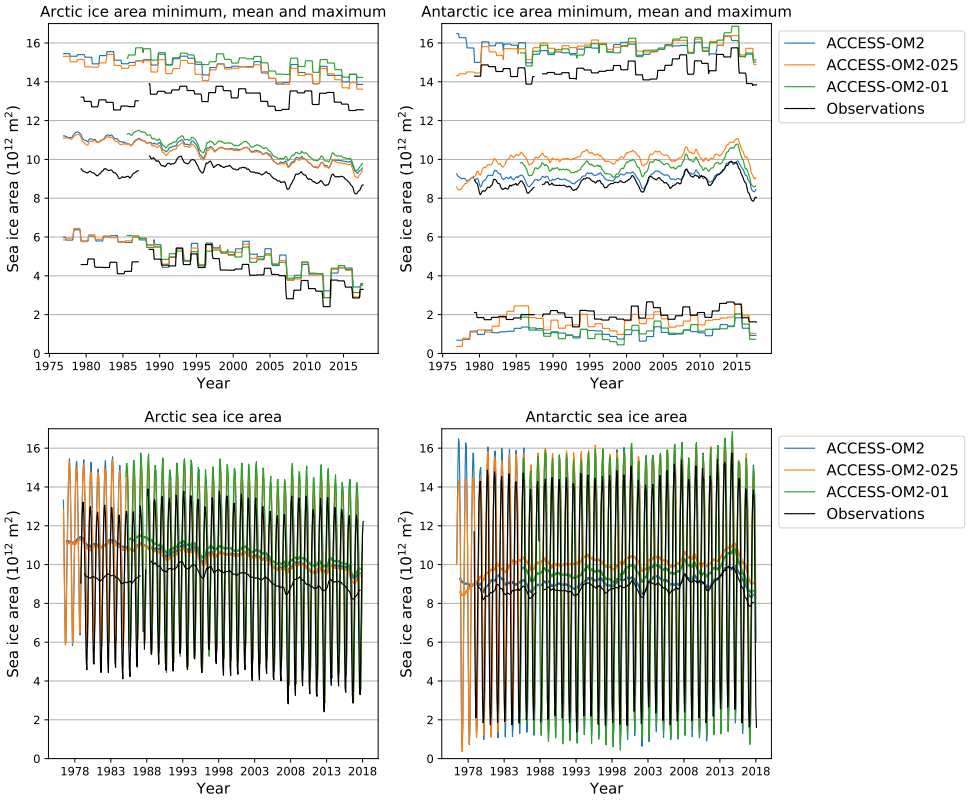

Figure 33: Sea ice area timeseries in the different configurations. Top row: running 12-month minimum, mean and maximum. Bottom row: timeseries (thick lines show the 12-month running mean). **FIXME:** missing obs data (-9999): Dec 1987, Jan 1988

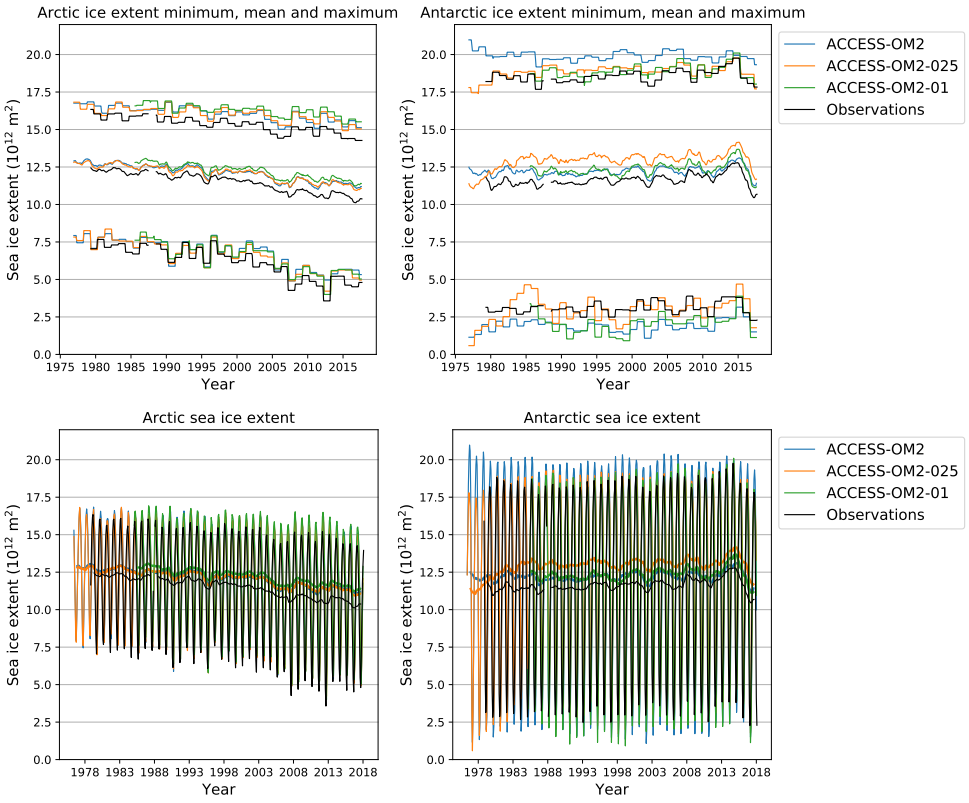

Figure 34: Sea ice extent timeseries in the different configurations. Top row: running 12-month minimum, mean and maximum. Bottom row: timeseries (thick lines show the 12-month running mean). **FIXME:** missing obs data (-9999): Dec 1987, Jan 1988

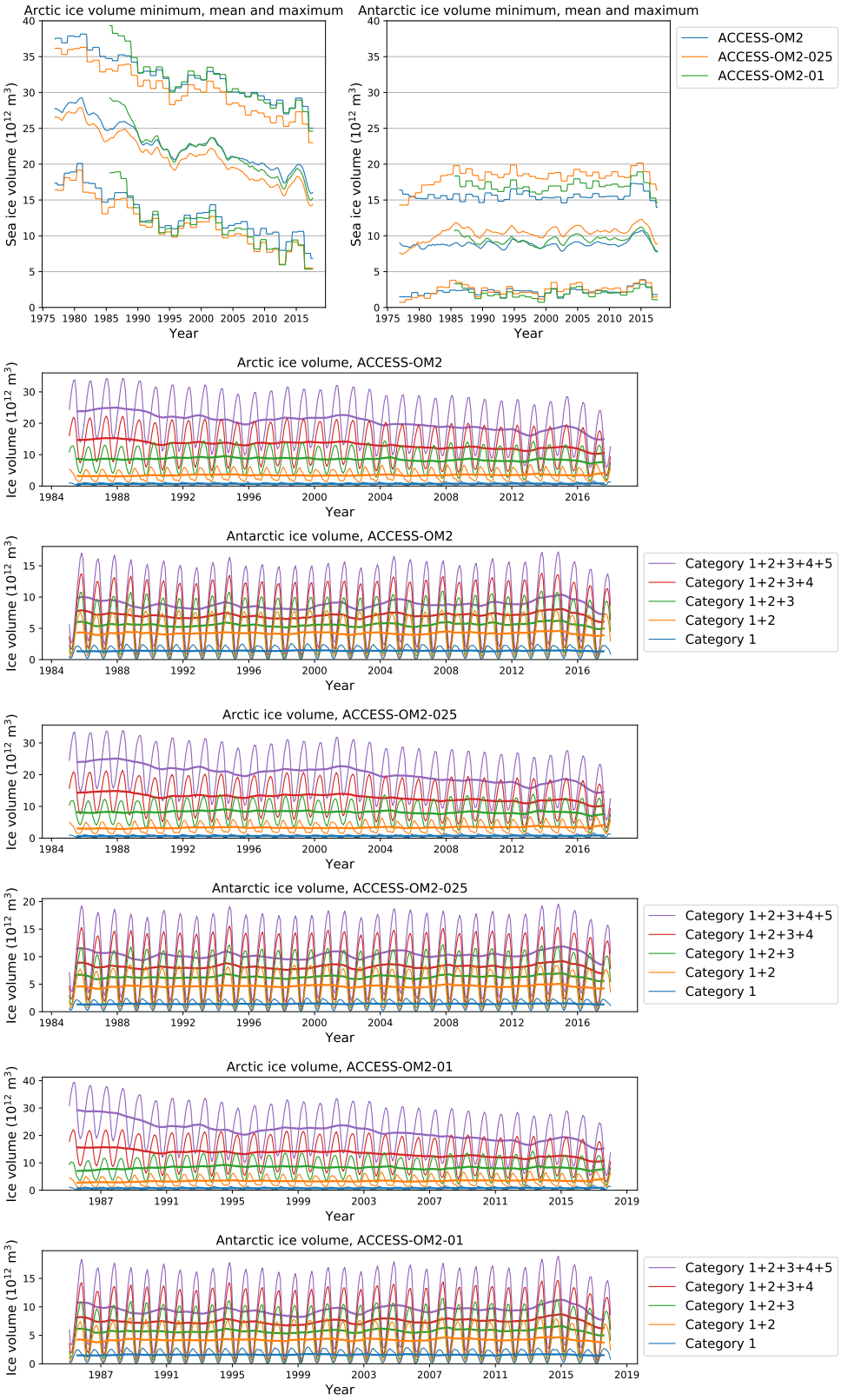

Figure 35: Sea ice volume timeseries in the different configurations. Top row: running 12-month minimum, mean and maximum. Remaining rows: breakdown of ice volume by category (thick lines show the 12-month running mean). Lower bound of ice thickness categories is 0, 0.64, 1.39, 2.47, 4.57m. **TODO:** use a common scale for the category plots in each hemisphere

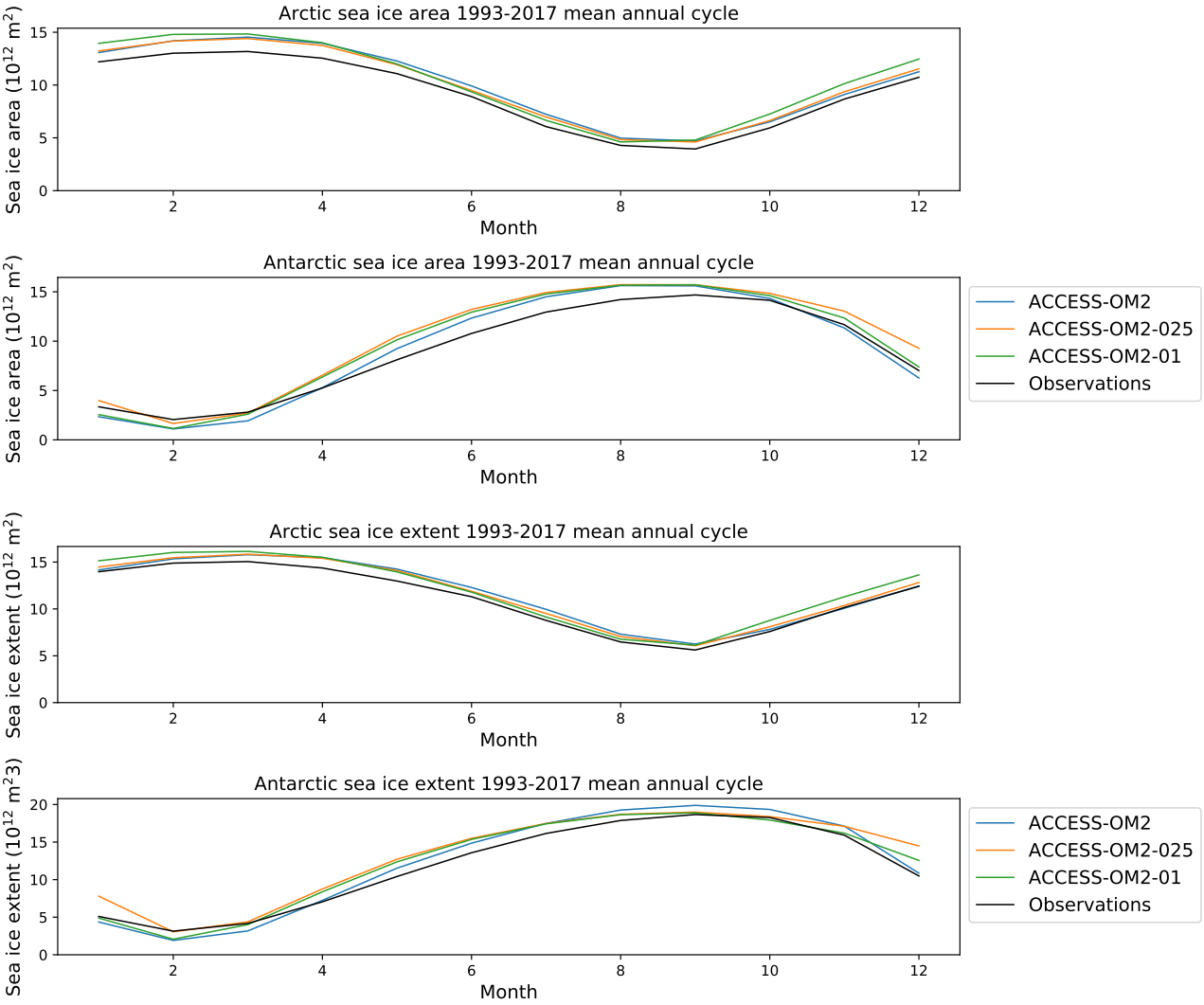

Figure 36: Seasonal cycle of ice area and extent compared to climatology of NOAA/NSIDC G02135 Sea Ice Index v3 (Fetterer et al., 2017, updated daily, http://nsidc.org/data/g02135)

4.16 Particularly important regions

Pick locations with detailed obs records for regional studies

4.16.1 ACC

Rintoul (2018)

cf SOSE Mazloff et al. (2010)

transport

EKE Farneti et al. (2015)

4.16.2 Antarctic margins

CONTRIBUTORS: Adele Morrison

dense water formation dense water transport down slope

4.16.3 East Australian Current

Laurindo et al. (2017) Archer et al. (2017a,b, 2018) Wijeratne et al. (2018) Zilberman et al. (2018, 2014) Feng et al. (2016) Sloyan et al. (2016)

http://www.clivar.org/clivar-panels/pacific/spice

4.16.4 Leeuwin Current

Wijeratne et al. (2018) Feng et al. (2016)

4.16.5 North Atlantic

North Atlantic mean state Danabasoglu et al. (2014) and variability Danabasoglu et al. (2016)

4.16.6 Arctic Ocean / Greenland-Iceland-Norway (GIN) Seas

cf. Behrendt et al. (2018) https://doi.pangaea.de/10.1594/PANGAEA.872931?

mixed layer depth

water properties

bottom water formation

bottom water transport over sills

Wang et al. (2016c) Ilicak et al. (2016)

4.16.7 Pacific

Tseng et al. (2016)

Kuroshio transport obs: Johns et al. (2001)

4.16.8 Agulhas

transport, structure, variability, leakage

5 Changes made in new version

Namelist changes from the original version are tabulated in Appendix D, and differences between the new namelists are tabulated in Appendix E.

5.1 For all resolutions

- switch to JRA55-do v1.4.0 https://github.com/COSIMA/access-om2/issues/155
- automatically sweep and resubmit on specific errors https://github.com/payu-org/payu/issues/241
- Update datetime-fortran and json-fortran https://github.com/COSIMA/libaccessom2/issues/29
- fixed units for temp: https://github.com/mom-ocean/MOM5/issues/295
- stop using -lother=hyperthread https://github.com/COSIMA/access-om2/issues/191
- fixed initial condition https://github.com/COSIMA/access-om2/issues/39
- use conservative temperature for initial condition: https://github.com/COSIMA/access-om2/issues/206
- updated compile scripts for gadi — library versions, compiler flags
- Compile with intel 19 and openMPI4.0.2 https://github.com/COSIMA/access-om2/issues/127
- move inputs and executables from /short/public to /g/data/ik11 for transition to gadi
- use new JRA55-do path https://github.com/COSIMA/access-om2/issues/120 — requires membership of qv56 via https://my.nci.org.au/mancini/project/ for all users.
- Fix calendar https://github.com/COSIMA/access-om2/issues/117
- Use relative wind for ice (set highfreq=true in group forcing_nml) since this is what use use for the ocean https://github.com/COSIMA/access-om2/issues/138
- Tidy up neutral physics namelist: https://github.com/COSIMA/access-om2/issues/197
- Set pottemp_equal_contemp to false: https://github.com/COSIMA/access-om2/issues/148
- Fix neutral density diagnostic levels: now set to neutralrho_min=1028.0 and neutralrho_max=1038.0 https://github.com/COSIMA/access-om2/issues/135
- Use updated payu (at least 0.11.2) that fixes cice coupling bug: https://github.com/COSIMA/access-om2/issues/123
- Set drhodz_mom4p1=true for 0.25 degree
- Set zmax_pen to 1e6 (the default — see comments in code)
- Set ncar_boundary_scaling=false at 0.25 and 0.1deg, since we're not using it anyway
- turn off MOM output/restart compression at 1 deg (since this can be done for both output and restart by payu in collation step): set deflate_level=-1 https://github.com/COSIMA/access-om2/issues/168
- dropped support for CORE and minimal configs (mark as deprecated) https://github.com/COSIMA/access-om2/issues/183
- use safer min_thickness https://github.com/mom-ocean/MOM5/issues/307 and https://github.com/mom-ocean/MOM5/pull/303
- fix PBS directives for gadi https://opus.nci.org.au/display/Help/Preparing+for+Gadi

- Fix salt restoring file at 0.1 and 0.25 deg https://github.com/COSIMA/access-om2/issues/74
- use mppnccombine-fast at 0.1 and 0.25 deg and https://github.com/COSIMA/access-om2/issues/154 and https://github.com/COSIMA/access-om2/issues/168
- tidy namelists for easy comparison across new configs; con: hard to compare to old configs (need to use nmltab) https://arccss.slack.com/archives/C6PP0GU9Y/p1589497779266600
- remove cdbot from MOM namelist - it is unused, since cdbot_law_of_wall=false (the default) https://github.com/COSIMA/access-om2/issues/200
- merge sync_output_to_gdata.sh and RM_SYNCHED_OUTPUT.sh into one script with a –remove-source-files option https://github.com/COSIMA/access-om2/issues/171
- delete any ice.log.task_* files that only have a 105-character header and nothing else
- Fixed up Rayleigh damping locations at 1 degree: see section 3.2.7 and https://github.com/COSIMA/access-om2/issues/156 and https://github.com/COSIMA/1deg_core_nyf/issues/1
- fixed vertical grid issue https://github.com/COSIMA/access-om2/issues/159
- Stop using 2nd order conservative remapping until we work out how to avoid negative values: https://github.com/COSIMA/access-om2/issues/71 and https://github.com/COSIMA/access-om2/issues/74#issuecomment-454660871
- Compress CICE output https://github.com/COSIMA/cice5/issues/26
- let payu determine the total ncpus https://github.com/payu-org/payu/issues/97
- put date in MOM output filenames, and make outputs a consistent length (e.g. monthly at 0.1 deg) https://github.com/COSIMA/access-om2/issues/185; also have one file per field
- use Large and Yeager (2009) latitude-dependent ocean albedo (cst_ocn_albedo=false) https://github.com/COSIMA/access-om2/issues/172. Note that this differs from MOM5's ocean_albedo_option=3 formula, which depends on zenith angle.
- removed some redundant items from input.nml
- Diagnostics
  - Consistent ocean and ice diag outputs across all resolutions, including monthly outputs of 3d fields in coarse runs
  - Output squared velocity components (for EKE)
  - Output all terms to close heat budget: https://github.com/COSIMA/access-om2/issues/139 and https://github.com/COSIMA/access-om2/issues/142
  - output min SST as well as mean — min is useful for comparison with foundation temperature or night time obs.
  - save max MLD as well as mean
  - Don't duplicate outputs from CICE and MOM (and prefer output from MOM as it is parallel)
  - Daily polynya and ice-production related diagnostics from CICE: f_frzmlt, f_frazil, f_congel
- updated model components to support WOMBAT BGC (https://github.com/mom-ocean/MOM5/pull/317 and https://github.com/COSIMA/cice5/pull/47 and https://github.com/COSIMA/access-om2/pull/199)
- automatically do run_summary.py

- New topography at 1 deg and 0.25 deg, now based on GEBCO 2014 and fixing many issues: https://github.com/COSIMA/access-om2/issues/141 and https://github.com/COSIMA/access-om2/issues/158 and https://github.com/mom-ocean/MOM5/issues/172 and https://github.com/COSIMA/access-om2/issues/210
- update MOM to fix ty_trans_int_z diagnostic bug: https://github.com/COSIMA/access-om2/issues/220
- turned off daily output from CICE as it is a serial bottleneck: https://github.com/COSIMA/cice5/issues/34
- update model components to support PIO for CICE https://github.com/COSIMA/cice5/issues/34
- update NetCDF version to get compression with parallel I/O (PIO) in CICE https://github.com/COSIMA/access-om2/issues/166
- generalised spatiotemporal forcing perturbations https://github.com/COSIMA/access-om2/wiki/Tutorials#Scaling-the-forcing-fields

5.2 At 0.1 degree

- Use improved bathymetry that
  - Sets min_thick to the top level thickness in bathymetry, removing terraces in shallow water: https://github.com/COSIMA/access-om2/issues/99
  - Removes Severny Island seamounts
  - Fills in very fine bathymetry near tripoles https://github.com/COSIMA/access-om2/issues/126
- Fixed misaligned CICE grid https://github.com/COSIMA/access-om2/issues/190
- Use conservative temperature https://github.com/COSIMA/access-om2/issues/97 and omit pottemp_equal_contemp so it defaults to false: https://github.com/COSIMA/access-om2/issues/148
- fixed 0.1 degree vertical grid issue https://github.com/COSIMA/access-om2/issues/161
- Use explicit vertical diffusivity, spatially uniform (j09_bgmax=j09_bgmin=$1 \times 10^{-6}\,\mathrm{m^2 s^{-1}}$). See https://github.com/COSIMA/access-om2/issues/134 see https://github.com/rmholmes/cosima-scripts/blob/master/Equatorial_Pacific_Analysis/Equatorial_Pacific_Thermal_Bias.ipynb

6 TODO for v2.0.0

- check parameter agreement with ACCESS-CM2 at 1deg
- set GM limits to 100-1200m2/s for 1deg to match ACCESS-CM2?
- use Langmuir mixing at 1 deg to match ACCESS-CM2 ?
- increase non-equatorial vertical diffusivity to match ACCESS-CM2?
- remove static fields from CICE output https://github.com/COSIMA/access-om2/issues/201

6.1 at 0.1 deg

- fix land masks for 0.1deg https://github.com/COSIMA/access-om2/issues/198
- calculate wavenumber spectra to see if we need different viscosity - see https://github.com/COSIMA/ACCESS-OM2-1-025-010deg-report/blob/master/figures/spectra/spectra.ipynb
- Try increased lateral viscosity to reduce vorticity noise? Or does non-terraced topography fix this? https://github.com/COSIMA/access-om2/issues/107

7 Things to improve for next time

See https://github.com/COSIMA/access-om2/issues.

7.1 For all resolutions

- explicit melt ponds in CCSM3, as in ACCESS-CM2 and Ridley et al. (2018)? only really relevant for Arctic
- distributed iceberg discharge (solid runoff) and latent heat — improves retention of Antarctic summer sea ice in ACCESS-CM2j
- Diagnostics
  - Make cice output more like SIMIP (Notz et al., 2016)?
  - Outputs like HighResMIP (Haarsma et al., 2016)?
- fix up access attributes at start of sync_data.sh (access seems to get stuffed up if this times out) https://climatefluidphysics.slack.com/archives/C0104HQ8K50/p1586838051081000 and https://climatefluidphysics.slack.com/archives/G010Q6Z28UA/p1589959710003200**TODO:** see comments in .tex
- when available, check whether normalbw is cheaper than gadi normal (may need to recompile for this) https://opus.nci.org.au/display/Help/Broadwell+Compute+Nodes
- Use an updated version of JRA55-do when they've fixed the cyclone sign problem: https://github.com/COSIMA/access-om2/issues/186
- Performance: Maybe the -ftz option could be worth trying, in case denormalised floats are hampering performance? or -fpe0?
- Consistent physical parameters: https://github.com/COSIMA/access-om2/issues/121 and https://github.com/COSIMA/access-om2/issues/22 - also see emails 26-27 Nov 2018
- Do separate forcing cycles rather than consecutive: https://github.com/COSIMA/access-om2/issues/149
- Upgrade OASIS https://github.com/COSIMA/access-om2/issues/85
- Use WOA2018 for initial condition and salt restoring? https://www.nodc.noaa.gov/OC5/woa18/ — like WOA13v2, WOA2018 has discontinuities and noise in Arctic surface salinity https://github.com/COSIMA/access-om2/issues/103 — but OMIP specifies WOA13v2
- As recommended by Tsujino et al. (2018a), for consistency with JRA55-do, use Gill (1982) bulk formulas instead of Large and Yeager (2004, 2009)? Also see Brodeau et al. (2017).
- Absolute or relative wind? https://github.com/COSIMA/access-om2/issues/79 and https://github.com/COSIMA/access-om2/issues/137 Add Rio et al. (2014) climatological mean surface ocean current to JRA55-do as recommended by Tsujino et al. (2018a)? But this suggestion has never been tested and is not widely supported (especially for high resolution) and no groups seem to be doing it — obs data may not be good enough. Also this attempts to deal with the adjustment of JRA55-do to match observed mean winds, but not the effect of ocean eddies in the scatterometer data ingested into the JRA55 reanalysis.
- TEOS-10? - requires conservative temp and absolute salinity; doing it properly requires an additional salt tracer, but nobody does it that way. It isn't more expensive than pre-TEOS-10 - https://github.com/COSIMA/access-om2/issues/140.
- Investigate wavy ice features in 0.25deg — poor EVP convergence? https://github.com/COSIMA/access-om2/issues/87

- increase ndte? Hunke said CICE consortium now uses ndte=240 instead of 120 - better for high resolution - worth doing some tests?
- parallel I/O in MOM? Yang et al. (2019)

7.2 At 1 degree

- disable NCAR boundary scaling of viscosity in tripole? https://github.com/mom-ocean/MOM5/issues/282#issuecomment-520634586

7.3 At 0.1 degree

Easy things:

- sort out run performance degradation https://github.com/COSIMA/access-om2/issues/192
- Use non-mushy ice thermodynamics for speed (may need to tweak restarts to make freezing point compatible?)
- Include Antarctic glacial ice tongues, e.g. Mertz, Dalton etc? they can produce polynyas in their lee but model can only represent them as peninsulas so will this cause more problems with currents? (and maybe no polynyas, if current separates and recirculates since it can't flow under ice tongue)
- experiment with EAP? Naughten (2018) found it improved things
- is runoff cap needed now we have Russ' ice salinity fix? try larger runoff caps, e.g. to avoid Ob outflow being smeared into the embayment to its west? e.g. see /g/data/hh5/tmp/cosima/access-om2-01/01deg_jra55v13_iaf/output194/ocean/ocean_month.nc
- fix Ob runoff misdirection https://github.com/COSIMA/access-om2/issues/130

Harder things:

- Sort out noise in surface vertical tracer diffusion https://github.com/COSIMA/access-om2/issues/110 - back-port MOM6 KPP fix to MOM5? or use this? https://github.com/mom-ocean/MOM5/issues/264 and https://github.com/mom-ocean/MOM5/issues/265 and https://github.com/mom-ocean/MOM5/issues/267
- Fix bug at tripole seam https://github.com/COSIMA/access-om2/issues/86
- Move tripoles further from ocean to increase minimum cell size
- Distributed iceberg freshwater and heat flux, using JRA55-do 1.4.0 solid runoff
- Separate solid and liquid runoff caps for JRA55-do v1.4.0
- Basal melt at depth
- Improve Gulf Stream variability distribution — see Renault et al. (2016, 2019a,b)
- Gulf Stream separation issue: https://github.com/COSIMA/access-om2/issues/151

8 Acknowledgments

Model development has been partly funded by ARC Linkage grant LP160100073. Runs were undertaken on the NCI National Facility in Canberra, which is supported by the Australian Commonwealth Government.

A Namelists

These tables show the namelist files used for the final run of each model spinup. Changes to namelists within these spinups are tabulated in Appendix B.

These tables are auto-generated by namelists/make_tables.py which uses nmltab (https://github.com/aekiss/nmltab). Variables are weblinks to source code searches. Variables that differ between the models are highlighted. Greyed values are ignored.

TODO: generate complete tables that include the default values of parameters not specified in namelists

A.1 ACCESS-OM2 namelist accessom2.nml

Group	Variable	./gadi/g/data/hh5/tmp/cosima/access-om2/1deg_jra55v13_iaf_spinup1_B1/output059/accessom2.nml	./gadi/g/data/hh5/tmp/cosima/access-om2-025/025deg_jra55v13_iaf_gmredi6/output153/accessom2.nml	./gadi/g/data/hh5/tmp/cosima/access-om2-01/01deg_jra55v13_iaf/output197/accessom2.nml
&accessom2_nml	ice_ocean_timestep	5400	1350	450
	log_level	'DEBUG'	'DEBUG'	'DEBUG'
&date_manager_nml	forcing_end_date	'2018-01-01T00:00:00'	'2018-01-01T00:00:00'	'2018-01-01T00:00:00'
	forcing_start_date	'1958-01-01T00:00:00'	'1958-01-01T00:00:00'	'1985-01-01T00:00:00'
	restart_period	5, 0, 0	1, 0, 0	0, 2, 0

A.2 MOM namelist input.nml

Group	Variable	./gadi/g/data/hh5/tmp/cosima/access-om2/1deg_jra55v13_iaf_spinup1_B1/output059/ocean/input.nml	./gadi/g/data/hh5/tmp/cosima/access-om2-025/025deg_jra55v13_iaf_gmredi6/output153/ocean/input.nml	./gadi/g/data/hh5/tmp/cosima/access-om2-01/01deg_jra55v13_iaf/output197/ocean/input.nml
&auscom_ice_nml	aice_cutoff	0.15	0.15	0.15
	chk_i2o_fields	False	False	False
	chk_o2i_fields	False	False	False
	do_ice_once	False	False	False
	fixmeltt	False	False	False
	frazil_factor	1.0	1.0	1.0
	iceform_adj_salt	False	False	False
	icemlt_factor	1.0	1.0	1.0

Group (continued)	Variable	./gadi/g/data/hh5/tmp/cosima/access-om2/1deg_jra55v13_-iaf_spinup1_B1/output059/ocean/input.nml	./gadi/g/data/hh5/tmp/cosima/access-om2-025/025deg_-jra55v13_iaf_-gmredi6/output153/ocean/input.nml	./gadi/g/data/hh5/tmp/cosima/access-om2-01/01deg_jra55v13_-iaf/output197/ocean/input.nml
	kmxice	5	5	5
	pop_icediag	True	True	True
	redsea_gulfbay_sfix	False		
	sign_stflx	1.0	1.0	1.0
	tmelt	−0.216	−0.216	−0.216
	use_ioaice	True	True	True
&diag_manager_nml	debug_diag_manager	False	True	True
	issue_oor_warnings	True	True	True
&fms_io_nml	checksum_required			False
	fileset_write	'single'	'single'	'multi'
	threading_read	'multi'	'multi'	'multi'
	threading_write	'single'	'single'	'multi'
&fms_nml	clock_grain	'LOOP'	'LOOP'	'ROUTINE'
	domains_stack_size	115200		115200
&mom_oasis3_interface_nml	fields_in	'u_flux', 'v_flux', 'lprec', 'fprec', 'salt_flx', 'mh_flux', 'sw_flux', 'q_flux', 't_flux', 'lw_flux', 'runof', 'p', 'aice', 'wfimelt', 'wfiform'	'u_flux', 'v_flux', 'lprec', 'fprec', 'salt_flx', 'mh_flux', 'sw_flux', 'q_flux', 't_flux', 'lw_flux', 'runof', 'p', 'aice', 'wfimelt', 'wfiform'	'u_flux', 'v_flux', 'lprec', 'fprec', 'salt_flx', 'mh_flux', 'sw_flux', 'q_flux', 't_flux', 'lw_flux', 'runof', 'p', 'aice', 'wfimelt', 'wfiform'
	fields_out	't_surf', 's_surf', 'u_surf', 'v_surf', 'dssldx', 'dssldy', 'frazil'	't_surf', 's_surf', 'u_surf', 'v_surf', 'dssldx', 'dssldy', 'frazil'	't_surf', 's_surf', 'u_surf', 'v_surf', 'dssldx', 'dssldy', 'frazil'
	num_fields_in	15	15	15
	num_fields_out	7	7	7
	send_after_ocean_update	True	True	True
	send_before_ocean_update	False	False	False
&monin_obukhov_nml	neutral	True	True	True
&mpp_io_nml	deflate_level	5	5	5
	shuffle	1	1	1
&ocean_adv_vel_diag_nml	diag_step	4320	4320	576
	large_cfl_value	10.0	10.0	10.0
	max_cfl_value	100.0	100.0	100.0
	verbose_cfl	True	True	True
&ocean_advection_velocity_nml	max_advection_velocity	0.5	0.5	0.3
&ocean_albedo_nml	ocean_albedo_option	2	2	2
&ocean_barotropic_nml	barotropic_halo	10	10	10
	barotropic_time_stepping_a	True	True	True
	barotropic_time_stepping_b	False	False	False
	debug_this_module	False	False	False
	diag_step	4320	4320	576
	eta_max	8.0	8.0	8.0
	frac_crit_cell_height	0.2	0.2	0.2
	pred_corr_gamma	0.2	0.2	0.2
	smooth_eta_diag_laplacian	True	True	True
	smooth_eta_t_biharmonic	False	False	False
	smooth_eta_t_laplacian	True	True	True
	smooth_pbot_t_biharmonic	False	False	False
	smooth_pbot_t_laplacian	True	True	True

Group (continued)	Variable	./gadi/g/data/hh5/tmp/cosima/access-om2/1deg_jra55v13_-iaf_spinup1_B1/output059/ocean/input.nml	./gadi/g/data/hh5/tmp/cosima/access-om2-025/025deg_-jra55v13_iaf_-gmredi6/output153/ocean/input.nml	./gadi/g/data/hh5/tmp/cosima/access-om2-01/01deg_jra55v13_-iaf/output197/ocean/input.nml
	truncate_eta	False	False	False
	use_legacy_barotropic_halos	False	False	False
	vel_micom_bih	0.01	0.01	0.01
	vel_micom_lap	0.05	0.05	0.05
	vel_micom_lap_diag	0.2	0.2	0.2
	verbose_truncate	True	True	True
	zero_tendency	False	False	False
&ocean_bbc_nml	bmf_implicit	True	True	True
	cdbot	0.001	0.001	0.001
	cdbot_hi	0.007	0.007	0.007
	cdbot_roughness_length	False	False	False
	cdbot_roughness_uamp	True	True	True
	uresidual	0.05	0.05	0.05
	use_geothermal_heating	False	False	False
&ocean_bih_friction_nml	bih_friction_scheme	'general'	'general'	'general'
&ocean_bih_tracer_nml	use_this_module	False	False	False
&ocean_bihcst_friction_nml	use_this_module	False	False	False
&ocean_bihgen_friction_nml	bottom_5point	True	False	False
	eq_lat_micom	0.0	0.0	0.0
	eq_vel_micom_aniso	0.0	0.0	0.0
	eq_vel_micom_iso	0.0	0.0	0.0
	equatorial_zonal	False	False	False
	k_smag_aniso	0.0	0.0	0.0
	k_smag_iso	2.0	2.0	2.0
	ncar_boundary_scaling	True	True	True
	ncar_boundary_scaling_read	False	False	False
	ncar_rescale_power	2	2	2
	ncar_vconst_4	2×10^{-8}	2×10^{-8}	2×10^{-8}
	ncar_vconst_5	5	5	5
	use_this_module	True	True	True
	vel_micom_aniso	0.0	0.0	0.0
	vel_micom_bottom	0.01	0.0	0.0
	vel_micom_iso	0.04	0.0	0.0
	visc_crit_scale	0.25	1.0	1.0
&ocean_convect_nml	use_this_module	False	False	False
&ocean_coriolis_nml	acor	0.5	0.5	0.5
	use_this_module	True	True	True
&ocean_density_nml	eos_linear	False	False	False
	eos_preteos10	True	True	True
	layer_nk	80	80	80
	neutralrho_max	1030.0	1030.0	1030.0
	neutralrho_min	1020.0	1020.0	1020.0
	potrho_max	1038.0	1038.0	1038.0
	potrho_min	1028.0	1028.0	1028.0
&ocean_domains_nml	max_tracers	5	5	5
&ocean_form_drag_nml	use_this_module	False	False	False
&ocean_frazil_nml	debug_this_module	False	False	False
	frazil_only_in_surface	False	False	False
	freezing_temp_preteos10	True	True	True
	freezing_temp_simple	False	False	False
	use_this_module	True	True	True

Group (continued)	Variable	./gadi/g/data/hh5/tmp/cosima/access-om2/1deg_jra55v13_-iaf_spinup1_B1/output059/ocean/input.nml	./gadi/g/data/hh5/tmp/cosima/access-om2-025/025deg_-jra55v13_iaf_-gmredi6/output153/ocean/input.nml	./gadi/g/data/hh5/tmp/cosima/access-om2-01/01deg_jra55v13_-iaf/output197/ocean/input.nml
&ocean_grids_nml	debug_this_module	False	False	False
&ocean_increment_eta_nml	use_this_module	False	False	False
&ocean_increment_tracer_nml	use_this_module	False	False	False
&ocean_increment_velocity_nml	use_this_module	False	False	False
&ocean_lap_friction_nml	lap_friction_scheme	'general'	'general'	'general'
&ocean_lap_tracer_nml	use_this_module	False	False	False
&ocean_lapcst_friction_nml	use_this_module	False	False	False
&ocean_lapgen_friction_nml	bottom_5point	True		
	k_smag_aniso	0.0		
	k_smag_iso	0.0		
	restrict_polar_visc	True		
	restrict_polar_visc_lat	60.0		
	restrict_polar_visc_ratio	0.35		
	use_this_module	True	False	False
	vel_micom_iso	0.1		
	viscosity_ncar	False		
	viscosity_ncar_2007	False		
	viscosity_scale_by_rossby	True		
	viscosity_scale_by_rossby_power	4.0		
&ocean_mixdownslope_nml	debug_this_module	False		
	mixdownslope_mask_gfdl	False		
	mixdownslope_npts	4		
	read_mixdownslope_mask	False		
	use_this_module	True	False	False
&ocean_model_nml	baroclinic_split	1	1	1
	barotropic_split	80	80	80
	cmip_units	True	True	True
	debug	False	False	False
	io_layout	4, 3	6, 5	5, 5
	layout	16, 15	48, 40	80, 75
	surface_height_split	1	1	1
	time_tendency	'twolevel'	'twolevel'	'twolevel'
	vertical_coordinate	'zstar'	'zstar'	'zstar'
&ocean_momentum_source_nml	rayleigh_damp_exp_from_bottom	False	False	False
	use_rayleigh_damp_table	True	True	True
	use_this_module	True	True	True
&ocean_nphysics_nml	debug_this_module	False	False	False
	use_nphysicsa	False	False	False
	use_nphysicsb	False	False	False
	use_nphysicsc	True	True	False
	use_this_module	True	True	False
&ocean_nphysics_util_nml	agm	600.0	200.0	100.0
	agm_closure	True	True	True
	agm_closure_baroclinic	True	True	True
	agm_closure_buoy_freq	0.004	0.004	0.004
	agm_closure_eady_ave_mixed	True	True	
	agm_closure_eady_cap	True	True	
	agm_closure_eady_smooth_horz	True	True	
	agm_closure_eady_smooth_vert	True	True	
	agm_closure_eden_gamma	0.0	0.0	
	agm_closure_eden_greatbatch	False	False	

Group (continued)	Variable	./gadi/g/data/hh5/tmp/cosima/access-om2/1deg_jra55v13_-iaf_spinup1_B1/output059/ocean/input.nml	./gadi/g/data/hh5/tmp/cosima/access-om2-025/025deg_-jra55v13_iaf_-gmredi6/output153/ocean/input.nml	./gadi/g/data/hh5/tmp/cosima/access-om2-01/01deg_jra55v13_-iaf/output197/ocean/input.nml
	agm_closure_grid_scaling	True	True	
	agm_closure_length	50 000.0	20 000.0	50 000.0
	agm_closure_length_bczone	False	False	False
	agm_closure_length_fixed	False	False	False
	agm_closure_length_rossby	False	False	False
	agm_closure_lower_depth	2000.0	2000.0	2000.0
	agm_closure_max	600.0	200.0	600.0
	agm_closure_min	50.0	1.0	100.0
	agm_closure_scaling	0.07	0.07	0.07
	agm_closure_upper_depth	100.0	100.0	100.0
	agm_damping_time	45.0	45.0	
	agm_smooth_space	False	False	
	agm_smooth_time	False	False	
	aredi	600.0	200.0	600.0
	aredi_diffusivity_grid_scaling		True	
	aredi_equal_agm	False	False	False
	drhodz_mom4p1	True	False	False
	drhodz_smooth_horz	False	False	False
	drhodz_smooth_vert	False	False	False
	nphysics_util_zero_init	True	True	
	rossby_radius_max	100 000.0	100 000.0	100 000.0
	rossby_radius_min	15 000.0	10 000.0	15 000.0
	tracer_mix_micom	False	False	False
	vel_micom	0.0	0.0	0.0
&ocean_nphysicsa_nml	use_this_module	False	False	False
&ocean_nphysicsb_nml	use_this_module	False	False	False
&ocean_nphysicsc_nml	bv_freq_smooth_vert	True	True	
	bvp_bc_mode	2	2	
	bvp_min_speed	0.1	0.1	
	bvp_speed	0.0	0.0	
	debug_this_module	False	False	
	do_gm_skewsion	True	True	
	do_neutral_diffusion	True	True	
	epsln_bv_freq	1×10^{-12}	1×10^{-12}	
	gm_skewsion_bvproblem	True	True	
	gm_skewsion_modes	False	False	
	neutral_eddy_depth	True	True	
	neutral_physics_limit	True	True	
	number_bc_modes	2	2	
	regularize_psi	False	False	
	smax_psi	0.01	0.01	
	smooth_psi	True	True	
	tmask_neutral_on	True	True	
	turb_blayer_min	50.0	50.0	
	use_this_module	True	True	False
&ocean_operators_nml	use_legacy_div_ud	False	False	False
&ocean_overexchange_nml	debug_this_module	False	False	False
	overexch_npts	4	4	4
	overexch_weight_far	False	False	False
	overflow_umax	5.0	5.0	5.0
	use_this_module	False	False	False

Group (continued)	Variable	./gadi/g/data/hh5/tmp/cosima/access-om2/1deg_jra55v13_-iaf_spinup1_B1/output059/ocean/input.nml	./gadi/g/data/hh5/tmp/cosima/access-om2-025/025deg_-jra55v13_iaf_-gmredi6/output153/ocean/input.nml	./gadi/g/data/hh5/tmp/cosima/access-om2-01/01deg_jra55v13_-iaf/output197/ocean/input.nml
&ocean_overflow_nml	use_this_module	False	False	False
&ocean_overflow_ofp_nml	use_this_module	False	False	False
&ocean_polar_filter_nml	use_this_module	False	False	False
&ocean_pressure_nml	zero_pressure_force	False	False	False
&ocean_rivermix_nml	debug_this_module	False	False	False
	river_diffuse_salt	True	True	True
	river_diffuse_temp	True	True	True
	river_diffusion_thickness	0.0	0.0	0.0
	river_diffusivity	0.0	0.0	0.0
	river_insertion_thickness	40.0	40.0	40.0
	use_this_module	True	True	True
&ocean_riverspread_nml	debug_this_module			False
	use_this_module	False	False	False
&ocean_rough_nml	rough_scheme	'beljaars'	'beljaars'	'beljaars'
&ocean_sbc_nml	avg_sfc_temp_salt_eta	True	True	True
	avg_sfc_velocity	True	True	True
	calvingspread	False	False	False
	do_bitwise_exact_sum	True	False	False
	do_flux_correction	False	False	False
	land_model_heat_fluxes	False	False	False
	max_delta_salinity_restore	−0.5	0.5	0.5
	max_ice_thickness	0.0	0.0	0.0
	ocean_ice_salt_limit			0.006
	read_restore_mask	False	False	False
	restore_mask_gfdl	False	False	False
	runoff_salinity	0.0	0.0	0.0
	runoffspread			False
	salt_correction_scale	0.0	0.0	0.0
	salt_restore_as_salt_flux	True	True	True
	salt_restore_tscale	21.28	21.28	10.0
	salt_restore_under_ice	True	True	True
	temp_restore_tscale	−10.0	−10.0	−10.0
	use_full_patm_for_sea_level	False	False	False
	use_waterflux	True	True	True
	zero_heat_fluxes	False	False	False
	zero_net_salt_correction	False	False	False
	zero_net_salt_restore	True	True	True
	zero_net_water_correction	False	False	False
	zero_net_water_couple_restore	True	True	True
	zero_net_water_coupler	True	True	True
	zero_net_water_restore	True	True	True
	zero_surface_stress	False	False	False
	zero_water_fluxes	False	False	False
&ocean_shortwave_csiro_nml	use_this_module	False	False	False
&ocean_shortwave_gfdl_nml	debug_this_module	False	False	False
	enforce_sw_frac	True	True	True
	optics_manizza	True	True	True
	optics_morel_antoine	False	False	False
	read_chl	True	True	True
	use_this_module	True	True	True
	zmax_pen	300.0	300.0	300.0

Group (continued)	Variable	./gadi/g/data/hh5/tmp/cosima/access-om2/1deg_jra55v13_-iaf_spinup1_B1/output059/ocean/input.nml	./gadi/g/data/hh5/tmp/cosima/access-om2-025/025deg_-jra55v13_iaf_-gmredi6/output153/ocean/input.nml	./gadi/g/data/hh5/tmp/cosima/access-om2-01/01deg_jra55v13_-iaf/output197/ocean/input.nml
&ocean_shortwave_jerlov_nml	use_this_module	False	False	False
&ocean_shortwave_nml	use_shortwave_csiro	False	False	False
	use_shortwave_gfdl	True	True	True
	use_shortwave_jerlov	False	False	False
	use_this_module	True	True	True
&ocean_sigma_transport_nml	use_this_module	True	False	False
&ocean_sponges_eta_nml	use_this_module	False	False	False
&ocean_sponges_tracer_nml	use_this_module	False	False	False
&ocean_sponges_velocity_nml	use_this_module	False	False	False
&ocean_submesoscale_nml	coefficient_ce	0.05	0.05	0.05
	debug_this_module	False	False	False
	front_length_const	5000.0	5000.0	5000.0
	front_length_deform_radius	True	True	True
	limit_psi	True	True	True
	limit_psi_velocity_scale	0.5	0.5	0.5
	min_kblt	4	4	4
	smooth_advect_transport	True	True	True
	smooth_advect_transport_num	2	4	4
	smooth_hblt	False	False	False
	smooth_psi	True	True	True
	smooth_psi_num	2	3	3
	submeso_advect_flux	False	False	False
	submeso_advect_limit	True	True	True
	submeso_advect_upwind	True	True	True
	submeso_advect_zero_bdy	True	True	True
	submeso_diffusion	False	False	False
	submeso_diffusion_biharmonic	True	True	True
	submeso_diffusion_scale	10.0	10.0	10.0
	submeso_skew_flux	True	True	True
	use_hblt_equal_mld	True	True	True
	use_psi_legacy	False	False	False
	use_this_module	True	True	True
&ocean_tempsalt_nml	debug_this_module	False	False	False
	pottemp_2nd_iteration	True	True	True
	pottemp_equal_contemp	True	True	True
	s_max	70.0	70.0	70.0
	s_max_limit	42.0	42.0	42.0
	s_min	0.0	0.0	0.0
	s_min_limit	2.0	2.0	2.0
	t_max	55.0	55.0	55.0
	t_max_limit	32.0	32.0	32.0
	t_min	−20.0	−20.0	−20.0
	t_min_limit	−5.0	−5.0	−5.0
	temperature_variable	'conservative_temp'	'conservative_temp'	'potential_temp'
&ocean_thickness_nml	debug_this_module	False	False	False
	debug_this_module_detail	False	False	False
	rescale_mass_to_get_ht_mod	False	False	False
	thickness_method	'energetic'	'energetic'	'energetic'
&ocean_tracer_advect_nml	debug_this_module	False	False	False
	read_basin_mask	False	False	False
&ocean_tracer_diag_nml	diag_step	4320	4320	576

Group (continued)	Variable	./gadi/g/data/hh5/tmp/cosima/access-om2/1deg_jra55v13_-iaf_spinup1_B1/output059/ocean/input.nml	./gadi/g/data/hh5/tmp/cosima/access-om2-025/025deg_-jra55v13_iaf_-gmredi6/output153/ocean/input.nml	./gadi/g/data/hh5/tmp/cosima/access-om2-01/01deg_jra55v13_-iaf/output197/ocean/input.nml
	do_bitwise_exact_sum	False	False	False
	tracer_conserve_days	30.0	30.0	30.0
&ocean_tracer_nml	age_tracer_max_init	0.0	0.0	0.0
	debug_this_module	False	False	False
	frazil_heating_after_vphysics	True	True	True
	frazil_heating_before_vphysics	False	False	False
	limit_age_tracer	True	True	True
	remap_depth_to_s_init	False	False	False
	use_tempsalt_check_range	True	True	True
	zero_tendency	False	False	False
	zero_tracer_source	False	False	False
&ocean_velocity_diag_nml	debug_this_module	False	False	False
	diag_step	4320	4320	576
	energy_diag_step	4320	4320	5760
	large_cfl_value	10.0	10.0	10.0
	max_cfl_value	100.0	100.0	100.0
&ocean_velocity_nml	adams_bashforth_third	True	True	True
	max_cgint	1.0	1.0	1.0
	truncate_velocity	False	False	False
	truncate_velocity_value	2.0	2.0	2.0
	truncate_verbose	True	True	True
	zero_tendency	False	False	False
	zero_tendency_explicit_a	False	False	False
	zero_tendency_explicit_b	False	False	False
	zero_tendency_implicit	False	False	False
&ocean_vert_kpp_iow_nml	use_this_module	False	False	False
&ocean_vert_kpp_mom4p1_nml	diff_cbt_iw	0.0	0.0	0.0
	double_diffusion	True	True	True
	kbl_standard_method	False	False	False
	ricr	0.3	0.3	0.3
	smooth_blmc	False	False	False
	smooth_ri_kmax_eq_kmu	True	True	True
	use_this_module	True	True	True
	visc_cbu_iw	0.0	0.0	0.0
&ocean_vert_mix_nml	aidif	1.0	1.0	1.0
	bryan_lewis_diffusivity	False	False	False
	bryan_lewis_lat_depend	False	False	False
	hwf_diffusivity	False	False	False
	hwf_min_diffusivity	2×10^{-6}	2×10^{-6}	2×10^{-6}
	hwf_n0_2omega	20.0	20.0	20.0
	j09_bgmax	5×10^{-6}		
	j09_bgmin	1×10^{-6}		
	j09_diffusivity	True		
	j09_lat	20.0		
	use_diff_cbt_table	False	False	False
	vert_diff_back_via_max	True	True	True
	vert_mix_scheme	'kpp_mom4p1'	'kpp_mom4p1'	'kpp_mom4p1'
&ocean_vert_tidal_nml	background_diffusivity	0.0	0.0	0.0
	background_viscosity	0.0001	0.0001	0.0001
	decay_scale	500.0	500.0	500.0
	drag_dissipation_use_cdbot	True	True	True

Group (continued)	Variable	./gadi/g/data/hh5/tmp/cosima/access-om2/1deg_jra55v13_iaf_spinup1_B1/output059/ocean/input.nml	./gadi/g/data/hh5/tmp/cosima/access-om2-025/025deg_jra55v13_iaf_gmredi6/output153/ocean/input.nml	./gadi/g/data/hh5/tmp/cosima/access-om2-01/01deg_jra55v13_iaf/output197/ocean/input.nml
	drhodz_min	1×10^{-10}	1×10^{-10}	1×10^{-10}
	fixed_wave_dissipation	False	False	False
	max_wave_diffusivity	0.01	0.01	0.01
	mixing_efficiency_n2depend	True	True	True
	read_roughness	True	True	True
	read_tide_speed	True	True	True
	read_wave_dissipation	False	False	False
	reading_roughness_amp	True	True	True
	reading_roughness_length	False	False	False
	roughness_scale	12 000.0	12 000.0	12 000.0
	shelf_depth_cutoff	−1000.0	−1000.0	−1000.0
	tide_speed_data_on_t_grid	True	True	True
	use_drag_dissipation	True	True	True
	use_legacy_methods	False	False	False
	use_this_module	True	True	True
	use_wave_dissipation	True	True	True
	wave_energy_flux_max	0.1	0.1	0.1
&ocean_xlandinsert_nml	use_this_module	False	False	False
&ocean_xlandmix_nml	use_this_module	False	False	False
&xgrid_nml	do_alltoall			True
	do_alltoallv			True
	interp_method	'second_order'	'second_order'	'second_order'
	make_exchange_reproduce	False	False	False
	nsubset	16	16	16

A.3 CICE namelists

See https://ncar.github.io/CICE/users_guide/ice_nml_var.html.

A.3.1 cice_in.nml

Group	Variable	./gadi/g/data/hh5/tmp/cosima/access-om2/1deg_jra55v13_iaf_spinup1_B1/output059/ice/cice_in.nml	./gadi/g/data/hh5/tmp/cosima/access-om2-025/025deg_jra55v13_iaf_gmredi6/output153/ice/cice_in.nml	./gadi/g/data/hh5/tmp/cosima/access-om2-01/01deg_jra55v13_iaf/output197/ice/cice_in.nml
&domain_nml	distribution_type	'cartesian'	'roundrobin'	'roundrobin'
	distribution_wght	'latitude'	'latitude'	'latitude'
	ew_boundary_type	'cyclic'	'cyclic'	'cyclic'
	maskhalo_bound	True	True	True
	maskhalo_dyn	True	True	True
	maskhalo_remap	True	True	True
	nprocs	24	361	1600
	ns_boundary_type	'tripole'	'tripole'	'tripole'
	processor_shape	'slenderX1'	'square-ice'	'square-ice'

Group (continued)	Variable	./gadi/g/data/hh5/tmp/cosima/access-om2/1deg_jra55v13_-iaf_spinup1_B1/output059/ice/cice_in.nml	./gadi/g/data/hh5/tmp/cosima/access-om2-025/025deg_-jra55v13_iaf_-gmredi6/output153/ice/cice_in.nml	./gadi/g/data/hh5/tmp/cosima/access-om2-01/01deg_jra55v13_-iaf/output197/ice/cice_in.nml
&dynamics_nml	advection	'remap'	'remap'	'remap'
	cosw	1.0	1.0	1.0
	dragio	0.005 36	0.005 36	0.005 36
	iceruf	0.0005	0.0005	0.0005
	kdyn	1	1	1
	krdg_partic	1	1	1
	krdg_redist	1	1	1
	kstrength	1	1	1
	mu_rdg	3	3	3
	ndte	120	120	120
	revised_evp	False	False	False
	sinw	0.0	0.0	0.0
&forcing_nml	atm_data_dir	'unknown_atm_-data_dir'	'unknown_atm_-data_dir'	'unknown_atm_-data_dir'
	atm_data_format	'nc'	'nc'	'nc'
	atm_data_type	'default'	'default'	'default'
	atmbndy	'default'	'default'	'default'
	calc_strair	True	True	True
	calc_tsfc	True	True	True
	formdrag	False	False	False
	fyear_init	1	1	1
	oceanmixed_file	'unknown_-oceanmixed_file'	'unknown_-oceanmixed_file'	'unknown_-oceanmixed_file'
	oceanmixed_ice	False	False	False
	ocn_data_dir	'unknown_ocn_-data_dir'	'unknown_ocn_-data_dir'	'unknown_ocn_-data_dir'
	ocn_data_format	'nc'	'nc'	'nc'
	precip_units	'mks'	'mks'	'mks'
	restore_ice	False	False	False
	restore_sst	False	False	False
	sss_data_type	'default'	'default'	'default'
	sst_data_type	'default'	'default'	'default'
	tfrz_option	'linear_salt'	'linear_salt'	'mushy'
	trestore	0	0	0
	update_ocn_f	True	True	True
	ustar_min	0.0005	0.0005	0.0005
	ycycle	1	1	1
&grid_nml	grid_file	'RESTART/grid.nc'	'RESTART/grid.nc'	'RESTART/grid.nc'
	grid_format	'nc'	'nc'	'nc'
	grid_type	'tripole'	'tripole'	'tripole'
	kcatbound	0	0	0
	kmt_file	'RESTART/kmt.nc'	'RESTART/kmt.nc'	'RESTART/kmt.nc'
&icefields_bgc_nml	f_aero	'x'	'x'	'x'
	f_bgc_am_ml	'x'	'x'	'x'
	f_bgc_am_sk	'x'	'x'	'x'
	f_bgc_c_sk	'x'	'x'	'x'
	f_bgc_chl_sk	'x'	'x'	'x'
	f_bgc_dms_sk	'x'	'x'	'x'
	f_bgc_dmsp_ml	'x'	'x'	'x'
	f_bgc_dmspd_sk	'x'	'x'	'x'
	f_bgc_dmspp_sk	'x'	'x'	'x'
	f_bgc_n_sk	'x'	'x'	'x'

Group (continued)	Variable	./gadi/g/data/hh5/tmp/cosima/access-om2/1deg_jra55v13_-iaf_spinup1_B1/output059/ice/cice_in.nml	./gadi/g/data/hh5/tmp/cosima/access-om2-025/025deg_-jra55v13_iaf_-gmredi6/output153/ice/cice_in.nml	./gadi/g/data/hh5/tmp/cosima/access-om2-01/01deg_jra55v13_-iaf/output197/ice/cice_in.nml
	f_bgc_nit_ml	'x'	'x'	'x'
	f_bgc_nit_sk	'x'	'x'	'x'
	f_bgc_sil_ml	'x'	'x'	'x'
	f_bgc_sil_sk	'x'	'x'	'x'
	f_bphi	'x'	'x'	'x'
	f_btin	'x'	'x'	'x'
	f_faero_atm	'x'	'x'	'x'
	f_faero_ocn	'x'	'x'	'x'
	f_fbri	'm'	'm'	'x'
	f_fn	'x'	'x'	'x'
	f_fn_ai	'x'	'x'	'x'
	f_fnh	'x'	'x'	'x'
	f_fnh_ai	'x'	'x'	'x'
	f_fno	'x'	'x'	'x'
	f_fno_ai	'x'	'x'	'x'
	f_fsil	'x'	'x'	'x'
	f_fsil_ai	'x'	'x'	'x'
	f_grownet	'x'	'x'	'x'
	f_hbri	'm'	'm'	'x'
	f_ppnet	'x'	'x'	'x'
&icefields_drag_nml	f_cdn_atm	'x'	'x'	'x'
	f_cdn_ocn	'x'	'x'	'x'
	f_drag	'x'	'x'	'x'
&icefields_mechred_nml	f_alvl	'm'	'm'	'm'
	f_aparticn	'x'	'x'	'x'
	f_araftn	'x'	'x'	'x'
	f_ardg	'm'	'm'	'm'
	f_ardgn	'x'	'x'	'x'
	f_aredistn	'x'	'x'	'x'
	f_dardg1dt	'x'	'x'	'x'
	f_dardg1ndt	'x'	'x'	'x'
	f_dardg2dt	'x'	'x'	'x'
	f_dardg2ndt	'x'	'x'	'x'
	f_dvirdgdt	'x'	'x'	'x'
	f_dvirdgndt	'x'	'x'	'x'
	f_krdgn	'x'	'x'	'x'
	f_opening	'x'	'm'	'm'
	f_vlvl	'm'	'm'	'x'
	f_vraftn	'x'	'x'	'x'
	f_vrdg	'm'	'm'	'x'
	f_vrdgn	'x'	'x'	'x'
	f_vredistn	'x'	'x'	'x'
&icefields_nml	f_aice	'm'	'm'	'md'
	f_aicen	'm'	'm'	'md'
	f_aisnap	'x'	'x'	'x'
	f_albice	'm'	'm'	'x'
	f_albpnd	'x'	'x'	'x'
	f_albsni	'm'	'm'	'x'
	f_albsno	'm'	'm'	'x'
	f_alidr	'x'	'x'	'x'
	f_alvdr	'x'	'x'	'x'
	f_angle	True	True	True

Group (continued)	Variable	./gadi/g/data/hh5/tmp/cosima/access-om2/1deg_jra55v13_-iaf_spinup1_B1/output059/ice/cice_in.nml	./gadi/g/data/hh5/tmp/cosima/access-om2-025/025deg_-jra55v13_iaf_-gmredi6/output153/ice/cice_in.nml	./gadi/g/data/hh5/tmp/cosima/access-om2-01/01deg_jra55v13_-iaf/output197/ice/cice_in.nml
	f_anglet	True	True	True
	f_bounds	False	False	False
	f_congel	'm'	'm'	'm'
	f_coszen	'x'	'x'	'x'
	f_daidtd	'm'	'm'	'x'
	f_daidtt	'm'	'm'	'x'
	f_divu	'm'	'm'	'md'
	f_dsnow	'x'	'x'	'x'
	f_dvidtd	'm'	'm'	'x'
	f_dvidtt	'm'	'm'	'x'
	f_dxt	True	True	True
	f_dxu	True	True	True
	f_dyt	True	True	True
	f_dyu	True	True	True
	f_evap	'x'	'x'	'x'
	f_evap_ai	'm'	'm'	'x'
	f_fcondtop_ai	'm'	'm'	'x'
	f_fcondtopn_ai	'm'	'm'	'x'
	f_fhocn	'x'	'x'	'x'
	f_fhocn_ai	'm'	'm'	'x'
	f_flat	'x'	'x'	'x'
	f_flat_ai	'm'	'm'	'x'
	f_flatn_ai	'm'	'm'	'm'
	f_flwdn	'm'	'm'	'x'
	f_flwup	'x'	'x'	'x'
	f_flwup_ai	'm'	'm'	'x'
	f_fmeltt_ai	'x'	'm'	'm'
	f_fmelttn_ai	'm'	'm'	'x'
	f_frazil	'm'	'm'	'm'
	f_fresh	'x'	'x'	'x'
	f_fresh_ai	'm'	'm'	'x'
	f_frz_onset	'm'	'm'	'm'
	f_frzmlt	'm'	'm'	'x'
	f_fsalt	'x'	'x'	'd'
	f_fsalt_ai	'm'	'x'	'd'
	f_fsens	'x'	'x'	'x'
	f_fsens_ai	'm'	'm'	'x'
	f_fsurf_ai	'x'	'x'	'x'
	f_fsurfn_ai	'm'	'm'	'x'
	f_fswabs	'x'	'x'	'x'
	f_fswabs_ai	'm'	'm'	'x'
	f_fswdn	'm'	'm'	'x'
	f_fswfac	'm'	'm'	'x'
	f_fswthru	'x'	'x'	'x'
	f_fswthru_ai	'm'	'm'	'x'
	f_fy	'x'	'x'	'x'
	f_hi	'm'	'm'	'md'
	f_hisnap	'x'	'x'	'x'
	f_hs	'm'	'm'	'md'
	f_hte	True	True	True
	f_htn	True	True	True
	f_iage	'm'	'm'	'm'

Group (continued)	Variable	./gadi/g/data/hh5/tmp/cosima/access-om2/1deg_jra55v13_-iaf_spinup1_B1/output059/ice/cice_in.nml	./gadi/g/data/hh5/tmp/cosima/access-om2-025/025deg_-jra55v13_iaf_-gmredi6/output153/ice/cice_in.nml	./gadi/g/data/hh5/tmp/cosima/access-om2-01/01deg_jra55v13_-iaf/output197/ice/cice_in.nml
	f_icepresent	'm'	'm'	'x'
	f_meltb	'm'	'm'	'x'
	f_meltl	'm'	'm'	'x'
	f_melts	'm'	'm'	'x'
	f_meltt	'm'	'm'	'x'
	f_mlt_onset	'm'	'm'	'm'
	f_ncat	True	True	True
	f_qref	'x'	'x'	'x'
	f_rain	'x'	'x'	'x'
	f_rain_ai	'm'	'm'	'x'
	f_shear	'm'	'm'	'md'
	f_sice	'm'	'm'	'x'
	f_sig1	'x'	'm'	'md'
	f_sig2	'x'	'm'	'md'
	f_sinz	'x'	'x'	'x'
	f_snoice	'm'	'm'	'x'
	f_snow	'x'	'x'	'x'
	f_snow_ai	'm'	'm'	'x'
	f_sss	'm'	'x'	'd'
	f_sst	'm'	'x'	'd'
	f_strairx	'm'	'm'	'md'
	f_strairy	'm'	'm'	'md'
	f_strcorx	'm'	'm'	'x'
	f_strcory	'm'	'm'	'x'
	f_strength	'm'	'm'	'm'
	f_strintx	'm'	'm'	'x'
	f_strinty	'm'	'm'	'x'
	f_strocnx	'm'	'm'	'x'
	f_strocny	'm'	'm'	'x'
	f_strtltx	'm'	'm'	'x'
	f_strtlty	'm'	'm'	'x'
	f_tair	'm'	'm'	'x'
	f_tarea	True	True	True
	f_tinz	'x'	'x'	'x'
	f_tmask	True	True	True
	f_tref	'x'	'x'	'x'
	f_trsig	'm'	'm'	'x'
	f_tsfc	'm'	'm'	'm'
	f_tsnz	'x'	'x'	'x'
	f_uarea	True	True	True
	f_uocn	'm'	'x'	'd'
	f_uvel	'm'	'm'	'md'
	f_vgrdb	False	False	False
	f_vgrdi	False	False	False
	f_vgrds	False	False	False
	f_vicen	'm'	'm'	'md'
	f_vocn	'm'	'x'	'd'
	f_vvel	'm'	'm'	'md'
&icefields_pond_nml	f_apeff	'm'	'm'	'x'
	f_apeff_ai	'm'	'm'	'x'
	f_apeffn	'x'	'x'	'x'
	f_apond	'm'	'm'	'x'

Group (continued)	Variable	./gadi/g/data/hh5/tmp/cosima/access-om2/1deg_jra55v13_-iaf_spinup1_B1/output059/ice/cice_in.nml	./gadi/g/data/hh5/tmp/cosima/access-om2-025/025deg_-jra55v13_iaf_-gmredi6/output153/ice/cice_in.nml	./gadi/g/data/hh5/tmp/cosima/access-om2-01/01deg_jra55v13_-iaf/output197/ice/cice_in.nml
	f_apond_ai	'm'	'm'	'x'
	f_apondn	'x'	'x'	'x'
	f_hpond	'm'	'm'	'x'
	f_hpond_ai	'm'	'm'	'x'
	f_hpondn	'x'	'x'	'x'
	f_ipond	'm'	'm'	'x'
	f_ipond_ai	'm'	'm'	'x'
&ponds_nml	dpscale	0.001	0.001	0.001
	frzpnd	'hlid'	'hlid'	'hlid'
	hp1	0.01	0.01	0.01
	hs0	0.0	0.0	0.0
	hs1	0.03	0.03	0.03
	pndaspect	0.8	0.8	0.8
	rfracmax	1.0	1.0	1.0
	rfracmin	0.15	0.15	0.15
&setup_nml	days_per_year	365	365	365
	dbug	False	False	False
	diag_file	'ice_diag.d'	'ice_diag.d'	'ice_diag.d'
	diag_type	'file'	'file'	'file'
	diagfreq	960	960	960
	dt	3600	1800	300
	dump_last	True	True	True
	dumpfreq	'y'	'y'	'm'
	dumpfreq_n	1	1	3
	hist_avg	True	True	True
	histfreq	'd', 'm', 'x', 'x', 'x'	'd', 'm', 'x', 'x', 'x'	'd', 'm', 'x', 'x', 'x'
	histfreq_n	1, 1, 1, 1, 1	1, 1, 1, 1, 1	1, 1, 1, 1, 1
	history_dir	'./OUTPUT/'	'./OUTPUT/'	'./OUTPUT/'
	history_file	'iceh'	'iceh'	'iceh'
	ice_ic	'default'	'default'	'default'
	incond_dir	'./OUTPUT/'	'./OUTPUT/'	'./OUTPUT/'
	incond_file	'iceh_ic'	'iceh_ic'	'iceh_ic'
	istep0	2067360	341496	3906432
	latpnt	90.0, −65.0	90.0, −65.0	66.75, 68.0
	lcdf64	False	True	True
	lonpnt	0.0, −45.0	0.0, −45.0	72.5, 74.0
	ndtd	1	1	3
	npt	35 040.0	2232.0	6480
	pointer_file	'./RESTART/ice.restart_file'	'./RESTART/ice.restart_file'	'./RESTART/ice.restart_file'
	print_global	False	False	False
	print_points	False	False	False
	restart	True	True	True
	restart_dir	'./RESTART/'	'./RESTART/'	'./RESTART/'
	restart_ext	False	False	False
	restart_file	'iced'	'iced'	'iced'
	restart_format	'nc'	'nc'	'nc'
	runtype	'continue'	'continue'	'continue'
	use_leap_years	False	False	False
	use_restart_time	True	True	True
	write_ic	False	False	False

Group (continued)	Variable	./gadi/g/data/hh5/tmp/cosima/access-om2/1deg_jra55v13_iaf_spinup1_B1/output059/ice/cice_in.nml	./gadi/g/data/hh5/tmp/cosima/access-om2-025/025deg_jra55v13_iaf_gmredi6/output153/ice/cice_in.nml	./gadi/g/data/hh5/tmp/cosima/access-om2-01/01deg_jra55v13_iaf/output197/ice/cice_in.nml
	year_init	1	1	1
&shortwave_nml	ahmax	0.1	0.1	0.1
	albedo_type	'default'	'default'	'default'
	albicei	0.44	0.44	0.44
	albicev	0.86	0.86	0.86
	albsnowi	0.7	0.7	0.7
	albsnowv	0.98	0.98	0.98
	dalb_mlt	−0.02	−0.02	−0.02
	dt_mlt	1.0	1.0	1.0
	r_ice	0.0	0.0	0.0
	r_pnd	0.0	0.0	0.0
	r_snw	0.0	0.0	0.0
	rsnw_mlt	1500.0	1500.0	1500.0
	shortwave	'default'	'default'	'default'
	tocnfrz	−1.8	−1.8	−1.8
&thermo_nml	a_rapid_mode	0.0005	0.0005	0.0005
	aspect_rapid_mode	1.0	1.0	1.0
	chio	0.004	0.004	0.004
	conduct	'bubbly'	'bubbly'	'bubbly'
	dsdt_slow_mode	-5×10^{-8}	-5×10^{-8}	-5×10^{-8}
	kitd	1	1	1
	ktherm	1	1	2
	phi_c_slow_mode	0.05	0.05	0.05
	phi_i_mushy	0.85	0.85	0.85
	rac_rapid_mode	10.0	10.0	10.0
&tracer_nml	restart_aero	False	False	False
	restart_age	False	False	False
	restart_fy	False	False	False
	restart_lvl	False	False	False
	restart_pond_cesm	False	False	False
	restart_pond_lvl	False	False	False
	restart_pond_topo	False	False	False
	tr_aero	False	False	False
	tr_fy	False	False	False
	tr_iage	False	False	False
	tr_lvl	False	False	False
	tr_pond_cesm	False	False	False
	tr_pond_lvl	False	False	False
	tr_pond_topo	False	False	False
&zbgc_nml	bgc_data_dir	'unknown_bgc_data_dir'	'unknown_bgc_data_dir'	'unknown_bgc_data_dir'
	bgc_flux_type	'Jin2006'	'Jin2006'	'Jin2006'
	nit_data_type	'default'	'default'	'default'
	phi_snow	0.5	0.5	0.5
	restart_bgc	False	False	False
	restart_hbrine	False	False	False
	restore_bgc	False	False	False
	sil_data_type	'default'	'default'	'default'
	skl_bgc	False	False	False
	tr_bgc_am_sk	False	False	False
	tr_bgc_c_sk	False	False	False
	tr_bgc_chl_sk	False	False	False

Group (continued)	Variable	./gadi/g/data/hh5/tmp/cosima/access-om2/1deg_jra55v13_-iaf_spinup1_B1/output059/ice/cice_in.nml	./gadi/g/data/hh5/tmp/cosima/access-om2-025/025deg_-jra55v13_iaf_-gmredi6/output153/ice/cice_in.nml	./gadi/g/data/hh5/tmp/cosima/access-om2-01/01deg_jra55v13_-iaf/output197/ice/cice_in.nml
	tr_bgc_dms_sk	False	False	False
	tr_bgc_dmspd_sk	False	False	False
	tr_bgc_dmspp_sk	False	False	False
	tr_bgc_sil_sk	False	False	False
	tr_brine	False	False	False

A.3.2 input_ice.nml

Group	Variable	./gadi/g/data/hh5/tmp/cosima/access-om2/1deg_jra55v13_-iaf_spinup1_B1/output059/ice/input_ice.nml	./gadi/g/data/hh5/tmp/cosima/access-om2-025/025deg_-jra55v13_iaf_-gmredi6/output153/ice/input_ice.nml	./gadi/g/data/hh5/tmp/cosima/access-om2-01/01deg_jra55v13_-iaf/output197/ice/input_ice.nml
&coupling_nml	chk_a2i_fields	False	False	False
	chk_frzmlt_sst		False	False
	chk_gfdl_roughness	False	False	False
	chk_i2a_fields		False	False
	chk_i2o_fields		False	False
	chk_o2i_fields		False	False
	cst_ocn_albedo	True	True	True
	gfdl_surface_flux	True	True	True
	ice_fwflux	True	True	True
	ice_pressure_on	True	True	True
	limit_icemelt	False	False	False
	meltlimit	−200.0	−200.0	−200.0
	ocn_albedo	0.1	0.1	0.1
	pop_icediag	True	True	True
	precip_factor	1.0	1.0	1.0
	rotate_winds	True	True	True
	use_ocnslope	False	False	False
	use_umask	False	False	False

A.3.3 input_ice_gfdl.nml

Group	Variable	./gadi/g/data/hh5/tmp/cosima/access-om2/1deg_jra55v13_-iaf_spinup1_B1/output059/ice/input_ice_gfdl.nml	./gadi/g/data/hh5/tmp/cosima/access-om2-025/025deg_-jra55v13_iaf_-gmredi6/output153/ice/input_ice_gfdl.nml	./gadi/g/data/hh5/tmp/cosima/access-om2-01/01deg_jra55v13_-iaf/output197/ice/input_ice_-gfdl.nml
&ocean_rough_nml	charnock	0.032	0.032	0.032
	do_cap40	False	False	False

Group (continued)	Variable	./gadi/g/data/hh5/tmp/cosima/access-om2/1deg_jra55v13_-iaf_spinup1_B1/output059/ice/input_ice_gfdl.nml	./gadi/g/data/hh5/tmp/cosima/access-om2-025/025deg_-jra55v13_iaf_-gmredi6/output153/ice/input_ice_gfdl.nml	./gadi/g/data/hh5/tmp/cosima/access-om2-01/01deg_jra55v13_-iaf/output197/ice/input_ice_-gfdl.nml
	do_highwind	False	False	False
	rough_scheme	'beljaars'	'beljaars'	'beljaars'
	roughness_heat	5.8×10^{-5}	5.8×10^{-5}	5.8×10^{-5}
	roughness_min	1×10^{-6}	1×10^{-6}	1×10^{-6}
	roughness_moist	5.8×10^{-5}	5.8×10^{-5}	5.8×10^{-5}
	roughness_mom	5.8×10^{-5}	5.8×10^{-5}	5.8×10^{-5}
	zcoh1	0.0	0.0	0.0
	zcoq1	0.0	0.0	0.0
&surface_flux_nml	alt_gustiness	False	False	False
	gust_const	1.0	1.0	1.0
	gust_min	0.0	0.0	0.0
	ncar_ocean_flux	True	True	True
	ncar_ocean_flux_orig	False	False	False
	no_neg_q	False	False	False
	old_dtaudv	False	False	False
	raoult_sat_vap	False	False	False
	use_mixing_ratio	False	False	False
	use_virtual_temp	True	True	True

A.3.4 input_ice_monin.nml

Group	Variable	./gadi/g/data/hh5/tmp/cosima/access-om2/1deg_jra55v13_-iaf_spinup1_B1/output059/ice/input_ice_-monin.nml	./gadi/g/data/hh5/tmp/cosima/access-om2-025/025deg_-jra55v13_iaf_-gmredi6/output153/ice/input_ice_-monin.nml	./gadi/g/data/hh5/tmp/cosima/access-om2-01/01deg_jra55v13_-iaf/output197/ice/input_ice_-monin.nml
&monin_obukhov_nml	neutral	True	True	True

A.4 YATM namelist atm.nml

Group	Variable	./gadi/g/data/hh5/tmp/cosima/access-om2/1deg_jra55v13_-iaf_spinup1_B1/output059/atmosphere/atm.nml	./gadi/g/data/hh5/tmp/cosima/access-om2-025/025deg_-jra55v13_iaf_-gmredi6/output153/atmosphere/atm.nml	./gadi/g/data/hh5/tmp/cosima/access-om2-01/01deg_jra55v13_-iaf/output197/atmosphere/atm.nml
&runoff_nml	num_runoff_caps			4
	remap_weights_file	'INPUT/rmp_jrar_to_cict_-CONSERV.nc'	'INPUT/rmp_jrar_to_cict_-CONSERV.nc'	'INPUT/rmp_jrar_to_cict_-CONSERV.nc'

Group (continued)	Variable	./gadi/g/data/hh5/tmp/cosima/access-om2/1deg_jra55v13_-iaf_spinup1_B1/output059/atmosphere/atm.nml	./gadi/g/data/hh5/tmp/cosima/access-om2-025/025deg_-jra55v13_iaf_-gmredi6/output153/atmosphere/atm.nml	./gadi/g/data/hh5/tmp/cosima/access-om2-01/01deg_jra55v13_-iaf/output197/atmosphere/atm.nml
	runoff_caps			0.03, 0.001, 0.003, 0.003
	runoff_caps_ie			1000000, 3530, 240, 560
	runoff_caps_is			0, 3470, 180, 300
	runoff_caps_je			1000000, 2650, 99999, 2470
	runoff_caps_js			0, 2270, 2670, 2260

B Namelist changes within runs

These are auto-generated by namelists/make_tables.py which uses nmltab (https://github.com/aekiss/nmltab). Variables are weblinks to source code searches. Only differences are shown, and consecutive identical namelists in a run are omitted. Differences in timestep counters are ignored. Tables are omitted if there are no differences at all.

B.1 ACCESS-OM2 namelist accessom2.nml

Group	Variable	./gadi/g/data/hh5/tmp/cosima/access-om2-025/025deg_-jra55v13_iaf_-gmredi6/output000/accessom2.nml	./gadi/g/data/hh5/tmp/cosima/access-om2-025/025deg_-jra55v13_iaf_-gmredi6/output022/accessom2.nml	./gadi/g/data/hh5/tmp/cosima/access-om2-025/025deg_-jra55v13_iaf_-gmredi6/output078/accessom2.nml	./gadi/g/data/hh5/tmp/cosima/access-om2-025/025deg_-jra55v13_iaf_-gmredi6/output082/accessom2.nml	./gadi/g/data/hh5/tmp/cosima/access-om2-025/025deg_-jra55v13_iaf_-gmredi6/output085/accessom2.nml	./gadi/g/data/hh5/tmp/cosima/access-om2-025/025deg_-jra55v13_iaf_-gmredi6/output086/accessom2.nml	./gadi/ hh5/tmp/ access-om 02 jra55v1 gr outp accesso
&acc	nml							
	ice_-ocea time	1800	1350	1800	1350	1200	1350	
&da	man ager nml resta pe-riod	2, 0, 0	2, 0, 0	2, 0, 0	2, 0, 0	2, 0, 0	2, 0, 0	

Group Variable	./gadi/g/data/hh5/tmp/cosima/access-om2-01/01deg_jra55v13_-iaf/output001/accessom2.nml	./gadi/g/data/hh5/tmp/cosima/access-om2-01/01deg_jra55v13_-iaf/output005/accessom2.nml	./gadi/g/data/hh5/tmp/cosima/access-om2-01/01deg_jra55v13_-iaf/output021/accessom2.nml	./gadi/g/data/hh5/tmp/cosima/access-om2-01/01deg_jra55v13_-iaf/output022/accessom2.nml	./gadi/g/data/hh5/tmp/cosima/access-om2-01/01deg_jra55v13_-iaf/output023/accessom2.nml	./gadi/g/data/hh5/tmp/cosima/access-om2-01/01deg_jra55v13_-iaf/output029/accessom2.nml	./gadi/ hh5/tmp/ access-o 01deg_jra5 iaf/outp accesso
&acc nml ice_-ocea time	540	450	300	450	450	400	
&dat man ager nml resta pe-riod	0, 3, 0	0, 2, 0	0, 1, 0	0, 1, 0	0, 2, 0	0, 2, 0	

B.2 MOM namelist input.nml

B.3 CICE namelists

B.3.1 cice_in.nml

Changes to istep0 are ignored.

Group	Variable	./gadi/g/data/hh5/tmp/cosima/access-om2/1deg_jra55v13_-iaf_spinup1_B1/output000/ice/cice_in.nml	./gadi/g/data/hh5/tmp/cosima/access-om2/1deg_jra55v13_-iaf_spinup1_B1/output001/ice/cice_in.nml
&setup_nml	restart	False	True
	runtype	'initial'	'continue'

Group	Variable	./gadi/g/data/hh5/tmp/cosima/access-om2-025/025deg_-jra55v13_iaf_-gmredi6/output000/ice/cice_in.nml	./gadi/g/data/hh5/tmp/cosima/access-om2-025/025deg_-jra55v13_iaf_-gmredi6/output001/ice/cice_in.nml
&setup_nml	restart	False	True
	runtype	'initial'	'continue'

Group	Variable	./gadi/g/data/hh5/tmp/cosima/access-om2-01/01deg_jra55v13_-iaf/output001/ice/cice_in.nml	./gadi/g/data/hh5/tmp/cosima/access-om2-01/01deg_jra55v13_-iaf/output002/ice/cice_in.nml	./gadi/g/data/hh5/tmp/cosima/access-om2-01/01deg_jra55v13_-iaf/output010/ice/cice_in.nml	./gadi/g/data/hh5/tmp/cosima/access-om2-01/01deg_jra55v13_-iaf/output115/ice/cice_in.nml
&domain_nml	distribution_type	'cartesian'	'cartesian'	'cartesian'	'roundrobin'
	nprocs	2000	2000	2000	1600
&icefields_nml	f_aicen	'd'	'd'	'md'	'md'
	f_hs	'm'	'm'	'md'	'md'
	f_vicen	'm'	'm'	'md'	'md'
&setup_nml	use_restart_time	False	True	True	True

B.3.2 input_ice.nml

B.3.3 input_ice_gfdl.nml

B.3.4 input_ice_monin.nml

B.4 YATM namelist atm.nml

C Namelist differences from profiling runs

These are auto-generated by namelists/make_tables.py which uses nmltab (https://github.com/aekiss/nmltab). Variables are weblinks to source code searches. Only differences are shown, and duplicate identical profiling namelists are omitted. Differences in timestep counters are ignored. Tables are omitted if there are no differences at all.

*deg runs were used for MOM5 profiling, and *cice runs were used for CICE5 profiling.

C.1 ACCESS-OM2 namelist accessom2.nml

Group	Variable	./gadi/g/data/hh5/tmp/cosima/raijin-short-public/mxw900/home/mxw157/om2bench/1cice/1cice_24p/accessom2.nml	./gadi/g/data/hh5/tmp/cosima/raijin-short-public/mxw900/home/mxw157/om2bench/1deg/1deg_216p/accessom2.nml	./gadi/g/data/hh5/tmp/cosima/access-om2/1deg_jra55v13_iaf_spinup1_B1/output059/accessom2.nml
&accessom2_nml	enable_simple_timers	True		
&date_manager_nml	restart_period	0, 2, 0	0, 2, 0	5, 0, 0

Group	Variable	./gadi/g/data/hh5/tmp/cosima/raijin-short-public/mxw900/home/mxw157/om2bench/025cice/025cice_1206p/accessom2.nml	./gadi/g/data/hh5/tmp/cosima/access-om2-025/025deg_jra55v13_iaf_gmredi6/output153/accessom2.nml
&accessom2_nml	ice_ocean_timestep	1800	1350
&date_manager_nml	restart_period	0, 0, 864000	1, 0, 0

Group	Variable	./gadi/g/data/hh5/tmp/cosima/raijin-short-public/mxw900/home/mxw157/om2bench/01deg/01deg_8489p/accessom2.nml	./gadi/g/data/hh5/tmp/cosima/access-om2-01/01deg_jra55v13_iaf/output197/accessom2.nml
&accessom2_nml	ice_ocean_timestep	400	450
&date_manager_nml	restart_period	0, 0, 86400	0, 2, 0

C.2 MOM namelist input.nml

Group Variable	./gadi/g/data/hh5/tmp/cosima/raijin-short-public/mxw900/home/mxw157/om2bench/1deg/1deg_216p/ocean/input.nml	./gadi/g/data/hh5/tmp/cosima/raijin-short-public/mxw900/home/mxw157/om2bench/1deg/1deg_60p/ocean/input.nml	./gadi/g/data/hh5/tmp/cosima/raijin-short-public/mxw900/home/mxw157/om2bench/1deg/1deg_407p/ocean/input.nml	./gadi/g/data/hh5/tmp/cosima/raijin-short-public/mxw900/home/mxw157/om2bench/1deg/1deg_116p/ocean/input.nml	./gadi/g/data/hh5/tmp/cosima/raijin-short-public/mxw900/home/mxw157/om2bench/1deg/1deg_784p/ocean/input.nml	./gadi/g/data/hh5/tmp/cosima/access-om2/1deg_jra55v13_iaf_spinup1_B1/output059/ocean/input.nml
&aui ice_nml red-sea_ gulf-bay_ sfix	True	True	True	True	True	False
&fm io_nml chec sum_ re-quire	False	False	False	False	False	
&fm nml do-mair stack size	115200	115200	152000	115200	152000	115200
&oc mod nml io_ lay-out	4, 3	3, 2	6, 4	3, 2	8, 6	4, 3
lay-out	16, 15	6, 10	24, 20	12, 10	32, 30	16, 15
&oc sbc_ nml max_ delta salin ity_ re-store	0.5	0.5	0.5	0.5	0.5	—0.5
salt_ re-store tscal	60.0	60.0	60.0	60.0	60.0	21.28

Group Variable	./gadi/g/data/hh5/tmp/cosima/raijin-short-public/mxw900/home/mxw157/om2bench/025deg/025deg_213p/ocean/input.nml	./gadi/g/data/hh5/tmp/cosima/raijin-short-public/mxw900/home/mxw157/om2bench/025deg/025deg_5425p/ocean/input.nml	./gadi/g/data/hh5/tmp/cosima/raijin-short-public/mxw900/home/mxw157/om2bench/025deg/025deg_395p/ocean/input.nml	./gadi/g/data/hh5/tmp/cosima/raijin-short-public/mxw900/home/mxw157/om2bench/025deg/025deg_1455p/ocean/input.nml	./gadi/g/data/hh5/tmp/cosima/raijin-short-public/mxw900/home/mxw157/om2bench/025deg/025deg_2801p/ocean/input.nml	./gadi/g/data/hh5/tmp/cosima/raijin-short-public/mxw900/home/mxw157/om2bench/025deg/025deg_761p/ocean/input.nml	./gadi/ hh5/tmp/ raijin public/mx home/mx om2 025deg/02 10634p/ in
&fms_io_nml checksum_required	False	False	False		False	False	
&ocean_model_nml io_layout	4, 5	12, 10	4, 5	6, 5	8, 6	4, 5	
layout	16, 15	96, 80	24, 20	48, 40	64, 60	32, 30	1
&ocean_sbc_nml salt_restore_tscale	60.0	60.0	60.0	60.0	60.0	60.0	

Group Variable	./gadi/g/data/hh5/tmp/cosima/raijin-short-public/mxw900/home/mxw157/om2bench/01deg/01deg_8489p/ocean/input.nml	./gadi/g/data/hh5/tmp/cosima/raijin-short-public/mxw900/home/mxw157/om2bench/01deg/01deg_2245p/ocean/input.nml	./gadi/g/data/hh5/tmp/cosima/raijin-short-public/mxw900/home/mxw157/om2bench/01deg/01deg_4358p/ocean/input.nml	./gadi/g/data/hh5/tmp/cosima/raijin-short-public/mxw900/home/mxw157/om2bench/01deg/01deg_16577p/ocean/input.nml	./gadi/g/data/hh5/tmp/cosima/raijin-short-public/mxw900/home/mxw157/om2bench/01deg/01deg_619p/ocean/input.nml	./gadi/g/data/hh5/tmp/cosima/raijin-short-public/mxw900/home/mxw157/om2bench/01deg/01deg_1180p/ocean/input.nml	./gadi/ hh5/tmp/ raijin public/mx home/mx om2bench/ 01deg_3 ocean/in
&ocean_model_nml io_layout	25, 16	6, 5	5, 5	16, 15	5, 5	3, 5	
layout	125, 96	60, 50	80, 75	160, 150	30, 25	30, 50	2

C.3 CICE namelists

C.3.1 cice_in.nml

Changes to istep0 are ignored.

Group Variable	./gadi/g/data/hh5/tmp/cosima/raijin-short-public/mxw900/home/mxw157/om2bench/1cice/1cice_24p/ice/cice_in.nml	./gadi/g/data/hh5/tmp/cosima/raijin-short-public/mxw900/home/mxw157/om2bench/1cice/1cice_180p/ice/cice_in.nml	./gadi/g/data/hh5/tmp/cosima/raijin-short-public/mxw900/home/mxw157/om2bench/1cice/1cice_45p/ice/cice_in.nml	./gadi/g/data/hh5/tmp/cosima/raijin-short-public/mxw900/home/mxw157/om2bench/1cice/1cice_90p/ice/cice_in.nml	./gadi/g/data/hh5/tmp/cosima/raijin-short-public/mxw900/home/mxw157/om2bench/1cice/1cice_12p/ice/cice_in.nml	./gadi/g/data/hh5/tmp/cosima/raijin-short-public/mxw900/home/mxw157/om2bench/1cice/1cice_6p/ice/cice_in.nml	./gadi/ hh5/tmp/ raijin public/mx home/mx om2bench 1cice_36 cice
&do nml npro	24	180	45	90	12	6	
&dy nml cosw	0.96	0.96	0.96	0.96	0.96	0.96	
sinw	0.28	0.28	0.28	0.28	0.28	0.28	
&set nml di- agfre	24	24	24	24	24	24	
resta	False	False	False	False	False	False	
runty	'initial'	'initial'	'initial'	'initial'	'initial'	'initial'	

Group Variable	./gadi/g/data/hh5/tmp/cosima/raijin-short-public/mxw900/home/mxw157/om2bench/025cice/025cice_-1206p/ice/cice_in.nml	./gadi/g/data/hh5/tmp/cosima/raijin-short-public/mxw900/home/mxw157/om2bench/025cice/025cice_-190p/ice/cice_in.nml	./gadi/g/data/hh5/tmp/cosima/raijin-short-public/mxw900/home/mxw157/om2bench/025cice/025cice_-99p/ice/cice_in.nml	./gadi/g/data/hh5/tmp/cosima/raijin-short-public/mxw900/home/mxw157/om2bench/025cice/025cice_-361p/ice/cice_in.nml	./gadi/g/data/hh5/tmp/cosima/raijin-short-public/mxw900/home/mxw157/om2bench/025cice/025cice_-2212p/ice/cice_in.nml	./gadi/g/data/hh5/tmp/cosima/raijin-short-public/mxw900/home/mxw157/om2bench/025cice/025cice_-697p/ice/cice_in.nml	./gadi/ hh5/tmp/ access-om 02 jra55v1 gr output1 cice
&do nml dis- tri- bu- tion_ type	'sectrobin'	'sectrobin'	'sectrobin'	'sectrobin'	'sectrobin'	'sectrobin'	'rou
npro	1206	190	99	361	2212	697	

Group (continued) Variable	./gadi/g/data/hh5/tmp/cosima/raijin-short-public/mxw900/home/mxw157/om2bench/025cice/025cice_1206p/ice/cice_in.nml	./gadi/g/data/hh5/tmp/cosima/raijin-short-public/mxw900/home/mxw157/om2bench/025cice/025cice_190p/ice/cice_in.nml	./gadi/g/data/hh5/tmp/cosima/raijin-short-public/mxw900/home/mxw157/om2bench/025cice/025cice_99p/ice/cice_in.nml	./gadi/g/data/hh5/tmp/cosima/raijin-short-public/mxw900/home/mxw157/om2bench/025cice/025cice_361p/ice/cice_in.nml	./gadi/g/data/hh5/tmp/cosima/raijin-short-public/mxw900/home/mxw157/om2bench/025cice/025cice_2212p/ice/cice_in.nml	./gadi/g/data/hh5/tmp/cosima/raijin-short-public/mxw900/home/mxw157/om2bench/025cice/025cice_697p/ice/cice_in.nml	./gadi/hh5/tmp/access-om02/jra55v1/gr/output1/cice
&icemecl	'x'	'x'	'x'	'x'	'x'	'x'	
nml							
f_-oper							
ing							
&icenml	'x'	'x'	'x'	'x'	'x'	'x'	
f_-fmel							
ai							
f_-fsalt	'm'	'm'	'm'	'm'	'm'	'm'	
ai							
f_-sig1	'x'	'x'	'x'	'x'	'x'	'x'	
f_-sig2	'x'	'x'	'x'	'x'	'x'	'x'	
f_-sss	'm'	'm'	'm'	'm'	'm'	'm'	
f_-sst	'm'	'm'	'm'	'm'	'm'	'm'	
f_-uocn	'm'	'm'	'm'	'm'	'm'	'm'	
f_-vocn	'm'	'm'	'm'	'm'	'm'	'm'	
&setnml	False	False	False	False	False	False	
resta							
runty	'initial'	'initial'	'initial'	'initial'	'initial'	'initial'	'c

Group Variable	./gadi/g/data/hh5/tmp/cosima/raijin-short-public/mxw900/home/mxw157/om2bench/01cice/01cice_-11935p/ice/cice_in.nml	./gadi/g/data/hh5/tmp/cosima/raijin-short-public/mxw900/home/mxw157/om2bench/01cice/01cice_-428p/ice/cice_in.nml	./gadi/g/data/hh5/tmp/cosima/raijin-short-public/mxw900/home/mxw157/om2bench/01cice/01cice_-1600p/ice/cice_in.nml	./gadi/g/data/hh5/tmp/cosima/raijin-short-public/mxw900/home/mxw157/om2bench/01cice/01cice_-828p/ice/cice_in.nml	./gadi/g/data/hh5/tmp/cosima/raijin-short-public/mxw900/home/mxw157/om2bench/01cice/01cice_-3116p/ice/cice_in.nml	./gadi/g/data/hh5/tmp/cosima/raijin-short-public/mxw900/home/mxw157/om2bench/01cice/01cice_-6077p/ice/cice_in.nml	./gadi/hh5/tmp/access-o 01deg_jra5 iaf/outp ice/cice
&do	'sectrobin'	'sectrobin'	'sectrobin'	'sectrobin'	'sectrobin'	'sectrobin'	'rou
nml							
dis-							
tri-							
bu-							
tion_							
type							
npro	11935	428	1600	828	3116	6077	
&set	False	False	False	False	False	False	
nml							
resta							
runty	'initial'	'initial'	'initial'	'initial'	'initial'	'initial'	'c

C.3.2 input_ice.nml

C.3.3 input_ice_gfdl.nml

C.3.4 input_ice_monin.nml

C.4 YATM namelist atm.nml

D Namelist differences between old and new configs

These are auto-generated by namelists/make_tables.py which uses nmltab (https://github.com/aekiss/nmltab). Variables are weblinks to source code searches. Only differences are shown, and duplicate identical profiling

namelists are omitted. Differences in timestep counters are ignored. Tables are omitted if there are no differences at all.

D.1 ACCESS-OM2 namelist accessom2.nml

Group	Variable	./gadi/g/data/hh5/tmp/cosima/access-om2/1deg_jra55v13_iaf_spinup1_B1/output059/accessom2.nml	github.com/COSIMA/1deg_jra55_iaf/accessom2.nml	github.com/COSIMA/1deg_jra55_ryf/accessom2.nml
&date_manager_nml	forcing_end_date	'2018-01-01T00:00:0(	'2019-01-01T00:00:0(	'1901-01-01T00:00:00'
	forcing_start_date	'1958-01-01T00:00:0(	'1958-01-01T00:00:0(	'1900-01-01T00:00:00'

Group	Variable	./gadi/g/data/hh5/tmp/cosima/access-om2-025/025deg_jra55v13_iaf_gmredi6/output153/accessom2.nml	github.com/COSIMA/025deg_jra55_iaf/accessom2.nml	github.com/COSIMA/025deg_jra55_ryf/accessom2.nml
&date_manager_nml	forcing_end_date	'2018-01-01T00:00:0(	'2019-01-01T00:00:0(	'1901-01-01T00:00:00'
	forcing_start_date	'1958-01-01T00:00:0(	'1958-01-01T00:00:0(	'1900-01-01T00:00:00'
	restart_period	1, 0, 0	2, 0, 0	2, 0, 0

Group	Variable	./gadi/g/data/hh5/tmp/cosima/access-om2-01/01deg_jra55v13_iaf/output197/accessom2.nml	./gadi/g/data/hh5/tmp/cosima/access-om2-01/01deg_jra55v13_ryf9091/output675/accessom2.nml	github.com/COSIMA/01deg_jra55_iaf/accessom2.nml	github.com/COSIMA/01deg_jra55_ryf/accessom2.nml
&accessom2_nml	ice_ocean_timestep	450	540	300	300
&date_manager_nml	forcing_end_date	'2018-01-01T00:00:0(	'1901-01-01T00:00:0(	'2019-01-01T00:00:0(	'1901-01-01T00:00:00'
	forcing_start_date	'1985-01-01T00:00:0(	'1900-01-01T00:00:0(	'1958-01-01T00:00:0(	'1900-01-01T00:00:00'
	restart_period	0, 2, 0	0, 3, 0	0, 3, 0	0, 3, 0

D.2 MOM namelist input.nml

Group	Variable	./gadi/g/data/hh5/tmp/cosima/access-om2/1deg_jra55v13_iaf_spinup1_B1/output059/ocean/input.nml	github.com/COSIMA/1deg_jra55_iaf/ocean/input.nml	github.com/COSIMA/1deg_jra55_ryf/ocean/input.nml
&diag_manager_nml	max_axes		400	400
	max_files		200	200
	max_num_axis_sets		200	200
&mom_oasis3_interface_nml	fields_in	'u_flux', 'v_flux', 'lprec', 'fprec', 'salt_flx', 'mh_flux', 'sw_flux', 'q_flux', 't_flux', 'lw_flux', 'runof', 'p', 'aice', 'wfimelt', 'wfiform'	'u_flux', 'v_flux', 'lprec', 'fprec', 'salt_flx', 'mh_flux', 'sw_flux', 'q_flux', 't_flux', 'lw_flux', 'runof', 'p', 'aice', 'wfimelt', 'wfiform', 'licefw', 'liceht'	'u_flux', 'v_flux', 'lprec', 'fprec', 'salt_flx', 'mh_flux', 'sw_flux', 'q_flux', 't_flux', 'lw_flux', 'runof', 'p', 'aice', 'wfimelt', 'wfiform', 'licefw', 'liceht'
	num_fields_in	15	17	17
&monin_obukhov_nml	neutral	True		
&mpp_io_nml	deflate_level	5	-1	-1
&ocean_albedo_nml	ocean_albedo_option	2		

Group (continued)	Variable	./gadi/g/data/hh5/tmp/cosima/access-om2/1deg_jra55v13_iaf_spinup1_B1/output059/ocean/input.nml	github.com/COSIMA/1deg_jra55_iaf/ocean/input.nml	github.com/COSIMA/1deg_jra55_ryf/ocean/input.nml
&ocean_barotropic_nml	debug_this_module	False		
&ocean_bbc_nml	cdbot	0.001		
	cdbot_roughness_length	False		
	use_geothermal_heating	False		
&ocean_density_nml	neutralrho_max	1030.0	1038.0	1038.0
	neutralrho_min	1020.0	1028.0	1028.0
&ocean_frazil_nml	debug_this_module	False		
&ocean_grids_nml	debug_this_module	False		
&ocean_mixdownslope_nml	debug_this_module	False		
&ocean_nphysics_nml	debug_this_module	False		
&ocean_nphysics_util_nml	agm	600.0		
	agm_closure_eden_gamma	0.0		
	agm_closure_eden_greatbatch	False		
	agm_closure_length_bczone	False		
	agm_closure_length_fixed	False		
	agm_closure_length_rossby	False		
	agm_damping_time	45.0		
	agm_smooth_space	False		
	agm_smooth_time	False		
	drhodz_smooth_horz	False		
	drhodz_smooth_vert	False		
	rossby_radius_max	100 000.0		
	rossby_radius_min	15 000.0		
	tracer_mix_micom	False		
	vel_micom	0.0		
&ocean_nphysicsc_nml	debug_this_module	False		
&ocean_operators_nml	use_legacy_div_ud	False		
&ocean_overexchange_nml	debug_this_module	False		
	overexch_npts	4		
	overexch_weight_far	False		
	overflow_umax	5.0		
&ocean_polar_filter_nml	use_this_module	False		
&ocean_pressure_nml	zero_pressure_force	False		
&ocean_rivermix_nml	debug_this_module	False		
&ocean_shortwave_gfdl_nml	debug_this_module	False		
	zmax_pen	300.0	1 000 000.0	1 000 000.0
&ocean_submesoscale_nml	debug_this_module	False		
&ocean_tempsalt_nml	debug_this_module	False		
	pottemp_equal_contemp	True		
&ocean_thickness_nml	debug_this_module	False		
&ocean_topog_nml	min_thickness		0.001	0.001
&ocean_tracer_advect_nml	debug_this_module	False		
&ocean_tracer_nml	debug_this_module	False		
&ocean_velocity_diag_nml	debug_this_module	False		
&ocean_vert_kpp_iow_nml	use_this_module	False		

Group	Variable	./gadi/g/data/hh5/tmp/cosima/access-om2-025/025deg_jra55v13_iaf_gmredi6/output153/ocean/input.nml	github.com/COSIMA/025deg_jra55_iaf/ocean/input.nml	github.com/COSIMA/025deg_jra55_ryf/ocean/input.nml
&diag_manager_nml	debug_diag_manager	True	False	False
	max_axes		400	400
	max_files		200	200
	max_num_axis_sets		200	200
&mom_oasis3_interface_nml	fields_in	'u_flux', 'v_flux', 'lprec', 'fprec', 'salt_flx', 'mh_flux', 'sw_flux', 'q_flux', 't_flux', 'lw_flux', 'runof', 'p', 'aice', 'wfimelt', 'wfiform'	'u_flux', 'v_flux', 'lprec', 'fprec', 'salt_flx', 'mh_flux', 'sw_flux', 'q_flux', 't_flux', 'lw_flux', 'runof', 'p', 'aice', 'wfimelt', 'wfiform', 'licefw', 'liceht'	'u_flux', 'v_flux', 'lprec', 'fprec', 'salt_flx', 'mh_flux', 'sw_flux', 'q_flux', 't_flux', 'lw_flux', 'runof', 'p', 'aice', 'wfimelt', 'wfiform', 'licefw', 'liceht'
	num_fields_in	15	17	17
&monin_obukhov_nml	neutral	True		
&ocean_albedo_nml	ocean_albedo_option	2		
&ocean_barotropic_nml	debug_this_module	False		
&ocean_bbc_nml	cdbot	0.001		
	cdbot_roughness_length	False		
	use_geothermal_heating	False		
&ocean_bihgen_friction_nml	ncar_boundary_scaling	True	False	False
&ocean_density_nml	neutralrho_max	1030.0	1038.0	1038.0
	neutralrho_min	1020.0	1028.0	1028.0
&ocean_frazil_nml	debug_this_module	False		
&ocean_grids_nml	debug_this_module	False		
&ocean_nphysics_nml	debug_this_module	False		
&ocean_nphysics_util_nml	agm	200.0		
	agm_closure_eden_gamma	0.0		
	agm_closure_eden_greatbatch	False		
	agm_closure_length_bczone	False		
	agm_closure_length_fixed	False		
	agm_closure_length_rossby	False		
	agm_damping_time	45.0		
	agm_smooth_space	False		
	agm_smooth_time	False		
	drhodz_mom4p1	False	True	True
	drhodz_smooth_horz	False		

Group (continued)	Variable	./gadi/g/data/hh5/tmp/cosima/access-om2-025/025deg_jra55v13_iaf_gmredi6/output153/ocean/input.nml	github.com/COSIMA/025deg_jra55_iaf/ocean/input.nml	github.com/COSIMA/025deg_jra55_ryf/ocean/input.nml
	drhodz_smooth_vert	False		
	rossby_radius_max	100 000.0		
	rossby_radius_min	10 000.0		
	tracer_mix_micom	False		
	vel_micom	0.0		
&ocean_nphysicsc_nml	debug_this_module	False		
&ocean_operators_nml	use_legacy_div_ud	False		
&ocean_overexchange_nml	debug_this_module	False		
	overexch_npts	4		
	overexch_weight_far	False		
	overflow_umax	5.0		
&ocean_polar_filter_nml	use_this_module	False		
&ocean_pressure_nml	zero_pressure_force	False		
&ocean_rivermix_nml	debug_this_module	False		
&ocean_sbc_nml	ocean_ice_salt_limit		0.006	0.006
&ocean_shortwave_gfdl_nml	debug_this_module	False		
	zmax_pen	300.0	1 000 000.0	1 000 000.0
&ocean_submesoscale_nml	debug_this_module	False		
&ocean_tempsalt_nml	debug_this_module	False		
	pottemp_equal_contemp	True		
&ocean_thickness_nml	debug_this_module	False		
&ocean_topog_nml	min_thickness		0.001	0.001
&ocean_tracer_advect_nml	debug_this_module	False		
&ocean_tracer_nml	debug_this_module	False		
&ocean_velocity_diag_nml	debug_this_module	False		
&ocean_vert_kpp_iow_nml	use_this_module	False		

Group	Variable	./gadi/g/data/hh5/tmp/cosima/access-om2-01/01deg_jra55v13_iaf/output197/ocean/input.nml	./gadi/g/data/hh5/tmp/cosima/access-om2-01/01deg_jra55v13_ryf9091/output675/ocean/input.nml	github.com/COSIMA/01deg_jra55_iaf/ocean/input.nml	github.com/COSIMA/01deg_jra55_ryf/ocean/input.nml
&diag_manager_nml	debug_diag_manager	True	False	False	False
	max_axes			400	400
	max_files			200	200

Group (continued)	Variable	./gadi/g/data/hh5/tmp/cosima/access-om2-01/01deg_jra55v13_iaf/output197/ocean/input.nml	./gadi/g/data/hh5/tmp/cosima/access-om2-01/01deg_jra55v13_ryf9091/output675/ocean/input.nml	github.com/COSIMA/01deg_jra55_iaf/ocean/input.nml	github.com/COSIMA/01deg_jra55_ryf/ocean/input.nml
	max_num_axis_sets			200	200
&mom_oasis3_interface_nml	fields_in	'u_flux', 'v_flux', 'lprec', 'fprec', 'salt_flx', 'mh_flux', 'sw_flux', 'q_flux', 't_flux', 'lw_flux', 'runof', 'p', 'aice', 'wfimelt', 'wfiform'	'u_flux', 'v_flux', 'lprec', 'fprec', 'salt_flx', 'mh_flux', 'sw_flux', 'q_flux', 't_flux', 'lw_flux', 'runof', 'p', 'aice', 'wfimelt', 'wfiform'	'u_flux', 'v_flux', 'lprec', 'fprec', 'salt_flx', 'mh_flux', 'sw_flux', 'q_flux', 't_flux', 'lw_flux', 'runof', 'p', 'aice', 'wfimelt', 'wfiform', 'licefw', 'liceht'	'u_flux', 'v_flux', 'lprec', 'fprec', 'salt_flx', 'mh_flux', 'sw_flux', 'q_flux', 't_flux', 'lw_flux', 'runof', 'p', 'aice', 'wfimelt', 'wfiform', 'licefw', 'liceht'
	num_fields_in	15	15	17	17
&monin_obukhov_nml	neutral	True	True		
&ocean_advection_velocity_nml	max_advection_velocity	0.3	0.2	0.3	0.3
&ocean_albedo_nml	ocean_albedo_option	2	2		
&ocean_barotropic_nml	debug_this_module	False	False		
&ocean_bbc_nml	cdbot	0.001	0.001		
	cdbot_roughness_length	False	False		
	use_geothermal_heating	False	False		
&ocean_bihgen_friction_nml	ncar_boundary_scaling	True	True	False	False
&ocean_density_nml	neutralrho_max	1030.0	1038.0	1038.0	1038.0
	neutralrho_min	1020.0	1028.0	1028.0	1028.0
&ocean_frazil_nml	debug_this_module	False	False		
&ocean_grids_nml	debug_this_module	False	False		
&ocean_nphysics_nml	debug_this_module	False	False		
&ocean_nphysics_util_nml	agm	100.0	100.0		
	agm_closure	True	True		
	agm_closure_baroclinic	True	True		
	agm_closure_buoy_freq	0.004	0.004		
	agm_closure_length	50 000.0	50 000.0		
	agm_closure_length_bczone	False	False		
	agm_closure_length_fixed	False	False		
	agm_closure_length_rossby	False	False		
	agm_closure_lower_depth	2000.0	2000.0		
	agm_closure_max	600.0	600.0		
	agm_closure_min	100.0	100.0		
	agm_closure_scaling	0.07	0.07		
	agm_closure_upper_depth	100.0	100.0		
	aredi	600.0	600.0		
	aredi_equal_agm	False	False		
	drhodz_mom4p1	False	False		

Group (continued)	Variable	./gadi/g/data/hh5/tmp/cosima/access-om2-01/01deg_jra55v13_iaf/output197/ocean/input.nml	./gadi/g/data/hh5/tmp/cosima/access-om2-01/01deg_jra55v13_ryf9091/output675/ocean/input.nml	github.com/COSIMA/01deg_jra55_iaf/ocean/input.nml	github.com/COSIMA/01deg_jra55_ryf/ocean/input.nml
	drhodz_smooth_horz	False	False		
	drhodz_smooth_vert	False	False		
	rossby_radius_max	100 000.0	100 000.0		
	rossby_radius_min	15 000.0	15 000.0		
	tracer_mix_micom	False	False		
	vel_micom	0.0	0.0		
&ocean_operators_nml	use_legacy_div_ud	False	False		
&ocean_overexchange_nml	debug_this_module	False	False		
	overexch_npts	4	4		
	overexch_weight_far	False	False		
	overflow_umax	5.0	5.0		
&ocean_polar_filter_nml	use_this_module	False	False		
&ocean_pressure_nml	zero_pressure_force	False	False		
&ocean_rivermix_nml	debug_this_module	False	False		
&ocean_riverspread_nml	debug_this_module	False	False		
&ocean_shortwave_gfdl_nml	debug_this_module	False	False		
	zmax_pen	300.0	300.0	1 000 000.0	1 000 000.0
&ocean_submesoscale_nml	debug_this_module	False	False		
&ocean_tempsalt_nml	debug_this_module	False	False		
	pottemp_equal_contemp	True			
	temperature_variable	'potential_temp'	'conservative_temp'	'conservative_temp'	'conservative_temp'
&ocean_thickness_nml	debug_this_module	False	False		
&ocean_topog_nml	min_thickness		1.0	0.001	0.001
&ocean_tracer_advect_nml	debug_this_module	False	False		
&ocean_tracer_nml	debug_this_module	False	False		
&ocean_velocity_diag_nml	debug_this_module	False	False		
&ocean_vert_kpp_iow_nml	use_this_module	False	False		
&ocean_vert_mix_nml	j09_bgmax		1×10^{-6}	1×10^{-6}	1×10^{-6}
	j09_bgmin		1×10^{-6}	1×10^{-6}	1×10^{-6}
	j09_diffusivity		True	True	True
	j09_lat		20.0	20.0	20.0

D.3 CICE namelists

D.3.1 cice_in.nml

Group	Variable	./gadi/g/data/hh5/tmp/cosima/access-om2/1deg_jra55v13_iaf_spinup1_B1/output059/ice/cice_in.nml	github.com/COSIMA/1deg_jra55_iaf/ice/cice_in.nml	github.com/COSIMA/1deg_jra55_ryf/ice/cice_in.nml
&forcing_nml	highfreq		True	True
&icefields_bgc_nml	f_fbri	'm'	'x'	'x'
	f_hbri	'm'	'x'	'x'
&icefields_mechred_nml	f_opening	'x'	'm'	'm'
&icefields_nml	f_aice	'm'	'md'	'md'
	f_congel	'm'	'md'	'md'
	f_dvidtd	'm'	'md'	'md'
	f_dvidtt	'm'	'md'	'md'
	f_fmeltt_ai	'x'	'm'	'm'
	f_frazil	'm'	'md'	'md'
	f_frz_onset	'm'	'x'	'x'
	f_frzmlt	'm'	'md'	'md'
	f_fsalt	'x'	'm'	'm'
	f_hi	'm'	'md'	'md'
	f_hs	'm'	'md'	'md'
	f_mlt_onset	'm'	'x'	'x'
	f_snoice	'm'	'md'	'md'
	f_sss	'm'	'x'	'x'
	f_sst	'm'	'x'	'x'
	f_uocn	'm'	'x'	'x'
	f_uvel	'm'	'md'	'md'
	f_vocn	'm'	'x'	'x'
	f_vvel	'm'	'md'	'md'
&icefields_pond_nml	f_apeff	'm'	'x'	'x'
	f_apeff_ai	'm'	'x'	'x'
	f_apond	'm'	'x'	'x'
	f_apond_ai	'm'	'x'	'x'
	f_hpond	'm'	'x'	'x'
	f_hpond_ai	'm'	'x'	'x'
	f_ipond	'm'	'x'	'x'
	f_ipond_ai	'm'	'x'	'x'
&setup_nml	history_chunksize_x		180	180
	history_chunksize_y		150	150
	history_deflate_level		1	1
	istep0	2067360	0	0
	lcdf64	False		
	restart	True	False	False
	restart_format	'nc'		
	runtype	'continue'	'initial'	'initial'

Group	Variable	./gadi/g/data/hh5/tmp/cosima/access-om2-025/025deg_jra55v13_iaf_gmredi6/output153/ice/cice_in.nml	github.com/COSIMA/025deg_jra55_iaf/ice/cice_in.nml	github.com/COSIMA/025deg_jra55_ryf/ice/cice_in.nml
&forcing_nml	highfreq		True	True
&icefields_bgc_nml	f_fbri	'm'	'x'	'x'
	f_hbri	'm'	'x'	'x'
&icefields_nml	f_aice	'm'	'md'	'md'
	f_congel	'm'	'md'	'md'
	f_dvidtd	'm'	'md'	'md'
	f_dvidtt	'm'	'md'	'md'
	f_frazil	'm'	'md'	'md'
	f_frz_onset	'm'	'x'	'x'
	f_frzmlt	'm'	'md'	'md'
	f_fsalt	'x'	'm'	'm'
	f_fsalt_ai	'x'	'm'	'm'
	f_hi	'm'	'md'	'md'
	f_hs	'm'	'md'	'md'
	f_mlt_onset	'm'	'x'	'x'
	f_sig1	'm'	'x'	'x'
	f_sig2	'm'	'x'	'x'
	f_snoice	'm'	'md'	'md'
	f_uvel	'm'	'md'	'md'
	f_vvel	'm'	'md'	'md'
&icefields_pond_nml	f_apeff	'm'	'x'	'x'
	f_apeff_ai	'm'	'x'	'x'
	f_apond	'm'	'x'	'x'
	f_apond_ai	'm'	'x'	'x'
	f_hpond	'm'	'x'	'x'
	f_hpond_ai	'm'	'x'	'x'
	f_ipond	'm'	'x'	'x'
	f_ipond_ai	'm'	'x'	'x'
&setup_nml	history_chunksize_x		720	720
	history_chunksize_y		540	540
	history_deflate_level		1	1
	istep0	341496	0	0
	lcdf64	True		
	restart	True	False	False
	restart_format	'nc'		
	runtype	'continue'	'initial'	'initial'

Group	Variable	./gadi/g/data/hh5/tmp/cosima/access-om2-01/01deg_jra55v13_iaf/output197/ice/cice_in.nml	./gadi/g/data/hh5/tmp/cosima/access-om2-01/01deg_jra55v13_ryf9091/output675/ice/cice_in.nml	github.com/COSIMA/01deg_jra55_iaf/ice/cice_in.nml	github.com/COSIMA/01deg_jra55_ryf/ice/cice_in.nml
&domain_nml	distribution_type	'roundrobin'	'sectrobin'	'sectrobin'	'sectrobin'
	nprocs	1600	799	722	722
&forcing_nml	highfreq		True	True	True
&icefields_nml	f_aice	'md'	'm'	'md'	'md'
	f_aicen	'md'	'm'	'm'	'm'
	f_congel	'm'	'm'	'md'	'md'
	f_daidtd	'x'	'x'	'm'	'm'
	f_daidtt	'x'	'x'	'm'	'm'
	f_divu	'md'	'm'	'm'	'm'
	f_dvidtd	'x'	'x'	'md'	'md'
	f_dvidtt	'x'	'x'	'md'	'md'
	f_frazil	'm'	'm'	'md'	'md'
	f_frz_onset	'm'	'm'	'x'	'x'
	f_frzmlt	'x'	'x'	'md'	'md'
	f_fsalt	'd'	'm'	'm'	'm'
	f_fsalt_ai	'd'	'm'	'm'	'm'
	f_hi	'md'	'm'	'md'	'md'
	f_hs	'md'	'm'	'md'	'md'
	f_mlt_onset	'm'	'm'	'x'	'x'
	f_shear	'md'	'm'	'm'	'm'
	f_sig1	'md'	'm'	'x'	'x'
	f_sig2	'md'	'm'	'x'	'x'
	f_snoice	'x'	'x'	'md'	'md'
	f_sss	'd'	'm'	'x'	'x'
	f_sst	'd'	'm'	'x'	'x'
	f_strairx	'md'	'm'	'm'	'm'
	f_strairy	'md'	'm'	'm'	'm'
	f_uocn	'd'	'm'	'x'	'x'
	f_uvel	'md'	'm'	'md'	'md'
	f_vicen	'md'	'm'	'm'	'm'
	f_vocn	'd'	'm'	'x'	'x'
	f_vvel	'md'	'm'	'md'	'md'
&setup_nml	history_chunksize_x			360	360
	history_chunksize_y			270	270
	history_deflate_level		1	1	1
	istep0	3906432	4374000	0	0
	latpnt	66.75, 68.0	66.75, 68.0	90.0, −65.0	90.0, −65.0
	lcdf64	True			
	lonpnt	72.5, 74.0	72.5, 74.0	0.0, −45.0	0.0, −45.0
	ndtd	3	2	2	2
	restart	True	True	False	False
	restart_format	'nc'	'nc'		
	runtype	'continue'	'continue'	'initial'	'initial'

D.3.2 input_ice.nml

Group	Variable	./gadi/g/data/hh5/tmp/cosima/access-om2/1deg_jra55v13_iaf_spinup1_B1/output059/ice/input_ice.nml	github.com/COSIMA/1deg_jra55_iaf/ice/input_ice.nml	github.com/COSIMA/1deg_jra55_ryf/ice/input_ice.nml
&coupling_nml	chk_frzmlt_sst		False	False
	chk_i2a_fields		False	False
	chk_i2o_fields		False	False
	chk_o2i_fields		False	False
	cst_ocn_albedo	True	False	False
	fields_from_atm		'swfld_i', 'lwfld_i', 'rain_i', 'snow_i', 'press_i', 'runof_i', 'tair_i', 'qair_i', 'uwnd_i', 'vwnd_i', 'licalvf_i'	'swfld_i', 'lwfld_i', 'rain_i', 'snow_i', 'press_i', 'runof_i', 'tair_i', 'qair_i', 'uwnd_i', 'vwnd_i', 'licalvf_i'
	fields_from_ocn		'sst_i', 'sss_i', 'ssu_i', 'ssv_i', 'sslx_i', 'ssly_i', 'pfmice_i'	'sst_i', 'sss_i', 'ssu_i', 'ssv_i', 'sslx_i', 'ssly_i', 'pfmice_i'
	fields_to_ocn		'strsu_io', 'strsv_io', 'rain_io', 'snow_io', 'stflx_io', 'htflx_io', 'swflx_io', 'qflux_io', 'shflx_io', 'lwflx_io', 'runof_io', 'press_io', 'aice_io', 'melt_io', 'form_io', 'licefw_io', 'licefh_io'	'strsu_io', 'strsv_io', 'rain_io', 'snow_io', 'stflx_io', 'htflx_io', 'swflx_io', 'qflux_io', 'shflx_io', 'lwflx_io', 'runof_io', 'press_io', 'aice_io', 'melt_io', 'form_io', 'licefw_io', 'licefh_io'

Group	Variable	./gadi/g/data/hh5/tmp/cosima/access-om2-025/025deg_jra55v13_iaf_gmredi6/output153/ice/input_ice.nml	github.com/COSIMA/025deg_jra55_iaf/ice/input_ice.nml	github.com/COSIMA/025deg_jra55_ryf/ice/input_ice.nml
&coupling_nml	cst_ocn_albedo	True	False	False
	fields_from_atm		'swfld_i', 'lwfld_i', 'rain_i', 'snow_i', 'press_i', 'runof_i', 'tair_i', 'qair_i', 'uwnd_i', 'vwnd_i', 'licalvf_i'	'swfld_i', 'lwfld_i', 'rain_i', 'snow_i', 'press_i', 'runof_i', 'tair_i', 'qair_i', 'uwnd_i', 'vwnd_i', 'licalvf_i'
	fields_from_ocn		'sst_i', 'sss_i', 'ssu_i', 'ssv_i', 'sslx_i', 'ssly_i', 'pfmice_i'	'sst_i', 'sss_i', 'ssu_i', 'ssv_i', 'sslx_i', 'ssly_i', 'pfmice_i'
	fields_to_ocn		'strsu_io', 'strsv_io', 'rain_io', 'snow_io', 'stflx_io', 'htflx_io', 'swflx_io', 'qflux_io', 'shflx_io', 'lwflx_io', 'runof_io', 'press_io', 'aice_io', 'melt_io', 'form_io', 'licefw_io', 'licefh_io'	'strsu_io', 'strsv_io', 'rain_io', 'snow_io', 'stflx_io', 'htflx_io', 'swflx_io', 'qflux_io', 'shflx_io', 'lwflx_io', 'runof_io', 'press_io', 'aice_io', 'melt_io', 'form_io', 'licefw_io', 'licefh_io'

Group	Variable	./gadi/g/data/hh5/tmp/cosima/access-om2-01/01deg_jra55v13_iaf/output197/ice/input_ice.nml	./gadi/g/data/hh5/tmp/cosima/access-om2-01/01deg_jra55v13_ryf9091/output675/ice/input_ice.nml	github.com/COSIMA/01deg_jra55_iaf/ice/input_ice.nml	github.com/COSIMA/01deg_jra55_ryf/ice/input_ice.nml
&coupling_nml	cst_ocn_albedo	True	True	False	False
	fields_from_atm			'swfld_i', 'lwfld_i', 'rain_i', 'snow_i', 'press_i', 'runof_i', 'tair_i', 'qair_i', 'uwnd_i', 'vwnd_i', 'licalvf_i'	'swfld_i', 'lwfld_i', 'rain_i', 'snow_i', 'press_i', 'runof_i', 'tair_i', 'qair_i', 'uwnd_i', 'vwnd_i', 'licalvf_i'
	fields_from_ocn			'sst_i', 'sss_i', 'ssu_i', 'ssv_i', 'sslx_i', 'ssly_i', 'pfmice_i'	'sst_i', 'sss_i', 'ssu_i', 'ssv_i', 'sslx_i', 'ssly_i', 'pfmice_i'
	fields_to_ocn			'strsu_io', 'strsv_io', 'rain_io', 'snow_io', 'stflx_io', 'htflx_io', 'swflx_io', 'qflux_io', 'shflx_io', 'lwflx_io', 'runof_io', 'press_io', 'aice_io', 'melt_io', 'form_io', 'licefw_io', 'licefh_io'	'strsu_io', 'strsv_io', 'rain_io', 'snow_io', 'stflx_io', 'htflx_io', 'swflx_io', 'qflux_io', 'shflx_io', 'lwflx_io', 'runof_io', 'press_io', 'aice_io', 'melt_io', 'form_io', 'licefw_io', 'licefh_io'

D.3.3 input_ice_gfdl.nml

D.3.4 input_ice_monin.nml

D.4 YATM namelist atm.nml

Group	Variable	./gadi/g/data/hh5/tmp/cosima/access-om2-01/01deg_jra55v13_iaf/output197/atmosphere/atm.nml	./gadi/g/data/hh5/tmp/cosima/access-om2-01/01deg_jra55v13_ryf9091/output675/atmosphere/atm.nml	github.com/COSIMA/01deg_jra55_iaf/atmosphere/atm.nml	github.com/COSIMA/01deg_jra55_ryf/atmosphere/atm.nml
&runoff_nml	runoff_caps	0.03, 0.001, 0.003, 0.003, 0.003	0.03, 0.003, 0.003, 0.003, 0.003	0.03, 0.003, 0.003, 0.003, 0.003	0.03, 0.003, 0.003, 0.003, 0.003
	runoff_caps_is	0, 3470, 180, 300	0, 3420, 180, 300	0, 3420, 180, 300	0, 3420, 180, 300
	runoff_caps_je	1000000, 2650, 99999, 2470	1000000, 2680, 99999, 2470	1000000, 2680, 99999, 2470	1000000, 2680, 99999, 2470

E Namelist differences between new configs

These are auto-generated by namelists/make_tables.py which uses nmltab (https://github.com/aekiss/nmltab). Variables are weblinks to source code searches. Only differences are shown, and duplicate identical profiling namelists are omitted. Differences in timestep counters are ignored. Tables are omitted if there are no differences at all.

E.1 ACCESS-OM2 namelist accessom2.nml

Group	Variable	github.com/COSIMA/01deg_jra55_iaf/accessom2.nml	github.com/COSIMA/01deg_jra55_ryf/accessom2.nml	github.com/COSIMA/025deg_jra55_iaf/accessom2.nml	github.com/COSIMA/025deg_jra55_ryf/accessom2.nml	github.com/COSIMA/1deg_jra55_iaf/accessom2.nml	github.com/COSIMA/1deg_jra55_ryf/accessom2.nml
&accessom2_nml	ice_ocean_timestep	300	300	1350	1350	5400	5400
&date_manager_nml	forcing_end_date	'2019-01-01T00:00:0	'1901-01-01T00:00:0	'2019-01-01T00:00:0	'1901-01-01T00:00:0	'2019-01-01T00:00:0	'1901-01-01T00:00:00'

Group (continued)	Variable	github.com/COSIMA/01deg_jra55_iaf/accessom2.nml	github.com/COSIMA/01deg_jra55_ryf/accessom2.nml	github.com/COSIMA/025deg_jra55_iaf/accessom2.nml	github.com/COSIMA/025deg_jra55_ryf/accessom2.nml	github.com/COSIMA/1deg_jra55_iaf/accessom2.nml	github.com/COSIMA/1deg_jra55_ryf/accessom2.nml
	forcing_start_date	'1958-01-01T00:00:0	'1900-01-01T00:00:0	'1958-01-01T00:00:0	'1900-01-01T00:00:0	'1958-01-01T00:00:0	'1900-01-01T00:00:00'
	restart_period	0, 3, 0	0, 3, 0	2, 0, 0	2, 0, 0	5, 0, 0	5, 0, 0

E.2 MOM namelist input.nml

Group	Variable	github.com/COSIMA/01deg_jra55_iaf/ocean/input.nml	github.com/COSIMA/01deg_jra55_ryf/ocean/input.nml	github.com/COSIMA/025deg_jra55_iaf/ocean/input.nml	github.com/COSIMA/025deg_jra55_ryf/ocean/input.nml	github.com/COSIMA/1deg_jra55_iaf/ocean/input.nml	github.com/COSIMA/1deg_jra55_ryf/ocean/input.nml
&auscom_ice_nml	redsea_gulfbay_sfix					False	False
&fms_io_nml	checksum_required	False	False				
	fileset_write	'multi'	'multi'	'single'	'single'	'single'	'single'
	threading_write	'multi'	'multi'	'single'	'single'	'single'	'single'
&fms_nml	clock_grain	'ROUTINE'	'ROUTINE'	'LOOP'	'LOOP'	'LOOP'	'LOOP'
	domains_stack_size	115200	115200			115200	115200
&mpp_io_nml	deflate_level	5	5	5	5	-1	-1
&ocean_adv_vel_diag_nml	diag_step	576	576	4320	4320	4320	4320
&ocean_advection_velocity_nml	max_advection_velocity	0.3	0.3	0.5	0.5	0.5	0.5
&ocean_barotropic_nml	diag_step	576	576	4320	4320	4320	4320
&ocean_bihgen_friction_nml	bottom_5point	False	False	False	False	True	True
	ncar_boundary_scaling	False	False	False	False	True	True
	vel_micom_bottom	0.0	0.0	0.0	0.0	0.01	0.01
	vel_micom_iso	0.0	0.0	0.0	0.0	0.04	0.04
	visc_crit_scale	1.0	1.0	1.0	1.0	0.25	0.25
&ocean_lapgen_friction_nml	bottom_5point					True	True
	k_smag_aniso					0.0	0.0
	k_smag_iso					0.0	0.0
	restrict_polar_visc					True	True
	restrict_polar_visc_lat					60.0	60.0
	restrict_polar_visc_ratio					0.35	0.35
	use_this_module	False	False	False	False	True	True
	vel_micom_iso					0.1	0.1
	viscosity_ncar					False	False
	viscosity_ncar_2007					False	False
	viscosity_scale_by_rossby					True	True
	viscosity_scale_by_rossby_power					4.0	4.0
&ocean_mixdownslope_nml	mixdownslope_mask_gfdl					False	False
	mixdownslope_npts					4	4
	read_mixdownslope_mask					False	False
	use_this_module	False	False	False	False	True	True
&ocean_model_nml	io_layout	5, 5	5, 5	6, 5	6, 5	4, 3	4, 3
	layout	80, 75	80, 75	48, 40	48, 40	16, 15	16, 15
&ocean_nphysics_nml	use_nphysicsc	False	False	True	True	True	True
	use_this_module	False	False	True	True	True	True
&ocean_nphysics_util_nml	agm_closure			True	True	True	True
	agm_closure_baroclinic			True	True	True	True

Group (continued)	Variable	github.com/COSIMA/01deg_jra55_iaf/ocean/input.nml	github.com/COSIMA/01deg_jra55_ryf/ocean/input.nml	github.com/COSIMA/025deg_jra55_iaf/ocean/input.nml	github.com/COSIMA/025deg_jra55_ryf/ocean/input.nml	github.com/COSIMA/1deg_jra55_iaf/ocean/input.nml	github.com/COSIMA/1deg_jra55_ryf/ocean/input.nml
	agm_closure_buoy_freq			0.004	0.004	0.004	0.004
	agm_closure_eady_ave_mixed			True	True	True	True
	agm_closure_eady_cap			True	True	True	True
	agm_closure_eady_smooth_horz			True	True	True	True
	agm_closure_eady_smooth_vert			True	True	True	True
	agm_closure_grid_scaling			True	True	True	True
	agm_closure_length			20 000.0	20 000.0	50 000.0	50 000.0
	agm_closure_lower_depth			2000.0	2000.0	2000.0	2000.0
	agm_closure_max			200.0	200.0	600.0	600.0
	agm_closure_min			1.0	1.0	50.0	50.0
	agm_closure_scaling			0.07	0.07	0.07	0.07
	agm_closure_upper_depth			100.0	100.0	100.0	100.0
	aredi			200.0	200.0	600.0	600.0
	aredi_diffusivity_grid_scaling			True	True		
	aredi_equal_agm			False	False	False	False
	drhodz_mom4p1			True	True	True	True
	nphysics_util_zero_init			True	True	True	True
&ocean_nphysicsc_nml	bv_freq_smooth_vert			True	True	True	True
	bvp_bc_mode			2	2	2	2
	bvp_min_speed			0.1	0.1	0.1	0.1
	bvp_speed			0.0	0.0	0.0	0.0
	do_gm_skewsion			True	True	True	True
	do_neutral_diffusion			True	True	True	True
	epsln_bv_freq			1×10^{-12}	1×10^{-12}	1×10^{-12}	1×10^{-12}
	gm_skewsion_bvproblem			True	True	True	True
	gm_skewsion_modes			False	False	False	False
	neutral_eddy_depth			True	True	True	True
	neutral_physics_limit			True	True	True	True
	number_bc_modes			2	2	2	2
	regularize_psi			False	False	False	False
	smax_psi			0.01	0.01	0.01	0.01
	smooth_psi			True	True	True	True
	tmask_neutral_on			True	True	True	True
	turb_blayer_min			50.0	50.0	50.0	50.0
	use_this_module	False	False	True	True	True	True
&ocean_sbc_nml	do_bitwise_exact_sum	False	False	False	False	True	True
	max_delta_salinity_restore	0.5	0.5	0.5	0.5	−0.5	−0.5
	ocean_ice_salt_limit	0.006	0.006	0.006	0.006		
	runoffspread	False	False				
	salt_restore_tscale	10.0	10.0	21.28	21.28	21.28	21.28
&ocean_sigma_transport_nml	use_this_module	False	False	False	False	True	True
&ocean_submesoscale_nml	smooth_advect_transport_num	4	4	4	4	2	2
	smooth_psi_num	3	3	3	3	2	2
&ocean_tracer_diag_nml	diag_step	576	576	4320	4320	4320	4320
&ocean_velocity_diag_nml	diag_step	576	576	4320	4320	4320	4320
	energy_diag_step	5760	5760	4320	4320	4320	4320
&ocean_vert_mix_nml	j09_bgmax	1×10^{-6}	1×10^{-6}			5×10^{-6}	5×10^{-6}
	j09_bgmin	1×10^{-6}	1×10^{-6}			1×10^{-6}	1×10^{-6}
	j09_diffusivity	True	True			True	True

Group (continued)	Variable	github.com/COSIMA/01deg_jra55_iaf/ocean/input.nml	github.com/COSIMA/01deg_jra55_ryf/ocean/input.nml	github.com/COSIMA/025deg_jra55_iaf/ocean/input.nml	github.com/COSIMA/025deg_jra55_ryf/ocean/input.nml	github.com/COSIMA/1deg_jra55_iaf/ocean/input.nml	github.com/COSIMA/1deg_jra55_ryf/ocean/input.nml
	j09_lat	20.0	20.0			20.0	20.0
&xgrid_nml	do_alltoall	True	True				
	do_alltoallv	True	True				

E.3 CICE namelists

E.3.1 cice_in.nml

Group	Variable	github.com/COSIMA/01deg_jra55_iaf/ice/cice_in.nml	github.com/COSIMA/01deg_jra55_ryf/ice/cice_in.nml	github.com/COSIMA/025deg_jra55_iaf/ice/cice_in.nml	github.com/COSIMA/025deg_jra55_ryf/ice/cice_in.nml	github.com/COSIMA/1deg_jra55_iaf/ice/cice_in.nml	github.com/COSIMA/1deg_jra55_ryf/ice/cice_in.nml
&domain_nml	distribution_type	'sectrobin'	'sectrobin'	'roundrobir	'roundrobir	'cartesian'	'cartesian'
	nprocs	722	722	361	361	24	24
	processor_shape	'square-ice'	'square-ice'	'square-ice'	'square-ice'	'slenderX1'	'slenderX1'
&forcing_nml	tfrz_option	'mushy'	'mushy'	'linear_salt'	'linear_salt'	'linear_salt'	'linear_salt'
&icefields_mechred_nml	f_vlvl	'x'	'x'	'm'	'm'	'm'	'm'
	f_vrdg	'x'	'x'	'm'	'm'	'm'	'm'
&icefields_nml	f_albice	'x'	'x'	'm'	'm'	'm'	'm'
	f_albsni	'x'	'x'	'm'	'm'	'm'	'm'
	f_albsno	'x'	'x'	'm'	'm'	'm'	'm'
	f_evap_ai	'x'	'x'	'm'	'm'	'm'	'm'
	f_fcondtop_ai	'x'	'x'	'm'	'm'	'm'	'm'
	f_fcondtopn_ai	'x'	'x'	'm'	'm'	'm'	'm'
	f_fhocn_ai	'x'	'x'	'm'	'm'	'm'	'm'
	f_flat_ai	'x'	'x'	'm'	'm'	'm'	'm'
	f_flwdn	'x'	'x'	'm'	'm'	'm'	'm'
	f_flwup_ai	'x'	'x'	'm'	'm'	'm'	'm'
	f_fmelttn_ai	'x'	'x'	'm'	'm'	'm'	'm'
	f_fresh_ai	'x'	'x'	'm'	'm'	'm'	'm'
	f_fsens_ai	'x'	'x'	'm'	'm'	'm'	'm'
	f_fsurfn_ai	'x'	'x'	'm'	'm'	'm'	'm'
	f_fswabs_ai	'x'	'x'	'm'	'm'	'm'	'm'
	f_fswdn	'x'	'x'	'm'	'm'	'm'	'm'
	f_fswfac	'x'	'x'	'm'	'm'	'm'	'm'
	f_fswthru_ai	'x'	'x'	'm'	'm'	'm'	'm'
	f_icepresent	'x'	'x'	'm'	'm'	'm'	'm'
	f_meltb	'x'	'x'	'm'	'm'	'm'	'm'
	f_meltl	'x'	'x'	'm'	'm'	'm'	'm'
	f_melts	'x'	'x'	'm'	'm'	'm'	'm'
	f_meltt	'x'	'x'	'm'	'm'	'm'	'm'
	f_rain_ai	'x'	'x'	'm'	'm'	'm'	'm'
	f_sice	'x'	'x'	'm'	'm'	'm'	'm'
	f_snow_ai	'x'	'x'	'm'	'm'	'm'	'm'
	f_strcorx	'x'	'x'	'm'	'm'	'm'	'm'

Group (continued)	Variable	github.com/COSIMA/01deg_jra55_iaf/ice/cice_in.nml	github.com/COSIMA/01deg_jra55_ryf/ice/cice_in.nml	github.com/COSIMA/025deg_jra55_iaf/ice/cice_in.nml	github.com/COSIMA/025deg_jra55_ryf/ice/cice_in.nml	github.com/COSIMA/1deg_jra55_iaf/ice/cice_in.nml	github.com/COSIMA/1deg_jra55_ryf/ice/cice_in.nml
	f_strcory	'x'	'x'	'm'	'm'	'm'	'm'
	f_strintx	'x'	'x'	'm'	'm'	'm'	'm'
	f_strinty	'x'	'x'	'm'	'm'	'm'	'm'
	f_strocnx	'x'	'x'	'm'	'm'	'm'	'm'
	f_strocny	'x'	'x'	'm'	'm'	'm'	'm'
	f_strtltx	'x'	'x'	'm'	'm'	'm'	'm'
	f_strtlty	'x'	'x'	'm'	'm'	'm'	'm'
	f_tair	'x'	'x'	'm'	'm'	'm'	'm'
	f_trsig	'x'	'x'	'm'	'm'	'm'	'm'
&setup_nml	dt	300	300	1800	1800	3600	3600
	dumpfreq	'm'	'm'	'y'	'y'	'y'	'y'
	dumpfreq_n	3	3	1	1	1	1
	history_chunksize_x	360	360	720	720	180	180
	history_chunksize_y	270	270	540	540	150	150
	ndtd	2	2	1	1	1	1
	npt	6480	6480	2232	2232	35040	35040
&thermo_nml	ktherm	2	2	1	1	1	1

E.3.2 input_ice.nml

E.3.3 input_ice_gfdl.nml

E.3.4 input_ice_monin.nml

E.4 YATM namelist atm.nml

Group	Variable	github.com/COSIMA/01deg_jra55_iaf/atmosphere/atm.nml	github.com/COSIMA/01deg_jra55_ryf/atmosphere/atm.nml	github.com/COSIMA/025deg_jra55_iaf/atmosphere/atm.nml	github.com/COSIMA/025deg_jra55_ryf/atmosphere/atm.nml	github.com/COSIMA/1deg_jra55_iaf/atmosphere/atm.nml	github.com/COSIMA/1deg_jra55_ryf/atmosphere/atm.nml
&runoff_nml	num_runoff_caps	4	4				
	runoff_caps	0.03, 0.003, 0.003, 0.003	0.03, 0.003, 0.003, 0.003				
	runoff_caps_ie	1000000, 3530, 240, 560	1000000, 3530, 240, 560				
	runoff_caps_is	0, 3420, 180, 300	0, 3420, 180, 300				

Group (continued)	Variable	github.com/COSIMA/01deg_jra55_iaf/atmosphere/atm.nml	github.com/COSIMA/01deg_jra55_ryf/atmosphere/atm.nml	github.com/COSIMA/025deg_jra55_iaf/atmosphere/atm.nml	github.com/COSIMA/025deg_jra55_ryf/atmosphere/atm.nml	github.com/COSIMA/1deg_jra55_iaf/atmosphere/atm.nml	github.com/COSIMA/1deg_jra55_ryf/atmosphere/atm.nml
	runoff_caps_je	1000000, 2680, 99999, 2470	1000000, 2680, 99999, 2470				
	runoff_caps_js	0, 2270, 2670, 2260	0, 2270, 2670, 2260				

F Namelist differences from ACCESS, ACCESS-CM2, ACCESS-ESM, OFAM3

F.1 ACCESS-OM2-01 MOM compared to OFAM3

input.ofam3_spinup03 is the namelist that was used for the spinup that was the version after "ofam3_spinup01" which was referred to the in Oke et al. (2013). The main difference between these experiments was that spinup01 was forced with ERA fluxes directly, whereas spinup03 used ERA atmosphere fields with bulk formulas.

input.ofam2017.nml is the most recent spinup namelist with several differences.

Only differences are shown.

Group	Variable	OFAM3/input.ofam3_spinup03.nml	OFAM3/input.ofam2017.nml	./gadi/g/data/hh5/tmp/cosima/access-om2-01/01deg_jra55v13_iaf/output197/ocean/input.nml
&auscom_ice_nml	aice_cutoff			0.15
	chk_i2o_fields			False
	chk_o2i_fields			False
	do_ice_once			False
	fixmeltt			False
	frazil_factor			1.0
	iceform_adj_salt			False
	icemlt_factor			1.0
	kmxice			5
	pop_icediag			True
	sign_stflx			1.0
	tmelt			−0.216
	use_ioaice			True
&coupler_nml	atmos_npes	0	0	
	calendar	'gregorian'	'gregorian'	
	check_stocks	-1	-1	
	current_date	1993, 1, 1, 0, 0, 0	1990, 1, 1, 0, 0, 0	
	days	6	0	
	do_atmos	False	False	
	do_ice	True	True	
	do_land	False	False	
	do_ocean	True	True	
	dt_atmos	10800	10800	
	dt_cpld	10800	10800	

Group (continued)	Variable	OFAM3/input.ofam3_-spinup03.nml	OFAM3/input.ofam2017.nml	./gadi/g/data/hh5/tmp/cosima/access-om2-01/01deg_jra55v13_-iaf/output197/ocean/input.nml
	hours	0	0	
	minutes	0	0	
	months	0	1	
	ocean_npes	0	0	
	seconds	0	0	
	use_lag_fluxes		False	
&diag_manager_nml	debug_diag_manager			True
	issue_oor_warnings		False	True
	max_axes	100		
&flux_exchange_nml	do_area_weighted_flux	False	False	
	do_runoff	False	False	
&fms_io_nml	checksum_required		False	False
&fms_nml	clock_grain	'LOOP'	'LOOP'	'ROUTINE'
	domains_stack_size			115200
&ice_model_nml	io_layout	32, 16	2, 10	
	layout	32, 32	48, 30	
	nsteps_adv	0	0	
	nsteps_dyn	0	0	
	spec_ice		False	
&mom_oasis3_interface_nml	fields_in			'u_flux', 'v_flux', 'lprec', 'fprec', 'salt_flx', 'mh_flux', 'sw_flux', 'q_flux', 't_flux', 'lw_flux', 'runof', 'p', 'aice', 'wfimelt', 'wfiform'
	fields_out			't_surf', 's_surf', 'u_surf', 'v_surf', 'dssldx', 'dssldy', 'frazil'
	num_fields_in			15
	num_fields_out			7
	send_after_ocean_update			True
	send_before_ocean_update			False
&monin_obukhov_nml	neutral	True	False	True
&mpp_io_nml	deflate_level			5
	shuffle			1
&ocean_adv_vel_diag_nml	diag_step	144	144	576
	verbose_cfl	False	False	True
&ocean_advection_velocity_nml	max_advection_velocity	0.5	0.5	0.3
&ocean_barotropic_nml	barotropic_halo			10
	barotropic_leap_frog	False		
	barotropic_pred_corr	True		
	barotropic_time_stepping_a		True	True
	barotropic_time_stepping_b		False	False
	barotropic_time_stepping_mom4p0	True		
	barotropic_time_stepping_mom4p1	False		
	diag_step	144	144	576
	eta_max	9.0	2.5	8.0
	frac_crit_cell_height	0.25	0.25	0.2
	pbot_offset	1×10^{-12}	1×10^{-12}	
	smooth_eta_diag_laplacian			True
	smooth_pbot_t_biharmonic			False

Group (continued)	Variable	OFAM3/input.ofam3_-spinup03.nml	OFAM3/input.ofam2017.nml	./gadi/g/data/hh5/tmp/cosima/access-om2-01/01deg_jra55v13_-iaf/output197/ocean/input.nml
	smooth_pbot_t_laplacian			True
	use_legacy_barotropic_halos			False
	vel_micom_lap_diag			0.2
	verbose_truncate	False	False	True
&ocean_bbc_nml	bmf_implicit			True
	cdbot	0.0015	0.0015	0.001
	cdbot_hi			0.007
	cdbot_roughness_length			False
	cdbot_roughness_uamp			True
	use_geothermal_heating			False
&ocean_bbc_ofam_nml	read_tide_speed	False	False	
	uresidual2_max	1.0	1.0	
&ocean_bihgen_friction_nml	eq_lat_micom			0.0
	eq_vel_micom_aniso			0.0
	eq_vel_micom_iso			0.0
	equatorial_zonal			False
	k_smag_aniso	3.0	3.0	0.0
	k_smag_iso	3.0	3.0	2.0
	ncar_boundary_scaling			True
	ncar_boundary_scaling_read			False
	ncar_rescale_power			2
	ncar_vconst_4			2×10^{-8}
	ncar_vconst_5			5
	use_this_module	True	True	True
	vel_micom_aniso	0.005	0.005	0.0
	vel_micom_bottom	0.01	0.01	0.0
	vel_micom_iso	0.005	0.005	0.0
	visc_crit_scale			1.0
&ocean_convect_nml	convect_full_scalar	True	True	
	convect_full_vector	False	False	
	convect_ncon	False	False	
	use_this_module	False	False	False
&ocean_coriolis_nml	acor	1.0	1.0	0.5
	use_this_module	True	True	True
&ocean_density_nml	eos_linear		False	False
	eos_preteos10		True	True
	layer_nk			80
	linear_eos	False		
	neutralrho_max			1030.0
	neutralrho_min			1020.0
	potrho_max			1038.0
	potrho_min			1028.0
&ocean_domains_nml	max_tracers			5
&ocean_frazil_nml	debug_this_module			False
	frazil_only_in_surface			False
	freezing_temp_preteos10			True
	freezing_temp_simple			False
	use_this_module	False	False	True
&ocean_increment_eta_nml	days_to_increment	0	0	
	fraction_increment	1.0	1.0	
	secs_to_increment	3600	3600	
	use_this_module	False	False	False
&ocean_increment_tracer_nml	days_to_increment	0	0	

Group (continued)	Variable	OFAM3/input.ofam3_-spinup03.nml	OFAM3/input.ofam2017.nml	./gadi/g/data/hh5/tmp/cosima/access-om2-01/01deg_jra55v13_-iaf/output197/ocean/input.nml
	fraction_increment	1.0	1.0	
	secs_to_increment	3600	3600	
	use_this_module	False	False	False
&ocean_increment_velocity_nml	days_to_increment	0	0	
	fraction_increment	1.0	1.0	
	secs_to_increment	3600	3600	
	use_this_module	False	False	False
&ocean_lap_friction_nml	lap_friction_scheme	'const'	'const'	'general'
&ocean_mixdownslope_nml	debug_this_module	False	False	
	use_this_module	False	False	False
&ocean_model_nml	barotropic_split	60	75	80
	cmip_units			True
	dt_ocean	450	600	
	impose_init_from_restart		False	
	io_layout	32, 16	2, 10	5, 5
	layout	32, 32	48, 30	80, 75
&ocean_momentum_source_nml	rayleigh_damp_exp_from_bottom	True	True	False
	rayleigh_damp_exp_scale	1000.0	1000.0	
	rayleigh_damp_exp_time	86 400.0	86 400.0	
	use_rayleigh_damp_table			True
	use_this_module	False	False	True
&ocean_nphysics_mom4p0_nml	debug_this_module	True	True	
	use_this_module	False	False	
&ocean_nphysics_mom4p1_nml	use_this_module	False	False	
&ocean_nphysics_nml	use_nphysicsa			False
	use_nphysicsb			False
	use_nphysicsc			False
	use_this_module	False	False	False
&ocean_nphysics_util_nml	agm			100.0
	agm_closure			True
	agm_closure_baroclinic			True
	agm_closure_buoy_freq			0.004
	agm_closure_length			50 000.0
	agm_closure_length_bczone			False
	agm_closure_length_fixed			False
	agm_closure_length_rossby			False
	agm_closure_lower_depth			2000.0
	agm_closure_max			600.0
	agm_closure_min			100.0
	agm_closure_scaling			0.07
	agm_closure_upper_depth			100.0
	aredi			600.0
	aredi_equal_agm			False
	drhodz_mom4p1			False
	drhodz_smooth_horz			False
	drhodz_smooth_vert			False
	rossby_radius_max			100 000.0
	rossby_radius_min			15 000.0
	tracer_mix_micom			False
	vel_micom			0.0
&ocean_nphysicsa_nml	use_this_module			False
&ocean_nphysicsb_nml	use_this_module			False
&ocean_nphysicsc_nml	use_this_module			False

Group (continued)	Variable	OFAM3/input.ofam3_-spinup03.nml	OFAM3/input.ofam2017.nml	./gadi/g/data/hh5/tmp/cosima/access-om2-01/01deg_jra55v13_-iaf/output197/ocean/input.nml
&ocean_ofam_diag_nml	debug_this_module	False	False	
	do_eta_tendency	False	False	
&ocean_operators_nml	use_legacy_div_ud			False
&ocean_overexchange_nml	debug_this_module			False
	overexch_npts			4
	overexch_weight_far			False
	overflow_umax			5.0
	use_this_module	False	False	False
&ocean_overflow_nml	debug_this_module	False	False	
	use_this_module	False	False	False
&ocean_overflow_ofp_nml	use_this_module			False
&ocean_pressure_nml	zero_pressure_force			False
&ocean_rivermix_nml	river_diffuse_salt	False	False	True
	river_diffuse_temp	False	False	True
	river_insertion_thickness	15.0	15.0	40.0
	use_this_module	True	True	True
&ocean_riverspread_nml	debug_this_module			False
	use_this_module	True	True	False
&ocean_rough_nml	rough_scheme		'beljaars'	'beljaars'
&ocean_sbc_nml	avg_sfc_temp_salt_eta			True
	avg_sfc_velocity			True
	calvingspread			False
	do_bitwise_exact_sum		False	False
	do_flux_correction			False
	land_model_heat_fluxes			False
	max_delta_salinity_restore			0.5
	max_ice_thickness			0.0
	ocean_ice_salt_limit			0.006
	restore_mask_gfdl			False
	runoff_salinity			0.0
	runoffspread			False
	salt_correction_scale			0.0
	salt_restore_tscale	180.0	14.0	10.0
	salt_restore_under_ice			True
	use_full_patm_for_sea_level			False
	zero_heat_fluxes			False
	zero_net_salt_correction			False
	zero_net_salt_restore			True
	zero_net_water_correction			False
	zero_net_water_couple_restore			True
	zero_net_water_coupler		True	True
	zero_net_water_restore			True
	zero_surface_stress			False
	zero_water_fluxes			False
&ocean_sbc_ofam_nml	do_override_stress_ofam		False	
	restore_mask_ofam	False	False	
	river_temp_ofam	False	False	
&ocean_shortwave_csiro_nml	read_depth	True	True	
	use_this_module	True	False	False
	zmax_pen	6000.0	6000.0	
&ocean_shortwave_gfdl_nml	optics_manizza		True	True
	optics_morel_antoine		False	False
	use_this_module	False	True	True

Group (continued)	Variable	OFAM3/input.ofam3_-spinup03.nml	OFAM3/input.ofam2017.nml	./gadi/g/data/hh5/tmp/cosima/access-om2-01/01deg_jra55v13_-iaf/output197/ocean/input.nml
	zmax_pen	100.0	6000.0	300.0
&ocean_shortwave_jerlov_nml	use_this_module			False
&ocean_shortwave_nml	use_shortwave_csiro	True	False	False
	use_shortwave_gfdl	False	True	True
	use_shortwave_jerlov			False
	use_this_module	True	True	True
&ocean_sponges_eta_ofam_nml	athresh	0.5	0.5	
	days_to_restore	-1	-1	
	lambda	0.0083	0.0083	
	npower	1.0	1.0	
	secs_to_restore	0	0	
	taumin	1200	1200	
	use_adaptive_restore	False	False	
	use_hard_thump	False	False	
	use_normalising	True	True	
&ocean_sponges_tracer_nml	damp_coeff_3d	True	True	
	use_this_module	True	True	False
&ocean_sponges_tracer_ofam_nml	athresh	0.5	0.5	
	days_to_restore	-1	-1	
	lambda	0.0083	0.0083	
	limit_salt		True	
	limit_salt_min		0.25	
	limit_temp		True	
	limit_temp_restore		1800.0	
	npower	1.0	1.0	
	secs_to_restore	0	0	
	taumin	1200	1200	
	use_adaptive_restore	False	False	
	use_hard_thump	False	False	
	use_normalising	True	True	
&ocean_sponges_velocity_nml	damp_coeff_3d	False	False	
	use_this_module	False	False	False
&ocean_sponges_velocity_ofam_nml	athresh	0.5	0.5	
	days_to_restore	-1	-1	
	lambda	0.0083	0.0083	
	npower	1.0	1.0	
	secs_to_restore	0	0	
	taumin	1200	1200	
	use_adaptive_restore	True	True	
	use_hard_thump	False	False	
	use_normalising	True	True	
&ocean_submesoscale_nml	coefficient_ce			0.05
	debug_this_module			False
	front_length_const			5000.0
	front_length_deform_radius			True
	limit_psi			True
	limit_psi_velocity_scale			0.5
	min_kblt			4
	smooth_advect_transport			True
	smooth_advect_transport_num			4
	smooth_hblt			False
	smooth_psi			True
	smooth_psi_num			3
	submeso_advect_flux			False

Group (continued)	Variable	OFAM3/input.ofam3_-spinup03.nml	OFAM3/input.ofam2017.nml	./gadi/g/data/hh5/tmp/cosima/access-om2-01/01deg_jra55v13_-iaf/output197/ocean/input.nml
	submeso_advect_limit			True
	submeso_advect_upwind			True
	submeso_advect_zero_bdy			True
	submeso_diffusion			False
	submeso_diffusion_biharmonic			True
	submeso_diffusion_scale			10.0
	submeso_skew_flux			True
	use_hblt_equal_mld			True
	use_psi_legacy			False
	use_this_module	False	False	True
&ocean_tempsalt_nml	debug_this_module			False
	pottemp_equal_contemp			True
	reinit_ts_with_ideal	False	False	
	s_max	55.0	55.0	70.0
	s_min_limit	5.0	5.0	2.0
	t_min	−5.0	−5.0	−20.0
	t_min_limit	−1.5	−1.5	−5.0
&ocean_thickness_nml	debug_this_module			False
	debug_this_module_detail			False
	rescale_mass_to_get_ht_mod			False
	update_dzwu_k0	True	True	
&ocean_tracer_advect_nml	advect_sweby_all	True	True	
	read_basin_mask			False
	zero_tracer_advect_horz	False	False	
	zero_tracer_advect_vert	False	False	
&ocean_tracer_diag_nml	diag_step	144	144	576
	tracer_conserve_days	3.0	3.0	30.0
&ocean_tracer_nml	age_tracer_max_init			0.0
	compute_tmask_limit_on	False	False	
	frazil_heating_before_vphysics			False
	limit_age_tracer			True
	remap_depth_to_s_init			False
	use_tempsalt_check_range			True
	zero_tracer_source			False
&ocean_velocity_diag_nml	diag_step	144	144	576
	energy_diag_step	960	288	5760
&ocean_velocity_nml	max_cgint			1.0
	truncate_velocity_value	0.2	0.2	2.0
	truncate_verbose			True
	zero_tendency_explicit_a			False
	zero_tendency_explicit_b			False
	zero_tendency_implicit			False
&ocean_vert_chen_nml	debug_this_module	False	False	
	diff_cbt_iw	1×10^{-5}	0.0	
	diff_cbt_limit	0.005	0.005	
	diff_con_limit	0.1	0.1	
	use_this_module	False	False	
	visc_cbu_iw	0.0001	0.0	
	visc_cbu_limit	0.005	0.005	
	visc_con_limit	0.1	0.01	
&ocean_vert_const_nml	use_this_module	False	False	
&ocean_vert_gotm_nml	advect_gotm_method		'upwind'	
	correct_adv_errors		True	

Group (continued)	Variable	OFAM3/input.ofam3_-spinup03.nml	OFAM3/input.ofam2017.nml	./gadi/g/data/hh5/tmp/cosima/access-om2-01/01deg_jra55v13_-iaf/output197/ocean/input.nml
	debug_this_module		False	
	diff_cbt_min		0.0001	
	do_advection_gotm		True	
	do_turbulence_gotm		True	
	min_diss		1×10^{-10}	
	min_tke		1×10^{-6}	
	use_this_module	False	True	
	visc_cbu_min		1×10^{-5}	
	write_a_restart		True	
	z0b		0.002	
	z0s		0.2	
&ocean_vert_kpp_iow_nml	use_this_module			False
&ocean_vert_kpp_mom4p1_nml	diff_cbt_iw			0.0
	double_diffusion			True
	kbl_standard_method		False	False
	ricr			0.3
	smooth_blmc			False
	smooth_ri_kmax_eq_kmu		True	True
	use_this_module		True	True
	visc_cbu_iw			0.0
&ocean_vert_kpp_nml	kbl_standard_method	False		
	smooth_ri_kmax_eq_kmu	True		
	use_this_module	True		
&ocean_vert_mix_nml	bryan_lewis_lat_depend			False
	hwf_diffusivity			False
	hwf_min_diffusivity			2×10^{-6}
	hwf_n0_2omega			20.0
	use_diff_cbt_table			False
	vert_diff_back_via_max			True
	vert_mix_scheme	'kpp'	'gotm'	'kpp_mom4p1'
&ocean_vert_tidal_nml	background_viscosity	0.0	0.0	0.0001
	decay_scale			500.0
	drag_dissipation_use_cdbot			True
	fixed_wave_dissipation			False
	max_wave_diffusivity			0.01
	mixing_efficiency_n2depend			True
	read_roughness	False	False	True
	read_wave_dissipation			False
	reading_roughness_amp			True
	reading_roughness_length			False
	roughness_scale			12 000.0
	shelf_depth_cutoff			−1000.0
	tide_speed_data_on_t_grid			True
	use_legacy_methods			False
	use_this_module	True	True	True
	use_wave_dissipation	False	False	True
	wave_energy_flux_max			0.1
&ocean_xlandinsert_nml	use_this_module	False	False	False
	verbose_init	True	True	
&ocean_xlandmix_nml	use_this_module	False	False	False
	verbose_init	True	True	
&sat_vapor_pres_nml	construct_table_wrt_liq_and_ice	True	True	
	show_all_bad_values	True	True	

Group (continued)	Variable	OFAM3/ input.ofam3_-spinup03.nml	OFAM3/ input.ofam2017.nml	./gadi/g/data/ hh5/tmp/cosima/ access-om2-01/ 01deg_jra55v13_-iaf/output197/ ocean/input.nml
&surface_flux_nml	ncar_ocean_flux	False		
	raoult_sat_vap	True		
&xgrid_nml	do_alltoall		True	True
	do_alltoallv		True	True
	nsubset			16

F.2 ACCESS-OM2-01 MOM compared to MOM-SIS-01 and GFDL

F.3 ACCESS-OM2-01 CICE compared to RASM and NCAR

ice_in_RASM **TODO:** get permisssion

ncar_ice_in **TODO:** get permisssion

F.4 ACCESS-OM2 MOM and CICE compared to ACCESS, ACCESS-CM2, ACCESS-ESM

Only differences are shown. See https://www.dropbox.com/s/lktfwl3da0jpzp6/Fabio2018_Namelist_meeting_final.pdf?dl=0.

F.4.1 MOM namelist input.nml

Group	Variable	ACCESS-CM2/ input.nml	./gadi/g/data/ hh5/tmp/cosima/ access-om2/ 1deg_jra55v13_-iaf_spinup1_B1/ output059/ocean/ input.nml
&auscom_ice_nml	dt_cpl	1800	
	ige	345	
	igs	328	
	ire1	324	
	ire2	335	
	irs1	314	
	irs2	325	
	jge	198	
	jgs	189	
	jre1	196	
	jre2	180	
	jrs1	169	
	jrs2	169	
	kmxice	15	5
	redsea_gulfbay_sfix	True	False
	sfix_hours	24	
&bg_diff_lat_dependence_nml	bg_diff_eq	1×10^{-6}	
	lat_low_bgdiff	20.0	
&diag_manager_nml	debug_diag_manager		False
	issue_oor_warnings	False	True

Group (continued)	Variable	ACCESS-CM2/ input.nml	./gadi/g/data/ hh5/tmp/cosima/ access-om2/ 1deg_jra55v13_- iaf_spinup1_B1/ output059/ocean/ input.nml
&fms_nml	domains_stack_size		115200
&mom_oasis3_interface_nml	fields_in	'u_flux', 'v_flux', 'lprec', 'fprec', 'salt_flx', 'mh_flux', 'sw_flux', 'q_flux', 't_flux', 'lw_flux', 'runof', 'p', 'aice', 'wfimelt', 'wfiform', 'co2_io', 'wnd_io', 'licefw', 'liceht'	'u_flux', 'v_flux', 'lprec', 'fprec', 'salt_flx', 'mh_flux', 'sw_flux', 'q_flux', 't_flux', 'lw_flux', 'runof', 'p', 'aice', 'wfimelt', 'wfiform'
	fields_out	't_surf', 's_surf', 'u_surf', 'v_surf', 'dssldx', 'dssldy', 'frazil', 'co2_o', 'co2fx_o'	't_surf', 's_surf', 'u_surf', 'v_surf', 'dssldx', 'dssldy', 'frazil'
	num_fields_in	19	15
	num_fields_out	9	7
	send_after_ocean_update	False	True
	send_before_ocean_update	True	False
&monin_obukhov_nml	neutral		True
&mpp_io_nml	deflate_level		5
	shuffle		1
&ocean_adv_vel_diag_nml	diag_step	120	4320
	verbose_cfl	False	True
&ocean_albedo_nml	ocean_albedo_option		2
&ocean_barotropic_nml	barotropic_halo		10
	diag_step	120	4320
	smooth_eta_t_biharmonic	True	False
	smooth_eta_t_laplacian	False	True
	smooth_pbot_t_biharmonic	True	False
	smooth_pbot_t_laplacian	False	True
	use_legacy_barotropic_halos		False
	zero_tendency		False
&ocean_bbc_nml	bmf_implicit		True
	cdbot_hi		0.007
	cdbot_law_of_wall	False	
	cdbot_roughness_length		False
	cdbot_roughness_uamp		True
	uresidual		0.05
&ocean_bbc_ofam_nml	read_tide_speed	False	
	uresidual2_max	1.0	
&ocean_bihgen_friction_nml	ncar_boundary_scaling_read		False
	use_this_module	True	True
&ocean_convect_nml	convect_full_scalar	True	
	convect_full_vector	False	
	use_this_module	False	False
&ocean_domains_nml	max_tracers	20	5
&ocean_form_drag_nml	cprime_aiki	0.6	
	use_this_module	False	False
&ocean_frazil_nml	debug_this_module		False
	frazil_only_in_surface	True	False
	freezing_temp_preteos10		True

Group (continued)	Variable	ACCESS-CM2/ input.nml	./gadi/g/data/ hh5/tmp/cosima/ access-om2/ 1deg_jra55v13_- iaf_spinup1_B1/ output059/ocean/ input.nml
	freezing_temp_simple	True	False
	use_this_module	True	True
&ocean_grids_nml	debug_this_module	True	False
	read_rho0_profile	False	
&ocean_increment_eta_nml	days_to_increment	0	
	fraction_increment	1.0	
	secs_to_increment	3600	
	use_this_module	False	False
&ocean_increment_tracer_nml	days_to_increment	0	
	fraction_increment	1.0	
	secs_to_increment	3600	
	use_this_module	False	False
&ocean_increment_velocity_nml	days_to_increment	0	
	fraction_increment	1.0	
	secs_to_increment	3600	
	use_this_module	False	False
&ocean_lapgen_friction_nml	ncar_only_equatorial	True	
	use_this_module	True	True
	vconst_1	8 000 000.0	
	vconst_2	0.0	
	vconst_3	0.8	
	vconst_4	5×10^{-9}	
	vconst_5	3	
	vconst_6	300 000 000.0	
	vconst_7	100.0	
	viscosity_ncar	True	False
	viscosity_ncar_2000	False	
	viscosity_ncar_2007	True	False
&ocean_model_nml	barotropic_split	100	80
	do_wave	True	
	dt_ocean	1800	
	io_layout		4, 3
	layout	8, 14	16, 15
&ocean_momentum_source_nml	rayleigh_damp_exp_from_bottom		False
	use_this_module	True	True
&ocean_nphysics_util_nml	agm_closure_max	1200.0	600.0
	agm_closure_min	100.0	50.0
	aredi	300.0	600.0
	smax	0.002	
	swidth	0.0002	
&ocean_nphysicsa_nml	debug_this_module	False	
	neutral_linear_gm_taper	True	
	neutral_physics_limit	True	
	neutral_physics_simple	'.false'	
	neutral_sine_taper	True	
	tmask_neutral_on	True	
	use_this_module	False	False
&ocean_operators_nml	use_legacy_div_ud		False
&ocean_overexchange_nml	overexch_check_extrema	False	
	use_this_module	False	False
&ocean_overflow_nml	debug_this_module	False	
	use_this_module	False	False

Group (continued)	Variable	ACCESS-CM2/ input.nml	./gadi/g/data/ hh5/tmp/cosima/ access-om2/ 1deg_jra55v13_- iaf_spinup1_B1/ output059/ocean/ input.nml
&ocean_overflow_ofp_nml	use_this_module		False
&ocean_pressure_nml	zero_pressure_force		False
&ocean_rivermix_nml	river_diffuse_salt	False	True
	river_diffuse_temp	False	True
	use_this_module	True	True
&ocean_riverspread_nml	use_this_module	True	False
&ocean_rough_nml	rough_scheme		'beljaars'
&ocean_sbc_nml	calvingspread		False
	do_bitwise_exact_sum		True
	do_flux_correction		False
	ice_salt_concentration	0.004	
	land_model_heat_fluxes		False
	max_delta_salinity_restore	0.5	−0.5
	max_ice_thickness	8.0	0.0
	salt_correction_scale		0.0
	salt_restore_tscale	−1.0	21.28
	salt_restore_under_ice	False	True
	temp_restore_tscale	−1.0	−10.0
	use_full_patm_for_sea_level		False
	waterflux_tavg	False	
	zero_net_salt_correction		False
	zero_net_salt_restore	False	True
	zero_net_water_correction		False
	zero_net_water_couple_restore	False	True
	zero_net_water_coupler	False	True
	zero_net_water_restore	False	True
&ocean_sbc_ofam_nml	restore_mask_ofam	False	
	river_temp_ofam	False	
&ocean_shortwave_csiro_nml	read_depth	True	
	use_this_module	False	False
	zmax_pen	7000	
&ocean_shortwave_gfdl_nml	use_this_module	True	True
	zmax_pen	7000.0	300.0
&ocean_sigma_transport_nml	sigma_advection_on	False	
	sigma_advection_sgs_only	False	
	sigma_diffusion_on	True	
	sigma_diffusivity_ratio	1×10^{-6}	
	sigma_just_in_bottom_cell	True	
	sigma_umax	0.01	
	smooth_sigma_thickness	True	
	smooth_sigma_velocity	True	
	smooth_velmicom	0.2	
	thickness_sigma_layer	100.0	
	thickness_sigma_max	100.0	
	thickness_sigma_min	100.0	
	tmask_sigma_on	False	
	tracer_mix_micom	True	
	use_this_module	True	True
	vel_micom	0.05	
&ocean_solo_nml	calendar	'gregorian'	
	date_init	301, 1, 1, 0, 0, 0	
	days	30	

Group (continued)	Variable	ACCESS-CM2/ input.nml	./gadi/g/data/ hh5/tmp/cosima/ access-om2/ 1deg_jra55v13_- iaf_spinup1_B1/ output059/ocean/ input.nml
	dt_cpld	1800	
	hours	0	
	minutes	0	
	months	0	
	seconds	0	
	years	0	
&ocean_sponges_tracer_nml	damp_coeff_3d	False	
	use_this_module	False	False
&ocean_submesoscale_nml	coefficient_ce		0.05
	smooth_advect_transport		True
	smooth_advect_transport_num		2
	smooth_psi		True
	smooth_psi_num		2
	submeso_advect_flux		False
	submeso_advect_limit		True
	submeso_advect_upwind		True
	submeso_advect_zero_bdy		True
	submeso_diffusion		False
	submeso_diffusion_biharmonic		True
	submeso_diffusion_scale		10.0
	submeso_limit_flux	True	
	submeso_skew_flux		True
	use_psi_legacy		False
	use_this_module	True	True
&ocean_tempsalt_nml	debug_this_module		False
	pottemp_equal_contemp	False	True
	s_max	55.0	70.0
	s_min	−1.0	0.0
	s_min_limit	0.0	2.0
	t_min	−5.0	−20.0
	t_min_limit	−2.0	−5.0
&ocean_thickness_nml	initialize_zero_eta	False	
	read_rescale_rho0_mask	False	
	rescale_mass_to_get_ht_mod		False
	rescale_rho0_basin_label	7.0	
	rescale_rho0_mask_gfdl	False	
	rescale_rho0_value	0.75	
	thickness_dzt_min	1.0	
	thickness_dzt_min_init	2.0	
&ocean_topog_nml	min_thickness	25.0	
&ocean_tracer_advect_nml	advect_sweby_all	True	
	read_basin_mask		False
&ocean_tracer_diag_nml	diag_step	120	4320
	tracer_conserve_days	1.0	30.0
&ocean_tracer_nml	debug_this_module	True	False
	use_tempsalt_check_range		True
&ocean_velocity_diag_nml	diag_step	120	4320
	energy_diag_step	120	4320
&ocean_velocity_nml	truncate_verbose	False	True
	zero_tendency_explicit_a		False
	zero_tendency_explicit_b		False
	zero_tendency_implicit		False

Group (continued)	Variable	ACCESS-CM2/ input.nml	./gadi/g/data/ hh5/tmp/cosima/ access-om2/ 1deg_jra55v13_- iaf_spinup1_B1/ output059/ocean/ input.nml
&ocean_vert_gotm_nml	advect_gotm_method	'sweby'	
	correct_adv_errors	True	
	debug_this_module	False	
	diff_cbt_min	0.0001	
	do_advection_gotm	False	
	do_turbulence_gotm	True	
	min_diss	1×10^{-10}	
	min_tke	1×10^{-6}	
	use_this_module	False	
	visc_cbu_min	1×10^{-5}	
	write_a_restart	True	
	z0b	0.002	
	z0s	0.2	
&ocean_vert_kpp_iow_nml	use_this_module		False
&ocean_vert_kpp_mom4p1_nml	diff_con_limit	0.1	
	do_langmuir	True	
	kbl_standard_method	True	False
	smooth_blmc	True	False
	smooth_ri_kmax_eq_kmu		True
	use_this_module	True	True
	visc_con_limit	0.1	
&ocean_vert_mix_nml	afkph_00	0.65	
	afkph_90	0.75	
	bryan_lewis_lat_depend	True	False
	bryan_lewis_lat_transition	35.0	
	dfkph_00	1.15	
	dfkph_90	0.95	
	hwf_diffusivity		False
	hwf_min_diffusivity		2×10^{-6}
	hwf_n0_2omega		20.0
	j09_bgmax		5×10^{-6}
	j09_bgmin		1×10^{-6}
	j09_diffusivity		True
	j09_lat		20.0
	linear_taper_diff_cbt_table	False	
	sfkph_00	4.5×10^{-5}	
	sfkph_90	4.5×10^{-5}	
	zfkph_00	250 000.0	
	zfkph_90	250 000.0	
&ocean_vert_tidal_nml	background_diffusivity	5×10^{-6}	0.0
	decay_scale	300.0	500.0
	drag_dissipation_use_cdbot		True
	drhodz_min	1×10^{-12}	1×10^{-10}
	max_drag_diffusivity	0.005	
	roughness_scale	20 000.0	12 000.0
	shelf_depth_cutoff	160.0	−1000.0
	use_legacy_methods		False
	use_this_module	True	True
&ocean_xlandinsert_nml	use_this_module	False	False
	verbose_init	True	
&ocean_xlandmix_nml	use_this_module	False	False
	verbose_init	True	

Group (continued)	Variable	ACCESS-CM2/ input.nml	./gadi/g/data/ hh5/tmp/cosima/ access-om2/ 1deg_jra55v13_- iaf_spinup1_B1/ output059/ocean/ input.nml
	xlandmix_kmt	True	
&xgrid_nml	interp_method		'second_order'
	make_exchange_reproduce		False
	nsubset		16

F.4.2 CICE namelist cice_in.nml

Group	Variable	ACCESS-CM2/ cice_in.nml	./gadi/g/data/ hh5/tmp/cosima/ access-om2/ 1deg_jra55v13_- iaf_spinup1_B1/ output059/ice/ cice_in.nml
&domain_nml	distribution_wght	'block'	'latitude'
	maskhalo_bound	False	True
	maskhalo_dyn	False	True
	maskhalo_remap	False	True
	nprocs	16	24
	processor_shape	'square-pop'	'slenderX1'
&dynamics_nml	cosw		1.0
	dragio		0.005 36
	iceruf		0.0005
	sinw		0.0
&forcing_nml	calc_strair	False	True
	calc_tsfc	False	True
	cap_fluxes	True	
	fyear_init	1997	1
	tfrz_option		'linear_salt'
&grid_nml	grid_file	'INPUT/grid.nc'	'RESTART/grid.nc'
	kcatbound	1	0
	kmt_file	'INPUT/kmt.nc'	'RESTART/kmt.nc'
&icefields_bgc_nml	f_aero		'x'
	f_bgc_am_ml		'x'
	f_bgc_am_sk		'x'
	f_bgc_c_sk		'x'
	f_bgc_chl_sk		'x'
	f_bgc_dms_sk		'x'
	f_bgc_dmsp_ml		'x'
	f_bgc_dmspd_sk		'x'
	f_bgc_dmspp_sk		'x'
	f_bgc_n_sk		'x'
	f_bgc_nit_ml		'x'
	f_bgc_nit_sk		'x'
	f_bgc_sil_ml		'x'
	f_bgc_sil_sk		'x'
	f_bphi		'x'
	f_btin		'x'
	f_faero_atm		'x'
	f_faero_ocn		'x'

Group (continued)	Variable	ACCESS-CM2/ cice_in.nml	./gadi/g/data/ hh5/tmp/cosima/ access-om2/ 1deg_jra55v13_- iaf_spinup1_B1/ output059/ice/ cice_in.nml
	f_fbri		'm'
	f_fn		'x'
	f_fn_ai		'x'
	f_fnh		'x'
	f_fnh_ai		'x'
	f_fno		'x'
	f_fno_ai		'x'
	f_fsil		'x'
	f_fsil_ai		'x'
	f_grownet		'x'
	f_hbri		'm'
	f_ppnet		'x'
&icefields_drag_nml	f_cdn_atm		'x'
	f_cdn_ocn		'x'
	f_drag		'x'
&icefields_mechred_nml	f_alvl	'x'	'm'
	f_ardg	'x'	'm'
	f_dardg1dt	'm'	'x'
	f_dardg2dt	'm'	'x'
	f_dvirdgdt	'm'	'x'
	f_opening	'm'	'x'
	f_vlvl	'x'	'm'
	f_vrdg	'x'	'm'
&icefields_nml	f_aice	'dm'	'm'
	f_albice	'x'	'm'
	f_albsni	'x'	'm'
	f_albsno	'x'	'm'
	f_alidf	'x'	
	f_alidf_ai	'm'	
	f_alidr_ai	'm'	
	f_alvdf	'x'	
	f_alvdf_ai	'm'	
	f_alvdr_ai	'm'	
	f_congel	'x'	'm'
	f_daidtd	'x'	'm'
	f_daidtt	'x'	'm'
	f_dvidtd	'x'	'm'
	f_dvidtt	'x'	'm'
	f_dvsdtd	'm'	
	f_dvsdtt	'm'	
	f_dxt	False	True
	f_dxu	False	True
	f_dyt	False	True
	f_dyu	False	True
	f_evap_ai	'x'	'm'
	f_evap_ice_ai	'm'	
	f_evap_snow_ai	'm'	
	f_fcondtop_ai	'x'	'm'
	f_fhocn_ai	'x'	'm'
	f_flat_ai	'x'	'm'
	f_flatn_ai	'x'	'm'
	f_flwdn	'x'	'm'
	f_flwup_ai	'x'	'm'

Group (continued)	Variable	ACCESS-CM2/ cice_in.nml	./gadi/g/data/ hh5/tmp/cosima/ access-om2/ 1deg_jra55v13_- iaf_spinup1_B1/ output059/ice/ cice_in.nml
	f_fmelttn_ai	'x'	'm'
	f_frazil	'x'	'm'
	f_fresh_ai	'x'	'm'
	f_fsalt_ai	'x'	'm'
	f_fsens		'x'
	f_fsens_ai		'm'
	f_fsurf_ai	'm'	'x'
	f_fswabs_ai	'x'	'm'
	f_fswdn		'm'
	f_fswfac	'x'	'm'
	f_fswthru_ai	'x'	'm'
	f_hi		'm'
	f_hs		'm'
	f_hte	False	True
	f_htn	False	True
	f_iage		'm'
	f_icepresent	'x'	'm'
	f_meltb	'x'	'm'
	f_meltl	'x'	'm'
	f_melts		'm'
	f_meltt	'x'	'm'
	f_rain_ai	'x'	'm'
	f_shear	'x'	'm'
	f_siage	'm'	
	f_sialb	'm'	
	f_sice		'm'
	f_sicompstren	'm'	
	f_sidconcdyn	'm'	
	f_sidconcth	'm'	
	f_sidivvel	'm'	
	f_sidmassdyn	'm'	
	f_sidmassevapsubl	'm'	
	f_sidmassgrowthbot	'm'	
	f_sidmassgrowthwat	'm'	
	f_sidmasslat	'm'	
	f_sidmassmeltbot	'm'	
	f_sidmassmelttop	'm'	
	f_sidmasssi	'm'	
	f_sidmassth	'm'	
	f_sidmasstranx	'm'	
	f_sidmasstrany	'm'	
	f_sifb	'm'	
	f_siflcondbot	'm'	
	f_siflcondtop	'm'	
	f_siflfwbot	'm'	
	f_sifllatstop	'm'	
	f_sifllwdtop	'm'	
	f_sifllwutop	'm'	
	f_siflsaltbot	'm'	
	f_siflsenstop	'm'	
	f_siflsensupbot	'm'	
	f_siflswdbot	'm'	
	f_siflswdtop	'm'	

Group (continued)	Variable	ACCESS-CM2/ cice_in.nml	./gadi/g/data/ hh5/tmp/cosima/ access-om2/ 1deg_jra55v13_- iaf_spinup1_B1/ output059/ice/ cice_in.nml
	f_siflswutop	'm'	
	f_siforcecoriolx	'm'	
	f_siforcecorioly	'm'	
	f_siforceintstrx	'm'	
	f_siforceintstry	'm'	
	f_siforcetiltx	'm'	
	f_siforcetilty	'm'	
	f_sig1	'm'	'x'
	f_sig2	'm'	'x'
	f_sihc	'm'	
	f_sipr	'm'	
	f_sisaltmass	'm'	
	f_sisnconc	'm'	
	f_sisnhc	'm'	
	f_sisnthick	'dm'	
	f_sispeed	'dm'	
	f_sistrxdtop	'm'	
	f_sistrxubot	'm'	
	f_sistrydtop	'm'	
	f_sistryubot	'm'	
	f_sitempbot	'm'	
	f_sitempsnic	'm'	
	f_sitemptop	'dm'	
	f_sithick	'dm'	
	f_siu	'dm'	
	f_siv	'dm'	
	f_sndmassmelt	'm'	
	f_sndmasssnf	'm'	
	f_snoice	'x'	'm'
	f_snow_ai	'x'	'm'
	f_snowfrac	'm'	
	f_snowfracn	'm'	
	f_strairx	'x'	'm'
	f_strairy	'x'	'm'
	f_strcorx	'x'	'm'
	f_strcory	'x'	'm'
	f_strength	'x'	'm'
	f_strintx	'x'	'm'
	f_strinty	'x'	'm'
	f_strocnx	'x'	'm'
	f_strocny	'x'	'm'
	f_strtltx	'x'	'm'
	f_strtlty	'x'	'm'
	f_tsfc		'm'
	f_uocn	'x'	'm'
	f_uvel		'm'
	f_vgrdb		False
	f_vocn	'x'	'm'
	f_vsnon	'm'	
	f_vvel		'm'
&icefields_pond_nml	f_apeffn	'm'	'x'
	f_apondn	'm'	'x'

Group (continued)	Variable	ACCESS-CM2/ cice_in.nml	./gadi/g/data/ hh5/tmp/cosima/ access-om2/ 1deg_jra55v13_- iaf_spinup1_B1/ output059/ice/ cice_in.nml
	f_hpondn	'm'	'x'
&ponds_nml	frzpnd	'cesm'	'hlid'
	hs0	0.03	0.0
	rfracmax	0.85	1.0
&setup_nml	diagfreq	24	960
	dt	1800	3600
	dumpfreq	'm'	'y'
	history_dir	'./HISTORY/'	'./OUTPUT/'
	incond_dir	'./HISTORY/'	'./OUTPUT/'
	istep0	17280	2067360
	lcdf64		False
	npt	1488	35 040.0
	print_global	True	False
	print_points	True	False
	restart_ext	True	False
	use_leap_years	True	False
	use_restart_time	False	True
	year_init	301	1
&shortwave_nml	ahmax	0.5	0.1
	albicei	0.36	0.44
	albicev	0.78	0.86
	dalb_mlt		−0.02
	dt_mlt		1.0
	r_snw	1.5	0.0
	tocnfrz		−1.8
&thermo_nml	chio		0.004
	conduct	'MU71'	'bubbly'
	dsdt_slow_mode	-1.5×10^{-7}	-5×10^{-8}
	saltmax	9.6	
&tracer_nml	tr_iage	True	False
	tr_pond_topo	True	False

References

Abel, R., C. W. Böning, R. J. Greatbatch, H. T. Hewitt, and M. J. Roberts, 2017: Feedback of mesoscale ocean currents on atmospheric winds in high-resolution coupled models and implications for the forcing of ocean-only models. *Ocean Science Discussions*, 1–22, doi:10.5194/os-2017-24, URL http://dx.doi.org/10.5194/os-2017-24.

Abernathey, R. P., I. Cerovecki, P. R. Holland, E. Newsom, M. Mazloff, and L. D. Talley, 2016: Water-mass transformation by sea ice in the upper branch of the Southern Ocean overturning. *Nature Geoscience*, **9 (8)**, 596–601, doi:10.1038/ngeo2749, URL http://dx.doi.org/10.1038/ngeo2749.

Adcroft, A., C. Hill, and J. Marshall, 1997: Representation of topography by shaved cells in a height coordinate ocean model. *Monthly Weather Review*, **125**, 2293–2315.

Archer, M., M. Roughan, S. Keating, and A. Schaeffer, 2017a: On the variability of the East Australian Current: Jet structure, meandering, and influence on shelf circulation. *Journal of Geophysical Research: Oceans*, doi:10.1002/2017jc013097, URL http://dx.doi.org/10.1002/2017JC013097.

Archer, M. R., S. R. Keating, M. Roughan, W. E. Johns, R. Lumpkin, F. Beron-Vera, and L. K. Shay, 2018: The kinematic similarity of two western boundary currents revealed by sustained high-resolution observations. *Geophysical Research Letters*, doi:10.1029/2018gl078429, URL http://dx.doi.org/10.1029/2018GL078429.

Archer, M. R., L. K. Shay, and W. E. Johns, 2017b: The surface velocity structure of the Florida Current in a jet coordinate frame. *Journal of Geophysical Research: Oceans*, doi:10.1002/2017jc013286, URL http://dx.doi.org/10.1002/2017JC013286.

Atmadipoera, A., R. Molcard, G. Madec, S. Wijffels, J. Sprintall, A. Koch-Larrouy, I. Jaya, and A. Supangat, 2009: Characteristics and variability of the Indonesian throughflow water at the outflow straits. *Deep Sea Research Part I: Oceanographic Research Papers*, **56 (11)**, 1942–1954, doi:10.1016/j.dsr.2009.06.004, URL http://dx.doi.org/10.1016/j.dsr.2009.06.004.

Bailey, D., E. Hunke, A. DuVivier, B. Lipscomb, C. Bitz, M. Holland, B. Briegleb, and J. Schramm, 2018: CESM CICE5 users guide, Release CESM CICE5. Tech. rep. URL https://media.readthedocs.org/pdf/cesmcice/latest/cesmcice.pdf.

Bamber, J., M. van den Broeke, J. Ettema, J. Lenaerts, and E. Rignot, 2012: Recent large increases in freshwater fluxes from Greenland into the North Atlantic. *Geophysical Research Letters*, **39 (19)**, L19 501, doi:10.1029/2012gl052552, URL http://dx.doi.org/10.1029/2012GL052552.

Barthélemy, A., H. Goosse, T. Fichefet, and O. Lecomte, 2017: On the sensitivity of Antarctic sea ice model biases to atmospheric forcing uncertainties. *Climate Dynamics*, **51 (4)**, 1585–1603, doi:10.1007/s00382-017-3972-7, URL http://dx.doi.org/10.1007/s00382-017-3972-7.

Beckmann, A., and R. Döscher, 1997: A method for improved representation of dense water spreading over topography in geopotential-coordinate models. *Journal of Physical Oceanography*, **27 (4)**, 581–591, doi:10.1175/1520-0485(1997)027<0581:amfiro>2.0.co;2, URL http://dx.doi.org/10.1175/1520-0485(1997)027<0581:AMFIRO>2.0.CO;2.

Behrendt, A., H. Sumata, B. Rabe, and U. Schauer, 2018: UDASH - Unified Database for Arctic and Subarctic Hydrography. *Earth System Science Data*, **10 (2)**, 1119–1138, doi:10.5194/essd-10-1119-2018, URL https://www.earth-syst-sci-data.net/10/1119/2018/.

Behrens, E., A. Biastoch, and C. W. Böning, 2013: Spurious AMOC trends in global ocean sea-ice models related to subarctic freshwater forcing. *Ocean Modelling*, **69**, 39–49, doi:10.1016/j.ocemod.2013.05.004, URL http://dx.doi.org/10.1016/j.ocemod.2013.05.004.

Beljaars, A. C. M., 1995: The parametrization of surface fluxes in large-scale models under free convection. *Quarterly Journal of the Royal Meteorological Society*, **121 (522)**, 255–270, doi:10.1002/qj.49712152203, URL https://rmets.onlinelibrary.wiley.com/doi/abs/10.1002/qj.49712152203, https://rmets.onlinelibrary.wiley.com/doi/pdf/10.1002/qj.49712152203.

Bentley, J. L., 1975: Multidimensional binary search trees used for associative searching. *Commun. ACM*, **18 (9)**, 509–517, doi:10.1145/361002.361007, URL http://doi.acm.org/10.1145/361002.361007.

Bi, D., and S. Marsland, 2010: Australian Climate Ocean Model (AusCOM) users guide. CAWCR Technical Report 27, The Centre for Australian Weather and Climate Research. URL http://www.cawcr.gov.au/technical-reports/CTR_027.pdf.

Bi, D., H. Yan, and A. Sullivan, 2016: ACCESS-CM2 development. *COSIMA workshop 26-27 May 2016, Hobart*, URL http://cosima.org.au/wp-content/uploads/2016/06/BI-COSIMA-Hobart-20160526.ppt.pdf.

Bi, D., and Coauthors, 2013a: The ACCESS coupled model: description, control climate and evaluation. *Australian Meteorological and Oceanographic Journal*, **63 (1)**, 41–64.

Bi, D., and Coauthors, 2013b: ACCESS-OM: the ocean and sea-ice core of the ACCESS coupled model. *Australian Meteorological and Oceanographic Journal*, **63 (1)**, 213–232.

Bi, D., and Coauthors, 2019: Configuring the ACCESS-CM2 model for CMIP6 experiments. *AMOS Annual Meeting 2019 and the International Conference on Tropical Meteorology and Oceanography*.

Bitz, C. M., and W. H. Lipscomb, 1999: An energy-conserving thermodynamic model of sea ice. *Journal of Geophysical Research: Oceans*, **104 (C7)**, 15 669–15 677, doi:10.1029/1999jc900100, URL http://dx.doi.org/10.1029/1999JC900100.

Böning, C. W., E. Behrens, A. Biastoch, K. Getzlaff, and J. L. Bamber, 2016: Emerging impact of Greenland meltwater on deepwater formation in the North Atlantic Ocean. *Nature Geoscience*, **9 (7)**, 523–527, doi:10.1038/ngeo2740, URL http://dx.doi.org/10.1038/NGEO2740.

Bouillon, S., T. Fichefet, V. Legat, and G. Madec, 2013: The elastic–viscous–plastic method revisited. *Ocean Modelling*, **71**, 2–12, doi:10.1016/j.ocemod.2013.05.013, URL http://dx.doi.org/10.1016/j.ocemod.2013.05.013.

Brodeau, L., B. Barnier, S. K. Gulev, and C. Woods, 2017: Climatologically significant effects of some approximations in the bulk parameterizations of turbulent air–sea fluxes. *Journal of Physical Oceanography*, **47 (1)**, 5–28, doi:10.1175/jpo-d-16-0169.1, URL http://dx.doi.org/10.1175/JPO-D-16-0169.1.

Caesar, L., S. Rahmstorf, A. Robinson, G. Feulner, and V. Saba, 2018: Observed fingerprint of a weakening Atlantic Ocean overturning circulation. *Nature*, **556 (7700)**, 191–196, doi:10.1038/s41586-018-0006-5, URL https://doi.org/10.1038/s41586-018-0006-5.

Campin, J.-M., and H. Goosse, 1999: Parameterization of density-driven downsloping flow for a coarse-resolution ocean model in z-coordinate. *Tellus A: Dynamic Meteorology and Oceanography*, **51 (3)**, 412–430, doi:10.3402/tellusa.v51i3.13468, URL http://dx.doi.org/10.3402/tellusa.v51i3.13468.

Capet, X., J. C. McWilliams, M. J. Molemaker, and A. F. Shchepetkin, 2008: Mesoscale to submesoscale transition in the California Current system. Part I: Flow structure, eddy flux, and observational tests. *Journal of Physical Oceanography*, **38 (1)**, 29–43, doi:10.1175/2007JPO3671.1, URL http://dx.doi.org/10.1175/2007JPO3671.1.

Cassano, J. J., and Coauthors, 2017: Development of the Regional Arctic System Model (RASM): Near-surface atmospheric climate sensitivity. *Journal of Climate*, **30 (15)**, 5729–5753, doi:10.1175/jcli-d-15-0775.1, URL http://dx.doi.org/10.1175/JCLI-D-15-0775.1.

Cheon, W. G., Y.-G. Park, J. R. Toggweiler, and S.-K. Lee, 2014: The relationship of Weddell Polynya and open-ocean deep convection to the Southern Hemisphere Westerlies. *Journal of Physical Oceanography*, **44 (2)**, 694–713, doi:10.1175/jpo-d-13-0112.1, URL http://dx.doi.org/10.1175/JPO-D-13-0112.1.

Colella, P., and P. R. Woodward, 1984: The Piecewise Parabolic Method (PPM) for gas-dynamical simulations. *Journal of Computational Physics*, **54 (1)**, 174–201, doi:10.1016/0021-9991(84)90143-8, URL http://dx.doi.org/10.1016/0021-9991(84)90143-8.

Colin de Verdière, A., and M. Ollitrault, 2016: A direct determination of the world ocean barotropic circulation. *Journal of Physical Oceanography*, **46 (1)**, 255–273, doi:10.1175/jpo-d-15-0046.1, URL http://dx.doi.org/10.1175/JPO-D-15-0046.1.

Craig, A. P., S. A. Mickelson, E. C. Hunke, and D. A. Bailey, 2015: Improved parallel performance of the CICE model in CESM1. *The International Journal of High Performance Computing Applications*, **29 (2)**, 154–165, doi:10.1177/1094342014548771, URL http://dx.doi.org/10.1177/1094342014548771.

Dai, A., T. Qian, K. E. Trenberth, and J. D. Milliman, 2009: Changes in continental freshwater discharge from 1948 to 2004. *Journal of Climate*, **22 (10)**, 2773–2792, doi:10.1175/2008jcli2592.1, URL http://dx.doi.org/10.1175/2008JCLI2592.1.

Danabasoglu, G., and Coauthors, 2014: North Atlantic simulations in Coordinated Ocean-ice Reference Experiments phase II (CORE-II). Part I: Mean states. *Ocean Modelling*, **73**, 76–107, doi:10.1016/j.ocemod.2013.10.005, URL http://dx.doi.org/10.1016/j.ocemod.2013.10.005.

Danabasoglu, G., and Coauthors, 2016: North Atlantic simulations in Coordinated Ocean-ice Reference Experiments phase II (CORE-II). Part II: Inter-annual to decadal variability. *Ocean Modelling*, **97**, 65–90, doi:10.1016/j.ocemod.2015.11.007, URL http://dx.doi.org/10.1016/j.ocemod.2015.11.007.

Dansereau, V., J. Weiss, P. Saramito, and P. Lattes, 2016: A Maxwell elasto-brittle rheology for sea ice modelling. *The Cryosphere*, **10 (3)**, 1339–1359, doi:10.5194/tc-10-1339-2016, URL http://dx.doi.org/10.5194/tc-10-1339-2016.

de Boyer Montégut, C., G. Madec, A. S. Fischer, A. Lazar, and D. Iudicone, 2004: Mixed layer depth over the global ocean: An examination of profile data and a profile-based climatology. *Journal of Geophysical Research*, **109 (C12)**, doi:10.1029/2004jc002378, URL http://dx.doi.org/10.1029/2004JC002378.

de Lavergne, C., S. Falahat, G. Madec, F. Roquet, J. Nycander, and C. Vic, 2019: Toward global maps of internal tide energy sinks. *Ocean Modelling*, **137**, 52–75, doi:10.1016/j.ocemod.2019.03.010, URL http://dx.doi.org/10.1016/j.ocemod.2019.03.010.

Delworth, T. L., and Coauthors, 2012: Simulated climate and climate change in the GFDL CM2.5 high-resolution coupled climate model. *Journal of Climate*, **25 (8)**, 2755–2781, doi:10.1175/jcli-d-11-00316.1, URL http://dx.doi.org/10.1175/JCLI-D-11-00316.1.

Depoorter, M. A., J. L. Bamber, J. A. Griggs, J. T. M. Lenaerts, S. R. M. Ligtenberg, M. R. van den Broeke, and G. Moholdt, 2013: Calving fluxes and basal melt rates of Antarctic ice shelves. *Nature*, **502 (7469)**, 89–92, doi:10.1038/nature12567, URL http://dx.doi.org/10.1038/nature12567.

Dix, M., and Coauthors, 2013: The ACCESS coupled model: Documentation of core CMIP5 simulations and initial results. *Australian Meteorological and Oceanographic Journal*, **63 (1)**, 83–99.

Donat-Magnin, M., N. C. Jourdain, P. Spence, J. Le Sommer, H. Gallée, and G. Durand, 2017: Ice-shelf melt response to changing winds and glacier dynamics in the amundsen sea sector, antarctica. *Journal of Geophysical Research: Oceans*, **122 (12)**, 10 206–10 224, doi:10.1002/2017jc013059, URL http://dx.doi.org/10.1002/2017JC013059.

Donohue, K. A., K. L. Tracey, D. R. Watts, M. P. Chidichimo, and T. K. Chereskin, 2016: Mean Antarctic Circumpolar Current transport measured in Drake Passage. *Geophysical Research Letters*, **43 (22)**, 11,760–11,767, doi:10.1002/2016gl070319, URL http://dx.doi.org/10.1002/2016GL070319.

Dorn, W., A. Rinke, C. Köberle, K. Dethloff, and R. Gerdes, 2018: HIRHAM–NAOSIM 2.0: The upgraded version of the coupled regional atmosphere-ocean-sea ice model for Arctic climate studies. *Geoscientific Model Development Discussions*, 1–30, doi:10.5194/gmd-2018-278, URL http://dx.doi.org/10.5194/gmd-2018-278.

Döscher, R., and A. Beckmann, 2000: Effects of a bottom boundary layer parameterization in a coarse-resolution model of the North Atlantic Ocean. *Journal of Atmospheric and Oceanic Technology*, **17 (5)**, 698–707, doi:10.1175/1520-0426(2000)017<0698:eoabbl>2.0.co;2, URL http://dx.doi.org/10.1175/1520-0426(2000)017<0698:EOABBL>2.0.CO;2.

Downes, S. M., N. L. Bindoff, and S. R. Rintoul, 2009: Impacts of climate change on the subduction of mode and intermediate water masses in the Southern Ocean. *Journal of Climate*, **22 (12)**, 3289–3302, doi:10.1175/2008jcli2653.1, URL http://dx.doi.org/10.1175/2008JCLI2653.1.

Downes, S. M., A. Gnanadesikan, S. M. Griffies, and J. L. Sarmiento, 2011: Water mass exchange in the Southern Ocean in coupled climate models. *Journal of Physical Oceanography*, **41 (9)**, 1756–1771, doi:10.1175/2011jpo4586.1, URL http://dx.doi.org/10.1175/2011JPO4586.1.

Downes, S. M., and Coauthors, 2015: An assessment of Southern Ocean water masses and sea ice during 1988-2007 in a suite of interannual CORE-II simulations. *Ocean Modelling*, **94**, 67–94, doi:10.1016/j.ocemod.2015.07.022, URL http://dx.doi.org/10.1016/j.ocemod.2015.07.022.

Dufour, C. O., A. K. Morrison, S. M. Griffies, I. Frenger, H. Zanowski, and M. Winton, 2017: Preconditioning of the Weddell Sea polynya by the ocean mesoscale and dense water overflows. *Journal of Climate*, **30 (19)**, 7719–7737, doi:10.1175/jcli-d-16-0586.1, URL http://dx.doi.org/10.1175/JCLI-D-16-0586.1.

Dukowicz, J. K., and J. R. Baumgardner, 2000: Incremental remapping as a transport/advection algorithm. *Journal of Computational Physics*, **160 (1)**, 318–335, doi:10.1006/jcph.2000.6465, URL http://dx.doi.org/10.1006/jcph.2000.6465.

Dunne, J. P., and Coauthors, 2012: GFDL's ESM2 global coupled climate–carbon earth system models. Part I: Physical formulation and baseline simulation characteristics. *Journal of Climate*, **25 (19)**, 6646–6665, doi:10.1175/jcli-d-11-00560.1, URL http://dx.doi.org/10.1175/JCLI-D-11-00560.1.

Durran, D., J. A. Weyn, and M. Q. Menchaca, 2017: Practical considerations for computing dimensional spectra from gridded data. *Monthly Weather Review*, **145 (9)**, 3901–3910, doi:10.1175/mwr-d-17-0056.1, URL http://dx.doi.org/10.1175/MWR-D-17-0056.1.

Errico, R. M., 1985: Spectra computed from a limited area grid. *Monthly Weather Review*, **113 (9)**, 1554–1562, doi:10.1175/1520-0493(1985)113<1554:scfala>2.0.co;2, URL http://dx.doi.org/10.1175/1520-0493(1985)113<1554:SCFALA>2.0.CO;2.

Farneti, R., and Coauthors, 2015: An assessment of Antarctic Circumpolar Current and Southern Ocean meridional overturning circulation during 1958-2007 in a suite of interannual CORE-II simulations. *Ocean Modelling*, **93**, 84–120, doi:10.1016/j.ocemod.2015.07.009, URL http://dx.doi.org/10.1016/j.ocemod.2015.07.009.

Feng, M., X. Zhang, P. Oke, D. Monselesan, M. Chamberlain, R. Matear, and A. Schiller, 2016: Invigorating ocean boundary current systems around Australia during 1979–2014: As simulated in a near-global eddy-resolving ocean model. *Journal of Geophysical Research: Oceans*, **121 (5)**, 3395–3408, doi:10.1002/2016JC011842, URL http://dx.doi.org/10.1002/2016JC011842.

Fetterer, F., K. Knowles, W. Meier, M. Savoie, and A. K. Windnagel, 2017, updated daily: Sea ice index, version 3. Tech. rep., NSIDC: National Snow and Ice Data Center, Boulder, Colorado, USA. doi:https://doi.org/10.7265/N5K072F8, URL https://doi.org/10.7265/N5K072F8.

Fiedler, E. K., and Coauthors, 2019: Intercomparison of long-term sea surface temperature analyses using the GHRSST Multi-Product Ensemble (GMPE) system. *Remote Sensing of Environment*, **222**, 18–33, doi:10.1016/j.rse.2018.12.015, URL http://dx.doi.org/10.1016/j.rse.2018.12.015.

Flato, G., and Coauthors, 2013: *Evaluation of Climate Models*, book section 9, 741866. Cambridge University Press, Cambridge, United Kingdom and New York, NY, USA, doi:10.1017/CBO9781107415324.020, URL www.climatechange2013.org.

Fons, S., N. Kurtz, and M. Bagnardi, 2022a: Antarctic sea ice thickness estimates from CryoSat-2: 2010-2021. Zenodo, URL https://zenodo.org/record/7327711, doi:10.5281/ZENODO.7327711.

Fons, S., N. Kurtz, and M. Bagnardi, 2022b: A decade-plus of Antarctic sea ice thickness and volume estimates from CryoSat-2 using a physical model and waveform-fitting. doi:10.5194/egusphere-2022-1287, URL https://doi.org/10.5194%2Fegusphere-2022-1287.

Fox-Kemper, B., R. Ferrari, and R. Hallberg, 2008: Parameterization of mixed layer eddies. Part I: Theory and diagnosis. *J. Phys. Oceanogr.*, **38 (6)**, 1145–1165, doi:10.1175/2007JPO3792.1.

Frajka-Williams, E., and Coauthors, 2019: Atlantic meridional overturning circulation: Observed transport and variability. *Frontiers in Marine Science*, **6**, doi:10.3389/fmars.2019.00260, URL http://dx.doi.org/10.3389/fmars.2019.00260.

Fritzner, S., R. Graversen, K. H. Christensen, P. Rostosky, and K. Wang, 2018: Impact of assimilating sea ice concentration, sea ice thickness and snow depth in a coupled ocean-sea ice modeling system. *The Cryosphere Discussions*, 1–27, doi:10.5194/tc-2018-171, URL http://dx.doi.org/10.5194/tc-2018-171.

Ganachaud, A., and C. Wunsch, 2003: Large-scale ocean heat and freshwater transports during the world ocean circulation experiment. *Journal of Climate*, **16 (4)**, 696–705, doi:10.1175/1520-0442(2003)016<0696:LSOHAF>2.0.CO;2.

Garnier, F., and Coauthors, 2021: Advances in altimetric snow depth estimates using bi-frequency SARAL and CryoSat-2 Ka-Ku measurements. *The Cryosphere*, **15 (12)**, 5483–5512, doi:10.5194/tc-15-5483-2021, URL https://doi.org/10.5194%2Ftc-15-5483-2021.

Gent, P. R., and J. C. McWilliams, 1990: Isopycnal mixing in ocean circulation models. *J. Phys. Oceanogr.*, **20 (1)**, 150–155, doi:10.1175/1520-0485(1990)020<0150:IMIOCM>2.0.CO;2.

Giles, A., R. Massom, P. Heil, and G. Hyland, 2011: Semi-automated feature-tracking of East Antarctic sea ice from Envisat ASAR imagery. *Remote Sensing of Environment*, **115 (9)**, 2267–2276, doi:10.1016/j.rse.2011.04.027, URL http://ecite.utas.edu.au/76076, iSSN 0034-4257.

Gill, A. E., 1982: *Atmosphere-Ocean Dynamics*, International Geophysics, Vol. 30. 1st ed., Academic Press, San Diego.

Girard, L., J. Weiss, J. M. Molines, B. Barnier, and S. Bouillon, 2009: Evaluation of high-resolution sea ice models on the basis of statistical and scaling properties of Arctic sea ice drift and deformation. *Journal of Geophysical Research*, **114 (C8)**, doi:10.1029/2008jc005182, URL http://dx.doi.org/10.1029/2008JC005182.

Goosse, H., and T. Fichefet, 2001: Open-ocean convection and polynya formation in a large-scale ice-ocean model. *Tellus A*, **53 (1)**, 94–111, doi:10.3402/tellusa.v53i1.12175, URL https://doi.org/10.3402/tellusa.v53i1.12175.

Gordon, A. L., 1978: Deep Antarctic convection west of Maud Rise. *Journal of Physical Oceanography*, **8 (4)**, 600–612, doi:10.1175/1520-0485(1978)008<0600:dacwom>2.0.co;2, URL http://dx.doi.org/10.1175/1520-0485(1978)008<0600:DACWOM>2.0.CO;2.

Gregg, M. C., T. B. Sanford, and D. P. Winkel, 2003: Reduced mixing from the breaking of internal waves in equatorial waters. *Nature*, **422 (6931)**, 513–515, doi:10.1038/nature01507.

Gregory, J. M., and Coauthors, 2016: The flux-anomaly-forced model intercomparison project (FAFMIP) contribution to CMIP6: investigation of sea-level and ocean climate change in response to CO2 forcing. *Geoscientific Model Development*, **9 (11)**, 3993–4017, doi:10.5194/gmd-9-3993-2016, URL http://dx.doi.org/10.5194/gmd-9-3993-2016.

Griffies, S., 2004: *Fundamentals of Ocean Climate Models*. Princeton University Press, Princeton, USA.

Griffies, S., 2015: A handbook for the GFDL CM2-O model suite. Technical Report 1, GFDL Climate Processes and Sensitivity Group, NOAA/GFDL Princeton, USA.

Griffies, S., and R. Hallberg, 2000: Biharmonic friction with a Smagorinsky-like viscosity for use in large-scale eddy-permitting ocean models. *Monthly Weather Review*, **128**, 2935–2946.

Griffies, S., M. J. Harrison, R. C. Pacanowski, and A. Rosati, 2008: A technical guide to MOM4. GFDL Ocean Group Technical Report 5, NOAA/Geophysical Fluid Dynamics Laboratory, 342 pp.

Griffies, S. M., 1998: The Gent-McWilliams skew flux. *J. Phys. Oceanogr.*, **28 (5)**, 831–841, doi:10.1175/1520-0485(1998)028<0831:TGMSF>2.0.CO;2.

Griffies, S. M., 2012: Elements of the Modular Ocean Model (MOM) 5 (2012 release with updates). Technical Report 7, NOAA/Geophysical Fluid Dynamics Laboratory Ocean Group.

Griffies, S. M., and Coauthors, 2009: Coordinated ocean-ice reference experiments (COREs). *Ocean Modelling*, **26 (1-2)**, 1–46, doi:10.1016/j.ocemod.2008.08.007, URL http://dx.doi.org/10.1016/j.ocemod.2008.08.007.

Griffies, S. M., and Coauthors, 2014: An assessment of global and regional sea level for years 1993–2007 in a suite of interannual CORE-II simulations. *Ocean Modelling*, **78**, 35–89, doi:10.1016/j.ocemod.2014.03.004, URL http://dx.doi.org/10.1016/j.ocemod.2014.03.004.

Griffies, S. M., and Coauthors, 2015: Impacts on ocean heat from transient mesoscale eddies in a hierarchy of climate models. *Journal of Climate*, **28 (3)**, 952–977, doi:10.1175/jcli-d-14-00353.1, URL http://dx.doi.org/10.1175/JCLI-D-14-00353.1.

Griffies, S. M., and Coauthors, 2016: OMIP contribution to CMIP6: experimental and diagnostic protocol for the physical component of the Ocean Model Intercomparison Project. *Geoscientific Model Development*, **9 (9)**, 3231–3296, doi:10.5194/gmd-9-3231-2016, URL https://www.geosci-model-dev.net/9/3231/2016/.

Guerreiro, K., and S. Fleury, 2017: Legos altimetric sea ice thickness data product v1.0. Tech. rep., LEGOS/CTOH. URL http://ctoh.legos.obs-mip.fr/data/sea-ice-products/sea-ice-thickness/sea-ice-thickness-handbook.

Guerreiro, K., S. Fleury, E. Zakharova, A. Kouraev, F. Rémy, and P. Maisongrande, 2017: Comparison of CryoSat-2 and ENVISAT radar freeboard over Arctic sea ice: toward an improved Envisat freeboard retrieval. *The Cryosphere*, **11 (5)**, 2059–2073, doi:10.5194/tc-11-2059-2017, URL https://doi.org/10.5194%2Ftc-11-2059-2017.

Haarsma, R. J., and Coauthors, 2016: High Resolution Model Intercomparison Project (HighResMIP). *Geoscientific Model Development Discussions*, 1–35, doi:10.5194/gmd-2016-66, URL http://dx.doi.org/10.5194/gmd-2016-66.

Haidvogel, D., J. McWilliams, and P. Gent, 1992: Boundary current separation in a quasigeostrophic, eddy-resolving ocean circulation model. *J. Phys. Oceanogr.*, **22**, 882–902.

Hallberg, R., 2013: Using a resolution function to regulate parameterizations of oceanic mesoscale eddy effects. *Ocean Modelling*, **72**, 92 – 103, doi:http://dx.doi.org/10.1016/j.ocemod.2013.08.007, URL http://www.sciencedirect.com/science/article/pii/S1463500313001601.

Hallberg, R., 2014: Numerical instabilities of the ice/ocean coupled system. *CLIVAR Exchanges*, **65 (19/2)**, 38–42, URL http://www.clivar.org/sites/default/files/documents/exchanges65_0.pdf.

Hamman, J., B. Nijssen, A. Roberts, A. Craig, W. Maslowski, and R. Osinski, 2017: The coastal streamflow flux in the Regional Arctic System Model. *Journal of Geophysical Research: Oceans*, **122 (3)**, 1683–1701, doi:10.1002/2016jc012323, URL http://dx.doi.org/10.1002/2016JC012323.

Hammond, M. D., and D. C. Jones, 2016: Freshwater flux from ice sheet melting and iceberg calving in the Southern Ocean. *Geoscience Data Journal*, **3 (2)**, 60–62, doi:10.1002/gdj3.43, URL http://dx.doi.org/10.1002/gdj3.43.

Hautala, S. L., J. Sprintall, J. T. Potemra, J. C. Chong, W. Pandoe, N. Bray, and A. G. Ilahude, 2001: Velocity structure and transport of the Indonesian Throughflow in the major straits restricting flow into the Indian Ocean. *Journal of Geophysical Research: Oceans*, **106 (C9)**, 19 527–19 546, doi:10.1029/2000JC000577, URL https://agupubs.onlinelibrary.wiley.com/doi/abs/10.1029/2000JC000577.

Heil, P., R. Massom, I. Allison, and A. Worby, 2011: Physical attributes of sea-ice kinematics during spring 2007 off East Antarctica. *Deep-Sea Research. Part 2: Topical Studies in Oceanography*, **58 (9-10)**, 1158–1171, doi:10.1016/j.dsr2.2010.12.004, URL http://ecite.utas.edu.au/76077, iSSN 0967-0645.

Heorton, H. D. B. S., M. Tsamados, S. T. Cole, A. M. G. Ferreira, A. Berbellini, M. Fox, and T. W. K. Armitage, 2019: Retrieving sea ice drag coefficients and turning angles from in situ and satellite observations using an inverse modeling framework. *Journal of Geophysical Research: Oceans*, **124 (8)**, 6388–6413, doi:10.1029/2018jc014881, URL http://dx.doi.org/10.1029/2018JC014881.

Heuzé, C., K. J. Heywood, D. P. Stevens, and J. K. Ridley, 2013: Southern Ocean bottom water characteristics in CMIP5 models. *Geophysical Research Letters*, **40 (7)**, 1409–1414, doi:10.1002/grl.50287, URL http://dx.doi.org/10.1002/grl.50287.

Heuzé, C., J. K. Ridley, D. Calvert, D. P. Stevens, and K. J. Heywood, 2015: Increasing vertical mixing to reduce Southern Ocean deep convection in NEMO3.4. *Geoscientific Model Development*, **8 (10)**, 3119–3130, doi:10.5194/gmd-8-3119-2015, URL http://dx.doi.org/10.5194/gmd-8-3119-2015.

Hibler, W. D., 1979: A dynamic thermodynamic sea ice model. *Journal of Physical Oceanography*, **9 (4)**, 815–846, doi:10.1175/1520-0485(1979)009<0815:adtsim>2.0.co;2, URL http://dx.doi.org/10.1175/1520-0485(1979)009<0815:ADTSIM>2.0.CO;2.

Hirschi, J. J.-M., and Coauthors, 2020: The Atlantic Meridional Overturning Circulation in high resolution models. *Journal of Geophysical Research: Oceans*, **125 (4)**, e2019JC015 522, doi:10.1029/2019jc015522, URL http://dx.doi.org/10.1029/2019JC015522.

Hobbs, W. R., R. Massom, S. Stammerjohn, P. Reid, G. Williams, and W. Meier, 2016: A review of recent changes in Southern Ocean sea ice, their drivers and forcings. *Global and Planetary Change*, **143**, 228–250, doi:10.1016/j.gloplacha.2016.06.008, URL http://dx.doi.org/10.1016/j.gloplacha.2016.06.008.

Holliday, N. P., S. Bacon, S. A. Cunningham, S. F. Gary, J. Karstensen, B. A. King, F. Li, and E. L. Mcdonagh, 2018: Subpolar North Atlantic overturning and gyre-scale circulation in the summers of 2014 and 2016. *Journal of Geophysical Research: Oceans*, **123 (7)**, 4538–4559, doi:10.1029/2018jc013841, URL http://dx.doi.org/10.1029/2018JC013841.

Holte, J., L. D. Talley, J. Gilson, and D. Roemmich, 2017: An Argo mixed layer climatology and database. *Geophysical Research Letters*, **44 (11)**, 5618–5626, doi:10.1002/2017gl073426, URL http://dx.doi.org/10.1002/2017GL073426.

Hunke, E. C., 2001: Viscous–plastic sea ice dynamics with the EVP model: Linearization issues. *Journal of Computational Physics*, **170 (1)**, 18–38, doi:10.1006/jcph.2001.6710, URL http://dx.doi.org/10.1006/jcph.2001.6710.

Hunke, E. C., 2010: Thickness sensitivities in the CICE sea ice model. *Ocean Modelling*, **34 (3-4)**, 137–149, doi:10.1016/j.ocemod.2010.05.004, URL http://dx.doi.org/10.1016/j.ocemod.2010.05.004.

Hunke, E. C., and J. K. Dukowicz, 1997: An elastic–viscous–plastic model for sea ice dynamics. *Journal of Physical Oceanography*, **27 (9)**, 1849–1867, doi:10.1175/1520-0485(1997)027<1849:aevpmf>2.0.co;2, URL http://dx.doi.org/10.1175/1520-0485(1997)027<1849:AEVPMF>2.0.CO;2.

Hunke, E. C., and J. K. Dukowicz, 2002: The elastic–viscous–plastic sea ice dynamics model in general orthogonal curvilinear coordinates on a sphere—incorporation of metric terms. *Monthly Weather Review*, **130 (7)**, 1848–1865, doi:10.1175/1520-0493(2002)130<1848:tevpsi>2.0.co;2, URL http://dx.doi.org/10.1175/1520-0493(2002)130<1848:TEVPSI>2.0.CO;2.

Hunke, E. C., W. H. Lipscomb, A. K. Turner, N. Jeffery, and S. Elliott, 2015: CICE: the Los Alamos Sea Ice Model documentation and software user's manual version 5.1. Tech. Rep. LA-CC-06-012, Los Alamos National Laboratory, Los Alamos NM 87545. URL http://oceans11.lanl.gov/trac/CICE/attachment/wiki/WikiStart/cicedoc.pdf?format=raw.

Hutchings, J. K., P. Heil, and W. D. Hibler, 2005: Modeling linear kinematic features in sea ice. *Monthly Weather Review*, **133 (12)**, 3481–3497, doi:10.1175/mwr3045.1, URL http://dx.doi.org/10.1175/MWR3045.1.

Hutchings, J. K., A. Roberts, C. A. Geiger, and J. Richter-Menge, 2011: Spatial and temporal characterization of sea-ice deformation. *Annals of Glaciology*, **52 (57)**, 360–368, doi:10.3189/172756411795931769.

Hutter, N., M. Losch, and D. Menemenlis, 2018: Scaling properties of Arctic sea ice deformation in a high-resolution viscous-plastic sea ice model and in satellite observations. *Journal of Geophysical Research: Oceans*, **123 (1)**, 672–687, doi:10.1002/2017jc013119, URL http://dx.doi.org/10.1002/2017JC013119.

Ilicak, M., and Coauthors, 2016: An assessment of the Arctic Ocean in a suite of interannual CORE-II simulations. Part III: Hydrography and fluxes. *Ocean Modelling*, **100**, 141–161, doi:10.1016/j.ocemod.2016.02.004, URL http://dx.doi.org/10.1016/j.ocemod.2016.02.004.

Iovino, D., S. Masina, A. Storto, A. Cipollone, and V. N. Stepanov, 2016: A 1/16° eddying simulation of the global NEMO sea-ice–ocean system. *Geoscientific Model Development*, **9 (8)**, 2665–2684, doi:10.5194/gmd-9-2665-2016, URL http://dx.doi.org/10.5194/gmd-9-2665-2016.

Ivanova, D. P., P. J. Gleckler, K. E. Taylor, P. J. Durack, and K. D. Marvel, 2016: Moving beyond the total sea ice extent in gauging model biases. *Journal of Climate*, **29 (24)**, 8965–8987, doi:10.1175/jcli-d-16-0026.1, URL http://dx.doi.org/10.1175/JCLI-D-16-0026.1.

Ivanova, N., and Coauthors, 2015: Inter-comparison and evaluation of sea ice algorithms: towards further identification of challenges and optimal approach using passive microwave observations. *The Cryosphere*, **9 (5)**, 1797–1817, doi:10.5194/tc-9-1797-2015, URL http://dx.doi.org/10.5194/tc-9-1797-2015.

Jackett, D. R., T. J. McDougall, R. Feistel, D. G. Wright, and S. M. Griffies, 2006: Algorithms for density, potential temperature, conservative temperature, and the freezing temperature of seawater. *Journal of Atmospheric and Oceanic Technology*, **23 (12)**, 1709–1728, doi:10.1175/jtech1946.1, URL http://dx.doi.org/10.1175/JTECH1946.1.

Jayne, S. R., 2009: The impact of abyssal mixing parameterizations in an ocean general circulation model. *Journal of Physical Oceanography*, **39 (7)**, 1756–1775, doi:10.1175/2009jpo4085.1, URL http://dx.doi.org/10.1175/2009JPO4085.1.

Jayne, S. R., and L. C. St. Laurent, 2001: Parameterizing tidal dissipation over rough topography. *Geophysical Research Letters*, **28 (5)**, 811–814, doi:10.1029/2000gl012044, URL http://dx.doi.org/10.1029/2000GL012044.

Jin, M., and Coauthors, 2018: Effects of model resolution and ocean mixing on forced ice-ocean physical and biogeochemical simulations using global and regional system models. *Journal of Geophysical Research: Oceans*, **123 (1)**, 358–377, doi:10.1002/2017jc013365, URL http://dx.doi.org/10.1002/2017JC013365.

Jochum, M., 2009: Impact of latitudinal variations in vertical diffusivity on climate simulations. *Journal of Geophysical Research: Oceans*, **114 (C1)**, C01 010, doi:10.1029/2008JC005030.

Johns, W. E., T. N. Lee, D. Zhang, R. Zantopp, C.-T. Liu, and Y. Yang, 2001: The Kuroshio east of Taiwan: Moored transport observations from the WOCE PCM-1 array. *Journal of Physical Oceanography*, **31 (4)**, 1031–1053, doi:10.1175/1520-0485(2001)031<1031:tkeotm>2.0.co;2, URL http://dx.doi.org/10.1175/1520-0485(2001)031<1031:TKEOTM>2.0.CO;2.

Johnson, G. C., B. M. Sloyan, W. S. Kessler, and K. E. McTaggart, 2002: Direct measurements of upper ocean currents and water properties across the tropical Pacific during the 1990s. *Progress in Oceanography*, **52 (1)**, 31–61, doi:10.1016/s0079-6611(02)00021-6, URL http://dx.doi.org/10.1016/S0079-6611(02)00021-6.

Kerry, C., B. Powell, M. Roughan, and P. Oke, 2016: Development and evaluation of a high-resolution reanalysis of the East Australian Current region using the Regional Ocean Modelling System (ROMS 3.4) and incremental strong-constraint 4-dimensional variational (IS4D-Var) data assimilation. *Geoscientific Model Development*, **9 (10)**, 3779–3801, doi:10.5194/gmd-9-3779-2016, URL http://dx.doi.org/10.5194/gmd-9-3779-2016.

Khoei, A. R., and S. A. Gharehbaghi, 2007: The superconvergence patch recovery technique and data transfer operators in 3d plasticity problems. *Finite Elem. Anal. Des.*, **43 (8)**, 630–648, doi:10.1016/j.finel.2007.01.002, URL http://dx.doi.org/10.1016/j.finel.2007.01.002.

Kim, J. G., E. C. Hunke, and W. H. Lipscomb, 2006: Sensitivity analysis and parameter tuning scheme for global sea-ice modeling. *Ocean Modelling*, **14 (1-2)**, 61–80, doi:10.1016/j.ocemod.2006.03.003, URL http://dx.doi.org/10.1016/j.ocemod.2006.03.003.

Kim, W. M., R. J. Small, S. Yeager, G. Danabasoglu, H. Tsujino, and C. OMDP, 2018: A new dataset for forcing ocean sea-ice simulations: JRA55-do. *2018 OMWG Winter Meeting*, URL http://www.cesm.ucar.edu/events/wg-meetings/2018/presentations/omwg/kim.pdf.

Kimmritz, M., S. Danilov, and M. Losch, 2015: On the convergence of the modified elastic–viscous–plastic method for solving the sea ice momentum equation. *Journal of Computational Physics*, **296**, 90–100, doi:10.1016/j.jcp.2015.04.051, URL http://dx.doi.org/10.1016/j.jcp.2015.04.051.

Kimmritz, M., M. Losch, and S. Danilov, 2017: A comparison of viscous-plastic sea ice solvers with and without replacement pressure. *Ocean Modelling*, **115**, 59–69, doi:10.1016/j.ocemod.2017.05.006, URL http://dx.doi.org/10.1016/j.ocemod.2017.05.006.

Kirtman, B. P., and Coauthors, 2012: Impact of ocean model resolution on CCSM climate simulations. *Climate Dynamics*, **39 (6)**, 1303–1328, doi:10.1007/s00382-012-1500-3, URL http://dx.doi.org/10.1007/s00382-012-1500-3.

Kiss, A. E., and Coauthors, 2020: ACCESS-OM2 v1.0: a global ocean–sea ice model at three resolutions. *Geoscientific Model Development*, **13 (2)**, 401–442, doi:10.5194/gmd-13-401-2020, URL https://www.geosci-model-dev.net/13/401/2020/.

Kjellsson, J., and Coauthors, 2015: Model sensitivity of the weddell and ross seas, antarctica, to vertical mixing and freshwater forcing. *Ocean Modelling*, **94**, 141–152, doi:10.1016/j.ocemod.2015.08.003, URL http://dx.doi.org/10.1016/j.ocemod.2015.08.003.

Kobayashi, S., and Coauthors, 2015: The JRA-55 reanalysis: General specifications and basic characteristics. *Journal of the Meteorological Society of Japan. Ser. II*, **93 (1)**, 5–48, doi:10.2151/jmsj.2015-001, URL http://dx.doi.org/10.2151/jmsj.2015-001.

Koch-Larrouy, A., G. Madec, B. Blanke, and R. Molcard, 2008a: Water mass transformation along the Indonesian throughflow in an OGCM. *Ocean Dynamics*, **58 (3-4)**, 289–309, doi:10.1007/s10236-008-0155-4, URL http://dx.doi.org/10.1007/s10236-008-0155-4.

Koch-Larrouy, A., G. Madec, D. Iudicone, A. Atmadipoera, and R. Molcard, 2008b: Physical processes contributing to the water mass transformation of the Indonesian Throughflow. *Ocean Dynamics*, **58 (3-4)**, 275–288, doi:10.1007/s10236-008-0154-5, URL http://dx.doi.org/10.1007/s10236-008-0154-5.

Koldunov, N. V., V. Aizinger, N. Rakowsky, P. Scholz, D. Sidorenko, S. Danilov, and T. Jung, 2019a: Scalability and some optimization of the Finite-volumE Sea ice-Ocean Model, version 2.0 (FESOM2). *Geoscientific Model Development Discussions*, 1–30, doi:10.5194/gmd-2018-334, URL http://dx.doi.org/10.5194/gmd-2018-334.

Koldunov, N. V., and Coauthors, 2019b: Fast EVP solutions in a high-resolution sea ice model. *Journal of Advances in Modeling Earth Systems*, **11 (5)**, 1269–1284, doi:10.1029/2018ms001485, URL http://dx.doi.org/10.1029/2018MS001485.

Kritsikis, E., M. Aechtner, Y. Meurdesoif, and T. Dubos, 2017a: Conservative interpolation between general spherical meshes. *Geoscientific Model Development*, **10 (1)**, 425–431, doi:10.5194/gmd-10-425-2017, URL https://www.geosci-model-dev.net/10/425/2017/.

Kritsikis, E., M. Aechtner, Y. Meurdesoif, and T. Dubos, 2017b: Conservative interpolation between general spherical meshes. *Geoscientific Model Development*, **10 (1)**, 425–431, doi:10.5194/gmd-10-425-2017, URL http://dx.doi.org/10.5194/gmd-10-425-2017.

Kurtz, N. T., and T. Markus, 2012: Satellite observations of Antarctic sea ice thickness and volume. *Journal of Geophysical Research: Oceans*, **117 (C8)**, doi:10.1029/2012jc008141, URL http://dx.doi.org/10.1029/2012JC008141.

Kwok, R., 2018: Arctic sea ice thickness, volume, and multiyear ice coverage: losses and coupled variability (1958–2018). *Environmental Research Letters*, **13 (10)**, 105 005, doi:10.1088/1748-9326/aae3ec, URL http://dx.doi.org/10.1088/1748-9326/aae3ec.

Kwok, R., and G. F. Cunningham, 2008: ICESat over Arctic sea ice: Estimation of snow depth and ice thickness. *Journal of Geophysical Research*, **113 (C8)**, doi:10.1029/2008jc004753, URL http://dx.doi.org/10.1029/2008JC004753.

Kwok, R., E. C. Hunke, W. Maslowski, D. Menemenlis, and J. Zhang, 2008: Variability of sea ice simulations assessed with RGPS kinematics. *Journal of Geophysical Research*, **113 (C11)**, doi:10.1029/2008jc004783, URL http://dx.doi.org/10.1029/2008JC004783.

Kwok, R., S. S. Pang, and S. Kacimi, 2017: Sea ice drift in the Southern Ocean: Regional patterns, variability, and trends. *Elem. Sci. Anth.*, **5 (0)**, 32, doi:10.1525/elementa.226, URL http://dx.doi.org/10.1525/elementa.226.

Kwok, R., and D. A. Rothrock, 2009: Decline in Arctic sea ice thickness from submarine and ICESat records: 1958-2008. *Geophysical Research Letters*, **36 (15)**, n/a–n/a, doi:10.1029/2009gl039035, URL http://dx.doi.org/10.1029/2009GL039035.

Kwok, R., L. Toudal Pedersen, P. Gudmandsen, and S. S. Pang, 2010: Large sea ice outflow into the Nares Strait in 2007. *Geophysical Research Letters*, **37 (3)**, doi:10.1029/2009gl041872, URL http://dx.doi.org/10.1029/2009GL041872.

Large, W. G., J. C. McWilliams, and S. C. Doney, 1994: Oceanic vertical mixing: A review and a model with a nonlocal boundary layer parameterization. *Rev. Geophys.*, **32 (4)**, 363–403, doi:10.1029/94RG01872.

Large, W. G., and S. Yeager, 2004: Diurnal to decadal global forcing for ocean and sea-ice models: The data sets and flux climatologies. Technical Note NCAR/TN-460+STR, NCAR. URL http://dx.doi.org/10.5065/D6KK98Q6.

Large, W. G., and S. G. Yeager, 2009: The global climatology of an interannually varying air-sea flux data set. *Climate Dynamics*, **33 (2)**, 341–364, doi:10.1007/s00382-008-0441-3, URL http://dx.doi.org/10.1007/s00382-008-0441-3.

Laurindo, L. C., A. J. Mariano, and R. Lumpkin, 2017: An improved near-surface velocity climatology for the global ocean from drifter observations. *Deep Sea Research Part I: Oceanographic Research Papers*, **124**, 73–92, doi:10.1016/j.dsr.2017.04.009, URL http://dx.doi.org/10.1016/j.dsr.2017.04.009.

Lee, H.-C., A. Rosati, and M. J. Spelman, 2006: Barotropic tidal mixing effects in a coupled climate model: Oceanic conditions in the Northern Atlantic. *Ocean Modelling*, **11 (3-4)**, 464–477, doi:10.1016/j.ocemod.2005.03.003, URL http://dx.doi.org/10.1016/j.ocemod.2005.03.003.

Lemieux, J.-F., D. A. Knoll, B. Tremblay, D. M. Holland, and M. Losch, 2012: A comparison of the Jacobian-free Newton–Krylov method and the EVP model for solving the sea ice momentum equation with a viscous-plastic formulation: A serial algorithm study. *Journal of Computational Physics*, **231 (17)**, 5926–5944, doi:10.1016/j.jcp.2012.05.024, URL http://dx.doi.org/10.1016/j.jcp.2012.05.024.

Lemieux, J.-F., and B. Tremblay, 2009: Numerical convergence of viscous-plastic sea ice models. *Journal of Geophysical Research*, **114 (C5)**, doi:10.1029/2008jc005017, URL http://dx.doi.org/10.1029/2008JC005017.

Lemieux, J.-F., and Coauthors, 2015: The Regional Ice Prediction System (RIPS): verification of forecast sea ice concentration. *Quarterly Journal of the Royal Meteorological Society*, **142 (695)**, 632–643, doi:10.1002/qj.2526, URL http://dx.doi.org/10.1002/qj.2526.

Leppäranta, M., 2011: *The Drift of Sea Ice*. 2nd ed., Springer, doi:10.1007/978-3-642-04683-4, URL https://www.springer.com/gp/book/9783642046827.

Lin, X., F. Massonnet, T. Fichefet, and M. Vancoppenolle, 2021: SITool (v1.0) – a new evaluation tool for large-scale sea ice simulations: application to CMIP6 OMIP. *Geoscientific Model Development*, **14 (10)**, 6331–6354, doi:10.5194/gmd-14-6331-2021, URL https://doi.org/10.5194%2Fgmd-14-6331-2021.

Lindsay, R. W., J. Zhang, and D. A. Rothrock, 2003: Sea-ice deformation rates from satellite measurements and in a model. *Atmosphere-Ocean*, **41 (1)**, 35–47, doi:10.3137/ao.410103, URL http://dx.doi.org/10.3137/ao.410103.

Lipscomb, W. H., and E. C. Hunke, 2004: Modeling sea ice transport using incremental remapping. *Monthly Weather Review*, **132 (6)**, 1341–1354, doi:10.1175/1520-0493(2004)132<1341:msitui>2.0.co;2, URL http://dx.doi.org/10.1175/1520-0493(2004)132<1341:MSITUI>2.0.CO;2.

Lipscomb, W. H., E. C. Hunke, W. Maslowski, and J. Jakacki, 2007: Ridging, strength, and stability in high-resolution sea ice models. *Journal of Geophysical Research*, **112 (C3)**, C03S91, doi:10.1029/2005jc003355, URL http://dx.doi.org/10.1029/2005JC003355.

Locarnini, R. A., and Coauthors, 2013: World Ocean Atlas 2013, Volume 1: Temperature. NOAA Atlas NESDIS 73. URL https://data.nodc.noaa.gov/woa/WOA13/DOC/woa13_vol1.pdf.

Losch, M., and S. Danilov, 2012: On solving the momentum equations of dynamic sea ice models with implicit solvers and the elastic–viscous–plastic technique. *Ocean Modelling*, **41**, 42–52, doi:10.1016/j.ocemod.2011.10.002, URL http://dx.doi.org/10.1016/j.ocemod.2011.10.002.

Losch, M., A. Fuchs, J.-F. Lemieux, and A. Vanselow, 2014: A parallel Jacobian-free Newton–Krylov solver for a coupled sea ice-ocean model. *Journal of Computational Physics*, **257**, 901–911, doi:10.1016/j.jcp.2013.09.026, URL http://dx.doi.org/10.1016/j.jcp.2013.09.026.

Lozier, M. S., and Coauthors, 2017: Overturning in the Subpolar North Atlantic Program: A new international ocean observing system. *Bulletin of the American Meteorological Society*, **98 (4)**, 737–752, doi:10.1175/bams-d-16-0057.1, URL http://dx.doi.org/10.1175/BAMS-D-16-0057.1.

Lozier, M. S., and Coauthors, 2019: A sea change in our view of overturning in the subpolar north atlantic. *Science*, **363 (6426)**, 516–521, doi:10.1126/science.aau6592, URL http://dx.doi.org/10.1126/science.aau6592.

Lu, P., Z. Li, B. Cheng, and M. Leppäranta, 2011: A parameterization of the ice-ocean drag coefficient. *Journal of Geophysical Research*, **116 (C7)**, doi:10.1029/2010jc006878, URL http://dx.doi.org/10.1029/2010JC006878.

Lumpkin, R., and K. Speer, 2007: Global ocean meridional overturning. *Journal of Physical Oceanography*, **37 (10)**, 2550–2562, doi:10.1175/jpo3130.1, URL http://dx.doi.org/10.1175/JPO3130.1.

Manizza, M., C. Le Quéré, A. J. Watson, and E. T. Buitenhuis, 2005: Bio-optical feedbacks among phytoplankton, upper ocean physics and sea-ice in a global model. *Geophysical Research Letters*, **32 (5)**, L05 603, doi:10.1029/2004gl020778, URL http://dx.doi.org/10.1029/2004GL020778.

Martin, T., W. Park, and M. Latif, 2012: Multi-centennial variability controlled by Southern Ocean convection in the Kiel Climate Model. *Climate Dynamics*, **40 (7-8)**, 2005–2022, doi:10.1007/s00382-012-1586-7, URL http://dx.doi.org/10.1007/s00382-012-1586-7.

Martinson, D. G., and C. Wamser, 1990: Ice drift and momentum exchange in winter Antarctic pack ice. *Journal of Geophysical Research*, **95 (C2)**, 1741, doi:10.1029/jc095ic02p01741, URL http://dx.doi.org/10.1029/JC095iC02p01741.

Massonnet, F., H. Goosse, T. Fichefet, and F. Counillon, 2014: Calibration of sea ice dynamic parameters in an ocean-sea ice model using an ensemble Kalman filter. *Journal of Geophysical Research: Oceans*, **119 (7)**, 4168–4184, doi:10.1002/2013jc009705, URL http://dx.doi.org/10.1002/2013JC009705.

Mathiot, P., A. Jenkins, C. Harris, and G. Madec, 2017: Explicit representation and parametrised impacts of under ice shelf seas in the z* coordinate ocean model NEMO 3.6. *Geoscientific Model Development*, **10 (7)**, 2849–2874, doi:10.5194/gmd-10-2849-2017, URL http://dx.doi.org/10.5194/gmd-10-2849-2017.

Mazloff, M. R., P. Heimbach, and C. Wunsch, 2010: An eddy-permitting Southern Ocean state estimate. *Journal of Physical Oceanography*, **40 (5)**, 880–899, doi:10.1175/2009JPO4236.1, URL http://dx.doi.org/10.1175/2009JPO4236.1.

McPhee, M., 2008: *Air-Ice-Ocean Interaction: Turbulent Ocean Boundary Layer Exchange Processes*. Springer New York, doi:10.1007/978-0-387-78335-2, URL http://dx.doi.org/10.1007/978-0-387-78335-2.

Meehl, G. A., J. M. Arblaster, C. T. Y. Chung, M. M. Holland, A. DuVivier, L. Thompson, D. Yang, and C. M. Bitz, 2019: Sustained ocean changes contributed to sudden Antarctic sea ice retreat in late 2016. *Nature Communications*, **10 (1)**, 14, doi:10.1038/s41467-018-07865-9, URL https://doi.org/10.1038/s41467-018-07865-9.

Meier, W., F. Fetterer, M. Savoie, S. Mallory, R. Duerr, and J. Stroeve, 2017: Noaa/nsidc climate data record of passive microwave sea ice concentration, version 3. Tech. rep., NSIDC: National Snow and Ice Data Center, Boulder, Colorado USA. doi:10.7265/N59P2ZTG, URL https://doi.org/10.7265/N59P2ZTG.

Meier, W. N., G. Peng, D. J. Scott, and M. H. Savoie, 2014: Verification of a new NOAA/NSIDC passive microwave sea-ice concentration climate record. *Polar Research*, **33 (1)**, 21 004, doi:10.3402/polar.v33.21004, URL http://dx.doi.org/10.3402/polar.v33.21004.

Melsheimer, C., 2019: Asi version 5 sea ice concentration user guide, version v0.9.2 (august 4, 2019). Tech. rep., Institute of Environmental Physics, University of Bremen. URL https://seaice.uni-bremen.de/fileadmin/user_upload/ASIuserguide.pdf.

Melsheimer, C., and G. Spreen, 2019: AMSR2 ASI sea ice concentration data, Antarctic, version 5.4 (NetCDF) (July 2012 - December 2019). PANGAEA, URL https://doi.pangaea.de/10.1594/PANGAEA.898400, doi:10.1594/PANGAEA.898400.

Merino, N., N. C. Jourdain, J. Le Sommer, H. Goosse, P. Mathiot, and G. Durand, 2018: Impact of increasing Antarctic glacial freshwater release on regional sea-ice cover in the Southern Ocean. *Ocean Modelling*, **121**, 76–89, doi:10.1016/j.ocemod.2017.11.009, URL http://dx.doi.org/10.1016/j.ocemod.2017.11.009.

Merino, N., J. Le Sommer, G. Durand, N. C. Jourdain, G. Madec, P. Mathiot, and J. Tournadre, 2016: Antarctic icebergs melt over the Southern Ocean: Climatology and impact on sea ice. *Ocean Modelling*, **104**, 99–110, doi:10.1016/j.ocemod.2016.05.001, URL http://dx.doi.org/10.1016/j.ocemod.2016.05.001.

Miller, P. A., S. W. Laxon, D. L. Feltham, and D. J. Cresswell, 2006: Optimization of a sea ice model using basinwide observations of Arctic sea ice thickness, extent, and velocity. *Journal of Climate*, **19 (7)**, 1089–1108, doi:10.1175/jcli3648.1, URL http://dx.doi.org/10.1175/JCLI3648.1.

Morales Maqueda, M. A., 2004: Polynya dynamics: a review of observations and modeling. *Reviews of Geophysics*, **42 (1)**, doi:10.1029/2002rg000116, URL http://dx.doi.org/10.1029/2002RG000116.

Murray, R. J., 1996: Explicit generation of orthogonal grids for ocean models. *Journal of Computational Physics*, **126 (2)**, 251–273, doi:10.1006/jcph.1996.0136, URL http://dx.doi.org/10.1006/jcph.1996.0136.

NAS, 2017: *Antarctic Sea Ice Variability in the Southern Ocean-Climate System: Proceedings of a Workshop*. The National Academies Press, National Academies of Sciences, Engineering, and Medicine, Washington, DC, doi:10.17226/24696, URL https://www.nap.edu/catalog/24696/antarctic-sea-ice-variability-in-the-southern-ocean-climate-system.

Naughten, K., 2018: Modelling antarctic ice shelf, ocean, and sea ice interactions under present-day and future climate scenarios. Ph.D. thesis, Climate Change Research Centre (CCRC), Faculty of Science, University of New South Wales, URL https://www.unsworks.unsw.edu.au/primo-explore/fulldisplay?docid=unsworks_51321&context=L&vid=UNSWORKS&search_scope=unsworks_search_scope&tab=default_tab&lang=en_US.

Naughten, K. A., K. J. Meissner, B. K. Galton Fenzi, M. H. England, R. Timmermann, H. H. Hellmer, T. Hattermann, and J. B. Debernard, 2018: Intercomparison of Antarctic ice-shelf, ocean, and sea-ice interactions simulated by MetROMS-iceshelf and FESOM 1.4. *Geoscientific Model Development*, **11 (4)**, 1257–1292, doi:10.5194/gmd-11-1257-2018, URL https://www.geosci-model-dev.net/11/1257/2018/.

Newsom, E. R., C. M. Bitz, F. O. Bryan, R. Abernathey, and P. R. Gent, 2016: Southern Ocean deep circulation and heat uptake in a high-resolution climate model. *Journal of Climate*, **29 (7)**, 2597–2619, doi:10.1175/jcli-d-15-0513.1, URL http://dx.doi.org/10.1175/JCLI-D-15-0513.1.

Nihashi, S., and K. I. Ohshima, 2015: Circumpolar mapping of Antarctic coastal polynyas and landfast sea ice: Relationship and variability. *Journal of Climate*, **28 (9)**, 3650–3670, doi:10.1175/jcli-d-14-00369.1, URL http://dx.doi.org/10.1175/JCLI-D-14-00369.1.

Notz, D., F. A. Haumann, H. Haak, J. H. Jungclaus, and J. Marotzke, 2013: Arctic sea-ice evolution as modeled by Max Planck Institute for Meteorology's Earth system model. *Journal of Advances in Modeling Earth Systems*, **5 (2)**, 173–194, doi:10.1002/jame.20016, URL http://dx.doi.org/10.1002/jame.20016.

Notz, D., A. Jahn, M. Holland, E. Hunke, F. Massonnet, J. Stroeve, B. Tremblay, and M. Vancoppenolle, 2016: The CMIP6 Sea-Ice Model Intercomparison Project (SIMIP): understanding sea ice through climate-model simulations. *Geoscientific Model Development*, **9 (9)**, 3427–3446, doi:10.5194/gmd-9-3427-2016, URL https://www.geosci-model-dev.net/9/3427/2016/.

Nye, J. F., 1973: Is there any physical basis for assuming linear viscous behavior for sea ice? *AIDJEX Bull.*, **21**, 18–19, URL http://psc.apl.washington.edu/nonwp_projects/aidjex/files/AIDJEX-21.pdf.

Ohshima, K. I., S. Nihashi, and K. Iwamoto, 2016: Global view of sea-ice production in polynyas and its linkage to dense/bottom water formation. *Geoscience Letters*, **3 (1)**, doi:10.1186/s40562-016-0045-4, URL http://dx.doi.org/10.1186/s40562-016-0045-4.

Oke, P. R., and Coauthors, 2013: Evaluation of a near-global eddy-resolving ocean model. *Geoscientific Model Development*, **6 (3)**, 591–615, doi:10.5194/gmd-6-591-2013, URL http://www.geosci-model-dev.net/6/591/2013/.

Ollitrault, M., and A. Colin de Verdière, 2014: The ocean general circulation near 1000-m depth. *Journal of Physical Oceanography*, **44 (1)**, 384–409, doi:10.1175/jpo-d-13-030.1, URL http://dx.doi.org/10.1175/JPO-D-13-030.1.

Pacanowski, R. C., and A. Gnanadesikan, 1998: Transient response in a z-level ocean model that resolves topography with partial cells. *Monthly Weather Review*, **126 (12)**, 3248–3270, doi:10.1175/1520-0493(1998)126<3248:triazl>2.0.co;2, URL http://dx.doi.org/10.1175/1520-0493(1998)126<3248:TRIAZL>2.0.CO;2.

Park, H.-S., and A. L. Stewart, 2016: An analytical model for wind-driven Arctic summer sea ice drift. *The Cryosphere*, **10 (1)**, 227–244, doi:10.5194/tc-10-227-2016, URL http://dx.doi.org/10.5194/tc-10-227-2016.

Pellichero, V., J.-B. Sallée, C. C. Chapman, and S. M. Downes, 2018: The southern ocean meridional overturning in the sea-ice sector is driven by freshwater fluxes. *Nature Communications*, **9 (1)**, 1789, doi:10.1038/s41467-018-04101-2, URL https://doi.org/10.1038/s41467-018-04101-2.

Peng, G., W. N. Meier, D. J. Scott, and M. H. Savoie, 2013: A long-term and reproducible passive microwave sea ice concentration data record for climate studies and monitoring. *Earth System Science Data*, **5 (2)**, 311–318, doi:10.5194/essd-5-311-2013, URL http://dx.doi.org/10.5194/essd-5-311-2013.

Pringle, D. J., H. Eicken, H. J. Trodahl, and L. G. E. Backstrom, 2007: Thermal conductivity of landfast Antarctic and Arctic sea ice. *Journal of Geophysical Research*, **112 (C4)**, C04 017, doi:10.1029/2006jc003641, URL http://dx.doi.org/10.1029/2006JC003641.

Rae, J. G. L., H. T. Hewitt, A. B. Keen, J. K. Ridley, A. E. West, C. M. Harris, E. C. Hunke, and D. N. Walters, 2015: Development of the Global Sea Ice 6.0 CICE configuration for the Met Office Global Coupled model. *Geoscientific Model Development*, **8 (7)**, 2221–2230, doi:10.5194/gmd-8-2221-2015, URL https://www.geosci-model-dev.net/8/2221/2015/.

Rahmstorf, S., J. E. Box, G. Feulner, M. E. Mann, A. Robinson, S. Rutherford, and E. J. Schaffernicht, 2015: Exceptional twentieth-century slowdown in Atlantic Ocean overturning circulation. *Nature Climate Change*, **5**, 475 EP –, URL https://doi.org/10.1038/nclimate2554.

Redi, M. H., 1982: Oceanic isopycnal mixing by coordinate rotation. *J. Phys. Oceanogr.*, **12 (10)**, 1154–1158, doi:10.1175/1520-0485(1982)012<1154:OIMBCR>2.0.CO;2.

Renault, L., P. Marchesiello, S. Masson, and J. C. McWilliams, 2019a: Remarkable control of western boundary currents by eddy killing, a mechanical air-sea coupling process. *Geophysical Research Letters*, **46 (5)**, 2743–2751, doi:10.1029/2018gl081211, URL http://dx.doi.org/10.1029/2018GL081211.

Renault, L., S. Masson, T. Arsouze, G. Madec, and J. C. McWilliams, 2020: Recipes for how to force oceanic model dynamics. *Journal of Advances in Modeling Earth Systems*, **12 (2)**, doi:10.1029/2019ms001715, URL http://dx.doi.org/10.1029/2019MS001715.

Renault, L., S. Masson, V. Oerder, S. Jullien, and F. Colas, 2019b: Disentangling the mesoscale ocean-atmosphere interactions. *Journal of Geophysical Research: Oceans*, **124 (3)**, 2164–2178, doi:10.1029/2018jc014628, URL http://dx.doi.org/10.1029/2018JC014628.

Renault, L., M. J. Molemaker, J. Gula, S. Masson, and J. C. McWilliams, 2016: Control and stabilization of the Gulf Stream by oceanic current interaction with the atmosphere. *Journal of Physical Oceanography*, doi:10.1175/JPO-D-16-0115.1, URL http://dx.doi.org/10.1175/JPO-D-16-0115.1, http://dx.doi.org/10.1175/JPO-D-16-0115.1.

Richter, O., D. E. Gwyther, B. K. Galton-Fenzi, and K. A. Naughten, 2020: The Whole Antarctic Ocean Model (WAOM v1.0): Development and evaluation. *Geoscientific Model Development Discussions*, **2020**, 1–40, doi:10.5194/gmd-2020-164, URL https://gmd.copernicus.org/preprints/gmd-2020-164/.

Ridley, J. K., E. W. Blockley, A. B. Keen, J. G. L. Rae, A. E. West, and D. Schroeder, 2018: The sea ice model component of HadGEM3-GC3.1. *Geoscientific Model Development*, **11 (2)**, 713–723, doi:10.5194/gmd-11-713-2018, URL http://dx.doi.org/10.5194/gmd-11-713-2018.

Rintoul, S. R., 2018: The global influence of localized dynamics in the Southern Ocean. *Nature*, **558 (7709)**, 209–218, doi:10.1038/s41586-018-0182-3, URL https://doi.org/10.1038/s41586-018-0182-3.

Rio, M.-H., S. Mulet, and N. Picot, 2014: Beyond GOCE for the ocean circulation estimate: Synergetic use of altimetry, gravimetry, and in situ data provides new insight into geostrophic and Ekman currents. *Geophysical Research Letters*, **41 (24)**, 8918–8925, doi:10.1002/2014gl061773, URL http://dx.doi.org/10.1002/2014GL061773.

Roach, L. A., S. M. Dean, and J. A. Renwick, 2018: Consistent biases in Antarctic sea ice concentration simulated by climate models. *The Cryosphere*, **12 (1)**, 365–383, doi:10.5194/tc-12-365-2018, URL http://dx.doi.org/10.5194/tc-12-365-2018.

Roach, L. A., and Coauthors, 2020: Antarctic sea ice area in CMIP6. *Geophysical Research Letters*, **47 (9)**, doi:10.1029/2019gl086729, URL https://doi.org/10.1029%2F2019gl086729.

Roberts, A., W. Maslowski, J. Jakacki, M. Higgins, A. Craig, J. Cassano, W. Gutowski, and P. Lettenmaier, 2011: High frequency and wavenumber ocean-ice-atmosphere coupling in the Regional Arctic Climate Model. *AGU Fall Meeting Abstracts*, 4.

Roberts, A., and Coauthors, 2015: Simulating transient ice-ocean Ekman transport in the Regional Arctic System Model and Community Earth System Model. *Annals of Glaciology*, **56 (69)**, 211–228, doi:10.3189/2015aog69a760, URL http://dx.doi.org/10.3189/2015AoG69A760.

Roberts, A. F., E. C. Hunke, R. Allard, D. A. Bailey, A. P. Craig, J.-F. Lemieux, and M. D. Turner, 2018: Quality control for community-based sea-ice model development. *Philosophical Transactions of the Royal Society A: Mathematical, Physical and Engineering Sciences*, **376 (2129)**, 20170 344, doi:10.1098/rsta.2017.0344, URL http://dx.doi.org/10.1098/rsta.2017.0344.

Roberts, M. J., and Coauthors, 2019: Description of the resolution hierarchy of the global coupled HadGEM3-GC3.1 model as used in CMIP6 HighResMIP experiments. *Geoscientific Model Development Discussions*, 1–47, doi:10.5194/gmd-2019-148, URL http://dx.doi.org/10.5194/gmd-2019-148.

Roquet, F., G. Madec, T. J. McDougall, and P. M. Barker, 2015: Accurate polynomial expressions for the density and specific volume of seawater using the TEOS-10 standard. *Ocean Modelling*, **90**, 29–43, doi:10.1016/j.ocemod.2015.04.002, URL http://dx.doi.org/10.1016/j.ocemod.2015.04.002.

Röske, F., 2006: A global heat and freshwater forcing dataset for ocean models. *Ocean Modelling*, **11 (3-4)**, 235–297, doi:10.1016/j.ocemod.2004.12.005, URL http://dx.doi.org/10.1016/j.ocemod.2004.12.005.

Sallée, J.-B., E. Shuckburgh, N. Bruneau, A. J. S. Meijers, T. J. Bracegirdle, and Z. Wang, 2013: Assessment of Southern Ocean mixed-layer depths in CMIP5 models: Historical bias and forcing response. *Journal of Geophysical Research: Oceans*, **118 (4)**, 1845–1862, doi:10.1002/jgrc.20157, URL https://agupubs.onlinelibrary.wiley.com/doi/abs/10.1002/jgrc.20157.

Sallée, J.-B., N. Wienders, K. Speer, and R. Morrow, 2006: Formation of subantarctic mode water in the southeastern Indian Ocean. *Ocean Dynamics*, **56 (5-6)**, 525–542, doi:10.1007/s10236-005-0054-x, URL http://dx.doi.org/10.1007/s10236-005-0054-x.

Schmidt, M., 2007: A benchmark for the parallel code used in FMS and MOM-4. *Ocean Modelling*, **17 (1)**, 49–67, doi:10.1016/j.ocemod.2006.11.002, URL http://dx.doi.org/10.1016/j.ocemod.2006.11.002.

Schmidtko, S., G. C. Johnson, and J. M. Lyman, 2013: MIMOC: A global monthly isopycnal upper-ocean climatology with mixed layers. *Journal of Geophysical Research: Oceans*, **118 (4)**, 1658–1672, doi:10.1002/jgrc.20122, URL http://dx.doi.org/10.1002/jgrc.20122.

Schröder, D., D. L. Feltham, M. Tsamados, A. Ridout, and R. Tilling, 2019: New insight from CryoSat-2 sea ice thickness for sea ice modelling. *The Cryosphere*, **13 (1)**, 125–139, doi:10.5194/tc-13-125-2019, URL http://dx.doi.org/10.5194/tc-13-125-2019.

Schroeter, S., W. Hobbs, N. L. Bindoff, R. Massom, and R. Matear, 2018: Drivers of Antarctic sea ice volume change in CMIP5 models. *Journal of Geophysical Research: Oceans*, doi:10.1029/2018jc014177, URL http://dx.doi.org/10.1029/2018JC014177.

Schweiger, A., R. Lindsay, J. Zhang, M. Steele, H. Stern, and R. Kwok, 2011: Uncertainty in modeled Arctic sea ice volume. *Journal of Geophysical Research*, **116**, doi:10.1029/2011jc007084, URL http://dx.doi.org/10.1029/2011JC007084.

Shirasawa, K., and R. G. Ingram, 1997: Currents and turbulent fluxes under the first-year sea ice in Resolute Passage, Northwest Territories, Canada. *Journal of Marine Systems*, **11 (1-2)**, 21–32, doi:10.1016/s0924-7963(96)00024-3, URL http://dx.doi.org/10.1016/S0924-7963(96)00024-3.

Simmons, H. L., S. R. Jayne, L. C. S. Laurent, and A. J. Weaver, 2004: Tidally driven mixing in a numerical model of the ocean general circulation. *Ocean Model.*, **6 (3)**, 245–263, doi:10.1016/S1463-5003(03)00011-8.

Sloyan, B. M., K. R. Ridgway, and R. Cowley, 2016: The east australian current and property transport at 27°S from 2012 to 2013. *Journal of Physical Oceanography*, **46 (3)**, 993–1008, doi:10.1175/JPO-D-15-0052.1, URL http://dx.doi.org/10.1175/JPO-D-15-0052.1, http://dx.doi.org/10.1175/JPO-D-15-0052.1.

Smeed, D. A., and Coauthors, 2018: The North Atlantic Ocean is in a state of reduced overturning. *Geophysical Research Letters*, **45 (3)**, 1527–1533, doi:10.1002/2017gl076350, URL http://dx.doi.org/10.1002/2017GL076350.

Smith, G. C., and Coauthors, 2015: Sea ice forecast verification in the Canadian Global Ice Ocean Prediction System. *Quarterly Journal of the Royal Meteorological Society*, **142 (695)**, 659–671, doi:10.1002/qj.2555, URL http://dx.doi.org/10.1002/qj.2555.

Smith, W. H. F., and D. T. Sandwell, 1997: Global sea floor topography from satellite altimetry and ship depth soundings. *Science*, **277 (5334)**, 1956–1962, doi:10.1126/science.277.5334.1956, URL http://www.sciencemag.org/content/277/5334/1956.abstract, http://www.sciencemag.org/content/277/5334/1956.full.pdf.

Spence, P., R. M. Holmes, A. M. Hogg, S. M. Griffies, K. D. Stewart, and M. H. England, 2017: Localized rapid warming of West Antarctic subsurface waters by remote winds. *Nature Climate Change*, **7 (8)**, 595–603, doi:10.1038/nclimate3335, URL http://dx.doi.org/10.1038/nclimate3335.

Sprintall, J., S. E. Wijffels, R. Molcard, and I. Jaya, 2009: Direct estimates of the Indonesian Throughflow entering the Indian Ocean: 2004–2006. *Journal of Geophysical Research: Oceans*, **114 (C7)**, C07 001, doi:10.1029/2008JC005257, URL http://dx.doi.org/10.1029/2008JC005257.

Stewart, K., A. Hogg, S. Griffies, A. Heerdegen, M. Ward, P. Spence, and M. England, 2017: Vertical resolution of baroclinic modes in global ocean models. *Ocean Modelling*, **113**, 50–65, doi:10.1016/j.ocemod.2017.03.012, URL http://dx.doi.org/10.1016/j.ocemod.2017.03.012.

Stewart, K. D., and Coauthors, 2020: JRA55-do-based repeat year forcing datasets for driving ocean–sea-ice models. *Ocean Modelling*, **147**, 101 557, doi:10.1016/j.ocemod.2019.101557, URL http://dx.doi.org/10.1016/j.ocemod.2019.101557.

Storkey, D., and Coauthors, 2018: UK Global Ocean GO6 and GO7: a traceable hierarchy of model resolutions. *Geoscientific Model Development Discussions*, 1–43, doi:10.5194/gmd-2017-263, URL http://dx.doi.org/10.5194/gmd-2017-263.

Stössel, A., D. Notz, F. A. Haumann, H. Haak, J. Jungclaus, and U. Mikolajewicz, 2015: Controlling high-latitude Southern Ocean convection in climate models. *Ocean Modelling*, **86**, 58–75, doi:10.1016/j.ocemod.2014.11.008, URL http://dx.doi.org/10.1016/j.ocemod.2014.11.008.

Stössel, A., Z. Zhang, and T. Vihma, 2011: The effect of alternative real-time wind forcing on Southern Ocean sea ice simulations. *Journal of Geophysical Research*, **116 (C11)**, C11 021, doi:10.1029/2011jc007328, URL http://dx.doi.org/10.1029/2011JC007328.

Sumata, H., R. Gerdes, F. Kauker, and M. Karcher, 2015a: Empirical error functions for monthly mean Arctic sea-ice drift. *Journal of Geophysical Research: Oceans*, **120 (11)**, 7450–7475, doi:10.1002/2015jc011151, URL http://dx.doi.org/10.1002/2015JC011151.

Sumata, H., R. Kwok, R. Gerdes, F. Kauker, and M. Karcher, 2015b: Uncertainty of Arctic summer ice drift assessed by high-resolution SAR data. *Journal of Geophysical Research: Oceans*, **120 (8)**, 5285–5301, doi:10.1002/2015jc010810, URL http://dx.doi.org/10.1002/2015JC010810.

Sumata, H., T. Lavergne, F. Girard-Ardhuin, N. Kimura, M. A. Tschudi, F. Kauker, M. Karcher, and R. Gerdes, 2014: An intercomparison of Arctic ice drift products to deduce uncertainty estimates. *Journal of Geophysical Research: Oceans*, **119 (8)**, 4887–4921, doi:10.1002/2013jc009724, URL http://dx.doi.org/10.1002/2013JC009724.

Suresh, A., and H. Huynh, 1997: Accurate monotonicity-preserving schemes with Runge-Kutta time stepping. *Journal of Computational Physics*, **136 (1)**, 83–99, doi:10.1006/jcph.1997.5745, URL http://dx.doi.org/10.1006/jcph.1997.5745.

Suzuki, T., D. Yamazaki, H. Tsujino, Y. Komuro, H. Nakano, and S. Urakawa, 2018: A dataset of continental river discharge based on JRA-55 for use in a global ocean circulation model. *Journal of Oceanography*, **74 (4)**, 421–429, doi:10.1007/s10872-017-0458-5, URL https://doi.org/10.1007/s10872-017-0458-5.

Sweeney, C., A. Gnanadesikan, S. M. Griffies, M. J. Harrison, A. J. Rosati, and B. L. Samuels, 2005: Impacts of shortwave penetration depth on large-scale ocean circulation and heat transport. *J. Phys. Oceanogr.*, **35 (6)**, 1103–1119, doi:10.1175/JPO2740.1.

Szanyi, S., J. V. Lukovich, D. G. Barber, and G. Haller, 2016: Persistent artifacts in the NSIDC ice motion data set and their implications for analysis. *Geophysical Research Letters*, **43 (20)**, 10,800–10,807, doi:10.1002/2016gl069799, URL http://dx.doi.org/10.1002/2016GL069799.

Talley, L. D., 2013: Closure of the global overturning circulation through the Indian, Pacific, and Southern Oceans: Schematics and transports. *Oceanography*, **26 (1)**, 80–97, doi:10.5670/oceanog.2013.07, URL https://doi.org/10.5670/oceanog.2013.07.

Tamura, T., and K. I. Ohshima, 2011: Mapping of sea ice production in the Arctic coastal polynyas. *Journal of Geophysical Research*, **116 (C7)**, doi:10.1029/2010jc006586, URL http://dx.doi.org/10.1029/2010JC006586.

Tamura, T., K. I. Ohshima, A. D. Fraser, and G. D. Williams, 2016: Sea ice production variability in Antarctic coastal polynyas. *Journal of Geophysical Research: Oceans*, **121 (5)**, 2967–2979, doi:10.1002/2015jc011537, URL http://dx.doi.org/10.1002/2015JC011537.

Tamura, T., K. I. Ohshima, and S. Nihashi, 2008: Mapping of sea ice production for Antarctic coastal polynyas. *Geophysical Research Letters*, **35 (7)**, n/a–n/a, doi:10.1029/2007gl032903, URL http://dx.doi.org/10.1029/2007GL032903.

Toyota, T., and N. Kimura, 2018: An examination of the sea ice rheology for seasonal ice zones based on ice drift and thickness observations. *Journal of Geophysical Research: Oceans*, doi:10.1002/2017JC013627, URL http://dx.doi.org/10.1002/2017JC013627.

Tsamados, M., D. L. Feltham, and A. V. Wilchinsky, 2013: Impact of a new anisotropic rheology on simulations of Arctic sea ice. *Journal of Geophysical Research: Oceans*, **118 (1)**, 91–107, doi:10.1029/2012jc007990, URL http://dx.doi.org/10.1029/2012JC007990.

Tseng, Y.-H., and Coauthors, 2016: North and equatorial Pacific Ocean circulation in the CORE-II hindcast simulations. *Ocean Modelling*, **104**, 143–170, doi:10.1016/j.ocemod.2016.06.003, URL http://dx.doi.org/10.1016/j.ocemod.2016.06.003.

Tsujino, H., 2015a: On the use of JRA55 for driving ocean-sea ice models - biases, correction (adjustment), results from preliminary model run. *OMDP forcing mini workshop 29-30 Jan 2015, Grenoble, France*, URL http://www.clivar.org/sites/default/files/documents/wgomd/grenoble2015/OMDP_Grenoble2015_Tsujino.pdf.

Tsujino, H., 2015b: Short description of a JRA-55 based surface atmospheric data set for driving ocean-sea ice models. Tech. rep., JMA Meteorological Research Institute. URL https://mri-2.mri-jma.go.jp/owncloud/index.php/s/3d33d5a6ee3bd326abae2cecbea91bd0#pdfviewer.

Tsujino, H., 2016: JRA-55 based surface atmospheric data set for driving ocean-sea ice models. *OMDP extended meetng 14 January 2016, JAMSTEC, Yokohama, Japan*, URL http://www.clivar.org/sites/default/files/documents/wgomd/japan2016/OMDP_Meeting/Tsujino_OMDP2016.pdf.

Tsujino, H., 2018: Results of testing several wind forcing methods based on JRA55-do-v1.3: Application to MRI ocean - sea-ice models, URL https://jra55-do.slack.com/archives/C7LEZT4KY/p1524498479000123, posted to Slack JRA55-do channel https://jra55-do.slack.com.

Tsujino, H., and Coauthors, 2016: JRA-55 based data set for driving ocean - sea ice model (JRA55-do). *17 September 2016 ARP-OMDP joint session Qingdao, China*.

Tsujino, H., and Coauthors, 2018a: JRA-55 based surface dataset for driving ocean - sea-ice models (JRA55-do). *Ocean Modelling*, **130**, 79–139, doi:10.1016/j.ocemod.2018.07.002, URL http://dx.doi.org/10.1016/j.ocemod.2018.07.002.

Tsujino, H., and Coauthors, 2018b: *User manual for JRA-55 based surface dataset for driving ocean-sea-ice models (JRA55-do), version 1.3*. URL https://mri-2.mri-jma.go.jp/owncloud/index.php/s/cSntssoesw4ATRT.

Tsujino, H., and Coauthors, 2019: *User manual of JRA-55 based surface dataset for driving ocean-sea-ice models (JRA55-do), version 1.4*. JMA Meteorological Research Institute, Tsukuba, Japan, URL https://climate.mri-jma.go.jp/~htsujino/docs/JRA55-do/v1_4-manual/User_manual_jra55_do_v1_4.pdf.

Turner, A. K., E. C. Hunke, and C. M. Bitz, 2013: Two modes of sea-ice gravity drainage: A parameterization for large-scale modeling. *Journal of Geophysical Research: Oceans*, **118 (5)**, 2279–2294, doi:10.1002/jgrc.20171, URL http://dx.doi.org/10.1002/jgrc.20171.

Uotila, P., H. Goosse, K. Haines, M. Chevallier, A. Barthélemy, C. Bricaud, J. Carton, and Coauthors, 2019: An assessment of ten ocean reanalyses in the polar regions. *Climate Dynamics*, **52 (1613)**, doi:10.1007/s00382-018-4242-z, URL http://dx.doi.org/10.1007/s00382-018-4242-z.

Uotila, P., D. Iovino, M. Vancoppenolle, M. Lensu, and C. Rousset, 2017: Comparing sea ice, hydrography and circulation between NEMO3.6 LIM3 and LIM2. *Geoscientific Model Development*, **10 (2)**, 1009–1031, doi:10.5194/gmd-10-1009-2017, URL http://dx.doi.org/10.5194/gmd-10-1009-2017.

Uotila, P., S. O'Farrell, S. Marsland, and D. Bi, 2012: A sea-ice sensitivity study with a global ocean-ice model. *Ocean Modelling*, **51**, 1–18, doi:10.1016/j.ocemod.2012.04.002, URL http://dx.doi.org/10.1016/j.ocemod.2012.04.002.

Uotila, P., S. O'Farrell, S. J. Marsland, and D. Bi, 2013: The sea-ice performance of the Australian climate models participating in the CMIP5. *Australian Meteorological And Oceanographic Journal*, **63 (1)**, 121–143.

Urrego-Blanco, J. R., N. M. Urban, E. C. Hunke, A. K. Turner, and N. Jeffery, 2016: Uncertainty quantification and global sensitivity analysis of the Los Alamos sea ice model. *Journal of Geophysical Research: Oceans*, **121 (4)**, 2709–2732, doi:10.1002/2015jc011558, URL http://dx.doi.org/10.1002/2015JC011558.

Valcke, S., T. Craig, and L. Coquart, 2013: OASIS3-MCT User Guide: OASIS3-MCT 2.0. CERFACS/CNRS SUC URA No1875, CERFACS TR/CMGC/13/17, CERFACS/CNRS. URL http://www.cerfacs.fr/oa4web/oasis3-mct/oasis3mct_UserGuide.pdf.

Van Roekel, L., and Coauthors, 2018: The KPP boundary layer scheme for the ocean: Revisiting its formulation and benchmarking one-dimensional simulations relative to LES. *Journal of Advances in Modeling Earth Systems*, doi:10.1029/2018ms001336, URL http://dx.doi.org/10.1029/2018MS001336.

Vaughan, D., and Coauthors, 2013: *Observations: Cryosphere*, book section 4, 317382. Cambridge University Press, Cambridge, United Kingdom and New York, NY, USA, doi:10.1017/CBO9781107415324.012, URL www.climatechange2013.org.

Wang, G., H. H. Hendon, J. M. Arblaster, E.-P. Lim, S. Abhik, and P. van Rensch, 2019: Compounding tropical and stratospheric forcing of the record low Antarctic sea-ice in 2016. *Nature Communications*, **10 (1)**, 13, doi:10.1038/s41467-018-07689-7, URL https://doi.org/10.1038/s41467-018-07689-7.

Wang, K., and C. Wang, 2009: Modeling linear kinematic features in pack ice. *Journal of Geophysical Research*, **114 (C12)**, doi:10.1029/2008jc005217, URL http://dx.doi.org/10.1029/2008JC005217.

Wang, Q., S. Danilov, T. Jung, L. Kaleschke, and A. Wernecke, 2016a: Sea ice leads in the arctic ocean: Model assessment, interannual variability and trends. *Geophysical Research Letters*, **43 (13)**, 7019–7027, doi:10.1002/2016gl068696, URL http://dx.doi.org/10.1002/2016GL068696.

Wang, Q., and Coauthors, 2016b: An assessment of the Arctic Ocean in a suite of interannual CORE-II simulations. Part I: Sea ice and solid freshwater. *Ocean Modelling*, **99**, 110–132, doi:10.1016/j.ocemod.2015.12.008, URL http://dx.doi.org/10.1016/j.ocemod.2015.12.008.

Wang, Q., and Coauthors, 2016c: An assessment of the Arctic Ocean in a suite of interannual CORE-II simulations. Part II: Liquid freshwater. *Ocean Modelling*, **99**, 86–109, doi:10.1016/j.ocemod.2015.12.009, URL http://dx.doi.org/10.1016/j.ocemod.2015.12.009.

Waters, J. K., and M. S. Bruno, 1995: Internal wave generation by ice floes moving in stratified water: Results from a laboratory study. *Journal of Geophysical Research*, **100 (C7)**, 13 635, doi:10.1029/95jc01220, URL http://dx.doi.org/10.1029/95JC01220.

Weiss, J., 2003: Scaling of fracture and faulting of ice on Earth. *Surveys in Geophysics*, **24 (2)**, 185–227, doi:10.1023/A:1023293117309, URL https://doi.org/10.1023/A:1023293117309.

Weiss, J., 2017: Exploring the "solid turbulence" of sea ice dynamics down to unprecedented small scales. *Journal of Geophysical Research: Oceans*, **122 (8)**, 6071–6075, doi:10.1002/2017jc013236, URL http://dx.doi.org/10.1002/2017JC013236.

Weiss, J., and V. Dansereau, 2017: Linking scales in sea ice mechanics. *Philosophical Transactions of the Royal Society A: Mathematical, Physical and Engineering Sciences*, **375 (2086)**, 20150 352, doi:10.1098/rsta.2015.0352, URL http://dx.doi.org/10.1098/rsta.2015.0352.

Weiss, J., and E. M. Schulson, 2009: Coulombic faulting from the grain scale to the geophysical scale: lessons from ice. *Journal of Physics D: Applied Physics*, **42 (21)**, 214 017, URL http://stacks.iop.org/0022-3727/42/i=21/a=214017.

Weiss, J., E. M. Schulson, and H. L. Stern, 2007: Sea ice rheology from in-situ, satellite and laboratory observations: Fracture and friction. *Earth and Planetary Science Letters*, **255 (1-2)**, 1–8, doi:10.1016/j.epsl.2006.11.033, URL http://dx.doi.org/10.1016/j.epsl.2006.11.033.

Wijeratne, S., C. Pattiaratchi, and R. Proctor, 2018: Estimates of surface and subsurface boundary current transport around Australia. *Journal of Geophysical Research: Oceans*, doi:10.1029/2017jc013221, URL http://dx.doi.org/10.1029/2017JC013221.

Wijffels, S. E., and Coauthors, 2018: A fine spatial-scale sea surface temperature atlas of the Australian regional seas (SSTAARS): Seasonal variability and trends around Australasia and New Zealand revisited. *Journal of Marine Systems*, doi:10.1016/j.jmarsys.2018.07.005, URL http://dx.doi.org/10.1016/j.jmarsys.2018.07.005.

Wilchinsky, A. V., and D. L. Feltham, 2006: Modelling the rheology of sea ice as a collection of diamond-shaped floes. *Journal of Non-Newtonian Fluid Mechanics*, **138 (1)**, 22–32, doi:10.1016/j.jnnfm.2006.05.001, URL http://dx.doi.org/10.1016/j.jnnfm.2006.05.001.

Williams, K. D., and Coauthors, 2018: The Met Office Global Coupled Model 3.0 and 3.1 (GC3.0 and GC3.1) configurations. *Journal of Advances in Modeling Earth Systems*, **10 (2)**, 357–380, doi:10.1002/2017ms001115, URL http://dx.doi.org/10.1002/2017MS001115.

Worby, A. P., C. A. Geiger, M. J. Paget, M. L. Van Woert, S. F. Ackley, and T. L. DeLiberty, 2008: Thickness distribution of Antarctic sea ice. *Journal of Geophysical Research*, **113 (C5)**, doi:10.1029/2007jc004254, URL http://dx.doi.org/10.1029/2007JC004254.

Wu, Y., X. Zhai, and Z. Wang, 2017: Decadal-mean impact of including ocean surface currents in bulk formulas on surface air-sea fluxes and ocean general circulation. *Journal of Climate*, **30 (23)**, 9511–9525, doi:10.1175/jcli-d-17-0001.1, URL http://dx.doi.org/10.1175/JCLI-D-17-0001.1.

Xu, Y., and L.-L. Fu, 2011: Global variability of the wavenumber spectrum of oceanic mesoscale turbulence. *Journal of Physical Oceanography*, **41 (4)**, 802–809, doi:10.1175/2010JPO4558.1, URL http://dx.doi.org/10.1175/2010JPO4558.1.

Xu, Y., and L.-L. Fu, 2012: The effects of altimeter instrument noise on the estimation of the wavenumber spectrum of sea surface height. *Journal of Physical Oceanography*, **42 (12)**, 2229–2233, doi:10.1175/JPO-D-12-0106.1, URL http://dx.doi.org/10.1175/JPO-D-12-0106.1.

Yang, R., M. Ward, and B. Evans, 2019: Parallel I/O in FMS and MOM5. *Geoscientific Model Development Discussions*, **2019**, 1–31, doi:10.5194/gmd-2019-257, URL https://www.geosci-model-dev-discuss.net/gmd-2019-257/.

Zhang, J., and D. A. Rothrock, 2003: Modeling global sea ice with a thickness and enthalpy distribution model in generalized curvilinear coordinates. *Monthly Weather Review*, **131 (5)**, 845–861, doi:10.1175/1520-0493(2003)131<0845:mgsiwa>2.0.co;2, URL http://dx.doi.org/10.1175/1520-0493(2003)131<0845:MGSIWA>2.0.CO;2.

Zhang, R., R. Sutton, G. Danabasoglu, Y.-O. Kwon, R. Marsh, S. G. Yeager, D. E. Amrhein, and C. M. Little, 2019: A review of the role of the Atlantic Meridional Overturning Circulation in Atlantic multidecadal variability and associated climate impacts. *Reviews of Geophysics*, doi:10.1029/2019rg000644, URL http://dx.doi.org/10.1029/2019RG000644.

Zhang, Z., T. Vihma, A. Stössel, and P. Uotila, 2015: The role of wind forcing from operational analyses for the model representation of Antarctic coastal sea ice. *Ocean Modelling*, **94**, 95–111, doi:10.1016/j.ocemod.2015.07.019, URL http://dx.doi.org/10.1016/j.ocemod.2015.07.019.

Zilberman, N. V., D. H. Roemmich, and S. T. Gille, 2014: Meridional volume transport in the South Pacific: Mean and SAM-related variability. *Journal of Geophysical Research: Oceans*, **119 (4)**, 2658–2678, doi:10.1002/2013JC009688, URL https://agupubs.onlinelibrary.wiley.com/doi/abs/10.1002/2013JC009688.

Zilberman, N. V., D. H. Roemmich, S. T. Gille, and J. Gilson, 2018: Estimating the velocity and transport of western boundary current systems: A case study of the East Australian Current near Brisbane. *Journal of Atmospheric and Oceanic Technology*, **35 (6)**, 1313–1329, doi:10.1175/jtech-d-17-0153.1, URL http://dx.doi.org/10.1175/JTECH-D-17-0153.1.

Zilberman, N. V., M. Scanderbeg, A. R. Gray, and P. R. Oke, 2023: Scripps Argo trajectory-based velocity product: Global estimates of absolute velocity derived from core, biogeochemical, and deep argo float trajectories at parking depth. *Journal of Atmospheric and Oceanic Technology*, doi:10.1175/jtech-d-22-0065.1, URL https://doi.org/10.1175%2Fjtech-d-22-0065.1.

Zweng, M., and Coauthors, 2013: World Ocean Atlas 2013, Volume 2: Salinity. NOAA Atlas NESDIS 74. URL https://data.nodc.noaa.gov/woa/WOA13/DOC/woa13_vol2.pdf.

Index